Low spin pseudotetrahedral cobalt tris(phosphino)borate complexes

Thesis by

David Matthew Jenkins

In partial fulfillment of the requirements for the degree of

Doctor of Philosophy

California Institute of Technology

Pasadena, California

2005

(Defended January 31, 2005)

Acknowledgements

The number of people who have helped me throughout my education is too great for me to acknowledge everyone individually. I would, however, like to single out a few people. Foremost, I want to thank my advisor Jonas Peters for providing advice and encouragement. I will always remember the importance of doing the "best" chemistry in a thorough and accurate manner and of communicating the results in a precise fashion. I would also like to thank my boxmates, who have helped make day-to-day life so much more enjoyable. In particular, B.Q. (Baixin Qian) taught me the ropes of working in an inorganic laboratory and impressed on me the value of "life goals." Christine Thomas, in addition to her valuable help editing many of my papers, was always supportive in lab and a joy to be around in the office. I would like to thank the Peters's group in general for making sure life was never dull and, of course, "keepin' it real." I would also like to thank Héctor Abruña and Diego Diaz, who introduced me to chemical research at Cornell and for that have my utmost thanks.

There are several other people who helped me in the course of my research at Caltech. Angelo Di Bilio helped immensely with my EPR spectra acquisition and interpretation; Larry Henling and Mike Day provided superb assistance with X-ray crystallography; Mohan Sankaran taught me how to use the SQUID, which was a vital part of my research. Without your collective help, my graduate studies would not have been as fruitful and rewarding. I would also like to thank my graduate committee for their guidance and criticism.

Finally, I would like to thank my parents, William and Vicki Jenkins, for their steadfast love and support throughout my educational endeavors. I also must express my utmost gratitude to Mahogany Paulino, my future wife, for her tenderness and love.

Abstract

A synthetic protocol is developed for the preparation of a thallium complex featuring the tris(phosphino)borate ligand [$PhBP_3$] ([$PhBP_3$] = [$PhB(CH_2PPh_2)_3$]$^-$). The transmetallating reagent, [$PhBP_3$]Tl, is characterized by single crystal X-ray diffraction and solution NMR spectroscopy, and is the first example of a stable homoleptic Tl(I)-phosphine complex.

The synthesis and characterization of [$PhBP_3$]Co-X (X = I, Br or Cl) is discussed. These halide complexes are structurally characterized and magnetic investigations establish that they are low spin when monomeric. The low spin iodide complex is a monomer in solution and in the solid state. The other halides exhibit a monomer/dimer equilibrium that complicates their magnetic behavior. Theoretical calculations help provide a rationale as to why these pseudotetrahedral species are low spin. A classic high spin species supported by [$PhBP_3$] is compared to the low spin complexes.

Spin state control involving pseudotetrahedral [$PhBP_3$]Co(II) complexes is explored. Both high and low spin, as well as spin crossover, complexes are synthesized and structurally characterized. The complexes are discussed in terms of the relationship between local geometry and spin state. Changing the axial or tripodal ligand can cause a different spin state to be favored. Since the energy difference between the states is small, ligand changes at remote positions from the metal center have a significant effect on spin crossover phenomena. Theoretical calculations help illuminate why the low spin state is preferred for many of the complexes.

The first examples of cobalt imide complexes ([$PhBP_3$]Co≡NR (R = aryl or alkyl)) are prepared and they are supported by the [$PhBP_3$] ligand. These diamagnetic

species are evaluated by NMR and single crystal X-ray diffraction. Theoretical studies suggest that they have a similar molecular orbital bonding scheme as the previously prepared group 9 imides.

A cobalt μ_2-bridging nitride complex (($[PhBP_3]Co)_2(\mu\text{-}N)$) is synthesized and structurally characterized. This mixed-valence species is evaluated by magnetometry to determine its ground state, which is low spin ($S = ½$).

Several cobalt diazoalkane complexes are prepared. These diamagnetic species adopt two different bonding modes depending on the nature of the diazoalkane ligand.

Table of Contents

List of Figures

Chapter 1: Background and introduction to cobalt tris(phosphino)borate chemistry

Chapter 2: A homoleptic phosphine adduct of Tl(I)

Chapter 3: Elucidation of a low spin cobalt(II) system in a distorted tetrahedral geometry

List of Tables

List of Abbreviations and Nomenclature

[BP_3]	general abbreviation for [$PhBP_3$] or [$PhBP^{iPr}_3$]
[Cp]	cyclopentadienyl
[Cp*]	pentamethyl-cyclopentadienyl
[Me_2NN]	[$HC(CMeNC_6H_3\text{-}2,6\text{-}Me_2)_2]^-$
[$PhBP_3$]	[$PhB(CH_2PPh_2)_3]^-$
[$PhBP^{iPr}_3$]	[$PhB(CH_2P^iPr_2)_3]^-$
[Tp]	general tris(pyrazolyl)borate
[$Tp^{3,5\text{-}Me2}$]	hydro-tris(3,5-dimethyl-pyrazolyl)borate
[Tp’’]	hydro-tris(3-*tert*-butyl-5-methyl-pyrazolyl)borate
[$Tt^{tert\text{-}butyl}$]	[$PhB(CH_2S^tBu)_3]^-$
{^{1}H}	hydrogen-1 decoupled
°	degrees in measure of angles
°C	degrees Celsius
^{1}H	hydrogen-1
^{11}B	boron-11
^{13}C	carbon-13
^{19}F	fluorine-19
^{31}P	phosphorus-31
^{59}Co	cobalt-59
^{127}I	iodine-127
^{203}Tl	thallium-203
^{205}Tl	thallium-205

Å	Angstrom, 10^{-10} m
Ad	adamantyl
Anal. Calcd	elemental analysis calculated
Ar	general aryl group
av	average
A_X	EPR hyperfine coupling where X is the nucleus coupling to the unpaired electron (also sometimes abbreviated ^{X}A)
B3LYP	Becke three-parameter functional with Lee-Yang-Parr correlation functional
BM	Bohr magnetons
br	broad
Bu	butyl
C_{3v}, C_s	Schoenflies symmetry designations
Calcd	calculated
CCD	charge coupled device
cm	centimeter(s)
cm^{-1}	inverse centimeters or wavenumbers
cm^3	cubic centimeters
cont.	continued
d	doublet
DC	direct current
D_{calcd}	calculated density
deg	degrees in measure of angles

d^n	d-electron count of n electrons for a transition metal
DFT	density functional theory
dtbpe	1,2-bis(di-tert-butylphosphino)ethane
E	an atom or functional group forming a metal-ligand multiple bond
EPR	electron paramagnetic resonance
Eq.	equation
equiv.	equivalents
ESI/MS	electrospray ionization mass spectrometry
Et	ethyl
Exptl	experimental
fac	*facial* coordination
g	gram
G	gauss
GC/MS	gas chromatography mass spectrometry
GHz	gigahertz
g_{iso}	isotropic g-factor
h	hour(s)
H	applied magnetic field
HOMO	highest occupied molecular orbital
Hz	hertz
I_n	nuclear spin of atom n
^{i}Pr	*iso*-propyl
IR	infrared

K	degrees in Kelvin
kcal	kilocalories
kHz	kilohertz
L	dative ligand for a transition metal
LACVP	Los Alamos core valence potential
LFT	ligand field theory
LUMO	lowest unoccupied molecular orbital
m	multiplet
M	general metal
Me	methyl
Mes	mesityl
Me_3-tacn	1,4,7-trimethyl-1,4,7-triazocyclononane
mg	milligram(s)
MHz	megahertz, one million Hertz
min	minute(s)
mL	milliliter(s)
mmol	millimoles
MO	molecular orbital
mol	moles
ms	millisecond(s)
MS	mass spectrometry
mT	millitesla(s)
mV	millivolt(s)

mW	milliwatt(s)
NA	not applicable
^{n}Bu	*n*-butyl
near-IR	near-infrared
$^{n}J_{A-Z}$	in NMR spectroscopy, coupling constant between nuclei A and Z over n bonds (n, A, or Z omitted if not known)
nm	namometer(s)
NMR	nuclear magnetic resonance
np_3	tris(2-diphenylphosphino)ethyl)amine
OTf	$-OSO_2CF_3$
p-	*para* position on an aryl ring
Ph	phenyl
ppm	parts per million
q	quartet
R	general alkyl or aryl substituent
rt	room temperature
s	second(s)
s	solvent peak (in NMR spectrum)
S	spin
SOMO	singly occupied molecular orbital
SQUID	superconducting quantum interference device
S(*G*)	distance (i.e., deviation) of a given molecule from an idealized polyhedron of a symmetry point group defined as *G*

t	triplet
T	temperature
TBA	tetrabutylammonium
^{t}Bu	*tert*-butyl
THF	tetrahydrofuran
tmeda	tetramethylethylenediamine
TMS	trimethylsilyl
tolyl	$-C_6H_4CH_3$
triphos	$H_3CC(CH_2PPh_2)_3$
Ts	$-S(O)_2$-*p*-tolyl
tt	triplet of triplets
UV-vis	ultraviolet-visible
V	volume
X	monoanionic atom or group, such as a halide or thiolate
XRD	X-ray diffraction
δ	delta, chemical shift
ε	extinction coefficient in M^{-1} cm^{-1}
η^n	hapticity of order n
κ^n	number n of single ligating atom attachments of a polyatomic ligand
λ	wavelength
λ_{max}	wavelength of maximum absorption
μ	absorption coefficient (X-ray diffraction)

μ-A	bridging atom A
μ_2	atom bridging between two metal centers
μ_B	Bohr magnetons
μ_{eff}	effective magnetic moment, measured in Bohr magnetons
μL	microliter(s)
ν	frequency
θ	Weiss constant
χ	magnetic susceptibility
χ_m	molar magnetic susceptibility

Dedication

This work is dedicated to my father and mother, William and Vicki Jenkins.

I love you dearly.

Chapter 1: Background and introduction to cobalt tris(phosphino)borate chemistry

1.1 Introduction

Threefold symmetry is a successful design strategy for a myriad of inorganic transition metal complexes, in part because three-coordinate complexes in threefold symmetry have a site open for reactions (Figure 1.1). Many key advances have been achieved using this template, including the activation of dinitrogen and other small molecules.[1] Threefold symmetric complexes are particularly adept at stabilizing metal-ligand triple bonds. Since species that can be assigned to the C_{3v} point group (or higher symmetry with a threefold axis) have a set of orbitals of *e* symmetry, two energetically equivalent π-bonds can be formed. Some examples of C_{3v} pseudotetrahedral complexes with metal-ligand triple bonds are shown in Figure 1.2.[2] These complexes can contain three equivalent monodentate ligands[3] or a single tripodal ligand.[4] While d^0 and d^2 metal-ligand multiple bonds are ubiquitous, examples with higher electron counts are rare; however, this field of research has recently seen considerable growth.[5]

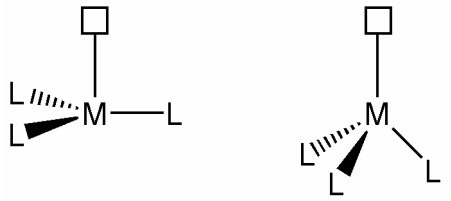

Figure 1.1. Two examples of threefold symmetric complexes with an available reaction site (□).

Many neutral and anionic tridentate ligands have been designed to take advantage of threefold symmetry in order to achieve *facial* coordination about a pseudotetrahedral metal complex. The tris(pyrazolyl)borates are among the most prominent anionic

ligands.[6] Neutral tripodal phosphine ligands, such as triphos (triphos = $H_3CC(CH_2PPh_2)_3$), have also been developed.[7] These and other prominent tridentate ligands are shown in Figure 1.3.

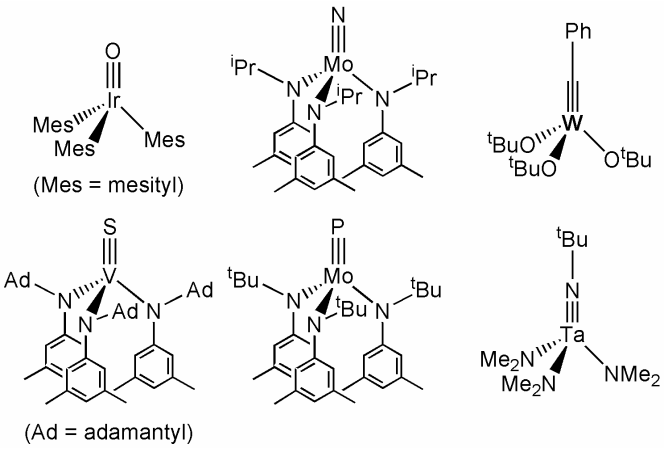

Figure 1.2. Some examples of metal-ligand triple bonds in threefold symmetry. See reference 2 for details.

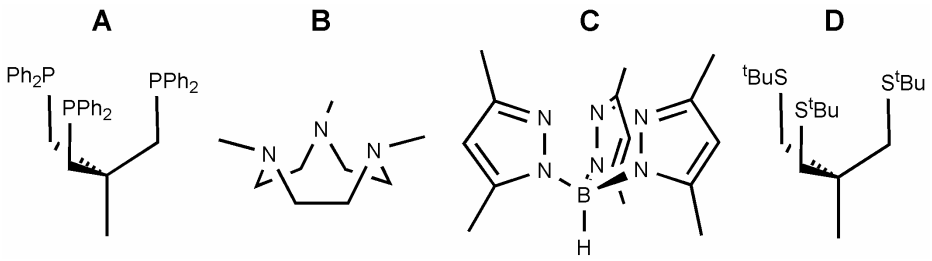

Figure 1.3. Prominent tridentate ligands that align in a *fac* arrangement on a metal center: (A) triphos ($H_3CC(CH_2PPh_2)_3$), (B) Me_3-tacn (1,4,7-trimethyl-1,4,7-triazocyclononane), (C) $Tp^{3,5\text{-}Me2}$ hydro-tris(3,5-dimethyl-pyrazolyl)borate, and (D) [$Tt^{tert\text{-}butyl}$] ([$PhB(CH_2S^tBu)_3$]$^-$).

1.2 Design of new tripodal anionic phosphine ligands

Phosphines are among the most ubiquitous ligands in transition metal chemistry, and their importance in catalysis has been well-documented.[8] Anionic monodentate and, to a more limited extent, bidentate phosphine ligands have also been prepared.[9] Many of these species incorporate a borate anion within the ligand backbone. Tripodal ligands incorporating a borate anion in the ligand backbone are well-established for nitrogen[10] and sulfur[11] donors (Figure 1.3), but there were no examples of anionic tridentate phosphorus ligands until the recent synthesis of a new class of tripodal anionic phosphines, [$PhBP_3$] ([$PhBP_3$] = [$PhB(CH_2PPh_2)_3]^-$) and [$PhBP^{iPr}_3$] ([$PhBP^{iPr}_3$] = [$PhB(CH_2P^iPr_2)_3]^-$).[12] These ligands have opened up new frontiers in synthesis (Figure 1.4), as the incorporation of an anionic charge into the ligand framework effectively makes these species more electron-releasing than their neutral analogs, such as triphos.[13] These six electron donor ligands (L_3) are isolobal to tris(pyrazolyl)borates ([Tp]) and the well-known cyclopendienyl ([Cp] = cyclopendienyl) ligands. This similarity to [Tp] and [Cp] suggests that it should be possible to prepare isoelectronic complexes that incorporating phosphine donors.

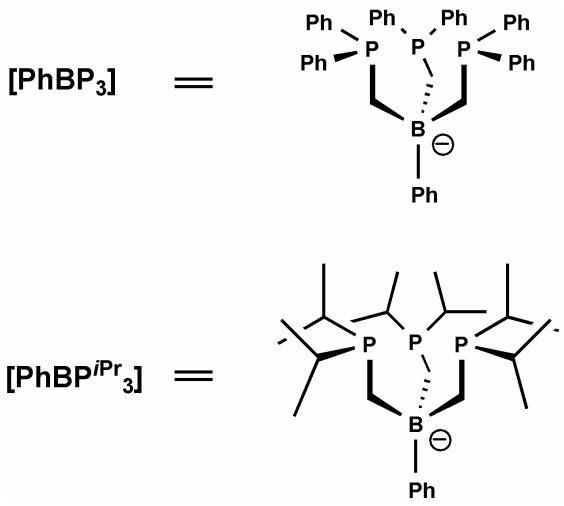

Figure 1.4. Chemical structures of [$PhBP_3$] and [$PhBP^{iPr}_3$].

1.3 Cobalt tris(phosphino)borate chemistry

Given the isolobal analogy between [$PhBP_3$] and [Cp] and [Tp] ligands, four-coordinate species featuring "[$PhBP_3$]CoX" can be expected to have the molecular orbital diagram shown in Figure 1.5, depending on the oxidation state of the metal center. This predicted molecular orbital diagram shows that Co(II) complexes would be high spin similar to ones previously prepared with "tetrahedral enforcer" ligands such as [Tp]. What became immediately apparent upon experimental investigation of [$PhBP_3$]Co-X complexes is that this molecular orbital diagram is incorrect. The Co(II) complexes obtained were not high spin (S = 3/2), but were in fact *low spin* (S = ½). This result was unexpected and unprecedented. Pseudotetrahedral Co(II) species were previously held to be always high spin with classic "three over two" splitting diagrams as derived from Ligand Field Theory.[14] Moreover, pseudotetrahedral Co(II) centers are generally assumed to adopt high spin arrangements within metalloenzymes.[15] The experimental data led to the establishment of a new molecular orbital diagram, shown in Figure 1.6, in order to explain these results. In the new interpretation, the C_{3v} symmetric manifold

undergoes an axial distortion away from the idealized tetrahedral geometry resulting in a new orbital diagram, which places the a_1 orbital at a much lower energy. This molecular orbital depiction is now reminiscent of octahedral coordination, as though the tridentate ancillary [$PhBP_3$] ligand occupies three *facial* sites of an octahedron with the fourth ligand occupying the vacant position opposite. The reasons for this low spin ground state will be discussed in additional detail in Chapter 3 (vide infra).

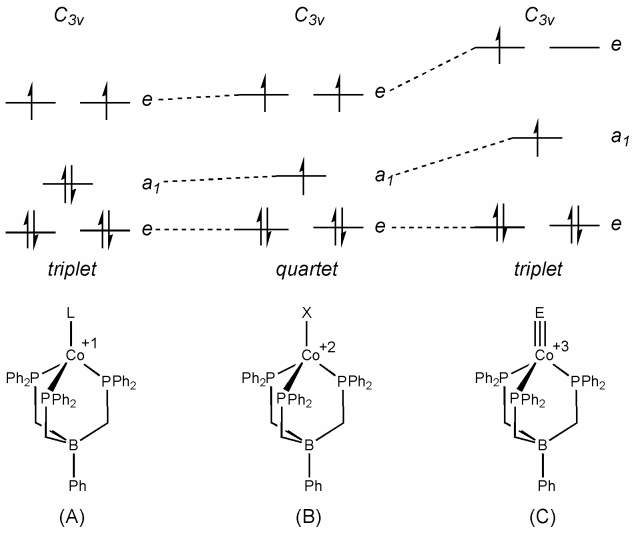

Figure 1.5. Qualitative splitting diagram assuming approximate C_{3v} symmetry for the frontier orbitals of (A) [$PhBP_3$]Co-L; (B) [$PhBP_3$]Co-X; and (C) [$PhBP_3$]Co≡E. The relative orbital energies are not accurately known.

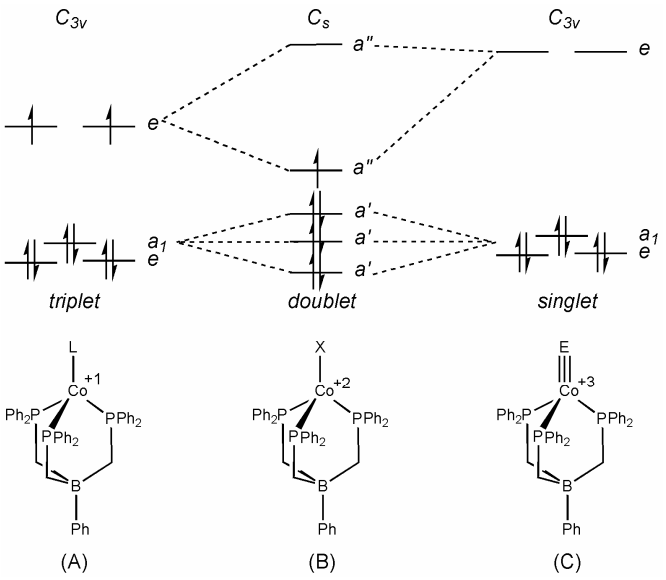

Figure 1.6. Qualitative splitting diagram assuming approximate C_{3v} or C_s symmetry for the frontier orbitals of (A) [$PhBP_3$]Co-L; (B) Jahn-Teller distorted low spin [$PhBP_3$]Co-X; and (C) [$PhBP_3$]Co≡E. The relative orbital energies are not accurately known.

Two hypotheses can be derived from the proposed new molecular orbital diagram shown in Figure 1.6. First, this diagram implies that it may be possible to stabilize a high spin species with the same tripodal ligand if the spin states of low and high spin Co(II) complexes are close in energy. This finding could lead to the preparation of four-coordinate spin crossover complexes. Although a limited number of five-coordinate spin crossover complexes have been prepared,[16] most Co(II) spin crossover complexes are six-coordinate;[17] no example of a four-coordinate spin crossover species had been established on any transition metal. In addition, the diagram suggests that the presence of strong donor ligands, combined with a threefold symmetry about the metal center, may allow for the stabilization of Co(III) metal-ligand triple bond. Excluding Fischer-type carbenes,[18] no cobalt-heteroatom multiple bond had previously been reported.

Bergman's imide, [Cp*]Ir≡N^{t}Bu ([Cp*] = pentamethyl-cyclopentadienyl) is a rare example of a group nine metal-ligand multiple bond.[19] An isolobal imido complex such as [$PhBP_3$]Co≡NR (R = alkyl or aryl) could be prepared employing [$PhBP_3$] instead of [Cp*] as the auxiliary L_2X ligand, which would give a closed shell 18 electron species.

It is worth asking why the "two over three" molecular orbital diagram is the preferred diagram for pseudotetrahedral complexes supported by [$PhBP_3$]. The d_z^2 (a_1) orbital is stabilized by an axial distortion caused by the narrow P-Co-P angles. Lowering the energy of this orbital allows for the stabilization of low spin Co(II) species as well as stable metal-ligand multiple bonds. A similar argument has been presented to explain the stability of [Cp*]IrN^{t}Bu. The detailed argument for the complexes' stabilization will be provided in Chapter 5.

The following chapters show how a strong anionic phosphine donor ligand that enforces threefold symmetry leads to two unprecedented results: a low spin pseudotetrahedral Co(II) complex and a stable Co(III) imide complex.

1.4 Chapter summaries

This chapter so far has presented the advantages of threefold symmetry from a molecular orbital perspective. Complexes featuring C_{3v} symmetry can form two equivalent π-bonds between a metal and a ligand, giving rise to stable metal-ligand triple bonds. Several tripodal L_2X type donor ligands, such as [Tp], are presented and compared to the new ligand [$PhBP_3$]. Experimental observations, which are presented in greater detail in the following chapters, show that the pseudotetrahedral Co(II) species can adopt a low spin rather than the expected high spin state. The strong electron donation and unusual local coordination geometry stabilizes these low spin species. A

new molecular orbital diagram suggests two hypotheses. First, it may be possible to synthesize an unprecedented pseudotetrahedral spin crossover complex. Second, a Co(III) species may be amenable to the formation of a metal-ligand triple bond. No examples of cobalt-ligand multiple bonds have been prepared previously, excluding Fischer carbenes.

The synthesis of the [$PhBP_3$] ligand is the focus of Chapter 2. While the ligand had been prepared previously as a tin or lithium complex, problems that arise during the attempted metalation onto transition metals have reduced its utility as a synthetic reagent. The preparation of the homoleptic thallium transmetalating reagent [$PhBP_3$]Tl allows for the easy preparation of a variety of late metal [$PhBP_3$] complexes. Furthermore, [$PhBP_3$]Tl is the first example of a stable homoleptic Tl(I) phosphine complex.

The study of [$PhBP_3$]Co-X (X = I, Br, or Cl) is the theme of Chapter 3, which focuses on the novel monomeric low spin pseudotetrahedral complex [$PhBP_3$]CoI. Structural and magnetic studies provide evidence for a low spin ground state, and DFT investigations help explain why this ground state is favorable. The bromide and chloride complexes are discussed in terms of their monomer/dimer equilibria. In addition, a high spin complex featuring the same [$PhBP_3$] ligand scaffold is presented. These complexes are compared structurally and magnetically to several other pseudotetrahedral Co(II) complexes.

Spin state control in pseudotetrahedral Co(II) complexes is the emphasis of Chapter 4. Low spin, spin crossover, and high spin complexes are prepared with a wide variety of X-type ligands following the general formula of [$PhBP_3$]Co-X (X = thiolate, aryloxide, or siloxide). The effects of sterics and electronics are investigated to

determine how each plays a role in determining the spin state of each complex. Structural comparisons show that the complexes can be arranged into two classes: umbrella distorted and off-axis distorted. Additional complexes featuring the more sterically encumbering ligand [$PhBP^{iPr}_3$] are also evaluated.

The preparation of stable cobalt imido complexes ([$PhBP_3$]Co≡NR, R = alkyl or aryl) is the subject of Chapter 5. The synthesis of these species and their structural characterization are described. Several different imido complexes were prepared by two different synthetic routes. In addition, the reactivity of these species is explored. The stabilization of the late-metal metal-ligand multiple bonds is discussed, aided by DFT calculations.

The synthesis and characterization of a bimetallic bridged cobalt nitride complex, ([$PhBP_3$]Co)$_2$(μ-N), is discussed in Chapter 6. This mixed-valent species is the first example of a μ_2-bridging nitride involving cobalt. Since the μ_2-bridging nitride is paramagnetic the nature of the unpaired electron is investigated. Finally, the complex is compared to other μ_2-bridging nitrides of iron.

Attempts to prepare a cobalt carbene from diazoalkanes are covered in Chapter 7. Diazoalkane adducts of "[$PhBP_3$]Co" were prepared and characterized. These species are compared to other late metal diazoalkane complexes as well as the related cobalt imide complexes. Both end-on and side-on diazoalkane species were prepared, making this one of the only systems that supports both diazoalkane bonding modes.

References cited

1) a) Laplaza, C. E.; Cummins, C. C. *Science* **1995**, *268*, 861-863. b) Peters, J. C.; Cherry, J. F.; Thomas, J. C.; Baraldo, L.; Mindiola, D. J.; Davis, W. M.; Cummins, C.

C. *J. Am. Chem. Soc.* **1999**, *121*, 10053-10067. c) Johnson, A. R.; Davis, W. M.; Cummins, C. C.; Serron, S.; Nolan, S. P.; Musaev, D. G.; Morokuma, K. *J. Am. Chem. Soc.* **1998**, *120*, 2071-2085. d) Yandulov, D. V.; Schrock, R. R. *Science* **2003**, *301*, 76-78.

2) a) Hay-Motherwell, R. S.; Wilkinson, G.; Hussain-Bates, B.; Hursthouse, M. B. *Polyhedron* **1993**, *12*, 2009-2012. b) Tsai, Y.; Johnson, M. J. A.; Mindiola, D. J.; Cummins, C. C.; Klooster, W. T.; Koetzle, T. F. *J. Am. Chem. Soc.* **1999**, *121*, 10426-10427. c) Cotton, F. A.; Schwotzer, W.; Shamshoum, E. S. *Organometallics* **1984**, *3*, 1770-1771. d) Brask, J. K.; Durà-Vilà, V.; Diaconescu, P. L.; Cummins, C. C. *Chem. Commun.* **2002**, 902-903. e) Laplaza, C. E.; Davis, W. M.; Cummins, C. C. *Angew. Chem., Int. Ed. Engl.* **1995**, *34*, 2042-2044. f) Nugent, W. A.; Harlow, R. L. *Chem. Commun.* **1978**, 579-580.

3) a) Tayebani, M.; Kasani, A.; Feghali, K.; Gambarotta, S.; Bensimon, C. *Chem. Commun.* **1997**, 2001-2002. b) Peters, J. C.; Odom, A. L.; Cummins, C. C. *Chem. Commun.* **1997**, 1995-1996. c) Agapie, T.; Odom, A. L.; Cummins, C. C. *Inorg. Chem.* **2000**, *39*, 174-179. d) Chisholm, M. H.; Hoffman, D. M.; Huffman, J. C. *Inorg. Chem.* **1983**, *22*, 2903-2906.

4) Blake, A. J.; Collier, P. E.; Gade, L. H.; Mountford, P.; Lloyd, J.; Pugh, S. M.; Schubart, M.; Skinner, M. E. G.; Troesch, D. J. M. *Inorg. Chem.* **2001**, *40*, 870-877.

5) a) Rohde, J.; In, J.; Lim, M. H.; Brennessel, W. W.; Bukowski, M. R.; Stubna, A.; Münck, E.; Nam, W.; Que, L., Jr. *Science* **2003**, *299*, 1037-1039. b) Anderson, T. M.; Neiwert, W. A.; Kirk, M. L.; Piccoli, P. M. B.; Schultz, A. J.; Koetzle, T. F.; Musaev, D. G.; Morokuma, K.; Cao, R.; Hill, C. L. S*cience* **2004**, *306*, 2074-2077.

6) a) Dias, H. V. R.; Wang, X. *Polyhedron* **2004**, *23*, 2533-2539. b) De Bari, H.; Zimmer, M. *Inorg. Chem.* **2004**, *43*, 3344-3348. c) Calabrese, J. C.; Domaille, P. J.; Thompson, J. S.; Trofimenko, S. *Inorg. Chem.* **1990**, *29*, 4429-4437.

7) a) Reger, D. L. *Comments Inorg. Chem.* **1999**, *121*, 1-28. b) Rupp, R.; Frick, A.; Huttner, G.; Rutsch, P.; Winterhalter, U.; Barth, A.; Kircher, P.; Zsolnai, L. *Eur. J. Inorg. Chem.* **2000**, 523-536. c) Teunissen, H. T. *Chem. Commun.* **1998**, 1367-1368.

8) a) Cotton, F. A.; Wilkinson, G.; Murillo, C. A.; Bochmann, M. *Advanced Inorganic Chemistry,* 6th ed.; Wiley & Sons: New York, 1999. b) Crabtree, R. H. *The Organometallic Chemistry of the Transition Metals,* 3rd ed.; Wiley & Sons: New York, 2001. c) Hegedus, L. S. *Transition Metals in the Synthesis of Complex Organic Molecules,* 2nd ed.; University Science Books: Sausalito, 1999. d) Tsuji, J. *Transition Metal Reagents and Catalysts;* Wiley & Sons: New York, 2000. e) Cotton, F. A.; Hong, B. *Prog. Inorg. Chem.* **1992**, *40*, 179-289.

9) a) Camus, A.; Marsich, N.; Nardin, G.; Randaccio, L. *J. Organomet. Chem.* **1973**, *60*, C39-C42. b) Balakrishna, M. S.; Reddy, V. S.; Krishnamurthy, S. S.; Nixon, J. F.; Burckett, J. C. T. R *Coord. Chem. Rev.* **1994**, *129*, 1-90. c) Karsch, H. H.; Appelt, A.; Riede, J.; Müller, G. *Organometallics* **1987**, *6*, 316-323. d) Hoic, D. A.; Davis, W. M.; Fu, G. C. *J. Am. Chem. Soc.* **1996**, *118*, 8176-8177.

10) a) Reinaud, O. M.; Rheingold, A. L.; Theopold, K. H. *Inorg. Chem.* **1994**, *33*, 2306-2308. b) Detrich, J. L.; Konečný, R.; Vetter, W. M.; Doren, D.; Rheingold, A. L.; Theopold, K. H. *J. Am. Chem. Soc.* **1996**, *118*, 1703-1712. c) Jewson, J. D.; Liable-Sands, L. M.; Yap, G. P. A.; Rheingold, A. L.; Theopold, K. H. *Organometallics* **1999**, *18*, 300-305. d) Shirasawa, N.; Akita, M.; Hikichi, S.;

Moro-oka, Y. *Chem. Commun.* **1999**, 417-418. e) Shirasawa, N.; Nguyet, T. T.; Hikichi, S.; Moro-oka, Y.; Akita, M. *Organometallics* **2001**, *20*, 3582-3598.

11) a) Schebler, P. J.; Riordan, C. G.; Guzei, I. A.; Rheingold, A. L. *Inorg. Chem.* **1998**, *37*, 4754-4755. b) Schebler, P. J.; Mandimutsira, B. S.; Riordan, C. G.; Liable-Sands, L. M.; Incarvito, C. D.; Rheingold, A. L. *J. Am. Chem. Soc.* **2001**, *123*, 331-332.

12) a) Peters J. C.; Feldman, J. D.; Tilley, T. D. *J. Am. Chem. Soc.* **1999**, *121*, 9871-9872. b) Barney, A. A.; Heyduk, A. F.; Nocera, D. G. *Chem. Commun.* **1999**, 2379-2380. c) Betley, T. A.; Peters, J. C. *Inorg. Chem.* **2003**, *43*, 5074-5084. d) Shapiro, I. R.; Jenkins, D. M.; Thomas, J. C.; Day, M. W.; Peters, J. C. *Chem. Commun.* **2001**, 2152-2153.

13) Thomas, J. C.; Peters, J. C. *J. Am. Chem. Soc.* **2003**, *125*, 8870-8888.

14) a) Lever, A. B. P. *Inorganic Electronic Spectroscopy*, 2nd ed.; Elsevier: New York, 1984. b) Cotton, F. A.; Wilkenson, G. *Advanced Inorganic Chemistry*, 5th ed.; Wiley: New York, 1988. c) Holm, R. H. *Acc. Chem. Res.* **1969**, *2*, 307-316. d) Jaynes, B. S.; Doerrer, L. H.; Liu, S.; Lippard, S. J. *Inorg. Chem.* **1995**, *34*, 5735-5744. e) Everett, G. W.; Holm, R. H. *J. Am. Chem. Soc.* **1965**, *87*, 5266-6267. f) Cotton, F. A.; Soderberg, R. H. *J. Am. Chem. Soc.* **1962**, *84*, 872-873.

15) a) Solomon, E. I.; Rawlings, J.; McMillin, J. R.; Stephens, P. J.; Gray, H. B. *J. Am. Chem. Soc*. **1976**, *98*, 8046-8048. b) Bertini, I.; Luchinat, C. *Acc. Chem. Res.* **1983**, *16*, 272-279. c) Bertini, I.; Lanini, G.; Luchinat, C. *J. Am. Chem. Soc*. **1983**, *105*, 5116-5118. d) Khalifah, R. G.; Rogers, J. I.; Harmon, P.; Morely, P. J.; Carroll, S. B. *Biochemistry* **1984**, *23*, 3129-3136. e) Briganti, F.; Pierattelli, R.; Scozzafava, A.; Supuran, C. T. *Eur. J. Med. Chem*. **1996**, *31*, 1001-1010.

16) a) Kennedy, B. J.; Murray, K. S. *Inorg. Chim. Acta* **1987**, *134*, 249-254. b) Kennedy, B. J.; Fallon, G. D.; Gatehouse, B. M. K. C.; Murray, K. S. *Inorg. Chem.* **1984**, *23*, 580-588. c) Thuéry, P.; Zarembowitch, J. *Inorg. Chem.* **1986**, *25*, 2001-2008. d) Zarembowitch, J.; Kahn, O. *Inorg. Chem.* **1984**, *23*, 589-593.

17) a) Zarembowitch, J. *New J. Chem.* **1992**, *16*, 255-267. b) Juhász, G.; Hayami, S.; Inoue, K.; Maeda, Y. *Chem. Lett.* **2003**, *32*, 882-883. c) Sieber, R.; Decurtins, S.; Stoeckli-Evans, H.; Wilson, C.; Yufit, D.; Howard, J. A. K.; Capelli, S. C.; Hauser, A. *Chem. Eur. J.* **2000**, *6*, 361-368. d) Gaspar, A. B.; Muñoz, M. C.; Niel, V.; Real, J. A. *Inorg. Chem.* **2001**, *40*, 9-10. e) Faus, J.; Julve, M.; Lloret, F.; Real, J. A.; Sletten, J. *Inorg. Chem.* **1994**, *33*, 5535-5540. f) Kremer, S.; Henke, W.; Reinen, D. *Inorg. Chem.* **1982**, *21*, 3013-3022.

18) a) Carre, F.; Cerveau, G.; Colomer, E.; Corriu, R. J. P.; Young, J. C.; Richard, L.; Weiss, R. *J. Organomet. Chem.* **1979**, *179*, 215-226. b) Filippou, A. C.; Herdtweck, E.; Alt, H. G. *J. Organomet. Chem.* **1988**, *355*, 437-447.

19) a) Glueck, D. S.; Wu, J.; Hollander, F. J.; Bergman, R. G. *J. Am. Chem. Soc.* **1991**, *113*, 2041-2054. b) Glueck, D. S.; Hollander, F. J.; Bergman, R. G. *J. Am. Chem. Soc.* **1989**, *111*, 2719-2721.

Chapter 2: A homoleptic phosphine adduct of Tl(I)

The text of this chapter is reproduced in part with permission from:

Shapiro, I. R.; Jenkins, D. M.; Thomas, J. C.; Day, M. W.; Peters, J. C. *Chem. Commun.* **2001**, 2152-2153.

Credit should be given to the following people for their work that appears in this chapter. I. R. Shapiro first synthesized and structurally characterized $[PhBP_3]Tl$. J. C. Peters wrote much of the following text, that also appears in the above cited work. J. C. Thomas helped with the NMR characterization. My specific contributions included the synthesis as it appears in the experimental section and NMR characterization.

2.1 Introduction

Although hard donor ligands are known to stabilize simple molecular complexes of thallium-(I) and -(III),[1] well-defined examples of thallium supported by correspondingly soft donor ligands are relatively rare.[2] With respect to phosphine donors specifically, only two phosphine adducts have been structurally characterized: both of thallium(III).[3] To our knowledge, there are no well-characterized phosphine adducts for thallium(I). By comparison, there are numerous structurally characterized examples of thallium(I) supported by hard N-donor ligands, including the tripodal ligands [Tp] ([Tp] = tris(pyrazolyl)borate) and Me_3-tacn (tacn = triazacyclononane).[4,5]

We set out to prepare a thallium adduct of the tris(phosphino)borate ligand, [$PhBP_3$] ([$PhBP_3$] = [$PhB(CH_2PPh_2)_3$]$^-$),[6] for two reasons. We were surprised by the dearth of well-defined phosphine complexes of thallium and hoped that the anionic [$PhBP_3$] ligand might support and stabilize a thallium(I) species. Additionally, the previously reported lithium salt of this ligand, [Li(tmeda)][$PhBP_3$] (tmeda = tetramethylethylenediamine), is not a reagent of general synthetic utility for clean delivery of the [$PhBP_3$] ligand to transition metals. A versatile thallium reagent of this ligand therefore seems highly desirable. Herein we report the isolation and structural characterization of a homoleptic phosphine adduct of thallium(I) stabilized by the [$PhBP_3$] ligand.

2.2 Results and discussion

2.2.1 Synthesis and ^{31}P NMR characterization of [$PhBP_3$]Tl

It was convenient to prepare the target complex, [$PhBP_3$]Tl, **2.1**, by transmetallation of lithium for thallium upon addition of $TlPF_6$ to a methanolic solution of

[Li(tmeda)][$PhBP_3$] (Eq. 2.1). The reaction occurred rapidly and cleanly at ambient temperature as indicated by ^{31}P NMR spectroscopy. Following work-up, the light yellow product was isolated in reasonable yield (65%). It is worth noting that the entire reaction sequence can be executed in air without decomposition. Furthermore, the thallium salt itself is stable to moisture and oxygen for an extended period, both in solution and in the solid state.

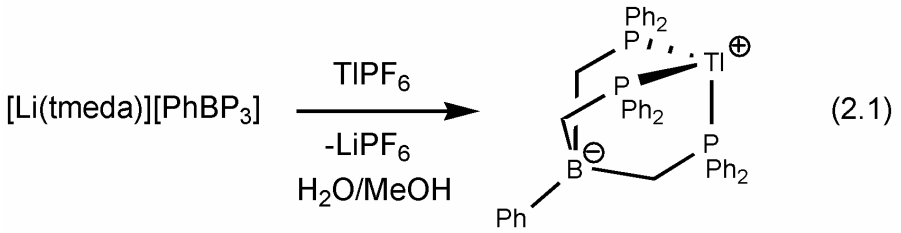

(2.1)

Examination of the ^{31}P NMR spectrum of **2.1** (C_6D_6) showed two resonances (1 1 ratio) separated by more than 40 ppm, each resonance bearing a resolvable shoulder. This spectrum represents two separate doublets from a very strong $^1J_{TlP}$ coupling interaction (5214, 5168 Hz) for each of the naturally occurring S = ½ thallium isotopes (^{205}Tl (70.5%), ^{203}Tl (29.5%), respectively). Notably, these coupling values are significantly larger than those reported for phosphine complexes of thallium(III) (approximately 1500 Hz).

2.2.2 Solid-state structure of [$PhBP_3$]Tl

In order to corroborate the NMR assignment consistent with a structure resulting from symmetric, tridentate binding of the [$PhBP_3$] ligand to the thallium cation, we sought independent structural confirmation. Slow evaporation of a benzene solution of **2.1** afforded crystals suitable for an X-ray diffraction study. A structural representation of complex **2.1** is shown in Figure 2.1 (top view, 50% ellipsoids). The structure confirms our assignment of **2.1** as a homoleptic phosphine adduct of thallium. The anionic [$PhBP_3$]

ligand coordinates the thallium cation in the expected tridentate conformation (top view). The large ionic radius of the thallium(I) ion forces it to sit well above the basal plane (2.074 Å), defined by its three phosphine donor atoms. This structural feature affords a significant separation between the thallium ion and the molecule's anionic borate counteranion (Tl1–B distance = 4.253 Å). It is interesting to compare the intramolecular Tl–B distance found in a host of structurally characterized thallium(I) adducts of variously substituted [Tp] ligands. The Tl–B distance is much longer in **2.1** than in all related [Tp] adducts of thallium(I) (range = 3.46–3.90 Å) and is approximately 0.6 Å longer than the mean distance (3.65 Å) for the related [Tp] systems. The pronounced Tl–B distance in **2.1**, in conjunction with the absence of simple resonance contributors that delocalize the anionic charge from the borate counteranion to the Tl center, suggests that **2.1** may be represented as a simple zwitterion (Eq. 2.1). Although equivalent phosphorus nuclei are observed by ^{31}P NMR spectroscopy, the three phosphine donors are not symmetrically bound in the solid state. The Tl1–P3 distance, 2.880 Å, is appreciably shorter than the Tl1–P1 and Tl1–P2 distances (2.953 and 2.934 Å, respectively).

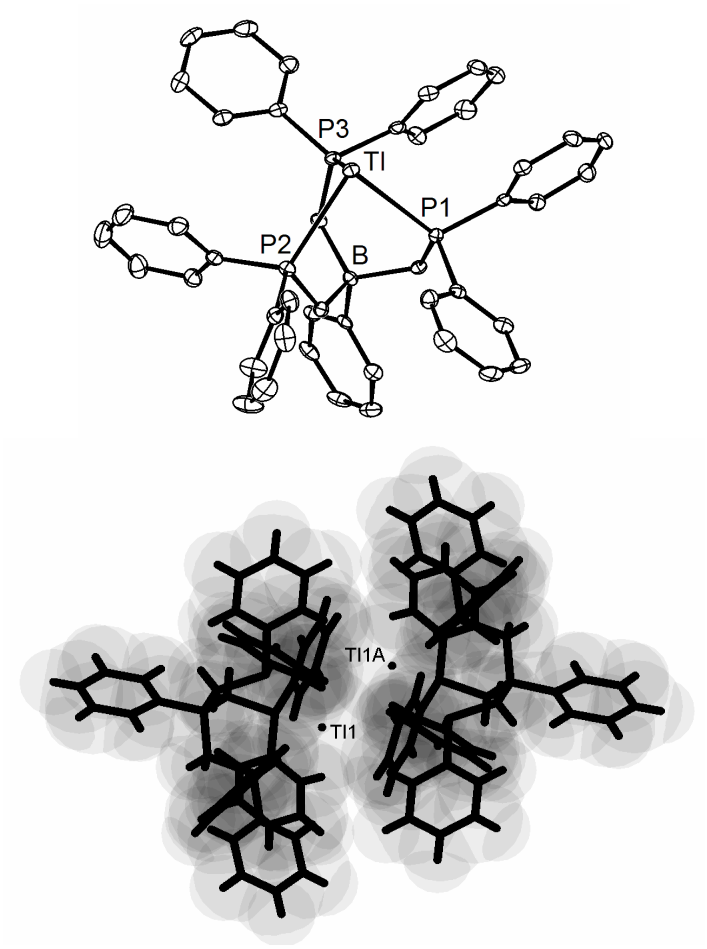

Figure 2.1. Displacement ellipsoid (50%) representation of [$PhBP_3$]Tl, **2.1**. Hydrogen atoms have been omitted for clarity. Selected interatomic distances (Å) and angles (°): Tl1–P1 2.878, Tl1–P2 2.953, Tl1–P3 2.932, Tl1–B 4.254; P1–Tl1–P2 70.82, P1–Tl1–P3 76.78, and P2–Tl1–P3 77.46. The bottom view shows a transparent space-filling model of **2.1** depicted as a dimer [Tl1–Tl1A = 3.5652(2) Å]. The [$PhBP_3$] ligands are highlighted as bold stick figures, and the positions of the Tl nuclei are labeled.

The bottom view of Figure 2.1 shows a transparent space-filling model of **2.1** and its neighboring thallium adduct. The asymmetric unit of **2.1** contains a single thallium

complex that is related to the neighboring thallium atom, Tl1A, by a center of symmetry. The distance between these thallium atoms is 3.5652(2) Å, which is considerably longer than twice the covalent radius (1.64 Å) of thallium, and is consistent with a thallium-thallium dimer resulting from weak interactions.

2.2.3 Evidence for a monomer of [PhBP$_3$]Tl in solution

Despite the solid state suggestion that **2.1** is a weak dimer in the solid state, the dimeric structure does not exist in solution. Direct evidence for assigning **2.1** as a monomer in solution is as follows: the ^{31}P NMR spectrum of **2.1** shows only $^{1}J_{\mathrm{TlP}}$ coupling. We would expect to observe a weaker $^{2}J_{\mathrm{TlP}}$ coupling to the neighboring Tl nucleus if the dimeric structure exists in solution. To buttress this argument, the ^{205}Tl NMR spectrum of **2.1** was obtained in C_6D_6:[7] a single resonance (2809 ppm) split into a quartet by the three equivalent phosphine donors was observed (Figure 2.2). There was no evidence for $^{1}J_{(205)\mathrm{Tl}(203)\mathrm{Tl}}$ coupling, ruling out Tl–Tl interactions in benzene solution. Finally, **2.1** was analyzed by electrospray mass spectroscopy (ESI/MS). The parent ion observed in positive mode (m/z = 891) was consistent with the protonated monomeric form of **2.1**. Thus, our data imply a monomeric formulation of **2.1** in solution.[8]

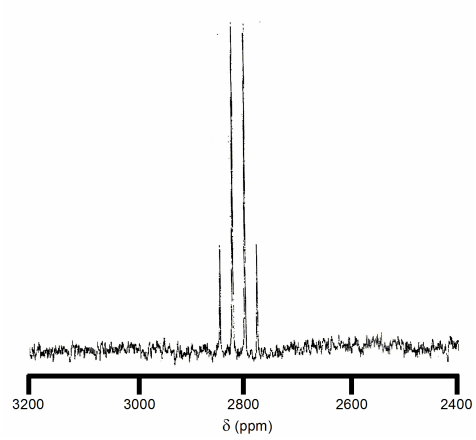

Figure 2.2. ^{205}Tl NMR for [PhBP$_3$]Tl (**2.1**) in C_6D_6.

2.2.4 Comparison to tris(thioether)borate

Regarding other soft, tripodal donor ligands supporting thallium(I), a good comparison to complex **2.1** comes from Riordan and co-workers, who recently reported a thallium(I) adduct of their second generation, anionic tris(thioether)borate ligand, [$Tt^{tert\text{-}butyl}$] ([$Tt^{tert\text{-}butyl}$] = [$PhB(CH_2S^tBu)_3$]$^-$).[9] Notably, [$Tt^{tert\text{-}butyl}$] does not enforce a simple 1:1 complex between thallium(I) and the tris(thioether) ligand in the solid state. This is despite the fact that the [$Tt^{tert\text{-}butyl}$]Tl reagent enables access to monomeric, pseudotetrahedral geometries for simple divalent nickel and cobalt chlorides.

2.3 Conclusion

In summary, we have isolated and structurally characterized a rare example of a simple phosphine adduct of thallium(I). It has been found that complex **2.1** displays a signature $^1J_{TlP}$ coupling constant of 5214 Hz. In addition to exposing new possibilities for thallium coordination chemistry within a phosphine donor sphere, complex **2.1** promises to be an important reagent for delivering the relatively unexplored [$PhBP_3$] ligand to transition metals.

2.4 Experimental section

2.4.1 General considerations

All manipulations were carried out using standard Schlenk or glovebox techniques under a dinitrogen atmosphere. Unless otherwise noted, solvents were deoxygenated and dried by thorough sparging with N_2 gas, followed by passage through an activated alumina column. Diethyl ether, tetrahydrofuran, petroleum ether, benzene, and toluene were periodically tested with a standard purple solution of sodium benzophenone ketyl in tetrahydrofuran to confirm that oxygen and moisture had been

effectively removed. Elemental analyses were performed by Desert Analytics, Tucson, AZ. A Varian Mercury-300 NMR spectrometer, a Varian Inova-500 NMR spectrometer, or a Joel 400 MHz was used to record ^{1}H, ^{13}C, ^{31}P, ^{11}B, and ^{19}F NMR spectra at ambient temperature. ^{1}H and ^{13}C chemical shifts were referenced to residual solvent. ^{31}P NMR chemical shifts are referenced to an external standard of H_3PO_4 with the ^{31}P signal being set at 0 ppm. ^{11}B NMR chemical shifts are referenced to an external standard of neat $BF_3{\cdot}Et_2O$ with the ^{11}B signal being set at 0 ppm. ^{19}F NMR chemical shifts are referenced to an external standard of neat hexafluorobenzene with the ^{19}F signal being set at -163 ppm. Deuterated toluene, benzene, and tetrahydrofuran were purchased from Cambridge Isotope Laboratories, Inc. and were degassed and dried over activated 3 Å molecular sieves prior to use. MS data were obtained by injection of a solution onto a Hewlett-Packard 1100MSD mass spectrometer (ESI/MS) or an Agilent 5973 mass selective detector (GC/MS). X-ray diffraction studies were carried out in the Beckman Institute Crystallographic Facility on a Bruker Smart 1000 CCD diffractometer.

2.4.2 Starting materials and reagents

$[PhBP_3][Li(tmeda)]$ and $Ph_2PCH_2Li(tmeda)$[10] were prepared by literature methods. $PhBCl_2$ and $TlPF_6$ were purchased from commercial vendors and used without any further purification.

2.4.3 Synthesis of compounds

Synthesis of $[PhBP_3]Tl$, **2.1**. This synthesis can be performed outside of a glovebox. Solid $[PhBP_3][Li(tmeda)]$ (7.1 g, 8.6 mmol) was suspended in methanol (60 mL). To this stirring suspension was added an aqueous solution (30 mL) of $TlPF_6$ (3.00 g, 8.6 mmol) over a period of 5 min. A cloudy white suspension resulted, which was stirred for an

additional 5 min, followed by extraction with dichloromethane (2 × 150 mL). Drying the organic extract in vacuo afforded a light yellow powder that was subsequently washed with hexanes and Et_2O (40 mL each). The remaining powder was extracted into benzene, stirred over $MgSO_4$, and dried thoroughly in vacuo to afford the thallium adduct **2.1** as a fine yellow powder (5.00 g, 65%). ^{1}H NMR (C_6D_6, 300 MHz, 25 °C): δ 8.13 (d, J = 6.6 Hz, 2H), 7.67 (m, J = 7.5 Hz, 2H), 7.42 (tt, J = 6.6, 1.2 Hz, 1H), 7.18–7.11 (m, 12H), 6.80–6.77 (m, 18H), 1.96 (br m, 6H). ^{31}P NMR (C_6D_6, 121.4 MHz, 25 °C): δ 21.6 [d, $^1J_{TlP}$ = 5214 Hz for ^{205}Tl (70.5% abundance), $^1J_{TlP}$ = 5168 Hz for ^{203}Tl (29.5% abundance)]. ^{205}Tl NMR (C_6D_6, 231.31 MHz, 25 °C): δ 2810 (q, $^1J_{TlP}$ = 5204 ± 116 Hz). ^{13}C NMR (C_6D_6, 125.7 MHz, 25 °C): δ 139.8, 132.5, 128.8–129.1 (overlapping resonances), 124.6, 17.0 (br). ^{11}B NMR (C_6D_6, 128.3 MHz, 25 °C): δ -10.96. ESI/MS (m/z): 891 (**2.1** + H^+). Anal. Calcd for $C_{47}H_{48}BP_3Tl$: C, 60.73; H, 4.64. Found: C, 61.75; H, 4.76%.

Alternative synthesis of [$PhBP_3$][Li(tmeda)]. The lithiophosphine reagent Ph_2PCH_2Li(tmeda) (12.55 g, 0.0390 mol) is added to a 250 mL filter flask and dissolved in 90 mL of toluene. This solution is stirred until the reagent is completely dissolved. The borane $PhBCl_2$ (2.00 g, 0.0126 mol) is diluted in 10 mL of toluene and added dropwise to the flask over 20 min. The reaction is allowed to continue for 90 min. The flask is then placed under dynamic vacuum to remove toluene. The vacuum is released as soon as precipitate starts to form (approximately 20 min). The filter flask is then stored at -35 °C for 16 h to achieve full precipitation of product. The solid precipitate is collected on a medium frit and washed with petroleum ether (2 x 20 mL). The white powder is dried and is spectroscopically pure (8.46 g, 83% yield).

Alternative synthesis of [PhBP$_3$]Tl, **2.1**. [PhBP$_3$][Li(tmeda)] (5.66 g, 0.00700 mol) is dissolved in a 250 mL Erlenmeyer flask in 120 mL of dried and degassed ethanol. The reagent is stirred until a homogenous solution is obtained. A THF (10 mL) solution of $TlPF_6$ (2.44 g, 0.00700 mol) is prepared, and this is added to the stirring ethanol solution over 10 min. The reaction is stirred for an additional 30 min as the product crashes out of solution as a fine light yellow powder. The product is collected on a medium frit and washed with petroleum ether (2 x 20 mL). The product is dried and is spectroscopically pure (4.90 g, 78% yield).

2.4.4 X-ray experimental information

A crystal of **2.1** was mounted on a glass fiber with Paratone-N oil. Crystallographic data was collected on a Bruker SMART 1000 diffractometer with a CCD area detector under a stream of dinitrogen. Data were collected using the Bruker SMART program, collecting ω scans at 5 ϕ settings. Data reduction was performed using Bruker SAINT v6.2. Structure solution and structure refinement were performed using SHELXS-97 (Sheldrick, 1990) and SHELXL-97 (Sheldrick, 1997). All structural representations were produced using the Diamond software program.

X-ray structure analysis for **2.1**: Data for $C_{45}H_{41}BP_3Tl$, pale yellow rhombohedral plate, formula weight (g mol^{-1}) = 889.87, T (°C) = -175, monoclinic space group $P2_1/n$, λ (Å) = 0.71073, a = 13.7449(7) Å, b = 13.5812(7) Å, c = 20.5487(10) Å, β = 94.536(1)°, V = 3823.9(3) Å^3, Z = 4, D_{calcd} (g cm^{-3})= 1.430, μ (cm^{-1}) = 43.81 R_1 = 0.0221 [$I > 2\sigma(I)$], wR_2 = 0.0381 [$I > 2\sigma(I)$] GOF = 1.308. CCDC reference number 162229.

References cited

1) a) Canty, A. J.; Mills, K.; Skelton, B. W.; White, A. H. *J. Chem. Soc., Dalton Trans.* **1986**, 939-945. b) Henrick, K.; Matthews, R. W.; Tasker, P. A. *Inorg. Chem.* **1977**, *16*, 3293-3298.

2) a) Blake, A. J.; Greig, J. A.; Schröder, M. *J. Chem. Soc., Dalton Trans.* **1991**, 529-532. b) Blake, J. A.; Reid, G.; Schröder, M. *J. Chem. Soc., Dalton Trans.* **1992**, 2987-2992.

3) a) Müller, G.; Lachmann, J. *Z. Naturforsch., Teil B* **1993**, *48*, 1544-1554. b) Baldwin, R. A.; Wells, R. L.; White, P. S. *Main Group Chem.* **1997**, *2*, 67-71.

4) For recent references see: a) Ghosh, P.; Churchill, D. G.; Rubinshtein, M.; Parkin, G. *New J. Chem.* **1999**, *23*, 961-963. b) Janiak, C.; Braun, L.; Girgsdies, F. *J. Chem. Soc., Dalton Trans.* **1999**, 3133-3136. c) Rheingold, A. L.; Haggerty, B. S.; Liable-Sands, L. M.; Trofimenko, S. *Inorg. Chem.* **1999**, *38*, 6306-6308.

5) Wieghardt, K.; Kleine-Boymann, M.; Nuber, B.; Weiss, J. *Inorg. Chem.* **1986**, *25*, 1309-1313.

6) a) Peters J. C.; Feldman, J. D.; Tilley, T. D. *J. Am. Chem. Soc.* **1999**, *121*, 9871-9872. b) Barney, A. A.; Heyduk, A. F.; Nocera, D. G. *Chem. Commun.* **1999**, 2379-2380.

7) Dr. Todd Alam from Sandia National Laboratory is acknowledged for obtaining the ^{205}Tl NMR spectrum of [$PhBP_3$]Tl (**2.1**).

8) Attempts to obtain a solution molecular weight estimate for [$PhBP_3$]Tl (**2.1**) by the Signer method have thus far been inconclusive due to its tendency to precipitate from solution on prolonged standing.

9) Schebler, P. J.; Riordan, C. G.; Guzei, I. A.; Rheingold, A. L. *Inorg. Chem.* **1998**, *37*, 4754-4755.

10) Fraenkel, G.; Winchester, W. R. *Organometallics* **1989**, *8*, 2308-2311.

Chapter 3: Elucidation of a low spin cobalt(II) system in a distorted tetrahedral geometry

The text of this chapter is reproduced in part with permission from:

Jenkins, D. M.; Di Bilio, A. J.; Allen, M. J.; Betley, T. A.; Peters, J. C. *J. Am. Chem. Soc.* **2002**, *124*, 15336-15350.

Credit should be given to the following people for their work that appears in this chapter. M. J. Allen first synthesized the $[PhBP_3]Co\text{-}X$ (X = I, Br, or Cl) complexes and structurally characterized them. A. J. Di Bilio helped with the EPR measurements.

3.1 Introduction

Metal centers that reside in unusual coordination geometries sometimes display unique physical properties that correlate to novel modes of chemical reactivity.[1] Metalloenzymes can exploit subtle structure/function relationships to achieve specific catalytic transformations by intimately tuning the local stereochemistry and ligand-field in a protein active site. An appreciation of specific ligand-to-metal interactions in protein active sites is therefore highly dependent on our basic understanding of elementary stereochemical and ligand-field relationships in coordination chemistry.[2] Moreover, our community's general desire to make use of these elementary principles to rationally design catalysts selective for specific transformations motivates ongoing interest in this area.[3,4] We suggest that coupling (i) an axial distortion in a pseudotetrahedral cobalt(II) complex of approximate threefold symmetry with (ii) a strong ligand-field donor strength can provide access to a doublet rather than a quartet electronic ground state. This result is of interest because, to the best of our knowledge, all previously characterized four-coordinate cobalt(II) systems that are low spin have adopted approximate square planar structure types.[5,6] Owing to its historically well-behaved and rich spectroscopy, there has been longstanding interest in using cobalt(II) substitution to probe local stereochemical environments in the active sites of native enzymes. Perhaps the most familiar example of this use is that of zinc carbonic anhydrase.[7] Establishing that pseudotetrahedral cobalt(II) can exhibit spectroscopic features consistent with a doublet rather than a quartet ground state is particularly interesting in this latter context.

The series of paramagnetic cobalt complexes described below is well suited to probing the ligand-field donor strength that is imposed by the tris(phosphino)borate

ligand $[PhB(CH_2PPh_2)_3]^-$, abbreviated throughout as $[PhBP_3]$.[8,9] The $[PhBP_3]$ ligand[10] is a structurally similar but anionic relative to the well-known tris(phosphine) ligand[11,12] $H_3CC(CH_2PPh_2)_3$ (abbreviated herein as triphos[13]) that was originally reported by Hewertson and Watson in 1964.[14] Our continued focus on developing neutral complexes that feature a partially insulated borate counteranion, fixed at a short but remote distance from a transition metal that is coordinated by neutral amine or phosphine donor arms, is in part due to the promise these formal zwitterions hold for catalytic applications.[15,16] Studying the elementary and catalytic reaction processes of zwitterions of this type, and comparing their reactivity to isostructural but more conventional cationic relatives, is paramount to defining the role zwitterionic systems might offer to homogeneous catalysis. It is also of interest to examine the impact that the fastened borate unit can have upon the intimate electronic structure of the coordinated metal center. This study describes our initial efforts to address this latter issue. We provide evidence to show that, when coordinated to a cobalt(II) ion, the $[PhBP_3]$ anion provides access to a unique low spin cobalt(II) complex, $[PhBP_3]CoI$ (**3.1**), whose stereochemical structure is best regarded as distorted tetrahedral. Given the intense spectroscopic and magnetic scrutiny divalent cobalt has received during the past several decades,[17,18] elucidation of this low spin system is particularly interesting. Complex **3.1** and its chloride and bromide relatives are structurally related to the well-known, but cationic, triphos supported cobalt(II) systems popularized by Sacconi and more recently by Huttner.[19,20] The data presented herein afford a first comparative glance at the dramatic electronic consequences that arise when the borate counteranion is embedded within the phosphine donor ligand framework.

The synthetic, structural, and spectroscopic data for the title complex **3.1** are presented below to corroborate its low spin assignment. Two related low spin cobalt(II) derivatives, ([$PhBP_3$]$Co^{II}X$) (X = Br (**3.2**), Cl (**3.3**)), are also described. These latter two complexes feature an added complexity in that they are dimeric in the solid-state, but predominantly monomeric in solution. The collection of comparative solid-state and solution EPR spectra for **3.1**, **3.2**, and **3.3** is presented. For comparison, structural and spectroscopic data for a high spin derivative that was obtained directly from **3.1** is also described.

3.2 Results

3.2.1 Synthesis and solid-state structures of ([$PhBP_3$]$Co^{II}X$) (X = I, Br, Cl)

Eq. 3.1 and Eq. 3.2 present the synthesis of the three halide derivatives ([$PhBP_3$]$Co^{II}X$) (X = I, Br, Cl). The high yield synthesis of the iodide complex [$PhBP_3$]CoI, (**3.1**), derived from the thallium reagent [$PhBP_3$]Tl, has been previously described. Although the bromide and chloride derivatives could be similarly prepared, they were best derived metathetically from the iodide complex: in situ iodide abstraction by $TlPF_6$ in THF, followed by addition of KBr or NaCl, converted [$PhBP_3$]CoI to ([$PhBP_3$]Co(μ-Br))$_2$, (**3.2**), and ([$PhBP_3$]Co(μ-Cl))$_2$, (**3.3**), respectively. Complexes **3.2** and **3.3** were isolated in yields typically greater than 80% when the metathesis protocol was repeated twice prior to workup. The halide derivatives **3.1**, **3.2**, and **3.3** gave rise to distinct and well-resolved, though paramagnetically shifted, ^{1}H NMR spectra.

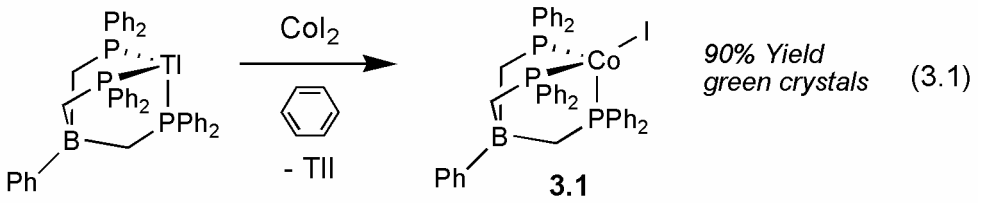

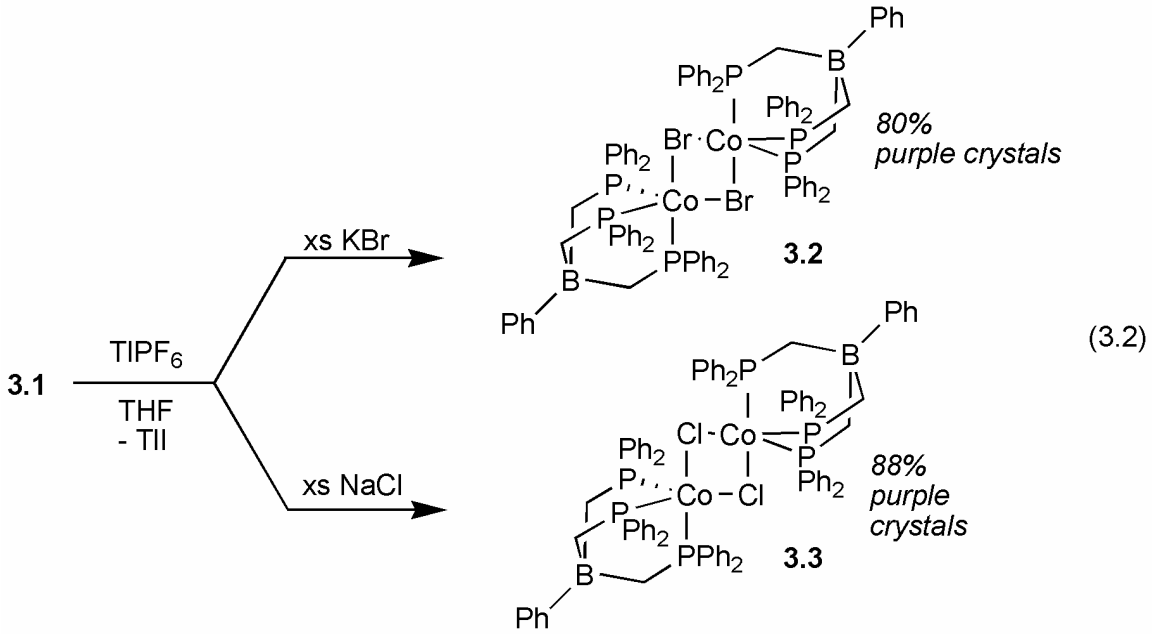

(3.2)

The iodide complex **3.1** is green whereas the chloride and bromide complexes **3.2** and **3.3** are purple in the crystalline state. This difference in color between polycrystalline samples of the three complexes correlates with their solid-state structures, which were determined by low temperature X-ray diffraction studies. Displacement ellipsoid representations for the solid-state structures (collected at 98 K) of **3.1**, **3.2**, and **3.3** are depicted in Figure 3.1, 3.2, and 3.3, respectively. The structure shown to the right for each complex provides a simplified representation in which the aryl carbon atoms from the diphenylphosphine donors have been omitted. Furthermore, the structures on the right of the bromide and chloride derivatives are rotated so that the bridging halide ligands are eclipsed. Only the bridged halide protruding out of the plane of the page is visible.

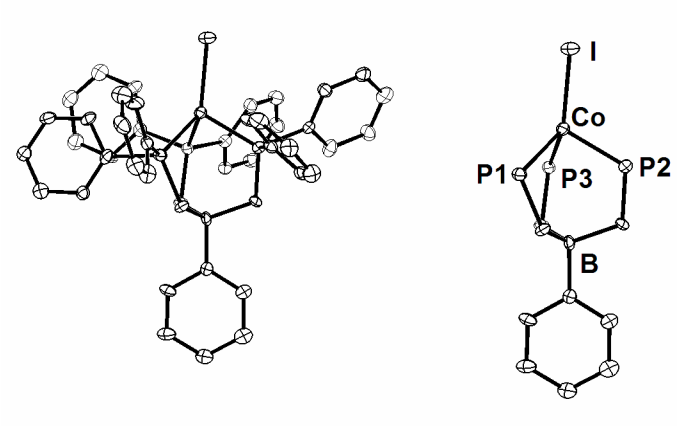

Figure 3.1. Displacement ellipsoids are represented at 50%. The structure on the right is shown without aryl carbon atoms for clarity. Selected interatomic distances (Å) and angles (deg) for [$PhBP_3$]CoI, (**3.1**): Co1-P1, 2.200(2); Co1-P2, 2.206(2); Co1-P3, 2.282(2); Co1-I1, 2.488(1); Co1-B1, 3.490(8). P1-Co1-P2, 90.33(8); P1-Co1-P3, 94.46(7); P2-Co1-P3, 91.95(7); P1-Co1-I1, 117.54(6); P2-Co1-I1, 129.19(6); P3-Co1-I1, 124.01(6).

Most striking in Figure 3.1 is the monomeric structure obtained for the iodide complex **3.1** in comparison to the dimeric solid-state structures obtained for the bromide and chloride complexes **3.2** and **3.3**, respectively. Although none of the three complexes adopts an idealized local geometry, they can be approximated as structure types typical of cobalt(II). The iodide **3.1** has pseudotetrahedral coordination, with low formal symmetry due to a strong axial distortion and inequivalent Co-phosphine bond lengths and angles. By contrast, the bromide and chloride derivatives can be regarded as square pyramidal structures at the localized cobalt center of each respective dimeric unit. In each of the three structures, the tridentate [$PhBP_3$] ligand exhibits two short and one modestly elongated Co-P bond. The P-Co-P angles vary only slightly from 90°.

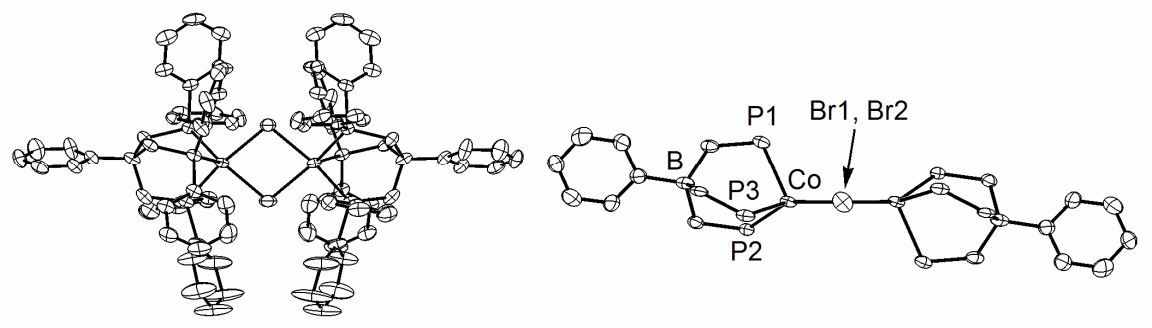

Figure 3.2. Displacement ellipsoids are represented at 50%. The structure on the right is shown without aryl carbon atoms for clarity, and the dimer is rotated such that the bridging halide ligands are eclipsed. Selected interatomic distances (Å) and angles (deg) for $([PhBP_3]Co(\mu\text{-}Br))_2$ (**3.2**): Co1-Co1(#1), 3.668(1); Co1-P3, 2.235(2); Co1-P2, 2.247(2); Co1-P1, 2.336(2); Co1-Br1, 2.413(1); Co1-Br2, 2.424(1); Co1-B1, 3.570(6). Co1-Br1-Co1(#1), 98.97(5); Co1-Br2-Co1(#1), 98.37(5); P2-Co1-P3, 87.42(6); P1-Co1-P3, 92.35(6); P1-Co1-P2, 93.44(6); P3-Co1-Br1, 165.70(5); P2-Co1-Br1, 93.63(5); P1-Co1-Br1, 101.81(4); P3-Co1-Br2, 91.35(5); P2-Co1-Br2, 153.37(5); P1-Co1-Br2, 113.19(4); Br1-Co1-Br2, 81.33(3). Symmetry transformations used to generate equivalent atoms: #1 - x, y, $-z + 1/2$.

The bromide complex **3.2** features a rigorously planar Co_2Br_2 rhombus that is bisected by a crystallographic C_2-axis running through the two bromide ligands. The C_2-axis effectively places the elongated axial Co-P bonds on opposite faces of the Co_2Br_2 plane. By comparison, the Co_2Cl_2 unit of the chloride complex **3.3** gently buckles from planarity. The two elongated, axial Co-P bonds in this case reside on the same face of the Co_2Cl_2 unit. The gentle buckling in **3.3**, along with the decreased size of the chloride bridge, effectively slides the two cobalt centers closer together by comparison to their

distance in **3.2** (3.668(1) Å in **3.2** versus 3.497(1) Å in **3.3**). Dimeric **3.3** is structurally very similar to its dicationic relative $[((triphos)Co(\mu\text{-}Cl))_2][BPh_4]_2$: the Co-Co distance in $[((triphos)Co(\mu\text{-}Cl))_2][BPh_4]_2$ is 3.52 Å, and its Co-Cl-Co angle is 100.0°, to be compared with an average Co-Cl-Co angle of 98.2° in **3.3**.[19c,20] The solid-state structure of $[((triphos)Co(\mu\text{-}OH))_2][BPh_4]_2$ has also been determined and is similarly dimeric, though the O-Co-O angles are much smaller and average 69.5°.[19c] Spectroscopic data confirms that the bromide derivative $[((triphos)Co(\mu\text{-}Br))_2][BPh_4]_2$ is dimeric as well;[19c] its solid-state crystal structure has not yet been reported.

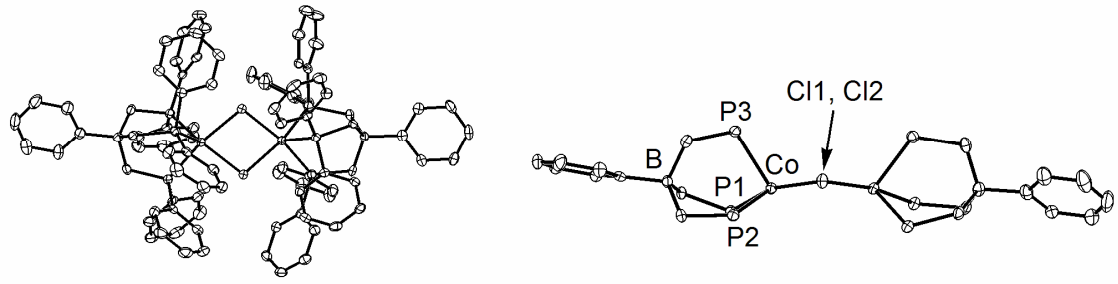

Figure 3.3. Displacement ellipsoids are represented at 50%. The structure on the right is shown without aryl carbon atoms for clarity, and the dimer is rotated such that the bridging halide ligands are eclipsed. Selected interatomic distances (Å) and angles (deg) for $([PhBP_3]Co(\mu\text{-}Cl))_2$ (**3.3**): Co1-Co2, 3.497(1); Co1-B1, 3.551(3); Co2-B2, 3.598(3); Co1-P1, 2.224(1); Co1-P2, 2.244(1); Co1-P3, 2.391(1); Co1-Cl1, 2.284(1); Co1-Cl2, 2.321(1); Co2-P4, 2.227(1); Co2-P5, 2.239(1); Co2-P6, 2.336(1); Co2-Cl1, 2.314(1); Co2-Cl2, 2.332(1). Co1-Cl1-Co2, 99.02(3); Co1-Cl2-Co2, 97.46(3); P1-Co1-P2, 88.16(3); P1-Co1-Cl1, 162.76(3); P2-Co1-Cl1, 92.82(3); P1-Co1-Cl2, 92.55(3); P2-Co1-Cl2, 159.70(3); Cl1-Co1-Cl2, 80.65(2); P1-Co1-P3, 91.09(3); P2-Co1-P3, 92.66(3); Cl1-Co1-P3, 106.04(3); Cl2-Co1-P3, 107.60(3); Cl1-Co2-Cl2, 79.79(2).

The solid-state structure of the iodide complex **3.1** exhibits approximate C_s symmetry.[21] An appreciable axial distortion gives rise to I-Co-P bond angles that are much larger than those found in idealized tetrahedral structures (P1-Co1-I1, 117.54(6); P2-Co1-I1, 129.19(6); P3-Co1-I1, 124.01(6)). Complex **3.1** is gently distorted from molecular threefold symmetry by a modest elongation of one of its phosphine donors by comparison to the other two (Co1-P1, 2.200(2); Co1-P2, 2.206(2); Co1-P3, 2.282(2)). Worth noting is that monomeric **3.1** is formally a 15 electron complex; this is very unusual for cobalt(II) systems supported by three phosphine donors. Similar 15 electron, monomeric, and pseudotetrahedral cobalt(II) halides supported by tris(pyrazolyl)- and tris(thioether)borate ligands have been reported previously.[22,23] An attempted synthesis of the analogous "[(triphos)CoI]$^{+}$" system was reported to have failed due to spontaneous reduction of the cobalt(II) center to cobalt(I).[19c]

3.2.2 Magnetic data (SQUID) for ([PhBP$_3$]Co^{II}X) (X = I, Br, Cl)

The temperature dependence of the magnetic susceptibility for complexes **3.1**, **3.2**, and **3.3** was studied by SQUID magnetometry. Average magnetic moments were adjusted for diamagnetic contributions using Pascal's constants and were fitted in the temperature range specified to use data that obeyed the Curie-Weiss law reasonably well. This was established from χ_m^{-1} versus T plots, which are shown in Figures 3.4B and 3.5B. For each case, the samples studied by SQUID magnetometry had provided satisfactory combustion analyses, as recorded in the Experimental section. These same sample batches were also used to obtain the EPR spectra that are discussed in the following section.

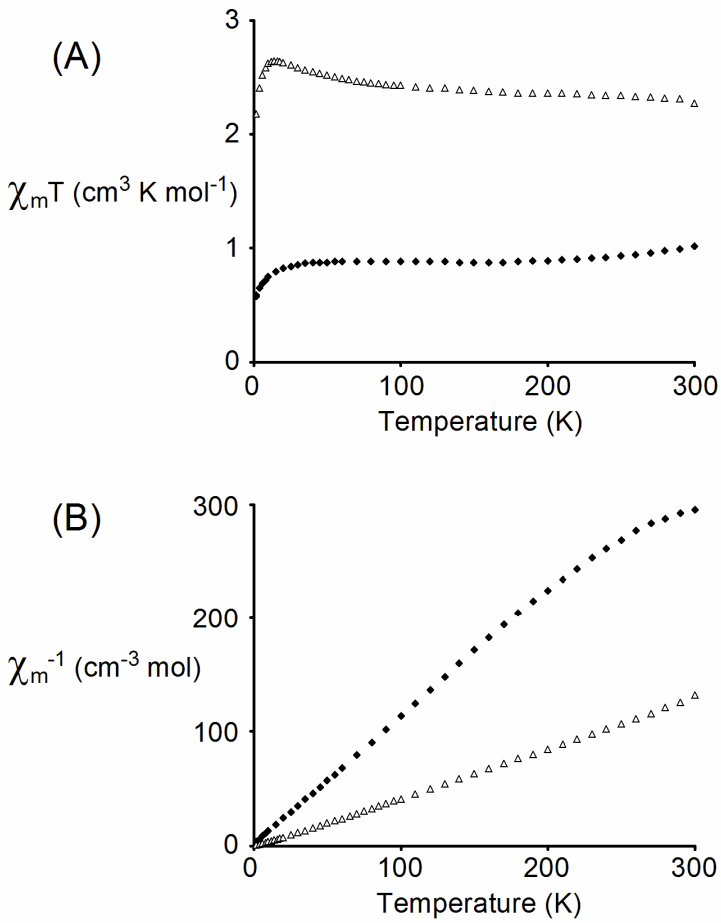

Figure 3.4. (A) SQUID plot of $\chi_m T$ (cm^3 K mol^{-1}) versus T: [$PhBP_3$]CoI, **3.1**, (♦) and [$PhBP_3$]CoO(2,6-dimethylphenyl), **3.4**, (Δ). (B) SQUID plot of χ_m^{-1} (mol/cm^3) versus T: [$PhBP_3$]CoI, **3.1**, (♦) and [$PhBP_3$]CoO(2,6-dimethylphenyl), **3.4**, (Δ).

Figure 3.4A displays the temperature dependence of the calculated magnetic moment $\chi_m T$ (see Experimental section for details) for complex **3.1**, and Figure 3.4B plots its χ_m^{-1} versus temperature. The magnetic data for **3.1** is unexpected for a 4-coordinate cobalt(II) system in a pseudo-tetrahedral coordination geometry. Its magnetic moment shows little variation in the temperature range between 30 and 220 K.

The Curie law observed in this range indicates that the doublet state is the only state that is thermally populated. Above 220 K, the effective moment increases, albeit very gradually, possibly suggesting that a high spin state is slightly but increasingly populated as the temperature rises above 220 K. The concentration of a high spin state at the elevated temperatures is very small, however, as even at 300 K the value for $\chi_m T$ only reaches 1.01. We note that the gradual rise in the moment that is observed above 220 K for **3.1** was reproducible and does not appear to be an artifact of the experiment. An average magnetic moment of 0.89 cm^3 K mol^{-1} was obtained for **3.1** by fitting the susceptibility data in the temperature range between 10 and 310 K. A fit to the region from 30 to 220 K, where the sample shows good Curie-Weiss behavior, provides an average moment of 0.88. For a 4-coordinate cobalt(II) complex, this moment would typically imply a cobalt(II) ion in an approximate *square planar* geometry.[24] Similar low spin moments are also common for cobalt(II) systems with higher coordination numbers (e.g., square pyramidal, trigonal bipyramidal, or octahedral type structures),[18,25] the value of 0.88 cm^3 K mol^{-1} tending toward the high side of what has been typically observed for low spin cobalt(II). By contrast, magnetic moments for tetrahedral and pseudo-tetrahedral structure types more closely related to $[PhBP_3]CoI$ (T_d, C_{3v}, and lower symmetries) typically fall within a range between 2.3 and 3.4 cm^3 K mol^{-1} and are assigned as high spin.[25,26] The average *g* value of 3.06 that is extracted from the SQUID magnetization data, assuming a moment of 2.65 μ_B ($\chi_m T = 0.88$), is much higher than the effective *g* value directly obtained by solid-state EPR spectroscopy ($g \approx 2.1$), as discussed below. The crude relationship between *g* and μ_{eff}, as defined by the simplified equation $\mu_{eff} = g\{S(S+1)\}^{1/2}$, assumes complete quenching of an orbital contribution,[27] which may be a

serious oversimplification in the present context. The room temperature benzene solution magnetic moment of **3.1** was estimated by the method of Evans and provided a value of 2.87 μ_B, assuming a diamagnetic correction from Pascal's constants, in close agreement with that obtained from the SQUID data at 300 K.[28] We suggest that the solid-state and solution moments are most consistent with a low spin assignment for **3.1**, and that a low spin ground state is very reasonable for a complex of this type based upon the rationale provided in the discussion section. Moreover, the low spin assignment is further corroborated by the EPR data for **3.1**.

The solid-state magnetic susceptibilities for polycrystalline samples of the dimeric bromide $([PhBP_3]Co(\mu\text{-}Br))_2$ and chloride $([PhBP_3]Co(\mu\text{-}Cl))_2$ were also measured by SQUID magnetometry and are plotted, *per dimeric unit*, in Figure 3.5. The magnetic data obtained for the dimers are more complex than the data obtained for monomeric **3.1**. Each set of susceptibility data was collected twice to verify its experimental reproducibility. Little, if any, evidence for detectable antiferromagnetic coupling in dimers **3.2** and **3.3** can be gleaned from the temperature-dependent plots of $\chi_m T$ and χ_m^{-1}. The acid test for antiferromagnetic exchange coupling in a dimeric complex consisting of two spin $^1/_2$ ions is that the susceptibility (χ_m) should reach a maximum as the temperature of the sample is lowered, but then fall precipitously to zero as the sample is cooled further. For both **3.2** and **3.3**, the magnetic moments decrease very gently from 310 K down to about 80 K, at which point they level off until reaching the lowest temperature region where intermolecular paramagnetic quenching begins to occur. The expected maximum in the susceptibility for **3.2** and **3.3** is not observed, in contrast to the temperature-dependent susceptibilities Sacconi reported for $[((triphos)Co(\mu\text{-}X))_2][BPh_4]_2$

(X = Br, Cl, OH), indicating the dicationic dimers exhibit strong antiferromagnetic coupling ($J < -100$ cm^{-1}) between their Co^{2+} centers.[19c]

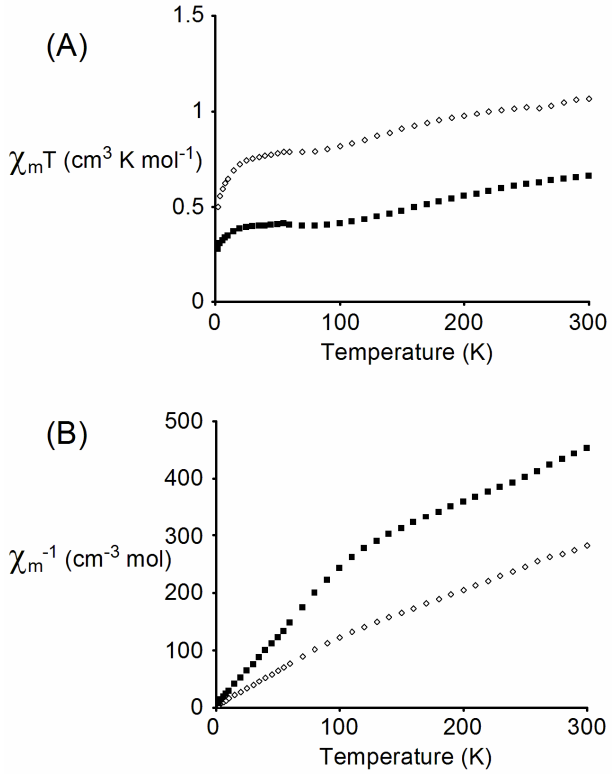

Figure 3.5. (A) SQUID plot of $\chi_m T$ (cm^3 K mol^{-1}) versus T: ([PhBP$_3$]Co(μ-Br))$_2$, **3.2**, (■) and ([PhBP$_3$]Co(μ-Cl))$_2$, **3.3**, (◊). (B) SQUID plot of χ_m^{-1} (mol/cm^3) versus T: ([PhBP$_3$]Co(μ-Br))$_2$, **3.2**, (■) and ([PhBP$_3$]Co(μ-Cl))$_2$, **3.3**, (◊).

Antiferromagnetic exchange behavior is most typical of halide-bridged cobalt(II), copper(II), and titanium(I) dimers, where an unpaired electron resides at each metal center,[29] and it is emphasized that antiferromagnetic exchange does not appear to be present in either **3.2** or **3.3**. The net change in the moment for both **3.2** and **3.3** is rather small between 300 and 80 K. For example, at 300 K the moment of chloride **3.3** is 1.06 cm^3 K mol^{-1}, which decreases to 0.79 at 80 K. For bromide **3.2**, the moment at 300 K

(0.66) is appreciably lower than for **3.3** and only decreases to a value of 0.40 at 80 K. For a simple ferromagnetic exchange interaction ($J > 0$) between the two spin $^1/_2$ ions in dimers **3.2** and **3.3**, a plot of $\chi_m T$ versus T is expected to show a rise in the curve as the temperature is lowered. Instead, we observe a gentle decrease in $\chi_m T$ (and likewise μ_{eff}) as the temperature is lowered, which decreases dramatically only at very low temperature due to the onset of intermolecular magnetic quenching interactions. A fit of the lower temperature data, where the Curie-Weiss law is obeyed reasonably well ($T < 110$ K), provided a magnetic moment 0.40 cm^3 K mol^{-1} and θ = -1.48 ± 0.49 K for complex **3.2**. A moment of 0.77 cm^3 K mol^{-1} and theta value of θ = -3.13 ± 0.67 K was obtained for complex **3.3** when fit in the same temperature regime. Zero-field splitting, weak exchange, and mixing of the triplet and singlet states of **3.2** and **3.3** likely complicate the observed magnetism and contribute to the gradual attenuation rather than rise of the moment of each sample as the temperature is lowered, as would have been expected for systems exhibiting pronounced ferromagnetic exchange. Regardless, we suggest that the magnetic data for **3.2** and **3.3** are most consistent when assigning them to $S = 1$ ground states. The EPR data for solid samples of **3.2** and **3.3** are also most consistent with a triplet ground state assignment (see below); the signal amplitude for these dimers increases as the temperature of each sample is lowered from 25 to 3.6 K, as is to be expected for a weak ferromagnetically coupled dimer with two $S = ^1/_2$ spin centers.

A dimeric cobalt(II) complex whose magnetism may be related to that observed for **3.2** and **3.3** was provided by Sacconi and co-workers in 1980.[30] They reported that the μ-thiolato complex $[((triphos)Co(\mu\text{-}SCH_3))_2][BPh_4]_2$ provided a μ_{eff} of 1.8 μ_B ($\chi_m T$ = 0.40) that gradually decreased to 0.8 μ_B at 130 K, at which point it leveled off down to

the lowest temperature for which data was recorded (87 K). The reasoning Sacconi and co-workers provided to explain the odd magnetic behavior of $[((triphos)Co(\mu\text{-}SCH_3))_2][BPh_4]_2$ was that antiferromagnetic exchange occurred between the spin $^1/_2$ cobalt centers through the μ-SCH_3 units, but that the limiting value represented a contribution from partial occupation of a higher triplet state. In our case, the limiting value at lower temperature represents a triplet state likely mixed with a singlet state that is close in energy.

It should be noted that the difference between the total $\chi_m T$ (and μ_{eff}) for solid samples of **3.2** and **3.3** is not so pronounced in solution. Evans method measurements for **3.2** and **3.3** in benzene-d_6 at 25 °C provided moments of 2.7 μ_B and 3.0 μ_B, respectively, similar to the solution moment obtained for **3.1**.[31] As will be suggested by the EPR data discussed in the following section, these solution moments reflect a change in both geometry and spin state for **3.2** and **3.3** in toluene solution.

3.2.3 EPR spectra for ($[PhBP_3]Co^{II}X$) (X = I, Br, Cl)

The EPR spectra for **3.1**, **3.2**, and **3.3** are extremely sensitive to oxygen due to a high spin impurity that results from a well-defined ligand oxidation process that has been carefully studied for the case of **3.1**. High-quality spectra for all three complexes were only acquired using thoroughly recrystallized samples that afforded satisfactory combustion analysis. The absence of high spin oxidation products was further confirmed by optical spectroscopy prior to EPR data collection.

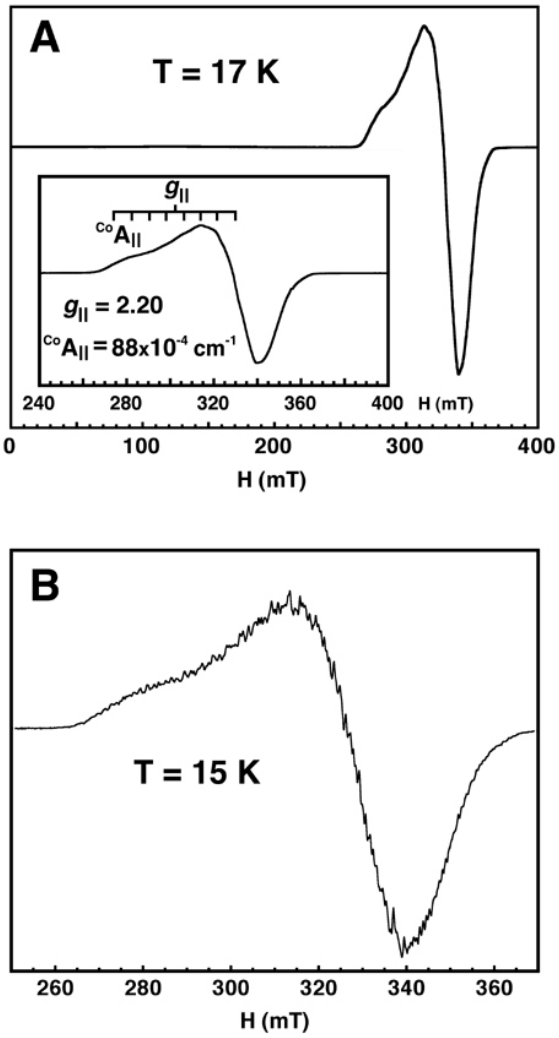

Figure 3.6. (A) EPR spectrum of a glassy toluene solution of [$PhBP_3$]CoI (**3.1**) at 17 K. $g_{||}$ and $A_{||}$ were estimated by simulating the EPR spectrum (inset). (B) EPR spectrum of a glassy toluene solution of [$PhBP_3$]CoI in toluene-d_8 at 15 K. See Experimental section for parameters.

The EPR spectrum in glassy toluene (17 K) of a pure sample of **3.1** is shown in Figure 3.6. Due to the high oxygen sensitivity of **3.1**, the spectra that were originally obtained showed a rather broad feature in the region $g \approx 4.8$ (ca. 120 mT). This feature

was entirely removed upon rigorous exclusion of oxygen from the sample. The broad feature at ~4.8 corresponds to a signal from the high spin complex $[PhB(CH_2PPh_2)(CH_2P(O)Ph_2)_2]CoI$ (see Experimental section for details). The spectrum of pure **3.1** is nearly independent of temperature (except for its intensity) in the temperature range 20 K to 140 K. It is characterized by an axial *g* factor ($g_{\|}$ = 2.20 and $g_{\perp}$ = 2.05) and poorly resolved ^{59}Co (I = 7/2) hyperfine splitting. However, a very complex super-hyperfine splitting pattern was resolved below 50 K in toluene-d_8 (Figure 3.6b),[32] ascribable to the ^{31}P (I = 1/2)[33] and possibly $^{127}I^-$ (I = 5/2) donor atoms. An isotropic EPR spectrum with g_{iso} = 2.1 was observable at room temperature, further confirming the low spin nature of **3.1**. The powder EPR spectrum of **3.1** shows features analogous to those of the frozen toluene sample. EPR signals for high spin cobalt(II) systems are typically observed only below ~30 K due to the fast spin-lattice relaxation times of the high spin Co(II) nucleus.[34] That we are able to observe an intense signal for **3.1** even at room temperature further supports the notion that **3.1** has a doublet ground state both in solution and in the solid-state.

The solid-state magnetic data that were presented above for **3.2** and **3.3** suggested that they each have triplet ground states close in energy to possibly mixed singlet excited states, and that the magnitude of exchange energy *J* is difficult to measure from the SQUID data alone. To the extent that ferromagnetic exchange is present, it is likely very small (<10 cm^{-1}). To further explore each of these systems, their EPR spectra were recorded using the same samples that had been carefully purified for the magnetic measurements. As for **3.1**, admission of adventitious oxygen to samples of **3.2** and **3.3** produced oxidation products that afforded spectra with signals centered at $g \approx 4.8$.

Problematic is that these features coincidentally overlap with the low field EPR signal expected (and observed in the solid-state) for the pure dimers of **3.2** and **3.3**. Again, rigorous exclusion of oxygen solved this problem and high quality spectra were obtained. The EPR spectra (Figure 3.7 and 3.9) for pure polycrystalline samples of both **3.2** and **3.3** are well-resolved below 30 K. Each spectrum supports the suggestion of the triplet species at low temperature: the intensity of these spectra were not attenuated, but rather increased, from 25 to 3.6 K, consistent with weak ferromagnetic coupling. The temperature dependence of the solid-state EPR spectrum of **3.2** is shown in Figure 3.8. We attempted to simulate the EPR spectra of the polycrystalline samples of **3.2** and **3.3** under the assumption that the exchange energy $|J| >>$ than the X-band microwave quantum (0.3 cm^{-1}). In such cases the triplet state can be described in terms of D and E using the standard spin-Hamiltonian for an $S = 1$ spin system (see the Experimental Section). We also made the crude assumption that the dipolar and g tensors were collinear.[35] Using this model, we could achieve only qualitative agreement between the simulated and experimental spectra. On the basis of these simulations, a zero-field splitting of roughly 0.2 cm^{-1} or less is consistent with the observed EPR spectra. Also, we note that the EPR spectrum of a monomeric triplet complex, $[PhBP_3]Co(PMe_3)$, has been recorded and contains features qualitatively similar to those of **3.2** and **3.3** in the solid-state, including the low field g signal ~4.8. This system has been described elsewhere (see Chapter 5).[15c]

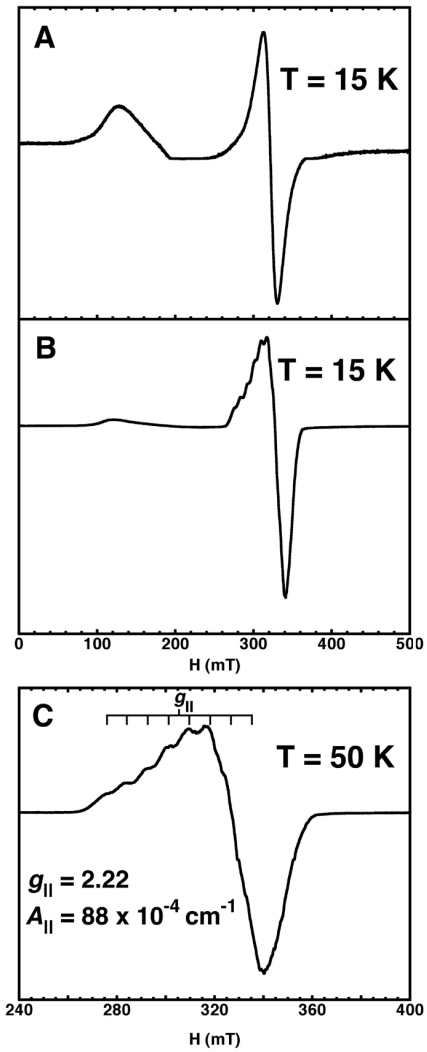

Figure 3.7. (A) EPR spectrum of a polycrystalline sample of ([$PhBP_3$]Co(μ-Br))$_2$ (**3.2**) at 15 K. (B) EPR spectrum of a glassy toluene solution of ([$PhBP_3$]Co(μ-Br))$_2$ at 12 K. (C) EPR spectrum of a glassy toluene solution of ([$PhBP_3$]Co(μ-Br))$_2$ at 50 K. $g_{||}$ and $A_{||}$ were estimated by simulating the EPR spectrum. See Experimental section for parameters.

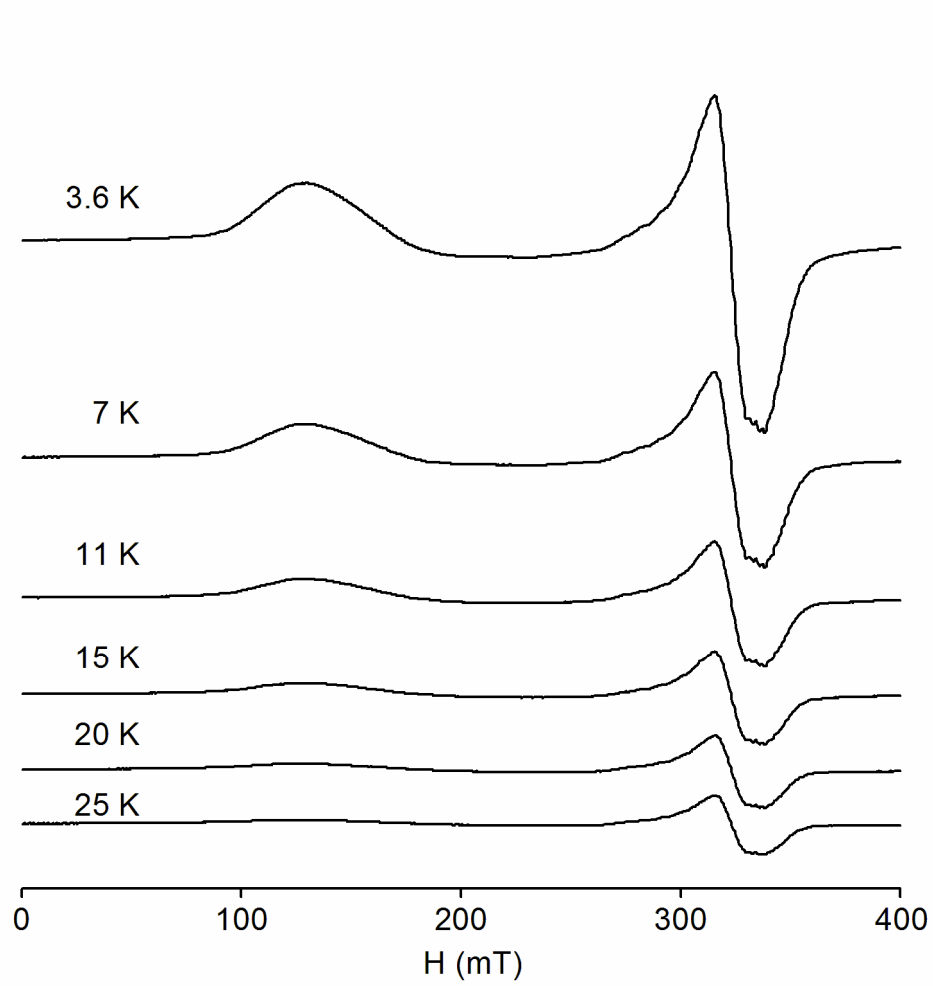

Figure 3.8. Series of EPR spectra for a polycrystalline sample of $([PhBP_3]Co(\mu\text{-}Br))_2$ (**3.2**) plotted to show the temperature dependence of the EPR signal. The signal amplitude increases as the temperature decreases, suggestive of a ferromagnetic triplet ground state.

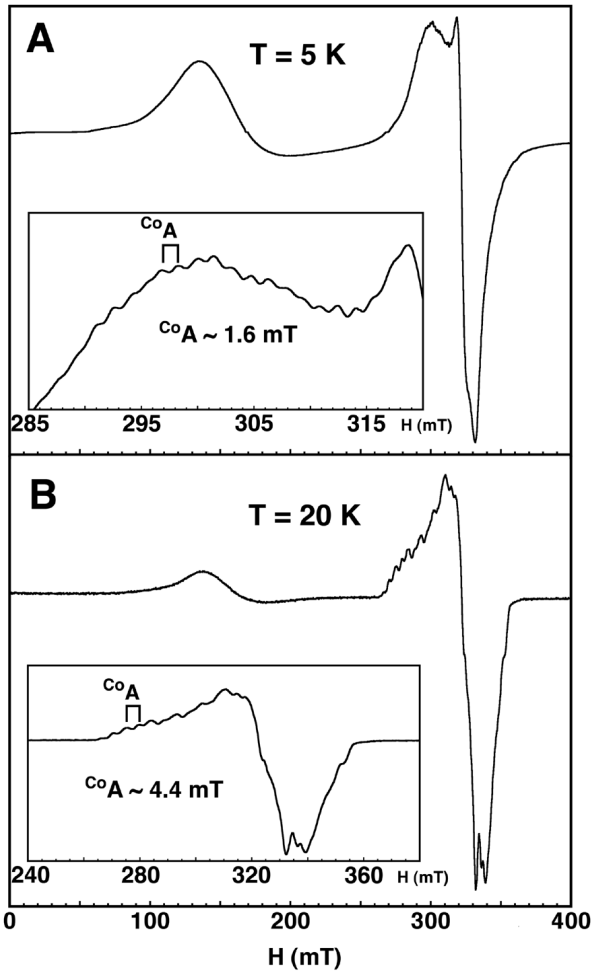

Figure 3.9. (A) EPR spectrum of a polycrystalline sample of $([PhBP_3]Co(\mu\text{-}Cl))_2$ (**3.3**) at 3.6 K. (B) EPR spectrum of a glassy toluene solution of $([PhBP_3]Co(\mu\text{-}Cl))_2$ at 12 K. See Experimental Section for parameters.

Dissolution of *purple* crystals of $([PhBP_3]Co(\mu\text{-}Br))_2$ (**3.2**) and $([PhBP_3]Co(\mu\text{-}Cl))_2$ (**3.3**) in toluene was accompanied by a drastic color change to bright green, similar to the color of $[PhBP_3]CoI$ both in solution and in the crystalline state. This behavior suggested to us a structural change in the dimers **3.2** and **3.3** upon dissolution.

Indeed, we found by EPR that in solution a temperature-dependent equilibrium between monomeric and dimeric species seems to exist (Eq. 3.3). The EPR spectrum of **3.2** in glassy toluene (15 K) is shown in Figure 3.7. This spectrum presumably represents a monomeric species akin to the structurally characterized iodide monomer, perhaps with an additional trace presence of the dimeric form of **3.2**. The observation that $g_{\|} > g_{\perp}$ for **3.2** in the frozen glass clearly establishes that the square-pyramidal arrangement of the cobalt complex, observed in the solid-state, is not preserved in solution. We suggest that the geometry of **3.2** in solution is that of a pseudotetrahedral, 4-coordinate monomer, as for the case of **3.1**. The similarity of the magnetic moments for solutions of **3.1** and **3.2** is also consistent with their having similar coordination geometries. We therefore conclude that the glassy toluene EPR spectrum of **3.2** represents the monomeric and low spin complex $[PhBP_3]CoBr$. The resolved hyperfine coupling in the $g_{\|}$ region is in accord with this model ($A_{\|} = 88 \times 10^{-4}$ cm^{-1}) as it shows an octet, indicative of coupling to a single cobalt nucleus. If the dimer of **3.2** were maintained in solution, we would have expected to observe a 15-line splitting pattern. A related EPR study was also performed for the chloride **3.3**. The polycrystalline and glassy EPR spectra of **3.3**, shown in Figure 3.8 are similar to that of **3.2**. The major difference is that a readily detectable population of the dimer of **3.3** appears to be present in glassy toluene at 12 K. The low spin monomer $[PhBP_3]CoCl$, however, is the major species present in the glass even at this low temperature. The additional hyperfine resonances observed in the $g_{\|}$ region (~2.2) for **3.3** are also suggestive of a modest concentration of the triplet $([PhBP_3]Co(\mu\text{-}Cl))_2$ in the glassy toluene spectrum, which is superimposed with the signal expected for $[PhBP_3]CoCl$. The hyperfine coupling for $[PhBP_3]CoCl$ is resolvable with $A_{\|} = 92 \times 10^{-4}$

cm^{-1}. The temperature dependence of the optical spectrum of **3.3** is discussed below and lends further support to the suggestion that **3.3** can dimerize in solution as a function of temperature.

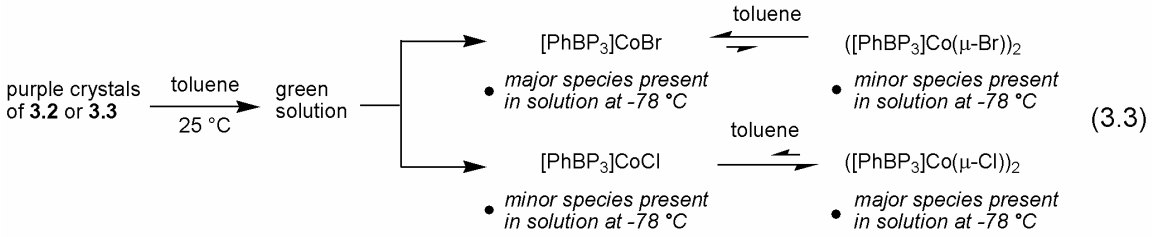

(3.3)

3.2.4 Conversion of low spin iodide to the high spin complex [PhBP$_3$]CoO(2,6-Me$_2$-C$_6$H$_4$)

It was prudent to prepare one or more complexes of similar geometry to **3.1** with a high spin ground state so that the relevant structural, magnetic, and spectroscopic data could be compared to the monomeric low spin derivatives already described.

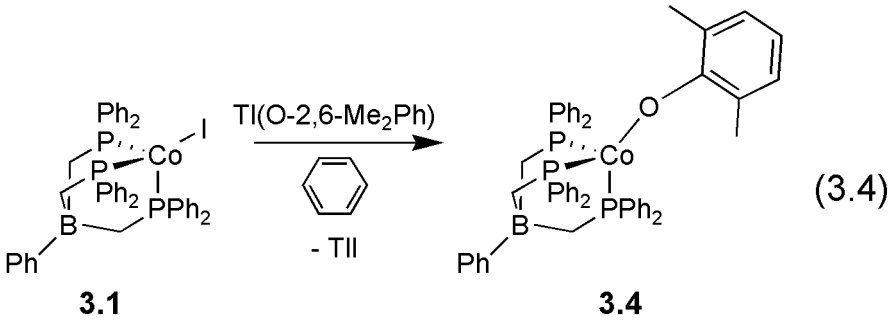

(3.4)

We prepared a more conventional four-coordinate and *high spin* complex supported by an intact [PhBP$_3$] ligand. The iodide complex **3.1** was allowed to react with the moderately bulky thallium aryloxide reagent Tl(O-2,6-Me$_2$-Ph), which smoothly generated the aryloxide species [PhBP$_3$]CoO(2,6-Me$_2$-Ph), (**3.4**), as a red-brown, crystalline solid (Eq. 3.4). The solid-state structure of **3.4**, depicted in Figure 3.10, reveals **3.4** to be monomeric, but grossly distorted from idealized threefold symmetry. Each of

the three O-Co-P angles is quite different (134.9(1)°, 120.4(1)°, and 105.3(1)°) and one of the phosphine donor arms is slightly elongated by comparison to the other two (2.366(1) Å versus 2.332(1) and 2.343(1) Å, respectively). High spin, four-coordinate cobalt(II) systems typically adopt higher symmetry when possible; the distorted structure obtained for **3.4** likely results from steric interactions between the bulky aryloxide and [$PhBP_3$] ligands. The Co-P bond lengths in **3.4** are, on average, appreciably elongated in comparison to **3.1** (~ 0.12 Å). This difference again qualitatively reflects their different spin states.

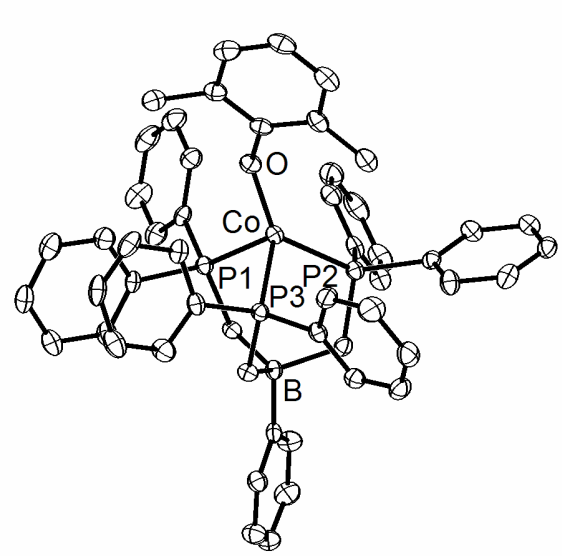

Figure 3.10. Displacement ellipsoid representation (50%) of [$PhBP_3$]CoO(2,6-dimethylphenyl), (**3.4**). Selected interatomic distances (Å) and angles (deg): Co-O, 1.851(2); Co-P3, 2.332(1); Co-P2, 2.366(1); Co-P1, 2.343(1); Co-B, 3.446(3); O-Co-P3, 120.39(5); O-Co-P2, 134.93(5); P3-Co-P2, 98.27(2); O-Co-P1, 105.27(5); P3-Co-P1, 92.72(2); P2-Co-P1, 94.22(2).

3.2.5 Comparative magnetic and EPR characterization of [PhBP$_3$]CoO(2,6-Me$_2$-C$_6$H$_4$)

The aryloxide complex **3.4** also appears to be a high spin species in the solid-state, as evident from its SQUID data provided in Figure 3.4. Its high spin moment was maintained in solution (4.3 μ_B, C_6D_6, 25 °C). It is also interesting to note that the $\chi_m T$ versus T plot for **3.4** reveals an unexpected rise in $\chi_m T$ as the sample temperature is lowered. This rise becomes more dramatic at temperatures < 100 K and reaches a maximum at 16 K, at which point it falls precipitously to zero as the temperature is lowered further, perhaps suggestive of intermolecular antiferromagnetic exchange. The glassy toluene EPR spectrum of **3.4** also suggests that it is high spin and its signal is not detected at elevated temperatures (> 50 K).

3.2.6 Comparative optical spectra of [PhBP$_3$]CoI, ([PhBP$_3$]Co(μ-Br))$_2$, and ([PhBP$_3$]Co(μ-Cl))$_2$

The room temperature optical spectra for green solutions of **3.1**, **3.2**, and **3.3** (250-1500 nm) were obtained in toluene and are shown in Figure 3.11. The spectra for the halides **3.1**, **3.2**, and **3.3** are very similar and are dominated by an apparent broad charge-transfer band in the visible region that displays an expected blue shift from I^- (638 nm) to Br^- (612 nm) to Cl^- (594 nm). Lower energy features that show less halide dependence are also present in the spectrum of each of the three halides. It is important to note that incubation of green toluene solutions of **3.1** and **3.2** at -78 °C did not effect an appreciable color change. In contrast, incubation of a green solution of chloride **3.3** at -78 °C gave rise to a distinctly purple solution whose green color was recovered on warming. The inset spectrum shown in Figure 3.11 was acquired upon rapid removal of the purple

solution containing **3.3** from a -78 °C cold bath. In accord with the EPR data, we presume that this spectrum represents a superposition of the spectrum for the dimeric form of **3.3** and its monomeric, pseudotetrahedral low spin form. The optical spectrum of high spin **3.4** was also obtained in toluene solution. The visible region of its spectrum was characterized by broad features between 400 and 800 nm with resolvable maxima at 530, 580, and 752 nm.

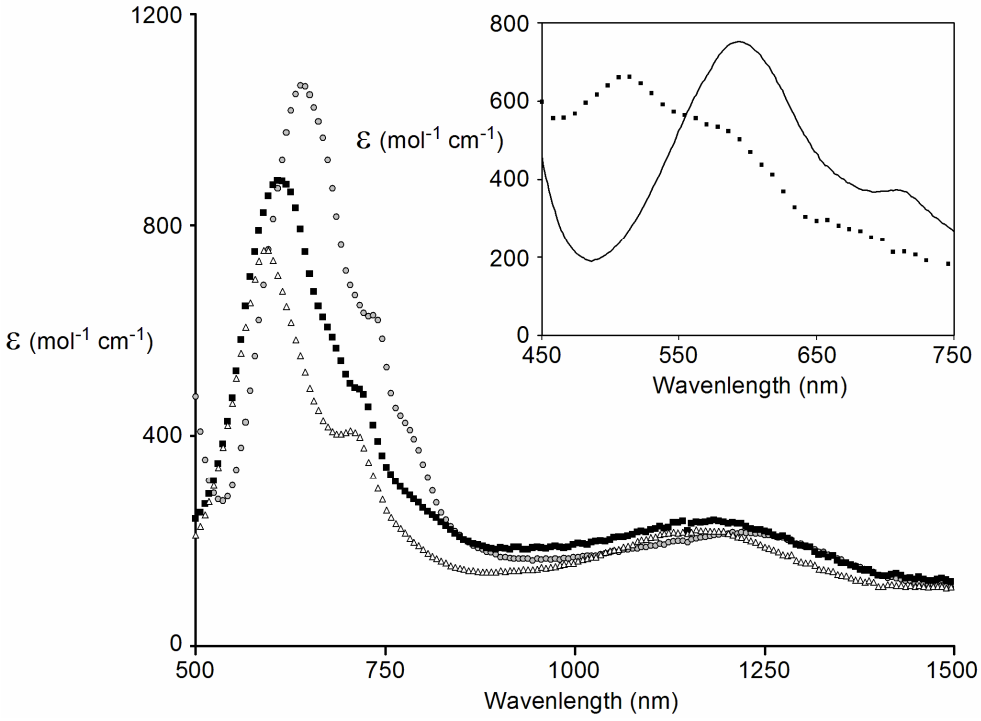

Figure 3.11. Absorption spectra for compounds [PhBP$_3$]CoI, **3.1**, (●), ([PhBP$_3$]Co(μ-Br))$_2$, **3.2**, (■), and ([PhBP$_3$]Co(μ-Cl))$_2$, **3.3**, (Δ), between 500 and 1500 nm. The similarity between each of the spectra suggests that each complex is predominantly monomeric at ambient temperature in toluene solution. **Inset:** ([PhBP$_3$]Co(μ-Cl))$_2$, **3.3**, at 298 K (——) and at 220 K (■) in toluene solution, illustrating the temperature dependence of the optical absorption that is associated with a monomer (298 K) to dimer (220 K) equilibrium.

3.3 Discussion

The preceding sections have presented structural, magnetic, and spectroscopic evidence to suggest that a low spin formulation is correct for *monomeric* $[PhBP_3]CoX$ systems, where X represents the halides I^-, Br^-, or Cl^-. Although the iodide complex **3.1** is a simple four-coordinate monomer both in the solid-state and in solution, the chloride **3.3**, and to a lesser extent the bromide **3.2**, are capable of dimerizing to a modest degree in solution at low temperature; they both crystallize in the dimeric form. The solid-state SQUID and EPR data collected for the dimers **3.2** and **3.3** prompt us to assign them to triplet ground states exhibiting weak ferromagnetic coupling. A more detailed analysis of their electronic structures is worth pursuing in future studies, though it is at present clear that the electronic structures of **3.2** and **3.3** are quite distinct from the structurally related dimers of Sacconi, these latter systems being characterized by singlet ground states due to pronounced antiferromagnetic exchange.

At room temperature, both **3.2** and **3.3** are *predominantly monomeric* in solution.[36] Room temperature solutions of **3.1**, **3.2**, and **3.3** in toluene are bright green; solutions of **3.1** and **3.2** remain green on cooling to 195 K, whereas a solution of **3.3** turns purple (reversibly) as it is cooled, indicative of the dimer concentration at low temperature. The solution EPR spectra are also consistent with this model. At low temperatures (< 50 K), the EPR spectra of iodide **3.1** and bromide **3.2** show only the monomer form. For the chloride **3.3**, however, the dimeric form also appears to be present below 50 K, superimposed with the spectrum for the monomer. The optical spectra for the three complexes are in accord with these data. Each of the spectra shows

very similar features at room temperature, suggesting analogous stereochemical environments in solution. Cooling the solution of **3.3** causes a dramatic change in color from green to purple, reflecting the increase in concentration of its dimeric form.

The most intriguing observation concerns the low spin character of the monomeric form of these simple halide complexes. Configurational solution equilibria between high and low spin complexes of cobalt were first observed more than three decades ago.[5,37,38] The typical situation is as follows: a low spin pentacoordinate cobalt(II) complex can dissociate one ligand to afford (i) a high spin, tetrahedral or distorted tetrahedral structure type, or (ii) a low spin, square planar or distorted square planar structure type. In certain cases, a solution equilibrium has been observed between strictly four-coordinate structures that are high spin (tetrahedral) and low spin (square planar), such as the bis(β-ketoamino)cobalt(II) complexes described by Holm and Everett.[5a] Stereochemical tuning of a series of tropocoronand ligands coordinated to divalent cobalt by Lippard and co-workers was shown to give rise to a range of intermediate structure types that were classified as either distorted tetrahedral (and high spin) or distorted square planar (and low spin). The halides described in the present manuscript are anomalous in that, for complexes **3.2** and **3.3**, solution equilibria between a low spin, five-coordinate, distorted square pyramidal structure and a low spin, four-coordinate, distorted tetrahedral structure apparently exist. The X-ray crystal structure of the iodide complex **3.1** provides a structural snapshot of the distorted tetrahedral, low spin four-coordinate structure, a structure that is not directly observable for complexes **3.2** and **3.3**, but which is inferred from the solution data available for these complexes. It becomes apparent that a low spin state for four-coordinate cobalt(II) can be

achieved by a distortion strikingly different from the severe distortion that takes a tetrahedral structure to a square planar structure. In the present case, a more subtle distortion, one that is distinctly axial in character, gives rise to the low spin configuration. The following discussion, accompanied by Figures 3.12 and 3.13, provides a simple orbital explanation for this phenomenon.

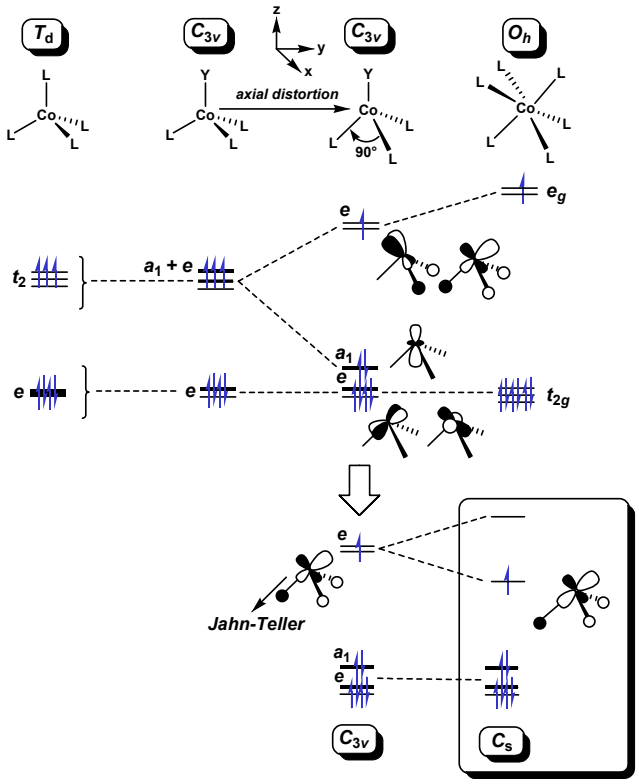

Figure 3.12. Qualitative d-orbital splitting diagram that depicts a descent in symmetry from T_d to C_{3v} symmetry for an axially distorted tetrahedral cobalt(II) system. As defined, the *z*-axis proceeds through one Co-L vector of the starting tetrahedron. The figure presents three limiting structure types: an idealized tetrahedron (CoL_4), a C_{3v} structure ($CoYL_3$) with bond angles analogous to the tetrahedral structure, and a C_{3v} structure resulting from a strong axial distortion ($CoYP_3$) in which the P-Co-P angle are fixed to ~90°.

A tetrahedral ligand-field for divalent cobalt places three degenerate orbitals, the *t* set, at a significantly higher energy than the nonbonding *e* set. Following Hund's rule, four electrons fill the *e* set, and three electrons fill the *t* set, one per orbital in a spin-aligned fashion. As is well-known, this is the origin of the typically observed quartet ground state that has been previously observed for tetrahedral and distorted tetrahedral cobalt(II) complexes. Breaking the symmetry, whether to C_3, C_s, or C_1, does not typically change this situation. The three orbitals at higher energy are only modestly split as the symmetry of the molecule descends from the tetrahedron. This splitting of the degenerate *t* set is typically small by comparison to the pairing energy that would be required to achieve a low spin state. However, if this splitting becomes large, and if an orbital of a_1 symmetry (predominantly dz^2) from the upper set is strongly stabilized on distortion, it should be possible to access a low spin population. We think that the stereochemical environment and the strong ligand-field donor-strength provided by the [$PhBP_3$] anion achieve this extreme and thereby provide access to the low spin ground state for pseudotetrahedral cobalt(II). The phosphine ligands of [$PhBP_3$] are good sigma-donors and should contribute to a strong ligand-field in pseudo-C_3 symmetry whereby the upper orbital set, σ* in character, lies well above the lower nonbonding orbital set. The dominant factor to consider is the extent to which a hybrid a_1 orbital (predominantly dz^2 with some admixed *s* and p_z) is stabilized as the cobalt center is axially distorted along the Co-I vector (i.e., along *z*). When stabilization of this a_1 orbital becomes strong enough, and when the ligand-field is sufficiently strong so as to destabilize the now high-lying *e*-set, electron pairing becomes energetically favorable and a low spin ground state is achieved. Figure 3.12 summarizes this model schematically by correlating the low

spin configuration in idealized C_{3v} symmetry to idealized T_d and O_h structures. Note that the natural choice of coordinate axes for all of the structures shown in Figure 3.12 places the *z*-axis through one face of an octahedral ML_6. Although this definition of axes is obvious for C_{3v} symmetry, it is not the typical choice for O_h ML_6. To describe the orbital character of the lower t_{2g} and upper e_g sets, the orbital functions need to be correlated to the new coordinate axis system. For an O_h ML_6 complex, these functions transform as:[39] **t_{2g} set:** z^2; $\{(2/3)^{1/2}(x^2 - y^2) - (1/3)^{1/2}yz\}$; $\{(2/3)^{1/2}xy - (1/3)^{1/2}xz\}$. **For e_g set:** $\{(1/3)^{1/2}x^2 - y^2 + (2/3)^{1/2}yz\}$; $\{(1/2)^{1/2}xy + (2/3)^{1/2}xz\}$. When the axial distortion is so severe that the angle (L-Co-L) between the three *fac* ligands becomes 90°, enforced in complex **3.1** by the [$PhBP_3$] ligand, the set of orbitals derived for O_h symmetry correlates very well with the axially distorted pseudotetrahedral structure type. For a low spin configuration we anticipate a Jahn-Teller distortion from C_{3v} to C_s symmetry. The lower portion of Figure 3.12 depicts this situation and suggests the final ground electronic configuration (using the functions given above) to be $(\{(2/3)^{1/2}(x^2 - y^2) - (1/3)^{1/2}yz\})^2(\{(2/3)^{1/2}xy - (1/3)^{1/2}xz\})^2(z^2)^2(\{(1/3)^{1/2}x^2 - y^2 + (2/3)^{1/2}yz\})^1(\{(1/2)^{1/2}xy + (2/3)^{1/2}xz\})^0$. The EPR spectrum of **3.1** ($g_{\|}$ = 2.20 and $g_{\perp}$ = 2.05) is consistent with this configuration to the extent that $g_{\|}$ is appreciably higher than the free electron value, suggesting that the unpaired spin is not localized in an orbital of dz^2 parentage. Rather, the unpaired spin resides in an orbital that is formally $\{(1/3)^{1/2}x^2 - y^2 + (2/3)^{1/2}yz\}$ within the present coordinate axis scheme.

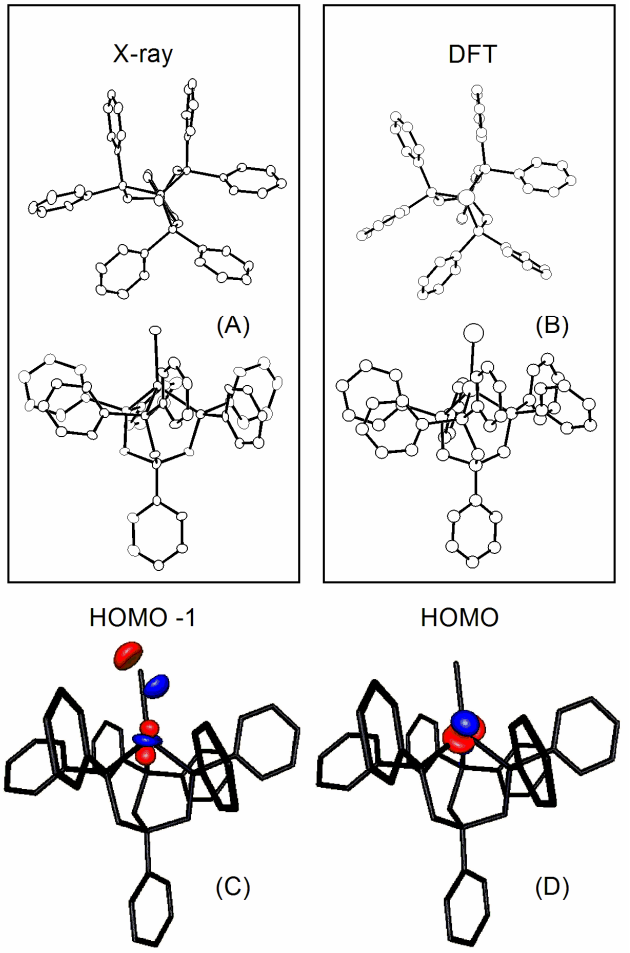

Figure 3.13. Figure shows the experimental (X-ray) **(A)** and calculated (DFT) **(B)** molecular structures for [$PhBP_3$]CoI (**3.1**). Representations of the HOMO-1 **(C)** and HOMO **(D)** orbitals obtained from the DFT electronic structure calculations are also shown. The calculated (DFT) bond distances (Å) and angles (deg) were theoretically determined to be as follows (the experimentally determined value is shown in parentheses): Co-I, 2.585 (2.474); Co-P(1), 2.282 (2.163); Co-P(2), 2.240 (2.208); Co-P(3), 2.402 (2.244); P(1)-Co-P(2), 88.6 (90.5); P(1)-Co-P(3), 96.0 (92.9); P(2)-Co-P(3), 90.5 (92.3); P(1)-Co-I, 119.0 (119.6); P(2)-Co-I, 131.6 (127.3); P(3)-Co-I, 121.6 (124.6).

Hoping to corroborate this conclusion, we performed a theoretical electronic structure calculation on the title complex **3.1**. The geometry of the complete complex, including the aryl rings of the [$PhBP_3$] ligand, was theoretically determined by performing a geometry optimization that used the experimentally determined structural coordinates for **3.1** as a starting point (see the Experimental Section for details). The structure calculation converged and reasonable, though not excellent, agreement between the theoretical structure of **3.1** and its experimentally determined structure was established (Figure 3.13). The electronic structure of **3.1** determined by DFT suggests the HOMO orbital to be one of π-antibonding character between the cobalt center and the iodide ligand, and the HOMO-1 orbital to be predominantly dz^2 in character, in accord with the qualitative MO scheme presented in Figure 3.12.

Although a great many high spin distorted tetrahedral complexes are known, two systems that deserve to be singled out with respect to the present discussion are the monomeric halides [Tp’’]CoI ([Tp’’] = hydrotris(3-*tert*-butyl-5-methylpyrazolyl)borate) and [$Tt^{tert\text{-butyl}}$]CoCl ([$Tt^{tert\text{-butyl}}$] = $[PhB(CH_2S^tBu)_3]^-$), each of which has been structurally characterized and assigned as high spin.[22,23] Like complex **3.1**, they each have approximate C_3 symmetry, and like complex **3.1**, they have a borate atom placed in close proximity to the cobalt center along the *z*-axis. The X-ray structures of [Tp’’]CoI and [$Tt^{tert\text{-butyl}}$]CoX also show a rather strong distortion in the axial direction (the average I-Co-N angle is ~122° for [Tp’’]CoI; the average Cl-Co-S angle is ~118° for [$Tt^{tert\text{-butyl}}$]CoCl). Geometric constraints for the facially capping [$PhBP_3$], [Tp’’] and [$Tt^{tert\text{-butyl}}$] donor ligands enforce the large X-Co-L (L = P, N, and S donor, respectively) bond angles in each case. As previously mentioned, low spin **3.1** is somewhat distorted

from C_3 symmetry by elongation of one of the phosphine donors. A similar distortion is not observed in [Tp'']CoI or [Tt$^{tert\text{-butyl}}$]CoCl. In these three cases, the three Co-L (L = N, S) bond lengths are very similar and the three X-Co-L bond angles show little variation. The solid-state structure of **3.1** is a reasonable consequence of its low spin configuration, expected to give rise to a Jahn-Teller distortion. That the related complexes [Tp'']CoI and [Tt$^{tert\text{-butyl}}$]CoCl do not adopt a low spin configuration and show a similar Jahn-Teller distortion likely reflects the relative ligand-field donor strengths of the three borate-derived donor ligands. The upper lying e-set (in C_{3v}) is σ^*. Its degree of destabilization should directly reflect the relative donor strength of three donor ligands. The [PhBP$_3$] ligand appears to be the strongest donor, destabilizing the upper orbital set to the greatest extent, but by a relative amount that has yet to be quantified. The ability of each ligand to accommodate a Jahn-Teller distortion (if a low spin configuration is to occur), however, is also a variable that needs to be considered. Tris(pyrazolyl)borate ligands, when coordinated in an η^3-fashion, are not very flexible. Geometric Jahn-Teller distortion to a stable low spin configuration might therefore be energetically unfavorable. Thus, [Tp]-derived ligands could provide a ligand-field strength similar to [PhBP$_3$], but still be coordinatively less flexible, thereby raising the energy of the doublet state above the quartet state for [Tp]CoX derivatives. Riordan's [Tt$^{tert\text{-butyl}}$]CoCl complex is another matter. That the monomeric complex [Tt$^{tert\text{-butyl}}$]CoCl is high spin is somewhat surprising based on the electronic scheme presented herein. It would seem that the tris(thioether)borate ligands are flexible enough to permit the Jahn-Teller distortion. The high-spin character of [Tt$^{tert\text{-butyl}}$]CoCl is perhaps reflective of their less pronounced axial elongation and an attenuated ligand-field strength by comparison to the [PhBP$_3$]CoX

systems. This would have the effect of narrowing the gap between the a_1 orbital and the upper *e* manifold, thereby making the high spin configuration of [Tt$^{tert\text{-butyl}}$]CoCl more stable. It would certainly be of interest to comparatively study the temperature dependence of the magnetic behavior of Theopold's and Riordan's cobalt(II) systems by SQUID magnetometry to establish whether any of the low spin forms for these complexes is populated at very low temperatures.

An interesting observation for the low spin complexes **3.1**, **3.2**, and **3.3** is that they bind a stoichiometric equivalent of CO readily to form the low spin, 5-coordinate carbonyl adducts [$PhBP_3$]Co(CO)(X) (X = I^-, Br^-, Cl^-). It is of interest in the present discussion to compare the relative CO donor strength of [$PhBP_3$]Co(CO)(Br) to the isostructural but cationic complex [$(H_3CC(CH_2PPh_2)_3)$Co(Br)(CO)][BPh_4] previously reported by Sacconi.[19d] The carbonyl stretching frequency of [$PhBP_3$]Co(CO)(Br) is 2030 cm^{-1}. The carbonyl stretching frequency of structurally characterized [$(H_3CC(CH_2PPh_2)_3)$Co(Br)(CO)][BPh_4] is 2060 cm^{-1}. That the cationic complex exhibits a CO stretch 30 cm^{-1} higher in energy than the neutral derivative suggests that the anionic borato ligand is an appreciably stronger donor than its neutral ligand counterpart. The increased donor strength likely accounts for the tendency of dimeric bromide **3.2** to dissociate to a 15 electron, low spin monomer in solution. Such an equilibrium has not been observed for any of the cationic cobalt(II) dimers supported by triphos, in which a halide or pseudohalide occupies the bridging position.[19,20] We highlight this distinction because it is important to bear in mind with respect to the degree of "zwitterionic" character ascribed to neutral complexes supported by (phosphino)borate ligands. From the perspective of a simple Lewis structure depiction, simple resonance contributors that

delocalize the anionic borate charge to the phosphine donor ligands are not available. This contrasts the situation for tris(pyrazolyl)borate ligands, where simple resonance delocalization is expected to partially distribute the negative charge to the N-donor atoms. That [$PhBP_3$] is such a strong field donor, however, suggests that there is appreciable communication between the borate anion and the bound metal center, either through space or through the sigma framework. Our ability to identify low spin, monomeric cobalt(II) halides that do not irreversibly dimerize might be a direct consequence of the strong field of the [$PhBP_3$] anion: it stabilizes complexes that are formally electron deficient. The high spin complex **3.4** is also monomeric, as are the high spin systems of Theopold and Riordan.[22,23] This is perhaps to be anticipated, as they do not possess an empty *d* orbital to accommodate the lone pair of a bridging halide ligand. In accord with this model, we note that the high spin cobalt(II) derivative **3.4**, in addition to the Riordan and Theopold systems, appears to be more resistant to coordination of carbon monoxide. This fact may, however, simply reflect other factors such as relative ligand-field donor strengths and steric considerations.

3.4 Conclusion

In summary, we have synthesized and studied a series of divalent cobalt complexes supported by [$PhBP_3$]. Structural, magnetic, and spectroscopic data for each of these systems is suggestive of low spin behavior for their monomeric, distorted tetrahedral structure types. The low spin nature of the monomeric form of these halides appears to be unique from related systems that have been previously studied. Two scenarios that transform a high spin, 4-coordinate tetrahedral complex to a four-coordinate species that is low spin can therefore be put forward. The first scenario

pertains to the traditional case in which a high spin tetrahedral structure is distorted to a low-spin square planar structure type. The second scenario, that which is described herein, occurs when coupling of a strong ligand-field donor strength with a pronounced axial distortion leads to a distorted tetrahedral geometry that can accommodate a cobalt(II) ion in a low spin ground-state configuration. The latter, more gentle distortion exposes an orbital at the cobalt(II) center appropriate for small molecule binding, a feature that could be exploited if tunable crossover systems for four-coordinate cobalt(II) prove accessible. We are pursuing this possibility by searching for new $[PhBP_3]CoX$ systems that display spin crossover phenomena while maintaining four-coordination in an approximate tetrahedral structure type. We are also pursuing new tris(phosphino)borate ligands to further test our electronic model.

3.5 Experimental section

3.5.1 General considerations

General procedures were performed according to Section 2.4.1. Three additional instruments were employed. UV-vis measurements were taken on a Hewlett-Packard 8452A diode array spectrometer using a quartz crystal cell with a Teflon cap. Near-IR measurements were taken on a Cary 14 spectrophotometer using a quartz crystal cell with a Teflon cap. IR measurements were obtained using a Bio Rad Excalibur FTS 3000 with a KBr solution cell. The ^1H NMR assignments for **3.1** were determined by a combination of T_1 relaxation rates and single scan integrations.

3.5.2 Magnetic measurements

Measurements were recorded using a Quantum Designs SQUID magnetometer running MPMSR2 software (Magnetic Property Measurement System Revision 2). Data

were recorded at 5000 G. Samples were suspended in the magnetometer in plastic straws sealed under nitrogen with Lilly No. 4 gel caps. Each measurement was performed on samples that had been recently subjected to combustion analysis to verify their purity. Loaded samples were centered within the magnetometer using the DC centering scan at 35 K and 5000 gauss. Data were acquired at 2-10 K (one data point every 2 K), 10-60 K (one data point every 5 K), 60-310 K (one data point every 10 K).

The magnetic susceptibility was adjusted for diamagnetic contributions using the constitutive corrections of Pascal's constants. The molar magnetic susceptibility (χ_m) was calculated by converting the calculated magnetic susceptibility (χ) obtained from the magnetometer to a molar susceptibility (using the multiplication factor {(molecular weight)/[(sample weight)(Field Strength)]}). Curie-Weiss behavior was verified by a plot of χ_m^{-1} versus T. Data were analyzed using Eqs. 3.5 and 3.6. Average magnetic moments were taken from the average of magnetic moments from the ranges indicated in the Experimental Section for each complex. The Weiss constant (θ) was taken as the x-intercept of the plot of χ_m^{-1} versus T. Error bars were established at 95% confidence using regression analysis or taking two standard deviations from the mean. Solution magnetic moments were measured by the method of Evans and were adjusted for diamagnetic contributions using the constitutive corrections of Pascal's constants.

$$\chi_m = \frac{\chi M}{mG} \quad (3.5) \qquad \mu_{eff} = \sqrt{7.997 \chi_m T} \quad (3.6)$$

Averaged *g*-factors can be extracted from the susceptibility data, assuming zero orbital contributions, using the following equation:

$$\chi_m = \frac{Ng^2\beta^2}{3kT}(S(S+1)) \quad (3.7)$$

3.5.3 EPR measurements

X-band EPR spectra were obtained on a Bruker EMX spectrometer equipped with a rectangular cavity working in the TE_{102} mode. Variable temperature measurements were conducted with an Oxford continuous-flow helium cryostat (temperature range 3.6-300 K). Accurate frequency values were provided by a frequency counter built in the microwave bridge. Solution spectra were acquired in toluene for all of the complexes. Sample preparation was performed under a nitrogen atmosphere, *particularly* important for handling the low spin complexes **3.1**, **3.2**, and **3.3**.

EPR simulations for the monomers were performed with the program WINEPR *SimFonia* (Version 1.25, Bruker Analytische Messtechnik GmbH); this software is based on second-order perturbation solution of the spin Hamiltonian: $H = H \cdot g \cdot S + \Sigma S \cdot A \cdot I$. For the dimers, the absolute values of the spin-Hamiltonian parameters were extracted from simulations of the EPR spectra. Calculations were carried out on a PC using FORTRAN code based on Gladney's general EPR fitting program[40] and adapted for simulations of EPR spectra of randomly oriented spin triplets. Transition fields and corresponding average transition moments[41] were computed in the magnetic field domain by matrix diagonalization of the $S = 1$ spin Hamiltonian.

$$\hat{H} = \beta(g_z H_z S_z + g_x H_x S_x + g_y H_y S_y) + D(S_z^2 - 3/2) + E(S_x^2 - S_y^2) \quad (3.8)$$

D and E are defined in terms of the components of the diagonal fine-structure tensor as follows:

$$D_{zz} = 2D/3; \quad D_{xx} = -D/3; \quad D_{yy} = (-D/3) - E \quad (3.9)$$

Instrumental parameters for the spectra shown are as follows:

For [$PhBP_3$]CoI (**3.1**) in Figure 3.6: (A) EPR spectrum of a glassy toluene solution of [$PhBP_3$]CoI at 17 K. Instrumental parameters: ν = 9.477 GHz, modulation frequency = 100 kHz, modulation amplitude = 4 G, microwave power = 0.51 mW, conversion time = 81.92 ms, time constant = 20.48 ms, 3 scans. $g \approx 2$ region and spectral assignment; $g_{\|}$ and $A_{\|}$ were estimated by simulating the EPR spectrum (inset). (B) EPR spectrum of a glassy toluene solution of [$PhBP_3$]CoI in toluene-d_8 at 15 K. Instrumental parameters: ν = 9.476 GHz, modulation frequency = 100 kHz, modulation amplitude = 3 G, microwave power = 0.202 mW, conversion time = 81.92 ms, time constant = 20.48 ms, sweep time = 83.9 s, 3 scans.

For ([$PhBP_3$]Co(μ-Br))$_2$ (**3.2**) in Figure 3.7: (A) EPR spectrum of a polycrystalline sample of ([$PhBP_3$]Co(μ-Br))$_2$ (15 K). Instrumental parameters: ν = 9.480 GHz, modulation frequency = 100 kHz, modulation amplitude = 4 G, microwave power = 1.01 mW, conversion time = 163.84 ms, time constant = 40.96 ms, 10 scans. (B) EPR spectrum of a glassy toluene solution of ([$PhBP_3$]Co(μ-Br))$_2$ at 12 K. Instrumental parameters: ν = 9.472 GHz, modulation frequency = 100 kHz, modulation amplitude = 4 G, microwave power = 0.101 mW, 1 scan. (C) EPR spectrum of a glassy toluene solution of ([$PhBP_3$]Co(μ-Br))$_2$ at 50 K. $g_{\|}$ and $A_{\|}$ were estimated by simulating the EPR spectrum. Instrumental parameters: ν = 9.477 GHz, modulation frequency = 100 kHz, modulation amplitude = 5 G, microwave power = 2.02 mW, conversion time = 20.48 ms, time constant = 5.12 ms, 20 scans. (D) Series of EPR spectra for a polycrystalline sample of ([$PhBP_3$]Co(μ-Br))$_2$ plotted to show the temperature dependence of the EPR signal.

The signal amplitude increases as the temperature decreases, suggestive of a ferromagnetic triplet ground state.

For $([PhBP_3]Co(\mu\text{-}Cl))_2$ (**3.3**) in Figure 3.9: (A) EPR spectrum of a polycrystalline sample of $([PhBP_3]Co(\mu\text{-}Cl))_2$ at 3.6 K. Instrumental parameters: ν = 9.477 GHz, modulation frequency = 100 kHz, modulation amplitude = 4 G, microwave power = 0.101 mW, conversion time = 163.84 ms, time constant = 40.96 ms, 4 scans. (B) EPR spectrum of a glassy toluene solution of $([PhBP_3]Co(\mu\text{-}Cl))_2$ at 12 K. Instrumental parameters: ν = 9.476 GHz, modulation frequency = 100 kHz, modulation amplitude = 4 G, microwave power = 0.202 mW, conversion time = 163.84 ms, time constant = 40.96 ms, 7 scans. The inset $g \approx 2$ region showing resolved cobalt hyperfine structure; $g_{\|}$ and $A_{\|}$ were estimated by simulating the EPR spectrum.

3.5.4 DFT calculations

A geometry optimization was performed for complex **3.1** using Jaguar (Version 4.1) starting from coordinates based on the solid-state structure that had been determined by X-ray diffraction. No symmetry constraints were imposed, and the calculation was performed on a doublet electronic state. The method used was B3LYP with LACVP** as the basis set (modified to LACVP**++ for the boron atom). Optimization was considered converged when energy changes in successive iterations fell below 0.3 kcal/mol. It should also be noted that convergence was also achieved for a system when the geometry was optimized assuming a quartet ground state.

3.5.5 Starting materials and reagents

The preparation of $[PhBP_3]Tl$ has been previously reported. $TlO\text{-}2,6\text{-}Me_2Ph$ was prepared according to a literature procedure.[42] The reagents CoI_2, $CoBr_2$, $CoCl_2$, CO, O_2,

KBr, NaCl, and $TlPF_6$ were purchased from commercial vendors and used without further purification.

3.5.6 Synthesis of compounds

Synthesis of [PhBP$_3$]CoI, 3.1. A benzene solution (50 mL) of the thallium reagent, [PhBP$_3$]Tl, (0.356 g, 0.400 mmol) was added to a stirring suspension of CoI_2 (0.250 g, 0.799 mmol) in benzene (20 mL). After stirring at ambient temperature for 24 h, the resulting green solution was filtered through diatomaceous earth, concentrated in vacuo (50% original volume), and filtered through diatomaceous earth once again. Vapor diffusion of petroleum ether into the resulting green filtrate afforded the pure crystalline product (0.317 g, 91.1%), which was analyzed: ^{1}H NMR (C_6D_6, 300 MHz): δ 22.3 (6 H, T_1 = 2.4 ms, PhB(C*H*$_2$PPh$_2$)$_3$), 10.8 (12 H, T_1 = 23.6 ms, *meta* P(C$_6$*H*$_5$)$_2$), 7.7 (2 H, T_1 = 40.5 ms, *ortho* B(C$_6$*H*$_5$)), 7.5 (3 H, T_1 = 205 ms, *meta* and *para* B(C$_6$*H*$_5$)), 4.3 (12 H, T_1 = 1.2 ms, *ortho* P(C$_6$*H*$_5$)$_2$), 2.2 (6 H, T_1 = 46.7 ms, *para* P(C$_6$*H*$_5$)$_2$). IR (cm^{-1}): 1433, 1091, 739. UV-vis (C_6H_6) λ_{max}, nm (ε): 638 (1112), 738 (627). SQUID (solid - average 30-220K): $\chi_m T$ = 0.88 cm^3 K mol^{-1}, θ = -1.43 K. Evans Method (C_6D_6): 2.76 μ_B. Anal. Calcd for $C_{45}H_{41}BCoIP_3$: C, 62.03; H, 4.74. Found: C, 61.76; H, 4.75.

Synthesis of ([PhBP$_3$]Co(μ-Br))$_2$, 3.2. A benzene solution (50 mL) of the thallium reagent, [PhBP$_3$]Tl (0.507 g, 0.570 mmol), was added to a stirring suspension of $CoBr_2$ (0.250 g, 1.14 mmol) in benzene (20 mL). After stirring at ambient temperature for 24 h, the resulting green solution was filtered through diatomaceous earth. The filtrate was pumped to dryness to leave a purple powder that was redissolved in benzene (20 mL), filtered over diatomaceous earth, and again thoroughly dried in vacuo. A UV-vis spectrum of this powder suggested a mixture of products. The powder was redissolved in

benzene (5 mL) and filtered over a fine sintered-glass frit. A microcrystalline purple powder precipitated from the solution; this powder (0.132 g, 28.1%) was dried and analyzed: ^{1}H NMR (C_6D_6, 300 MHz): δ 26.7, 11.0, 7.6, 7.4, 4.2, 2.2. UV-vis (C_6H_6) λ_{max}, nm (ε): 612 (1773), 718 (958). SQUID (solid, average 10-100 K): $\chi_m T$ = 0.39 cm^3 K mol^{-1}, θ = -1.48 ± 0.49 K; (solid, average 110-310 K) $\chi_m T$ = 0.56 cm^3 K mol^{-1}. Evans Method (C_6D_6, calculated for a monomer): 2.6 μ_B. Anal. Calcd for $C_{90}H_{82}B_2Br_2Co_2P_6$: C, 65.56; H, 5.01. Found: C, 65.23; H, 4.87. The sample used for the EPR and SQUID measurements, which was recrystallized two more times, analyzed as follows: C, 65.70; H, 5.04.

Synthesis of ([PhBP$_3$]Co(μ-Cl))$_2$, 3.3. A benzene solution (50 mL) of the thallium reagent, [PhBP$_3$]Tl (0.857 g, 0.963 mmol), was added to a stirring suspension of $CoCl_2$ (0.250 g, 1.93 mmol) in benzene (20 mL). After stirring at ambient temperature for 24 h, the resulting green solution was filtered through diatomaceous earth. The filtrate was dried in vacuo to a purple powder that was then redissolved in benzene (20 mL), filtered over diatomaceous earth, and again thoroughly dried. The resulting purple powder was redissolved in benzene (5 mL) and filtered over a fine sintered-glass frit; this caused a microcrystalline purple powder to precipitate from solution. The dried powder (0.195 g, 25.9%) was analyzed: ^{1}H NMR (C_6D_6, 300 MHz): δ 31.9, 11.2, 7.7, 7.4, 3.9, 2.2. UV-vis (C_6H_6) λ_{max}, nm (ε): 594 (1507), 712 (724). SQUID (solid - average 10-100 K): $\chi_m T$ = 0.76 cm^3 K mol^{-1}, θ = -3.13 ± 0.67 K; (solid - average 110-310 K) $\chi_m T$ = 0.97 cm^3 K mol^{-1}. Evans Method (C_6D_6, calculated for a monomer): 2.8 μ_B. Anal. Calcd for $C_{90}H_{82}B_2Cl_2Co_2P_6$: C, 69.30; H, 5.30. Found: C, 68.14; H, 5.18. The sample used for the

EPR and SQUID measurements, which was recrystallized two more times, analyzed as follows: C, 69.56; H, 5.36.

Alternative Preparation for 3.2 and 3.3. Thallium hexafluorophosphate (0.090 g, 0.26 mmol) was added to a stirring THF (20 mL) solution of **3.1** (0.201 g, 0.231 mmol). A yellow powder precipitated within 5 min and was subsequently removed by filtration through diatomaceous earth. NaCl (0.26 g, 4.4 mmol) was added to the filtrate, and the reaction solution was allowed to stir for 24 h. The above process was then repeated with additional $TlPF_6$ and NaCl. After another 24 h, the salts were removed by filtration; a UV-vis spectrum of the product solution indicated that **3.1** had been fully consumed, and the spectrum matched that of **3.3**. The solution was concentrated in vacuo to 50% of its original volume and allowed to stand for 24 h. White precipitate (NaCl) was removed by filtration, and the green solution was concentrated to dryness, redissolved in benzene, and once again allowed to stand for 12 h. Repeated filtration through diatomaceous earth ensured complete removal of salts. The final product was obtained by drying thoroughly in vacuo to afford purple **3.3** as a fine powder (0.159 g, 88.6%). An analogous protocol was effective for converting **3.1** to **3.2**, in this case using KBr instead of NaCl. Both UV-vis and ^{1}H NMR spectroscopies are useful in monitoring the metathesis procedure to ensure complete conversion.

Synthesis of [$PhBP_3$]CoO(2,6-dimethylphenyl), 3.4. A THF solution (5 mL) of the thallium reagent Tl-O-2,6-dimethylphenyl (0.0433 g, 0.133 mmol) was added to a stirring solution (10 mL) of **3.1** (0.116 g, 0.133 mmol). A yellow precipitate (TlI) formed within 15 min and was removed by filtration through diatomaceous earth. The remaining brown solution was stirred overnight. The reaction volatiles were removed in vacuo and the

resulting brown powder was redissolved in benzene. The benzene was lyophilized to thoroughly remove any remaining THF. The resulting fine powder was filtered once more through diatomaceous earth as a benzene (3 mL) solution. Vapor diffusion of petroleum ether into this benzene solution afforded the red-brown, crystalline product (0.067 g, 58.7% yield) that was analyzed. ^{1}H NMR (C_6D_6, 300 MHz): δ 67.0, 52.4, 17.9, 12.4, 11.6, 11.0, 9.0, 8.45, 7.80, 7.45, 7.06, -3.4, -6.5, -62.2. UV-vis (C_6H_6) λ_{max}, nm: 534 (1740), 752 (624). SQUID (solid, average 30-310 K): $\chi_m T$ = 2.41 cm^3 K mol^{-1}, θ = 7.48 K. Evans Method (C_6D_6): 4.4 μ_B. Anal. Calcd for $C_{53}H_{50}BCoP_3O$: C, 73.54; H, 5.82. Found: C, 73.32; H, 5.95.

Synthesis of [PhB(CH$_2$P(O)Ph$_2$)$_2$(CH$_2$PPh$_2$)]CoI, 3.5. A 100 mL Schlenk flask with a Teflon stir bar was charged with a benzene (30 mL) solution of **3.1** (0.278 g, 0.319 mmol) and stirred at room temperature. Oxygen (7.8 mL at 1 atm, 0.32 mmol) was added to the reaction vessel via syringe through a rubber septum. After 4 h, the solution, which had turned bright blue, was dried in vacuo to a fine blue powder. Washing this powder with petroleum ether (3 x 10 mL) and concentrating it to dryness afforded the final product (0.225 g, 79.1% yield) that was analyzed. ^{1}H NMR (C_6D_6, 300 MHz): δ 16.2, 13.8, 10.1, 9.47, 9.28, 7.90, 7.09, -2.1. UV-vis (C_6H_6) λ_{max}, nm (ε): 590 (450), 642 (461), 682 (520). IR (cm^{-1}): 1435, 1126, 1095, 1071, 752. SQUID (solid, average 30-310 K): $\chi_m T$ = 2.34 cm^3 K mol^{-1}, θ = -2.74 K. Evans Method (C_6D_6): 4.4 μ_B. Anal. Calcd for $C_{45}H_{41}BCoIP_3O_2$: C, 59.83; H, 4.57. Found: C, 59.62; H, 4.80.

Synthesis of [PhBP$_3$]Co(Br)(CO), 3.6. A 100 mL Schlenk flask with a Teflon stir bar was charged with a benzene (30 mL) solution of **3.2** (0.107 g, 0.0649 mmol) and stirred at room temperature until completely dissolved. Carbon monoxide (3.2 mL at 1 atm,

0.13 mmol) was added via syringe. After 4 h, the solution was frozen and the benzene was lyophilized, leaving a fine green powder. Washing this powder with petroleum ether (3 x 10 mL) and concentrating it to dryness afforded pure product (0.099 g, 89% yield). ^{1}H NMR (C_6D_6, 300 MHz): δ 13.8, 10.2, 8.1, 7.9, 7.5, 6.0. UV-vis (THF) λ_{max}, nm (ε): 676 (870). IR (THF, KBr solution cell, cm^{-1}): 2030. SQUID (solid – average 10 – 310 K): $\chi_m T$ = 0.50 cm^3 K mol^{-1}. EPR (THF, 100 K): $g_{\parallel}$ = 2.30, $A_{\parallel(Co)}$ = 33 gauss, $A_{\parallel(P)}$ = 35 gauss, $g_{\perp}$ = 2.05, $A_{\perp(Co)}$ = 17 gauss, $A_{\perp(P)}$ = 35 gauss. Anal. Calcd for $C_{46}H_{41}BBrCoP_3O$: C, 64.82; H, 4.85. Found: C, 65.03; H, 5.59.

3.5.7 X-ray experimental information

The general X-ray experimental procedure was performed according to section 2.4.4. Crystallographic information is provided in Table 3.1.

Table 3.1. X-ray diffraction experimental details for [$PhBP_3$]CoI (**3.1**), ([$PhBP_3$]Co(μ-Br))$_2$ (**3.2**), ([$PhBP_3$]Co(μ-Cl))$_2$ (**3.3**), and [$PhBP_3$]CoO(2,6-Me_2-Ph) (**3.4**).

	[$PhBP_3$]CoI, (**3.1**)	([$PhBP_3$]Co(μ-Br))$_2$ (**3.2**)
Chemical formula	$C_{45}H_{41}BCoIP_3 \cdot ½\ C_6H_6$	$C_{90}H_{82}B_2Br_2Co_2P_6$
Formula weight	910.38	1648.68
T (ºC)	-177	-177
λ (Å)	0.71073	0.71073
a (Å)	22.5443(17)	22.214(3)
b (Å)	12.7044(9)	19.286(3)
c (Å)	29.526(2)	18.008(3)
α (º)	90	90
β (º)	90.230(2)	90
γ (º)	90	90
V (Å^3)	8456.6(11)	7715.0(19)
Space group	$P2_1/c$	*Pbcn*
Z	8	4
Dcalcd (g/cm^3)	1.430	1.419
μ(cm^{-1})	12.74	16.37
R1, wR2 (I>2σ(I))[a]	0.0899, 0.0843	0.1432, 0.1012

[a] $R1 = \Sigma\ |\ |F_o| - |F_c|\ |\ /\ \Sigma\ |F_o|$, $wR2 = \{\ \Sigma\ [\ w(F_o^2 - F_c^2)^2\ ]\ /\ \Sigma\ [\ w(F_o^2)^2\ ]\ \}^{1/2}$

Table 3.1. (cont.)

	$([PhBP_3]Co(\mu\text{-}Cl))_2$ (**3.3**)	$[PhBP_3]CoO(2,6\text{-}Me_2\text{-}Ph)$ (**3.4**)
Chemical formula	$C_{90}H_{82}B_2Co_2Cl_2P_6 \cdot 2\ C_6H_6$	$C_{53}H_{50}BCoOP_3$
Formula weight	1715.97	865.58
T (ºC)	-177	-177
λ (Å)	0.71073	0.71073
a (Å)	26.340(3)	17.245(2)
b (Å)	13.2151(14)	16.484(1)
c (Å)	28.015(3)	16.494(1)
α (º)	90	90
β (º)	117.909(2)	109.181(1)
γ (º)	90	90
V ($Å^3$)	8617.6(16)	4428.3(6)
Space group	$P2_1/c$	*Cc*
Z	4	4
Dcalcd (g/cm^3)	1.323	1.298
μ(cm^{-1})	6.07	5.35
R1, wR2 (I>2σ(I))	0.0995, 0.0724	0.0454, 0.0624

References cited

1) Lippard, S. J.; Berg, J. M. *Principles of Bioinorganic Chemistry;* University Science Books: Mill Valley, CA, 1994; Chapter 12.

2) a) Halpern, J. *Science* **1985**, *227*, 869-875. b) Geno, M. K.; Halpern, J. *J. Am. Chem. Soc.* **1987**, *109*, 1238-1240. c) Perutz, M. F.; Fermi, G.; Luisi, B.; Shanon, B.; Liddington, R. C. *Acc. Chem. Res.* **1987**, *20*, 309-321. d) Raphael, A. L.; Gray, H. B.

J. Am. Chem. Soc. **1991**, *113*, 1038-1040. e) Garret, T. P. J.; Glingeleffer, D. J.; Guss, J. M.; Rogers, S. J.; Freeman, H. C. *J. Biol. Chem.* **1984**, *259*, 2822-2825.

3) Schultz, B. E.; Gheller, S. F.; Muetterties, M. C.; Scott, M. J.; Holm, R. H. *Acc. Chem. Res.* **1986**, *19*, 363-370.

4) Sellmann, D.; Sutter, J. *Acc. Chem. Res.* **1997**, *30*, 460-469.

5) a) Everett, G. W.; Holm, R. H. *J. Am. Chem. Soc*. **1965**, *87*, 5266-5267. b) Cotton, F. A.; Soderberg, R. H. *J. Am. Chem. Soc.* **1962**, *84*, 872-873.

6) Stereochemical tuning of 4-coordinate structure types of cobalt(II), and the ground spin state consequences of such tuning, has been recently described: Jaynes, B. S.; Doerrer, L. H.; Liu, S.; Lippard, S. J. *Inorg. Chem*. **1995**, 34, 5735-5744.

7) a) Solomon, E. I.; Rawlings, J.; McMillin, J. R.; Stephens, P. J.; Gray, H. B. *J. Am. Chem. Soc*. **1976**, *98*, 8046-8048. b) Bertini, I.; Luchinat, C. *Acc. Chem. Res.* **1983**, *16*, 272-279. c) Bertini, I.; Lanini, G.; Luchinat, C. *J. Am. Chem. Soc*. **1983**, *105*, 5116-5118. d) Khalifah, R. G.; Rogers, J. I.; Harmon, P.; Morely, P. J.; Carroll, S. B. *Biochemistry* **1984**, *23*, 3129-3136. e) Briganti, F.; Pierattelli, R.; Scozzafava, A.; Supuran, C. T. *Eur. J. Med. Chem*. **1996**, *31*, 1001-1010.

8) Cobalt complexes supported by tris(pyrazolyl)borate ligands have been studied extensively. For recent examples, see: a) Detrich, J.; Koneèny-Vetter, W. M.; Doren, D.; Rheingold, A. L.; Theopold, K. H. *J. Am. Chem. Soc*. **1996**, *118*, 1703-1712. b) Jewson, J. D.; Liable-Sands, L. M.; Yap, G. P. A.; Rheingold, A. L.; Theopold, K. H. *Organometallics* **1999**, *18*, 300-305. c) Thyagarajan, S.; Incarvito, C. D.; Rheingold, A. L.; Theopold, K. H. *Chem. Commun*. **2001**, 2198-2199.

9) Cobalt complexes supported by tris(thioether)borate ligands have been studied recently. See: Schebler, P.; Mondimutsira, B.; Riordan, C. G.; Liable-Sands, L. M.; Incarvito, C. D.; Rheingold, A. L. *J. Am. Chem. Soc*. **2001**, *123*, 331-332.

10) a) Peters, J. C.; Feldman, J. D.; Tilley, T. D. *J. Am. Chem. Soc*. **1999**, *121*, 9871-9872. b) Barney, A. A.; Heyduk, A. F.; Nocera, D. G. *Chem. Commun*. **1999**, 2379-2380.

11) a) Benelli, C.; DiVaira, M.; Noccioli, G.; Sacconi, L. *Inorg. Chem*. **1977**, *16*, 182-187. b) Ghilardi, C.; Midollina, S.; Orlandini, A.; Sacconi, L. *Inorg. Chem*. **1980**, *19*, 301-306. c) Dapparto, P.; Midollini, S.; Orlandini, A.; Sacconi, L. *Inorg. Chem*. **1976**, *15*, 2768-2744.

12) For recent papers dealing with (triphos)Co^{2+} chemistry, see: a) Heinze, K.; Huttner, G.; Walter, O. *Eur. J. Inorg. Chem*. **1999**, 593-600. b) Heinze, K.; Huttner, G.; Schober, P. *Eur. J. Inorg. Chem*. **1998**, 183-189. c) Heinze, K.; Huttner, G.; Zsolnai, L. *Z. Naturforsch. B* **1999**, *54*, 1147-1154. d) Winterhalter, U.; Zsolnai, L.; Kirscher, P.; Heinz, K.; Huttner, G. *Eur. J. Inorg. Chem*. **2001**, 89-103. e) Rupp, R.; Huttner, G.; Kirscher, P.; Soltek, R.; Büchner, M. *Eur. J. Inorg. Chem*. **2000**, 1745-1757.

13) The abbreviation *triphos* is used herein to designate the tripodal, tridentate ligand $RC(CH_2PPh_2)_3$ (R = alkyl or aryl). This abbreviation is often used to delineate tridentate phosphines of the type $PhP(CH_2PPh_2)_2$. In this manuscript, we restrict our use of the term *triphos* to represent the former ligand class.

14) Hewertson, W.; Watson, H. R. *J. Chem. Soc*. **1962**, 1490-1494.

15) a) Lu, C. C.; Peters, J. C. *J. Am. Chem. Soc*. **2002**, *124*, 5273-5273. b) Thomas, J. C.; Peters, J. C. *J. Am. Chem. Soc*. **2001**, *123*, 5100-5101. c) Jenkins, D. M.; Betley, T. A.; Peters, J. C. *J. Am. Chem. Soc*. **2002**, *124*, 11238-11239. Also see Chapter 5.

16) Shapiro, I. R.; Jenkins, D. M.; Thomas, J. C.; Day, M. W.; Peters, J. C. *Chem. Commun*. **2001**, 2152-2153. Also see Chapter 2.

17) For a lucid discussion of cobalt(II) EPR spectroscopy, see: Bencini, A.; Gatteschi, D. *Trans. Metal Chem.* **1982**, *8*, 97-119.

18) A thorough discussion of the electronic structure of cobalt(II) systems in four-, five-, and six-coordinate geometries has been provided by Lever: Lever, A. B. P. *Inorganic Electronic Spectroscopy*, 2nd ed.; Elsevier: New York, 1984; pp 480-505.

19) a) Sacconi, L.; Midollini, S. *J. Chem. Soc., Dalton. Trans*. **1972**, 1213-1216. b) Dapporto, P.; Midollini, S.; Sacconi, L. *Inorg. Chem*. **1975**, *14*, 1643-1650. c) Mealli, C.; Midollini, S.; Sacconi, L. *Inorg. Chem*. **1975**, *14*, 2513-2521. d) Ghilardi, C. A.; Midollini, S.; Sacconi, L. *J. Organomet. Chem*. **1980**, *186*, 279-287.

20) Heinze, K.; Huttner, G.; Zsolnai, L.; Schober, P. *Inorg. Chem*. **1997**, *36*, 5457-5469.

21) Complex **3.1** contained two crystallographically independent molecules in the asymmetric unit. For brevity, only one of the molecules is explicitly discussed in the text.

22) Reinaud, O.; Rheingold, A.; Theopold, K. *Inorg. Chem.* **1994**, *33*, 2306-2308.

23) For a discussion of high spin [Tt$^{tert\text{-butyl}}$]CoCl see: Schebler, P.; Riordan, C.; Guzei, I.; Rheingold, A. *Inorg. Chem.* **1998**, *37*, 4754-4755.

24) Casey, A. T.; Mitra, S. *Theory and Application of Molecular Paramagnetism* (Bourduaux, E. A., Mulay, N. L., Eds.); Wiley: New York, 1976.

25) Cotton, F. A.; Wilkinson, G. *Advanced Inorganic Chemistry*, 5th ed.; Wiley: New York, 1988; p 729.

26) For relevant references that deal with four-coordinate cobalt(II) in approximate C_3 or C_{3v} symmetry, see the following: a) Garrett, B. B.; Goedken, V. L.; Quagliano, J. V. *J. Am. Chem. Soc*. **1970**, *92*, 489-493. b) Bertini, I.; Gatteschi, D.; Mani, F. *Inorg. Chim. Acta* **1973**, *7*, 717-720. c) Gerloch, M.; Hanton, L. R. *Inorg. Chem*. **1980**, *19*, 1692-1698. d) Gerloch, M.; Manning, M. R. *Inorg. Chem*. **1981**, *20*, 1051-1056. e) Banci, L.; Benelli, C.; Gatteschi, D.; Mani, F. *Inorg. Chem*. **1982**, *21*, 1133-1136.

27) Kahn, O. *Molecular Magnetism*; VCH Publishers: New York, 1993; pp 1-10.

28) a) Sur, S. K. *J. Magn. Reson*. **1989**, *82*, 169-173. b) Evans, D. F. *J. Chem. Soc*. **1959**, 2003-2005.

29) a) Sinn, E. *Coord. Chem. Rev*. **1970**, *5*, 313-347, and references therein. b) Ball, P. W. *Coord. Chem. Rev*. **1969**, *4*, 361-383. c) Kato, M.; Jonassen, H. B.; Fanning, J. C. *Chem. Rev*. **1964**, *64*, 99-128.

30) Ghilardi, C. A.; Mealli, C.; Midollini, S.; Nefedov, V. I.; Orlandini, A.; Sacconi, L. *Inorg. Chem*. **1980**, *19*, 2454-2462.

31) Note that the solution susceptibilities for **3.2** and **3.3** are calculated by the Evans method assuming a *monomeric* formulation for each complex.

32) Sealy, R.; Hyde, J. S.; Antholine, W. E. *Modern Physical Methods in Biochemistry* (Neuberger, A., Van Deenen, L. L. M., Eds.); Elsevier: New York, 1985; p 69.

33) Superhyperfine coupling to phosphorous in a five-coordinate cobalt(II) phosphine complex has been treated previously. See: Stelzer, O.; Sheldrick, W. S.; Subramanian, J. *J. Chem. Soc., Dalton Trans*. **1976**, 966-970.

34) a) Pilbrow, J. R. *Transition Ion Electron Paramagnetic Resonance*; Clarendon Press: Oxford, 1990. b) Aasa, R.; Vänngård, T. *J. Magn. Resonance* **1975**, *19*, 308-315.

35) Gatteschi, D. *J. Mol. Catal.* **1985**, *23*, 145-150.

36) Osmometric measurements to determine the solution molecular weights of **3.2** and **3.3** by the method of Signer were vitiated due to the tendency of these species to precipitate from toluene and benzene solution at moderate concentrations.

37) Sacconi, L.; Ciampolini, M.; Speroni, C. P. *Inorg. Chem.* **1965**, *4*, 1116-1119.

38) Nicolini, M.; Pecile, C.; Turco, A. *J. Am. Chem. Soc.* **1965**, *87*, 2379-2384.

39) Orgel, L. E. *An Introduction to Transition-Metal Chemistry*; Wiley: New York, 1960; p 174.

40) Swalen, J. D.; Gladney, H. M. *IBM J. Res. Dev.* **1964**, *8*, 515-526.

41) van Veen, G. *J. Magn. Resonance* **1978**, *30*, 91-109.

42) Jazdzewski, B. A.; Holland, P. L.; Pink, M.; Young, V. G.; Spencer, D. J. E.; Tolman, W. B. *Inorg. Chem.* **2001**, *40*, 6097-6107.

Chapter 4: Spin state tuning at pseudotetrahedral d^7 ions: examining the structural and magnetic phenomena of 4-coordinate $[BP_3]Co^{II}$-X systems

The text of this chapter is reproduced in part with permission from:

Jenkins, D. M.; Peters, J. C. *J. Am. Chem. Soc.* **2003**, *125*, 11162-11163.

4.1 Introduction

Stereochemical and electronic structure phenomena of the first row transition ions are central issues in coordination chemistry. These properties are strongly coupled, and the experimental determination of one often intimates a great deal about the other. For instance, knowledge of a complex's solid-state crystal structure can reveal its electronic ground state configuration. The four-coordinate first row transition ions Fe(II), Co(II), and Ni(II) are exemplary. Each is high spin when approximately tetrahedral, occupying $S = 2$, $S = 3/2$, and $S = 1$ ground states, respectively. By contrast, when these same ions feature square planar structures, low spin (Co(II) and Ni(II)),[1] or intermediate spin (Fe(II)),[2] ground states are manifest. Knowledge of the interplay between stereochemistry and electronic structure thus lies at the heart of our ability to anticipate magnetic phenomena from key structural parameters. Indeed, the assignment of local stereochemical environments within complex metalloenzyme active sites is often achieved by the interpretation of spectroscopic data.[3,4] Moreover, chemical reactivity can be dramatically affected by subtle spin-state/stereochemical relationships, as in numerous biocatalytic transformations.[5] Inorganic complexes that expose new insights regarding the relationship between stereochemistry and electronic structure are therefore of broad concern.

From the perspective of Ligand Field Theory (LFT), one of the best-studied transition ions is Co^{2+}.[6] The most prominent coordination numbers encountered for this ion are four through six. Six coordinate pseudooctahedral species typically populate high spin configurations, though several low spin systems under the influence of unusually strong ligand fields have been characterized.[7] A host of six-coordinate systems also

exhibit spin crossover phenomena in the solid-state.[8] Sandwich and mixed-sandwich complexes (e.g., $[Cp]_2Co$, $[Cp]CoL_3^+$, [Tp]Co[Cp]; [Tp] = tris(pyrazolyl)borate) constitute a spectroscopically and magnetically rich subset of the octahedral Co(II) family.[9] Five-coordinate Co^{2+} ions exhibit both trigonal bipyramidal and square pyramidal limiting structures. In contrast to the octahedral systems, these five-coordinate ions are most commonly low spin,[10] though again, both spin forms are well-documented, as are systems that exhibit spin crossover in the solid-state.[11,12] Four-coordinate Co(II) systems are nominally either pseudotetrahedral or square planar, though a great many species are known to adopt structures that are highly distorted from these limiting structure types.[13] Nevertheless, prior to recent studies undertaken by our laboratory,[14,15,16] all of the four-coordinate cobalt(II) systems that were known to exhibit low spin ground state configurations were classified as square planar. Ions of approximate tetrahedral geometries, whether nearly perfect T_d symmetry (e.g., $CoCl_4^{2-}$) or species better described as pseudotetrahedral, distorted tetrahedral, or trigonal pyramidal, without exception had been classified as high spin.[17,18,19,20]

Our group has been exploring the nature of highly covalent pseudotetrahedral first row transition ions (L_3M-X) supported by relatively strong field tris(phosphino)borate ligands ($[BP_3]M$-X). The generic abbreviation used to denote these anionic tris(phosphino)borate ligands is $[BP_3]$. $[PhBP_3]$ and $[PhBP^{iPr}_3]$ designate the $[PhB(CH_2PPh_2)_3]^-$ and $[PhB(CH_2P^iPr_2)_3]^-$ anions, respectively (Figure 4.1). These $[BP_3]M$-X systems are striking in their propensity to populate low spin electronic configurations. For example, we have characterized a series of L_3Fe-N_x species that can accommodate low spin ground state configurations for cases where (i) the iron center is

either di-,[21] tri-,[22,23] or tetravalent[24] (i.e., d^6, d^5, or d^4), and (ii) a favorable interaction exists with the N_x-type ligand that is characterized by one sigma and two pi bonds (e.g., $S = 0$, $\{[PhBP_3]Fe^{II}{\equiv}NR\}^-$; S = ½, $[BP_3]Fe^{III}{\equiv}NR$;[22,23] $S = 0$, $[PhBP^{iPr}_3]Fe{\equiv}N$). When the degree of π-bonding is attenuated, as is the situation for the divalent halides $[BP_3]Fe\text{-}X$,[22,25] amides $[PhBP_3]Fe\text{-}NRR'$,[26] alkyls $[PhBP^{iPr}_3]Fe\text{-}R$,[27] and diazenidos $[PhBP^{iPr}_3]Fe\text{-}N{=}NR$, rigorously high spin ($S = 2$) ground states are invariably populated. By contrast, several divalent cobalt ions supported by these $[BP_3]$ platforms populate low spin (S = ½) ground state electronic configurations, even in the absence of a strongly π-bonding X ligand. For example, we have reported that in solution the simple halides $[PhBP_3]CoX$ (X = I, Br, Cl) each exhibit a doublet ground state that is predominantly populated at room temperature. The observed ground spin states of these complexes contrasts not only the numerous tetrahedral and distorted tetrahedral complexes studied previously, but also tripodal borate Co(II) systems that are structurally very similar. These systems include Theopold's[28] and Moro-oka's[29] S = 3/2 [Tp'']CoX ([Tp''] = hydrotris(3-isopropyl-5-methylpyrazoly1)borate species and Riordan's[30] S = 3/2 $[Tt^{tert\text{-}butyl}]CoX$ ($[Tt^{tert\text{-}butyl}] = [PhB(CH_2S^tBu)_3]^-$) derivatives. Moreover, a number of peculiar observations have been reported within the $[BP_3]Co^{II}\text{-}X$ family. For instance, a complex featuring an aryloxide X-type ligand, $[PhBP_3]CoO(2,6\text{-}Me_2\text{-}Ph)$ (**3.4**), exhibits a quartet rather than a doublet ground state. In addition, iodide and chloride complexes of the $[PhBP^{iPr}_3]$ anion ($[PhBP^{iPr}_3]CoI$ and $[PhBP^{iPr}_3]CoCl$) appear to populate rigorously high spin ground states. Each of these observations is somewhat counter-intuitive. The $[PhBP^{iPr}_3]$ anion is more electron-releasing than $[PhBP_3]$, and on the basis of electronic considerations its Co^{2+} complexes should be more likely to populate the low spin

configuration than [$PhBP_3$]Co(II) systems. The same is true of the aryloxide ligand. A more strongly π–donating aryloxide linkage might be expected to more favorably confer a low spin ground state configuration than a halide ligand.

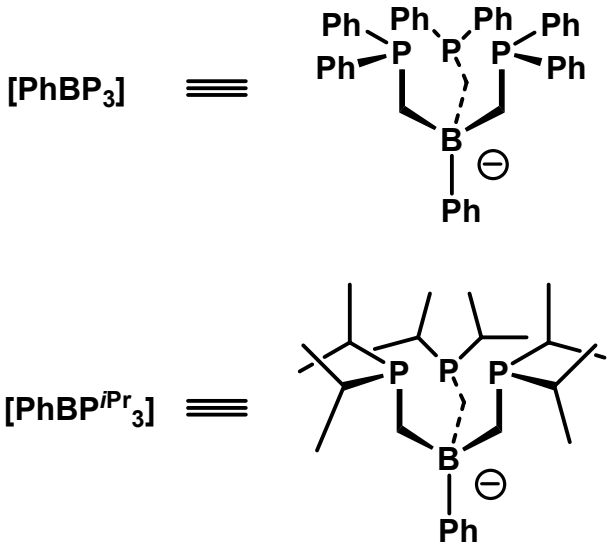

Figure 4.1. Chemical structures of [$PhBP_3$] and [$PhBP^{iPr}_3$].

Perceiving a need to broaden our appreciation of how the interplay between local stereochemistry, the L_3 donor ligand-field strength, and the nature of the X-type ligand work to confer a specific electronic configuration, we set out to systematically characterize a host of pseudotetrahedral d^7 [BP_3]Co-X ions amenable to structure/spin-state correlations. Herein we present the results of this study. Previous studies that have attempted to correlate steric factors with spin-state preferences have emphasized d^6 octahedral systems (e.g., $(L_3)_2$Fe(II)).[31] The systems described in this chapter afford the first opportunity to examine spin-state preferences in *four-coordinate pseudotetrahedral L_3MX structures* by correlating an observed spin-state to the identity of a single X-type ligand, or the identity of an L_3 donor scaffold.

A qualitative sketch of the d-orbital splitting diagrams anticipated for the various limiting stereochemical structures is shown in Figure 4.2. Structures **A** and **B** illustrate the most familiar coordination geometries for four-coordinate Co^{2+} ions. These structure types are square planar (**A**) and tetrahedral (**B**) and give rise to low spin (S = ½) and high spin (S = 3/2) ground state configurations, respectively. An intramolecular distortion that interconverts **A** and **B** is denoted as the "classic case" in Figure 4.2. This phenomenon is well-known for Co(II) ions. Configurational and spin-state equilibria in solution between Co(II) ions of these two limiting structure types is a phenomenon that was lucidly described by Holm and Everett nearly four decades ago.[18,20a] Also, stereochemical tuning of Co(II) complexes using macrocyclic tetradentate ligands can dictate one configuration versus another, and, therefore, different ground spin-states, as exemplified by Lippard and co-workers using tropocoronand ligands.

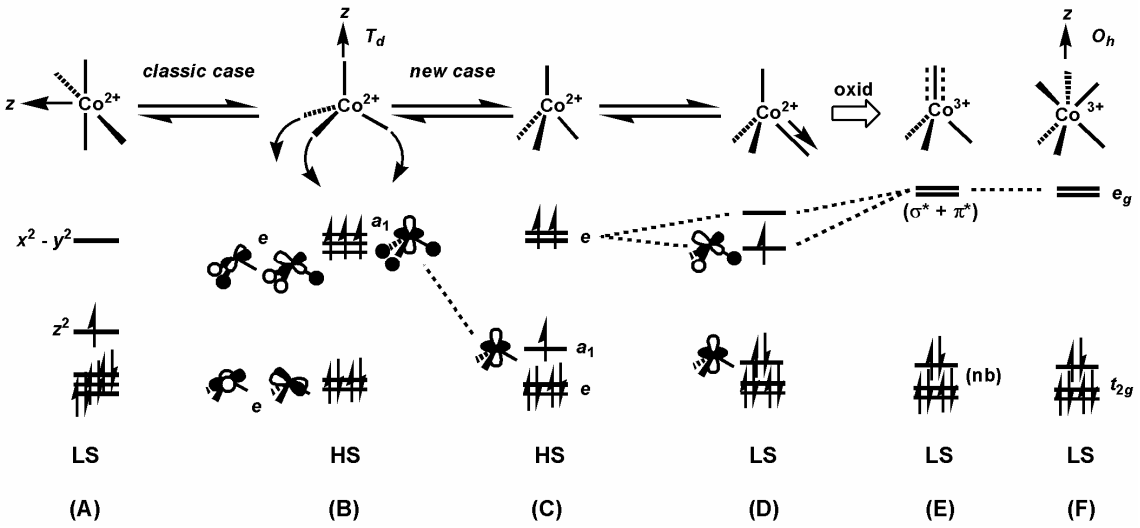

Figure 4.2. Qualitative stereochemical structures and d-orbital splitting diagrams relevant to the four-coordinate structures.

The interconversion between structures **A** and **B** is severe and is likely difficult to access in the crystalline state. A gentler distortion, denoted as the "new case" in Figure 4.2, is one of axial character and produces the pseudotetrahedral structure type **C**. Under three-fold symmetry (C_{3v}) a distortion of this type stabilizes an orbital of a_1 symmetry and provides a d-orbital splitting diagram comprised of $1a_1 + 2e$. This is a familiar orbital arrangement and has been frequently used to describe the electronic structures of sandwich ($[Cp^R]_2M$) and mixed-sandwich ($[Cp^R]ML_3$) complexes.[9,32] For sandwich complexes, the a_1 orbital is most typically placed slightly above a lowest-lying degenerate e-set, though the relative positioning of the lowest three orbitals ($a_1 + e$) has been debated. An important point to underscore is that, to a first approximation, pseudotetrahedral complexes of structure type **C** (i.e., those typically supported by tripodal L_3 donor sets) are electronically best described using a crude "two-over-three" d-orbital splitting diagram akin to that of sandwich complexes like $[Cp]_2Fe$. A tetrahedral splitting diagram is less appropriate. Therefore, while ligands that favor monomeric L_3MX structures are quite often referred to as "tetrahedral enforcers," owing to the pseudotetrahedral stereochemistry they confer, from an electronic structure perspective these ligands might be more appropriately regarded as "octahedral enforcers." The tripodal ligand enforces the requisite axial distortion that gives rise to an approximate two-over-three splitting of the d-orbitals under idealized three-fold symmetry. The ground state electronic structures of three-fold symmetric $[Tp"]Co^{II}$-X complexes are appropriately assigned as $^4A_{2g}$,[28,29,33] but, as discussed further below, these ground states bear a closer electronic relationship to high spin octahedral complexes such as $[Tp]_2Co$[34] than to high spin tetrahedral complexes such as $[Cs]_2[CoCl_4]$.[35] These general ideas help

to account for the relative ease with which complexes of the high spin structure type **C** can crossover to a related but low spin structure type **D** given appropriate choice of the donor ligand set.

4.2 Results and discussion

4.2.1 Synthesis and routine solution characterization of $[BP_3]Co^{II}$-X complexes

To more thoroughly examine structure/spin-state relationships within the $[BP_3]Co^{II}X$ system we prepared a series of $[BP_3]Co^{II}$-X complexes that feature O-atom and S-atom X-type linkages. Table 4.1 lists each of the $[BP_3]Co$ complexes featured in the present study, along with their numerical designations, color, and electrochemical characterization data. The magnetic characterization data are incorporated in Table 4.2. A fair number of alkoxide, aryloxide, thiolate, and arylthiolate derivatives of cobalt have been described previously, and several L_3MX systems that are structurally relevant to the present cobalt derivatives warrant specific mention. For instance, tris(pyrazolyl)borate ([Tp]) derivatives of cobalt[28,29,33] that feature X-type linkages related to the present systems have been reported. There are also several neutral tris(phosphine) Co(I) complexes, for example $(PPh_3)_3CoOPh$,[36,37] though we are unaware of any four-coordinate $P_3Co^{II}X$ species other than those supported by $[BP_3]$ ligands. A tripodal amine donor ligand system that supports complexes with a single aryloxide ligand on cobalt has also been described.[38]

The choice of $[BP_3]Co^{II}$-X complexes that feature O-atom and S-atom X-type linkages was due to the relative ease with which steric and electronic parameters could be tuned in a systematic fashion, and to the ease with which their Co(II) complexes could be generated and purified. Other X-type linkages were considered, for example alkyls and

amides, but these types of complexes have proven to be synthetically problematic within the [BP_3]Co-X family. Attempts to prepare them has led to side reactions indicative of undesirable redox chemistry rather than clean metallation.

Table 4.1. Summary of color and electrochemical data.

Complex Name and Number	Color	Co^{II}/Co^{III}, Co^{I}/Co^{II} (mV)
[$PhBP_3$]CoI, **3.1**	Green	10, -920
[$PhBP_3$]CoOSiPh_3, **4.1**	Purple	-360, -1290
[$PhBP_3$]CoO(4-^{t}Bu-Ph), **4.2**	Red-brown	-390, -1330
[$PhBP_3$]CoO(C_6F_5), **4.3**	Olive green	NA, NA
[$PhBP_3$]CoSPh, **4.4**	Red	-160, -1120
[$PhBP_3$]CoS(2,6-Me_2-Ph), **4.5**	Red	-170, -1100
[$PhBP_3$]CoS(2,4,6-$^{i}Pr_3$-Ph), **4.6**	Red-brown	-80, -1190
[$PhBP_3$]CoS(2,4,6-$^{t}Bu_3$-Ph), **4.7**	Red	-60, -1080
[$PhBP_3$]CoSSiPh_3, **4.8**	Green	-210 (irreversible), -1010
[$PhBP_3$]CoOSi(4-NMe_2-Ph)$_3$, **4.9**	Red	-360, -1300
[$PhBP_3$]CoOSi(4-CF_3-Ph)$_3$, **4.10**	Blue	-60 (irreversible), -1080
[$PhBP_3$]CoOCPh_3, **4.11**	Blue-green	-300, -1310
[$PhBP^{iPr}_3$]CoI, **4.12**	Green	60, -1250
[$PhBP^{iPr}_3$]CoOSiPh_3, **4.13**	Purple	100 (irreversible), -1690
[$PhBP^{iPr}_3$]CoSSiPh_3, **4.14**	Green	-140 (irreversible), -1330
{[$PhBP_3$]CoOSiPh_3} {B(3,5-(CF_3)$_2$-Ph)$_4$}, {**4.15**} {B(3,5-(CF_3)$_2$-Ph)$_4$}	Green	Oxidation product of **4.1**

Table 4.2. Summary of magnetic data.

Complex Number	Evans Method (μ_{eff} in BM, C_6D_6, 298 K)	SQUID $\chi_m T$ (cm^3 K mol^{-1}) at 20 K, 300 K
3.1	2.8	0.82, 1.01
4.1	3.4	0.47, 1.45
4.2	3.4	0.90, 1.90
4.3	3.8	1.32, 2.13 (at 240 K)
4.4	2.4	0.40, 0.49
4.5	2.3	0.50, 0.51
4.6	2.8	0.46, 0.63
4.7	3.9	2.05, 2.21
4.8	2.5	0.47, 0.44
4.9	3.5	0.46, 1.56
4.10	3.9	1.22, 1.95
4.11	3.8	2.08, 2.28
4.12	4.1	1.83, 1.90
4.13	4.3	2.19, 2.36
4.14	4.0	0.47, 1.23
{**4.15**} $\{B(3,5\text{-}(CF_3)_2\text{-}Ph)_4\}$	Diamagnetic	Diamagnetic

The family of complexes shown in Table 4.1 is conveniently accessible via the use of the soft thallium reagents TlEAr and $TlEZAr_3$ (E = O or S, Z = Si or C, Eq. 4.1). The typical method for preparation of these thallium reagents involves a metathesis reaction between commercially available thallium ethoxide and the desired phenol, arylthiol, silanol, or silylthiol.[39] The types of alcohols and thiols amenable to this method of preparation are restricted to those that have pK_a values lower than that of the ethanol byproduct (pK_a = 15.9). The addition of one equivalent of the desired thallium reagent as a THF solution to a THF solution of $[BP_3]CoX$ (X = I or Cl) affords the substituted product in high crude yield with TlX as an easily separable byproduct. Filtration of the crude reaction mixture followed by crystallization, typically by vapor diffusion of petroleum ether in benzene, provides each of the desired complexes in crystalline form in modest to high yields.

Despite the paramagnetic nature of these Co(II) derivatives, ^{1}H NMR spectroscopy aids in their characterization. While the signature proton resonances are listed for each isolated complex in the Experimental Section, we examined the paramagnetically shifted ^{1}H NMR spectra of the iodides $[PhBP_3]CoI$ (**3.1**) and $[PhBP^{iPr}_3]CoI$ (**4.12**) in some detail, as a representative sample of this family of complexes. Both complexes exhibit solution spectra (see Figure 4.3) consistent with approximate C_3 symmetry at room temperature, as only a single set of resonances arises from the phosphine donor arms. T_1 relaxation times can be used as a guide to determine the relative distances of ligand-based protons from a coordinated metal center containing unpaired spin.[40] By measuring a T_1 relaxation time for each proton resonance shown in

Figure 4.3 (top and bottom), and correlating these relaxation times with the integrated number of protons corresponding to each resonance, we are able to assign the spectrum of **3.1** with a high degree of confidence. The spectrum of **4.12** suffers from some ambiguity due to certain resonances having similar T_1 relaxation times and integration values. Notably, the chemical shift range of the resonances observed for **4.12** is much broader than that of **3.1**, likely due to their different respective spin states (vide infra).

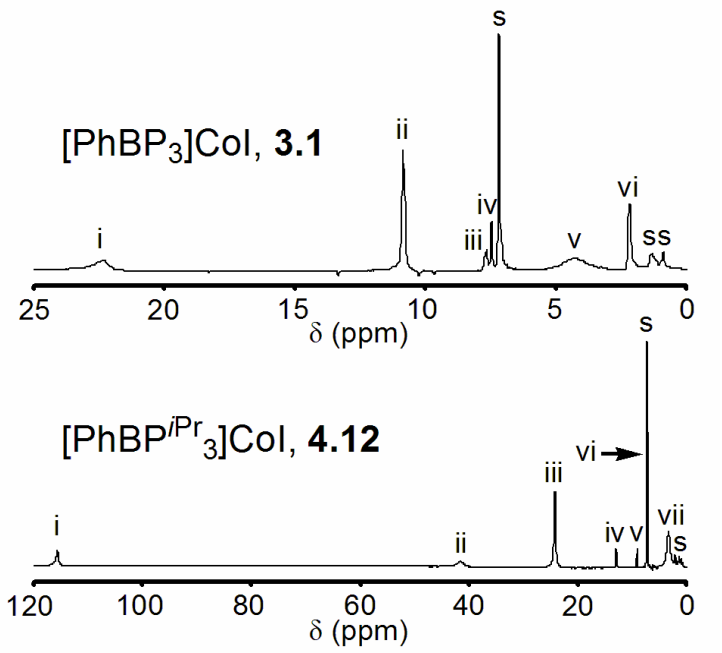

Figure 4.3. ^{1}H NMR spectra of **3.1** and **4.12** in C_6D_6. Assignments are based on the correlation between single scan integration values and T_1 relaxation times for each resonance. For **3.1**: (i) $PhB(CH_2PPh_2)_3$, (ii) *meta* $P(C_6H_5)_2$, (iii) *ortho* $B(C_6H_5)$, (iv) *meta* and *para* $B(C_6H_5)$, (v) *ortho* $P(C_6H_5)_2$, (vi) *para* $P(C_6H_5)_2$. For **4.12**: (i and ii) $PhB(CH_2P^iPr_2)_3$ and $P(CH(CH_3)_2)_2$, (iii and vii) $P(CH(CH_3)_2)_2$, (iv) *ortho* $B(C_6H_5)$, (v) *para* $B(C_6H_5)$, (vi) *meta* $B(C_6H_5)$.

4.2.2 Electrochemical data

The electrochemical response of each complex featured in this study was examined by cyclic voltammetry in THF solution using either $[^nBu_4N][PF_6]$ or $[^nBu_4N][ClO_4]$ as the supporting electrolyte, a glassy carbon working electrode, a platinum wire counter electrode, and a $Ag/AgNO_3$ reference electrode. The potentials of well-defined redox processes were recorded versus an external ferrocene standard and are listed in Table 4.1.

The electrochemical data are generally unremarkable and hence only a few comparative comments are warranted. For those $[PhBP_3]Co(II)$ complexes featuring a Co-OR linkage, specifically complexes **4.1**, **4.2**, **4.3**, **4.9**, **4.10**, and **4.11**, fully reversible Co(II/III) and Co(I/II) redox processes are observed. Relatively little shift in the potential of either redox event is observed within this family, with the exception of the *p*-CF_3-substituted silyloxide species $[PhBP_3]CoOSi(4\text{-}CF_3\text{-}Ph)_3$, **4.10**. For this complex the Co(I/II) redox event is anodically shifted by ca. 300 mV, and the Co(II/III) redox event is irreversible. These differences are likely due to the electron-withdrawing CF_3 substituent, which destabilizes the higher-valent Co(III) state but renders the lower-valent Co(I) state more accessible.

The $[PhBP_3]Co(II)$ arylthiolate complexes **4.4**-**4.8** also exhibit well-behaved Co(II/III) and Co(I/II) redox events. These thiolate species are, as might be expected, easier to reduce and more difficult to oxidize than their aryloxide relatives. Again, only a small degree of variance is observed for the potentials amongst the arylthiolate family of complexes. Two subtle differences worth noting are (i) complexes $[PhBP_3]CoS(2,4,6\text{-}^iPr_3\text{-}Ph)$, **4.6**, and $[PhBP_3]CoS(2,4,6\text{-}^tBu\text{-}Ph)$, **4.7**, are approximately

100 mV more difficult to oxidize than [PhBP$_3$]CoSPh, **4.4**, and [PhBP$_3$]CoS(2,6-Me$_2$-Ph), **4.5**, presumably reflecting the difference in electron-releasing character between the arylthiolate substituents; and (ii) it is ca. 100 mV more difficult to reduce **4.6** than **4.7**, an observation that is difficult to rationalize in simple terms. The triphenylsilylthiolato derivative [PhBP$_3$]CoSSiPh$_3$ (**4.8**) is the most easily reduced species (-1010 mV), but displays an irreversible oxidation event around -210 mV. The reduction potential recorded for complex **4.8** can be compared with that of its [PhBP$^{i\text{Pr}}_3$]-supported congener [PhBP$^{i\text{Pr}}_3$]CoSSiPh$_3$ (**4.14**). The latter complex **4.14** is ca. 300 mV more difficult to reduce (-1330 mV) due to its more electron-releasing P$_3$ donor scaffold, but still displays an irreversible Co(II/III) process. Comparison of the redox processes observed between [PhBP$_3$]CoOSiPh$_3$, **4.1**, and [PhBP$^{i\text{Pr}}_3$]CoOSiPh$_3$, **4.13**, reveals another curiosity of note. While **4.13** is appreciably more difficult to reduce (by ca. 400 mV), as should be expected, its oxidation to Co(III) is electrochemically irreversible. By contrast, {[PhBP$_3$]Co$^{\text{III}}$OSiPh$_3$}$^+$ is electrochemically accessible and stable (vide infra). This is difficult to rationalize, except to suggest that a putative {[PhBP$^{i\text{Pr}}_3$]Co$^{\text{III}}$OSiPh$_3$}$^+$ species may be more prone to loss of the triphenylsilyl substituent in the presence of a fluorinated counter-anion from the electrolyte.

Finally, it is interesting to compare the electrochemical data recorded for these cobalt systems with that of a related series of recently reported [BP$_3$]Ni-X systems.[41] For example, a reversible Ni(I/II) reduction event is observed for the complex [PhBP$_3$]NiOSiPh$_3$ at -1.47 V, which is ca. 180 mV more negative than the Co(I/II) event of **4.1**. More striking is how difficult it is to oxidize the nickel systems to the Ni(III) state. For the complex [PhBP$_3$]NiOSiPh$_3$, the first oxidative process is encountered at a

potential that is ca. 700 mV more positive than for its cobalt analogue **4.1**. This large difference appears to reflect the relative instability of a d^7 versus a d^6 electronic configuration within the $[BP_3]$Ni-X and $[BP_3]$Co-X platforms, respectively.

4.2.3 Chemical oxidation of $[PhBP_3]CoOSiPh_3$ to produce $\{[PhBP_3]CoOSiPh_3\}\{BAr_4\}$

Reversible oxidation waves for these $[BP_3]Co^{II}$-X derivatives suggest that their chemical oxidation might afford the corresponding trivalent $\{[BP_3]Co^{III}\text{-}X\}^+$ products, which would comprise a structurally unusual class of pseudotetrahedral Co(III) complexes (type **E** in Figure 4.2). We have prepared and thoroughly characterized one such example pertinent to the present study: $\{[PhBP_3]CoOSiPh_3\}\{BAr_4\}$, $\{\mathbf{4.15}\}\{BAr_4\}$ (Ar = C_6H_5, 3,5-$(CF_3)_2$-C_6H_3). The addition of THF to a solid mixture of **4.1** and $\{[Cp]_2Fe\}\{BAr_4\}$ effects a rapid oxidation process to generate the diamagnetic, green product $\{\mathbf{4.15}\}\{BAr_4\}$ (Eq. 4.2). Cationic $\{\mathbf{4.15}\}\{BAr_4\}$ exhibits a sharp singlet in its ^{31}P NMR spectrum at 64.6 ppm and also a sharp singlet in the ^{19}F NMR spectrum at -58.5 for the tetra(3,5-bis(trifluoromethyl)phenyl)borate salt derivative. The combined ^1H and ^{31}P NMR spectra obtained for this system reveal that it is threefold symmetric in solution on the NMR time scale. The diamagnetic ground state of $\{\mathbf{4.15}\}^+$ suggests that its electronic configuration is likely related to the diamagnetic imide $[PhBP_3]Co{\equiv}N$-*p*-tolyl, which is an $S = 0$ Co(III) species featuring a bona fide Co-N triple bond linkage.[42] However, whereas $\{\mathbf{4.15}\}^+$ can be reduced at a potential of ca. -360 mV, the imide species $[PhBP_3]Co{\equiv}N$-*p*-tolyl is stable to reduction at potentials as low as ca. – 3.0 V, reflecting both the difference in charge and the weaker strength of the π-bonding in $\{\mathbf{4.15}\}^+$.

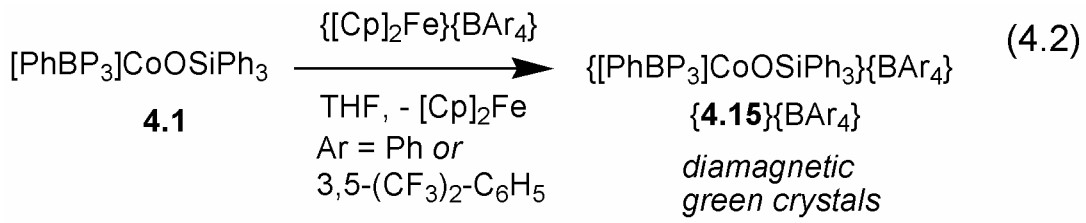

4.2.4 Structural characterization and stereochemical classification of $[BP_3]Co^{II}$-X derivatives

Solid-state crystal structures have been determined for many of the cobalt complexes listed in Table 4.1. These results are summarized by their core structure representations, collected in Figure 4.4 and Figure 4.5, and by a list of salient bond distances and angles, collected in Table 4.3. In each structure, the tris(phosphino)borate is κ^3-bound to a monomeric cobalt center. The pseudotetrahedral structures can be broadly divided into two separate classes based on the average length of the Co-P bonds. As will be corroborated by the SQUID and EPR data discussed below, complexes featuring average Co-P bond distances between 2.15 Å and 2.25 Å (e.g., **4.5** and **4.9**) are characteristic of low spin ground states (type **D** in Figure 4.2), whereas complexes with average Co-P bond distances between 2.30 Å and 2.35 Å (e.g., **4.7** and **4.11**) are characteristic of high spin ground states (type **C** is Figure 4.2).

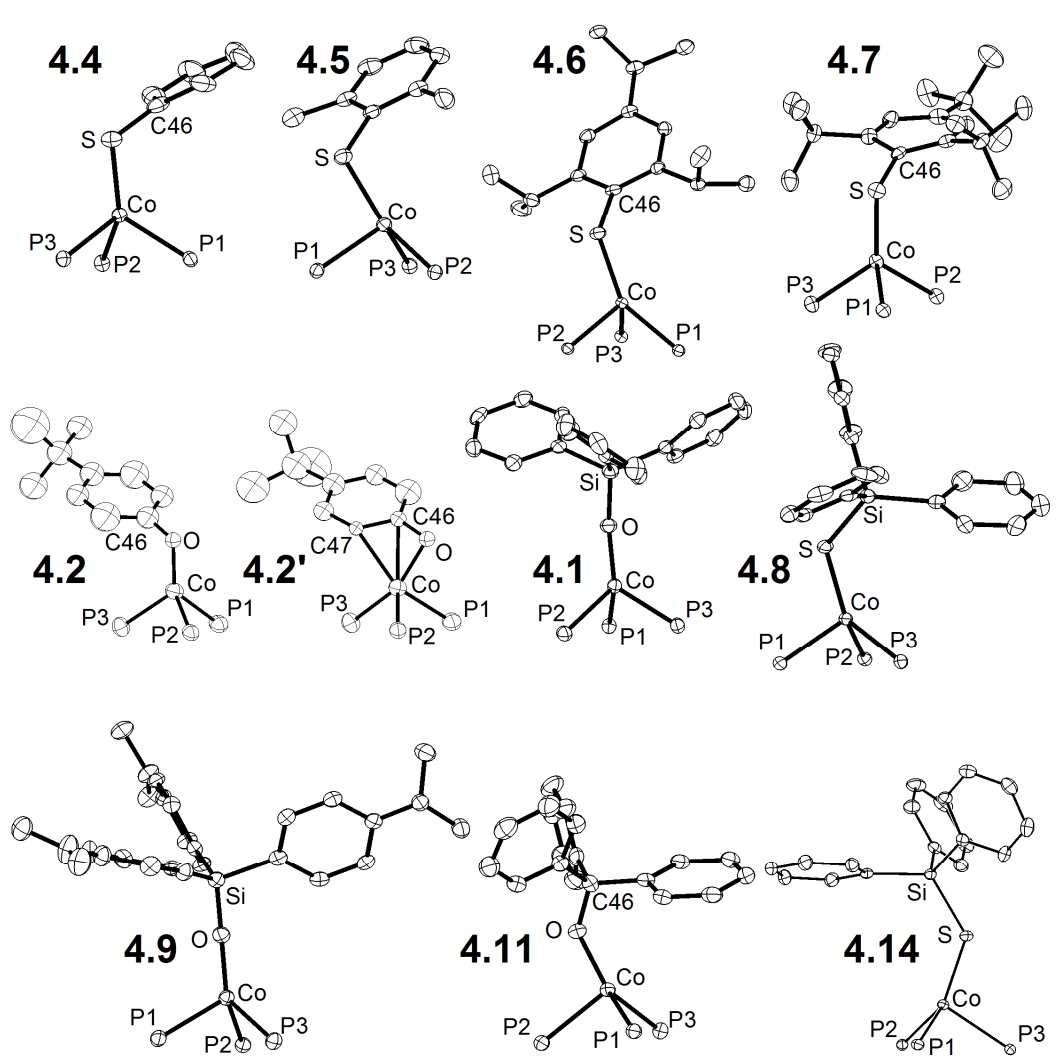

Figure 4.4. Displacement ellipsoid representations (50%) of the core structures of [PhBP$_3$]CoSPh (**4.4**); [PhBP$_3$]CoS(2,6-Me$_2$-Ph) (**4.5**); [PhBP$_3$]CoS(2,4,6-^{i}Pr$_3$-Ph) (**4.6**); [PhBP$_3$]CoS(2,4,6-^{t}Bu$_3$-Ph) (**4.7**); [PhBP$_3$]CoO(4-^{t}Bu-Ph) (**4.2**); [PhBP$_3$]CoOSiPh$_3$ (**4.1**); [PhBP$_3$]CoSSiPh$_3$ (**4.8**); [PhBP$_3$]CoOSi(4-NMe$_2$-Ph)$_3$ (**4.9**); [PhBP$_3$]CoOCPh$_3$ (**4.11**); and [PhBP$^{i\text{Pr}}_3$]CoSSiPh$_3$ (**4.14**). The **4.2** and **4.2**' structures show the disorder in the –O(4-^{t}Bu-Ph) ligand, which is bound either η^1 (left) or η^3 (right) to the cobalt center. See Table 4.3 for bond lengths and angles.

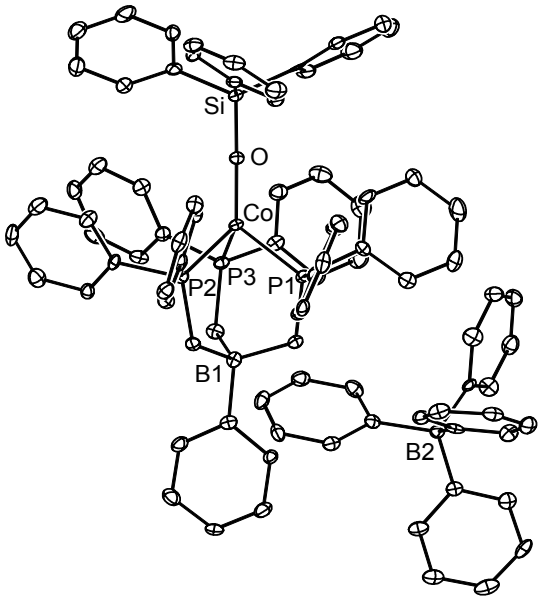

Figure 4.5. Displacement ellipsoid representations (50%) of {[$PhBP_3$]$CoOSiPh_3$}{BPh_4}, {**4.15**}{BPh_4}. Hydrogen atoms and solvent molecules have been omitted for clarity. See Table 4.3 for bond lengths and angles.

The basic stereochemical structures observed in the solid-state can be further classified, at least qualitatively, as having one of two general structure types that we will refer to throughout as either **umbrella** distorted or **off-axis** distorted (Figure 4.6). In an umbrella distorted structure, the X-type ligand is regarded as axial and trisects the three Co-P linkages, coincident with the B-Co vector. Distortions of an umbrella type are common for four-coordinate complexes supported by tripodal ligands, and it may be said that such ligands in fact enforce the umbrella distortion.[28,30] In an off-axis distorted structure, the X-type ligand cants away from the imaginary vector running through the B and Co atoms to such an appreciable extent that it is better regarded as an equatorial

ligand rather than an axial ligand. Four-coordinate complexes that exhibit an off-axis distortion are less frequently encountered and appear to arise from the population of a low spin ground state, as discussed in greater detail below.

Table 4.3. X-ray diffraction table showing key bond lengths (Å) and angles (deg) for **4.1**, **4.2**, **4.4**, **4.5**, **4.6**, **4.7**, **4.8**, **4.9**, **4.11**, **4.14**, and {**4.15**}{BPh_4}.

Complex Name and Number	Co-E[a]	E-Z[b]	Co-P1	Co-P2	Co-P3
[$PhBP_3$]$CoOSiPh_3$, **4.1**	1.799(2)	1.612(2)	2.156(1)	2.284(1)	2.169(1)
[$PhBP_3$]CoO(4-^{t}Bu-Ph), **4.2**[c]	1.832(7)	1.327(8)	2.247(1)	2.230(1)	2.227(1)
[$PhBP_3$]CoO(4-^{t}Bu-Ph), **4.2'**[c]	1.885(4)	1.330(6)	2.247(1)	2.230(1)	2.227(1)
[$PhBP_3$]CoSPh, **4.4**[d]	2.153(1)	1.742(4)	2.175(1)	2.178(1)	2.249(1)
[$PhBP_3$]CoS(2,6-Me_2-Ph), **4.5**	2.167(1)	1.781(2)	2.251(1)	2.199(1)	2.208(1)
[$PhBP_3$]CoS(2,4,6-$^i Pr_3$-Ph), **4.6**[d]	2.155(1)	1.802(2)	2.201(1)	2.280(1)	2.205(1)
[$PhBP_3$]CoS(2,4,6-$^t Bu_3$-Ph), **4.7**	2.207(1)	1.784(5)	2.354(1)	2.351(1)	2.387(1)
[$PhBP_3$]$CoSSiPh_3$, **4.8**	2.190(1)	2.120(1)	2.206(1)	2.167(1)	2.243(1)
[$PhBP_3$]CoOSi(4-NMe_2-Ph)$_3$, **4.9**	1.809(1)	1.618(2)	2.265(1)	2.144(1)	2.194(1)
[$PhBP_3$]$CoOCPh_3$, **4.11**[d]	1.839(1)	1.398(2)	2.349(1)	2.361(1)	2.387(1)
[$PhBP^{iPr}_3$]$CoSSiPh_3$, **4.14**	2.178(1)	2.113(1)	2.179(1)	2.179(1)	2.357(1)
{[$PhBP_3$]$CoOSiPh_3$}{BPh_4}, {**4.15**}{BPh_4}	1.766(3)	1.652(3)	2.187(1)	2.182(1)	2.184(1)

Table 4.3 (cont.)

Complex Number	Co-E-X	P1-Co-P2	P1-Co-P3	P2-Co-P3	P1-Co-E	P2-Co-E	P3-Co-E
4.1	172.5(1)	91.38(3)	85.88(3)	94.60(3)	129.45(7)	119.42(7)	125.82(7)
4.2	110.3(4)	91.48(4)	90.96(4)	96.35(4)	133.4(3)	106.9(2)	127.5(3)
4.2'	88.4(3)	91.48(4)	90.96(4)	96.35(4)	97.6(2)	110.8(1)	151.2(1)
4.4	104.3(1)	89.44(4)	97.52(4)	90.70(4)	121.14(4)	143.46(4)	103.24(4)
4.5	114.6(1)	89.44(2)	100.23(2)	86.73(2)	96.48(2)	147.37(2)	123.30(2)
4.6	123.2(1)	89.26(2)	88.14(2)	98.04(2)	143.37(2)	107.92(2)	119.75(2)
4.7	111.3(2)	96.11(5)	92.81(5)	96.30(5)	109.46(5)	125.24(5)	128.37(6)
4.8	128.0(1)	87.79(3)	99.63(3)	87.65(3)	108.15(3)	139.91(3)	123.62(3)
4.9	165.7(1)	90.43(2)	94.56(2)	86.47(2)	117.36(5)	127.61(5)	129.77(5)
4.11	138.0(1)	92.56(2)	95.67(2)	92.40(2)	126.83(5)	102.99(5)	133.18(5)
4.14	131.5(1)	90.30(2)	92.75(2)	93.27(2)	136.69(2)	126.30(2)	105.64(2)
{**4.15**}{BPh_4}	178.6(2)	90.67(5)	90.18(5)	90.50(5)	125.6(1)	124.4(1)	124.8(1)

Table 4.3 footnotes. a–E represents the fourth, non-phosphine atom directly bound to the Co center, either O or S; **b**–Z represents the non-cobalt atom bound to E, which is either C or Si; **c**–**4.2** shows the bond distances and angles for the η^1 conformation. **4.2'** shows the bond angles and distances for the η^3 conformation; **d**–There are two crystallographically independent molecules in the unit cell.

Rigorously distinguishing between structures that arise from these two limiting distortions is not readily apparent by inspection. An elegant method known as the *continuous symmetry measure*[13,43] proves very useful in this regard because it allows one to quantitatively discuss how close a given molecular geometry is to an idealized structure type. For example Alvarez and co-workers have used this approach to quantitatively compare true geometric structures to those of idealized tetrahedra or square planes. Under a continuous symmetry measurement, the distance (i.e., deviation) of a given molecule from an idealized polyhedron of a symmetry point group defined as *G* is numerically defined as *S(G)*. A perfect tetrahedron therefore has an $S(T_d) = 0$, and a perfect square plane has an $S(D_{4h}) = 0$. Construction of a 2-D plot of *S(G)* values can then be used to show that a perfect tetrahedron has an $S(D_{4h}) = 33.3$, and a perfect square plane has an $S(T_d) = 33.3$. As should be obvious, a trigonal pyramidal structure is geometrically much closer to a tetrahedron than to a square plane. This is reflected by its respective *S(G)* values; it features a relatively small $S(T_d)$ by comparison to a large $S(D_{4h})$ value ($S(T_d) = 3.57$; $S(D_{4h}) = 34.87$).

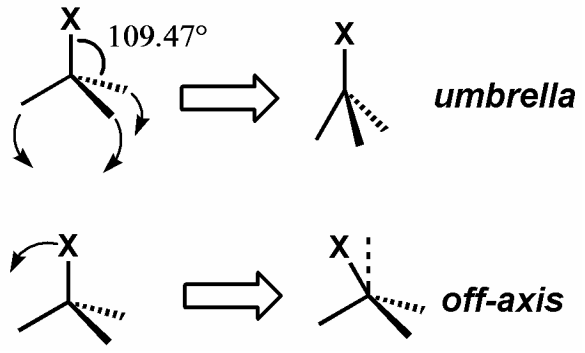

Figure 4.6. Limiting distortions relevant to the pseudotetrahedral structure types.

Plotting the data for the X-ray structures shown in Figures 4.4 and 4.5 on a 2-D continuous symmetry map allows us to see the deviations. Comparing the species on a S(T_d) versus S(D_{4h}) map shows that the complexes we have prepared are all reasonably close to an ideal tetrahedron (Figure 4.7). Complexes on the upper left portion of the graph exhibit a typical umbrella distortion and are high spin (vide infra). This class includes complexes [PhBP$_3$]CoS(2,4,6-^{t}Bu$_3$-Ph) (**4.7**), [PhBP$_3$]CoOCPh$_3$ (**4.11**), and [PhBP$^{i\text{Pr}}_3$]CoI (**4.12**). The ambient temperature solid-state structure of [PhBP$_3$]CoOSiPh$_3$ (**4.1**) is also in this class. The upper right box features low spin umbrella complexes including the siloxides: **4.1** (at 98 K), [PhBP$_3$]CoOSi(4-NMe$_2$-Ph)$_3$ (**4.9**), and {[PhBP$_3$]CoOSiPh$_3$}{BPh$_4$} ({**4.15**}{BPh$_4$}) and the iodide complex we previously reported, [PhBP$_3$]CoI (**3.1**). The complexes we denote as off-axis structure types are somewhat distinct from the [PhBP$_3$]Co^{II}-X complexes we have described in previous studies (lower right box in Figure 4.7).[14,15] These off-axis complexes all incorporate a thiolate as the fourth ligand. Furthermore, all of the off-axis species (**4.4**, **4.5**, **4.6**, **4.8**, and **4.14**) are low spin at 98 K. Not surprisingly, these five complexes feature one elongated Co-P bond in an axial position and two shorter Co-P bonds in the equatorial positions.

Given that all of these P$_3$Co^{II}X species show only a small distortion from an ideal tetrahedron, it is worth examining whether some of the species are better described as trigonal pyramidal. A continuous symmetry plot mapping the deviations from an ideal trigonal pyramid and a tetrahedron is shown in Figure 4.8. Almost all of the complexes fall within the middle portion of the graph, implying roughly equal distortions from both idealized geometries. Complexes **4.1**, **4.9**, **4.12**, and {**4.15**} have less distortion from a

tetrahedron than complex **4.5**, which, while distorted from both idealized geometries, is slightly closer to a trigonal pyramid. It is admittedly difficult to tease out a definitive difference between these two ideal geometries for the structures described. The dotted line shown in Figure 4.8 qualitatively draws the same distinction illustrated by the previous graph (Figure 4.7). The complexes on the left side feature typical umbrella distortions, and the complexes on the right feature off-axis distortions. The single discrepancy between this plot and the plot in Figure 4.7 is that this symmetry map suggests that complex **3.1** belongs to the off-axis class instead of the umbrella class. None of the complexes we have prepared is truly close to a trigonal pyramidal geometry since the equatorial L-Co-L angles are inequivalent. Known examples of trigonal pyramidal Co(II) species have been assigned as high spin and often feature a tetradentate ligand with three equivalent tripodal arms and one axial donor ligand giving equivalent L-Co-L angles near 120°.[17]

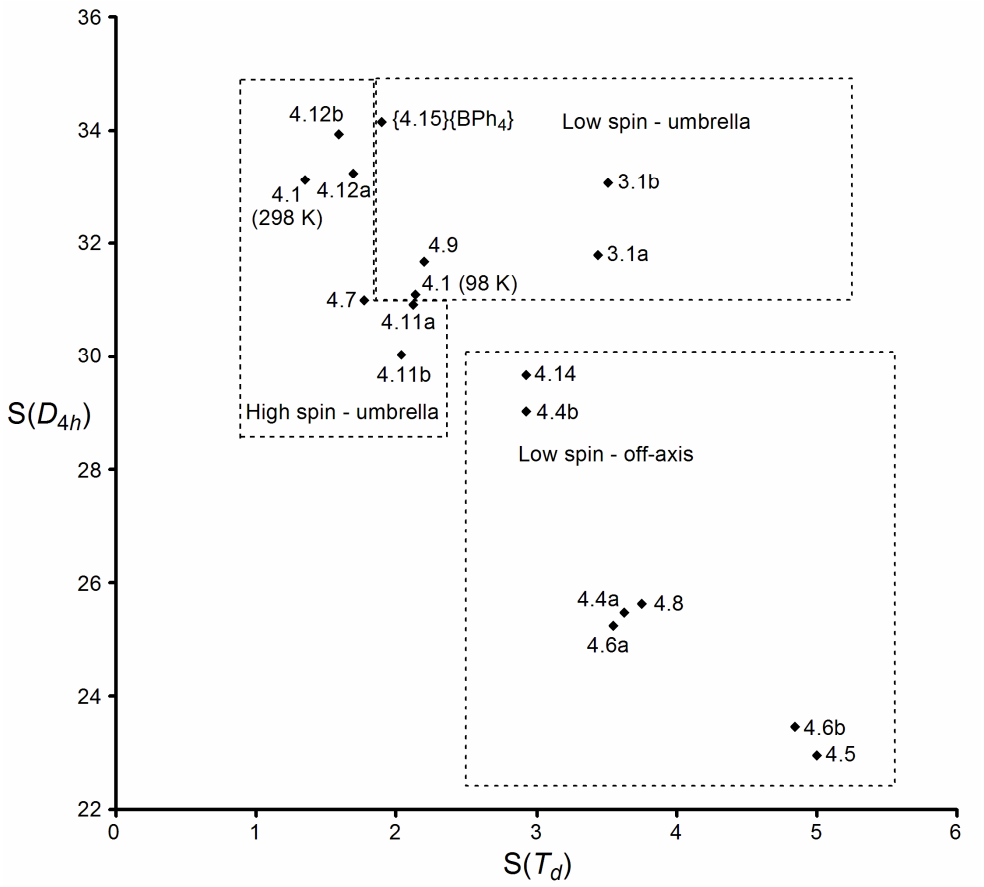

Figure 4.7. The calculated continuous symmetry deviation for each molecule is plotted on a continuous symmetry map of S(T_d) (tetrahedral) versus S(D_{4h}) (square planar). The complexes can be assigned to one of two classes based on their deviations from these two idealized structure types. The umbrella class can be subdivided into high spin and low spin complexes. Complexes with two components on the symmetry map (**a** and **b**) have two asymmetric molecules within the unit cell. The crystal structure of [$PhBP_3$]$CoOSiPh_3$ (**4.1**) was solved at two different temperatures.

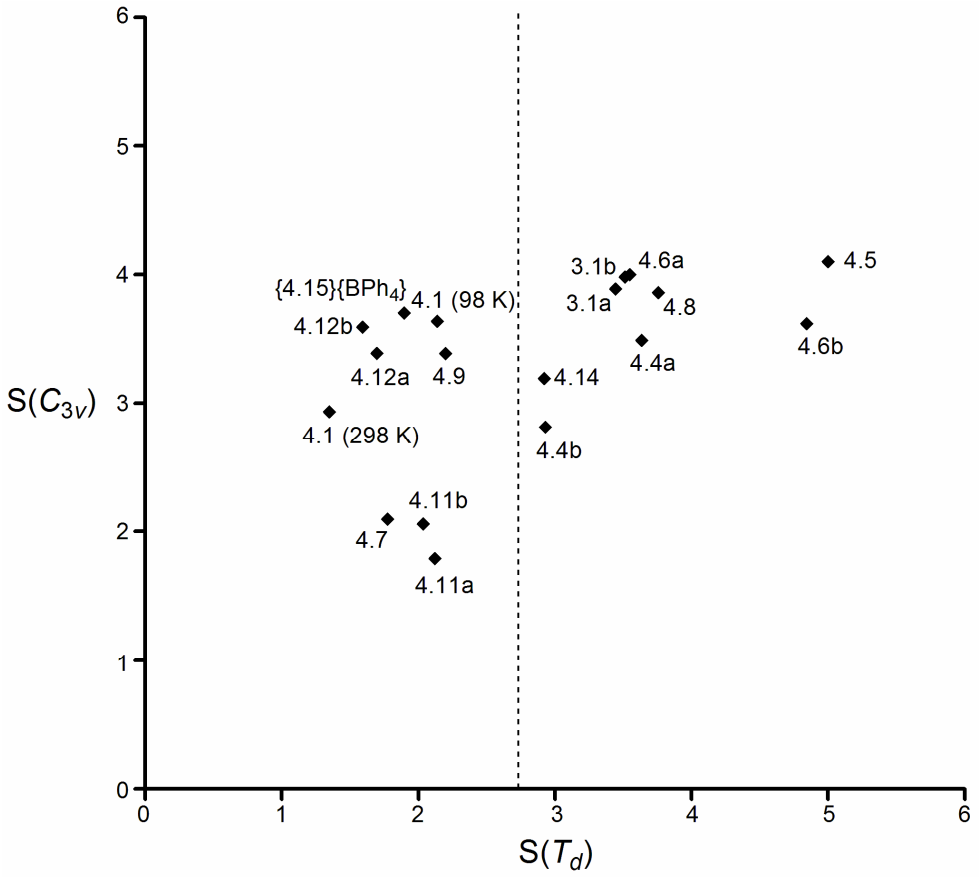

Figure 4.8. The calculated continuous symmetry deviation for each molecule is plotted on a continuous symmetry map of S(T_d) (tetrahedral) versus S(C_{3v}) (trigonal pyramidal). Complexes to the left of the dashed line can be assigned as umbrella distorted while those on the right can be assigned as off-axis distorted. Complexes with two components on the symmetry map (**a** and **b**) have two asymmetric molecules within the unit cell. The crystal structure of [$PhBP_3$]CoOSiPh_3 (**4.1**) was solved at two different temperatures.

Complex **4.2** does not follow the generalized descriptions discussed above since the aryloxide ligand is disordered over two positions, one that exhibits η^1-bonding to the

cobalt center (**4.2**) and one that displays η^3-bonding (**4.2'**) (Figure 4.4).[44] To our knowledge, an η^3-binding mode of an aryloxide ligand is unprecedented for cobalt complexes. In the η^3-bonding mode (**4.2'**), the Co-O bond distance is 1.885(4) Å, and the Co-C bond distances are 2.277(5) and 2.341(5) for C(46) and C(47), respectively. Furthermore, the Co-O-C(46) bond angle is highly bent (88.4(3)°) to accommodate favorable π-bonding to the aryl ring.

Two other solid-state structures are worth discussing in more detail. The solid-state structure determined for diamagnetic {**4.15**}{BPh_4} shows an umbrella distortion (Figure 4.5). The complex is markedly three-fold symmetric and represents an ideal example of structure type **E**, as shown in Figure 4.2. The Co-P distances display a variance of only 0.005 Å, and the average of the three Co-P distances is short at 2.185 Å (Table 4.3). The Co-O bond distance (1.766(3) Å) is only 0.03 Å shorter than in **4.1**, and the Co-O-Si bond angle is almost perfectly linear (178.6(2)°). [$PhBP^{iPr}_3$]$CoSSiPh_3$ (**4.14**) features an off-axis distortion. However, the axial elongation is much more pronounced for complex **4.14** than for the other off-axis complexes. In this case, the axial Co-P bond is greater than 0.17 Å longer than the other two Co-P bonds.

4.2.5 Magnetic characterization (SQUID and EPR) of [BP_3]Co^{II}-X derivatives

As mentioned in the introduction, experimental evidence for the preferred low spin ground state configuration in a L_3Co^{II}-X structure type was first provided by the complex [$PhBP_3$]CoI (**3.1**). In the solid-state this complex displays the distorted structure type represented as **D** in Figure 4.2. The related chloride and bromide complexes [$PhBP_3$]Co-X are also low spin species in their monomeric form in solution, but they give rise to dimeric structures in the crystalline state and are therefore of little utility to the

present discussion. In contrast to these low spin [$PhBP_3$]Co(II) halides, we have previously assigned quartet ground states to the complexes [$PhBP^{iPr}_3$]CoI (**4.12**), [$PhBP^{iPr}_3$]CoCl, and [$PhBP_3$]CoO(2,6-Me_2-Ph) (**3.4**) (type **C** in Figure 4.2). These assignments, considered collectively, suggested to us the possibility that the low and high spin ground states of pseudotetrahedral $L_3Co^{II}X$ structure types may in fact lie closer in energy (i.e., $\Delta H_{HS/LS} = k_BT$) than had been previously anticipated.[15,25]

For the collection of [$PhBP_3$]$Co^{II}X$ complexes presented in this chapter (see Table 4.2) it is clear that a low spin ground state is most typically, though not always, preferred. Moreover, this spin preference is in contrast to Co(II) species supported by the [$PhBP^{iPr}_3$] ligand, where the high spin configuration more typically dominates.

SQUID and EPR data have been collected for all of these [BP_3]Co(II) complexes. Rigorously high spin species include complexes **4.7**, **4.11**, **4.12**, and **4.13**. Each of these complexes adopts a structure that falls into the upper left portion of the symmetry plot shown in Figure 4.7, exhibiting a typical umbrella distortion. Complexes **3.1**, **4.4**, **4.5**, **4.6**, and **4.8** provide examples of rigorously low spin species. The species **4.1**, **4.9**, **4.10**, and **4.14** display spin crossover phenomena in the solid-state. The low spin Co(II) derivatives, type **D** in Figure 4.2, gives rise to stereochemical structures exhibiting both umbrella and off-axis distortions. The interpretation of the magnetic data for **4.2** and **4.3** is more complex due to the potential for η^3 interactions from the X-type ligand.

In examining the [$PhBP_3$] supported thiolates (**4.4**-**4.8**), it is apparent that the preferred ground state is a ^2E. Each complex, excluding **4.7**, has values of $\chi_m T_{av}$ (cm^3 K mol^{-1}) from 10-300 K slightly above the spin only value of $\chi_m T = 0.375$ for a single unpaired electron: **4.4**, 0.41; **4.5**, 0.50; **4.6**, 0.51; **4.8**, 0.45. The solid-state magnetic

moment of complexes **4.4** and **4.6** very gently increases as the temperature of each sample is raised above 250 K. We collected data from 4 K to 300 K, and then back to 4 K for complex **4.6**, and this gentle curvature at higher temperatures is reproducible. It appears likely that partial population of an $S = 3/2$ state is present at higher temperatures. A similar curvature is also observed for [$PhBP_3$]CoI (**3.1**). The low spin thiolates **4.4**, **4.5**, **4.6**, and **4.8** each exhibit an off-axis distortion in the solid-state and short average Co-P bond distances. The EPR data for these three species corroborates their doublet assignments, exhibiting an axial ($g_{\parallel} > g_{\perp}$) EPR signal centered near $g = 2$ (Figure 4.9). On the other hand, complex **4.7** exhibits a $\chi_m T_{av}$ (10-300 K) value of 2.11 cm^3 K mol^{-1} between 10 K and 300 K, an amount that is slightly greater than the spin only value for an $S = 3/2$ system (1.88 cm^3 K mol^{-1}). The low temperature EPR confirms this assignment by showing two signals, one at $g \approx 2$ and a second signal at low field centered at $g \approx 5.8$ (Figure 4.9). The $S = 3/2$ ground state of **4.7** must be due to high steric crowding by the bulky X-type thiolate ligand. Population of the quartet spin state expands the average Co-P bond distances thereby alleviating unfavorable steric contacts.

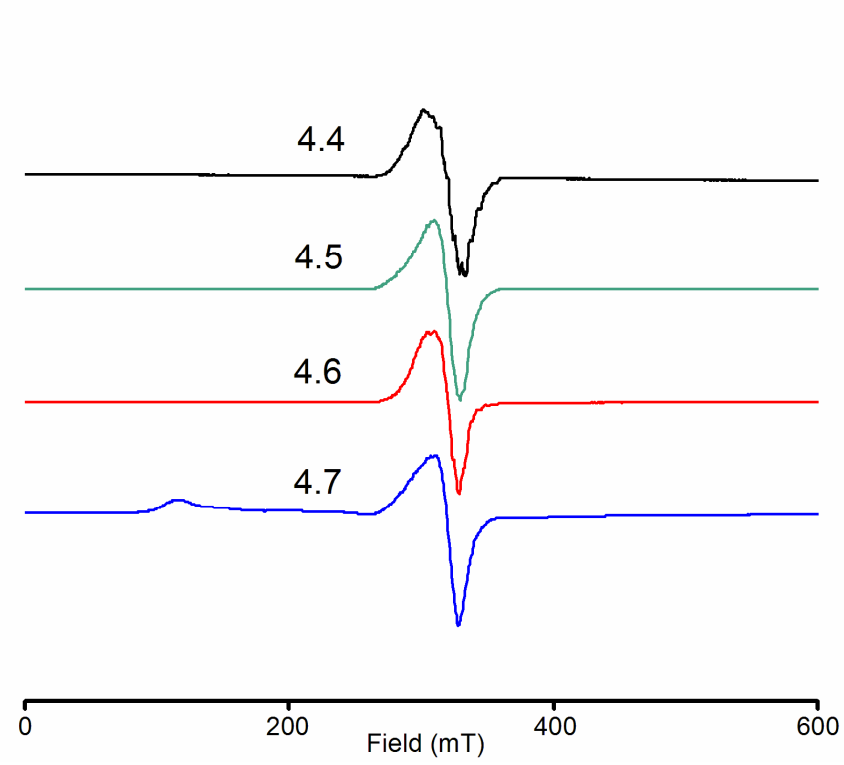

Figure 4.9. Glassy toluene EPR spectra (20 K) of [PhBP$_3$]CoSPh (**4.4**) (—), [PhBP$_3$]CoS(2,6-Me$_2$-Ph) (**4.5**) (—), [PhBP$_3$]CoS(2,4,6-^{i}Pr$_3$-Ph) (**4.6**) (—), and [PhBP$_3$]CoS(2,4,6-^{t}Bu$_3$-Ph) (**4.7**) (—). Instrumental parameters for the spectra can be found in the Experimental Section.

Many pseudotetrahedral Co(II) complexes supported by [Tp] ligands have been prepared, and all of them are high spin.[28,29] Given the preference we have found for [BP$_3$]Co-thiolates to populate low spin ground states, we were curious as to whether a thiolate ligand might confer the low spin configuration to a [Tp]Co(II) system. [Tp]Co thiolates have been prepared previously, and while magnetic data was not reported, they were presumed to be high spin.[33a] We therefore prepared one example of such a complex, [Tp$^{3,5\text{-Me2}}$]CoS(2,6-Me$_2$-Ph) (**4.16**), and obtained low temperature magnetic and structural data to accurately determine a ground spin state (Figure 4.10, see Experimental Section

for synthesis). The SQUID magnetometry data unequivocally shows that **4.16** populates a high spin ground state, with χT_{av} (10 – 300 K) = 2.41 cm^3 K mol^{-1}.

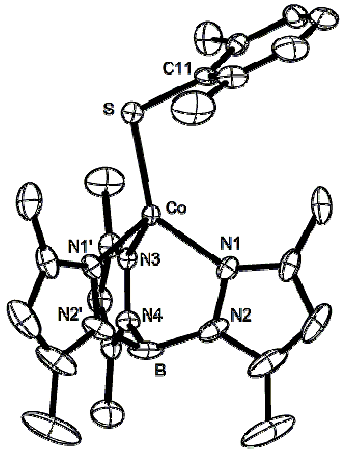

Figure 4.10. Displacement ellipsoid representations (50%) of [$Tp^{3,5\text{-}Me2}$]CoS(2,6-Me_2-Ph), **4.16**. Hydrogen atoms and solvent molecules have been omitted for clarity. Selected interatomic distances (Å) and angles (deg): Co-N1, 2.026(1); Co-N3, 2.021(2); Co-S, 2.273(1); N1-Co-N1', 93.39(8); N1-Co-N3, 93.16(5); N1-Co-S, 134.57(5); N1'-Co-S, 114.07(5); N3-Co-S, 119.04(6).

Whereas thiolate ligands typically confer low spin ground states in the case of [BP_3]Co(II) derivatives, weaker field siloxide ligands form complexes that exhibit spin crossover, as evinced by the complexes [$PhBP_3$]$CoOSiPh_3$ (**4.1**), [$PhBP_3$]CoOSi(4-NMe_2-Ph)$_3$ (**4.9**), and [$PhBP_3$]CoOSi(4-CF_3-Ph)$_3$ (**4.10**). Each of these complexes exhibits an umbrella distortion at low temperature. The structure of **4.1** has been examined both at 98 K (see Figure 4) and at 298 K, and while the average of the Co-P bond distances is expanded at 298 K (reflecting population of the high spin state, vide infra) both X-ray data sets confirm the umbrella distortion (Figure 4.7). Changing

the substituents at the *para* position on the siloxide aryl rings dramatically effects the spin state population at a given temperature (Figure 4.11). The presence of the electron-withdrawing CF_3 group in **4.10** serves to lower the T_c of the spin crossover event. As shown in Figure 4.11, there is a strong temperature dependence of the moment of **4.9**, and a relatively well-defined partial hysteresis is evident centered around 150 K. A more gradual and fully reversible change in $\chi_m T$ is observed above 170 K. This magnetic behavior is distinct from the data collected for **4.1**, which shows gradual crossover (Figure 4.11). EPR spectra were collected at 20 K for **4.1**, **4.9**, and **4.10** and the spectra are consistent with the low temperature SQUID data obtained for each sample.[45] The EPR spectrum of **4.1** shown in Figure 4.12A exhibits an axial signal (g_1 = 2.21, g_2 = 2.05, g_3 = 2.03) featuring well-defined hyperfine coupling (I_{Co} = 7/2) as well as superhyperfine coupling to phosphorus (3 x P, I_P = ½). The observation of phosphorous coupling reflects the highly covalent character of these systems.[46] The octet pattern ($A_{1(Co)}$ = 105 gauss) in the g_1 region of the spectrum suggests a monomeric species in solution (Figure 4.13). Noticeably absent from the spectra of **4.1** and **4.9** are any low field signals that would signify the presence of a high spin Co(II) component.[47] The EPR spectrum of **4.10** (Figure 4.12C) is more interesting. A broad but discernable signal at low field (near g = 5.5) is present at 20 K, suggesting the presence of a high spin component, as is also evident from the solid-state SQUID data. The hyperfine coupling, in the g = 2 region of the spectrum, can be attributed to the presence of the low spin component of **4.10** in the glass, in analogy to the spectra of **4.1** and **4.9**. The effect of solvent in the crystal lattice on the spin crossover process was measured for **4.1** in the solid-state and was found to be minimal.

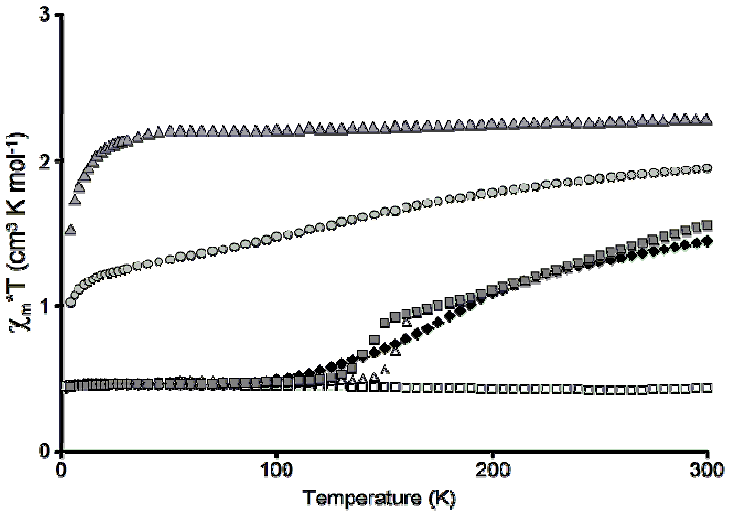

Figure 4.11. SQUID magnetization plot of χ_mT versus T: [PhBP$_3$]CoOSiPh$_3$ (**4.1**) (♦), [PhBP$_3$]CoOSi(4-CF$_3$-Ph)$_3$ (**4.10**) (●), [PhBP$_3$]CoOCPh$_3$ (**4.11**) (▲), [PhBP$_3$]CoSSiPh$_3$ (**4.8**) (□), and [PhBP$_3$]CoOSi(4-NMe$_2$-Ph)$_3$ (**4.9**) as the temperature was raised (Δ) and lowered (■).

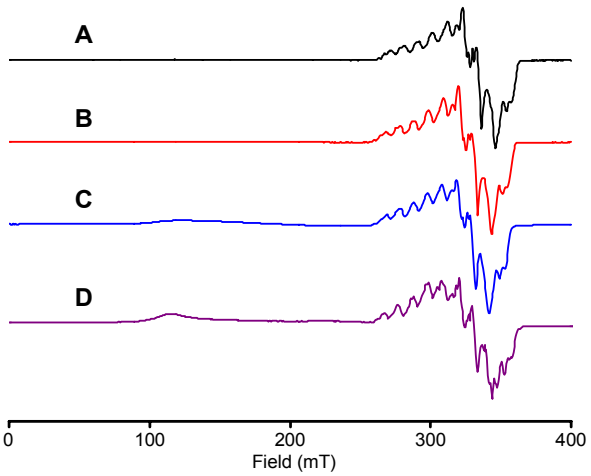

Figure 4.12. Glassy toluene EPR spectra (20 K) for (A) [PhBP$_3$]CoOSiPh$_3$ (**4.1**) (—), (B) [PhBP$_3$]CoOSi(4-NMe$_2$-Ph)$_3$ (**4.9**) (—), (C) [PhBP$_3$]CoOSi(4-CF$_3$-Ph)$_3$ (**4.10**) (—), and (D) [PhBP$_3$]CoOCPh$_3$ (**4.11**) (—). Instrumental parameters for the spectra can be found in the Experimental Section.

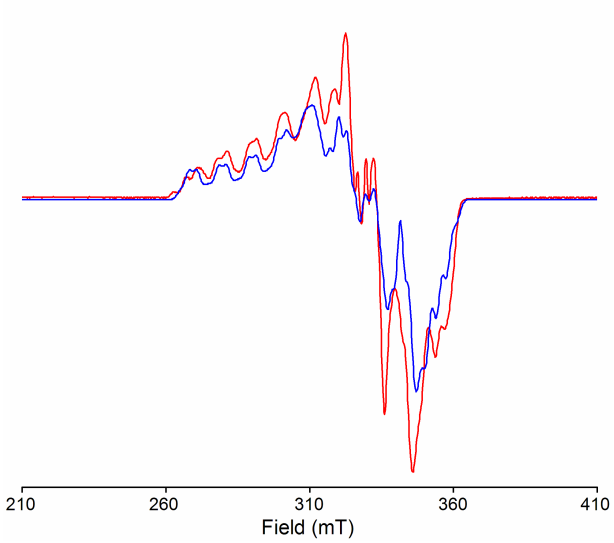

Figure 4.13. Experimental (—) and simulated (—) EPR spectra of $[PhBP_3]CoOSiPh_3$ (**4.1**). Instrumental parameters for the experimental spectrum can be found in the Experimental Section. The simulated parameters are as follows: $g_1 = 2.21$, $g_2 = 2.05$, $g_3 = 2.03$; $a_{1(Co)} = 105$ gauss, $a_{2(Co)} = 12$ gauss, $a_{3(Co)} = 65$ gauss; $a_{1(P)} = 28$ gauss, $a_{2(P)} = 27$ gauss, $a_{3(P)} = 34$ gauss.

Interestingly, the trityloxide complex $[PhBP_3]CoOCPh_3$ (**4.11**) exhibits a highly bent Co-O-C bond angle of 138.0(1)º, compared with the angle of 172.5(1)º for **4.1** and 165.7(1) for related **4.9**. Each of the Co-P bond distances in this umbrella distorted species are also expanded ($Co\text{-}P_{av} = 2.37$ Å). Moreover, each of the Co-P bond distances is expanded ($Co\text{-}P_{av} = 2.37$ Å), suggestive of a high spin ground state in accord with its solid-state SQUID (Figure 4.11) and glassy toluene EPR data (Figure 4.12D).

The magnetic data is complicated for **4.2** and **4.3** due to the possibility of η^3 interactions of the axial ligand. The solid-state crystal structure obtained for **4.2** at 98 K reveals the presence of two distinct conformational isomers. One of these isomers is a four-coordinate pseudotetrahedral species with a $Co\text{-}O\text{-}C_{ipso}$ angle of 110.3(4)º. The other

isomer is nominally five-coordinate and displays an η^3-binding mode of the aryloxide ligand that provides an acute Co-O-C_{ipso} angle of 88.4(3)º. SQUID magnetization data for **4.2** are shown in Figure 4.14. It is clear that the sample predominantly populates a doublet state at low temperature, though a weak signal at low field is discernable in the glassy toluene EPR spectrum of the sample. As the sample is warmed the $\chi_m T$ value gradually rises and at 300 K almost complete crossover to the high spin component is evident. Perhaps the simplest explanation of these data is that the pseudotetrahedral isomer of **4.2** is high spin at all temperatures, and that the isomer that exhibits an η^3-bonding mode is low spin at all temperatures. The magnetic data would then reflect variable populations of the two conformational isomers as a function of temperature in both solid and solution. Consistent with this explanation is the fact that the two other pseudotetrahedral aryloxide and alkoxide complexes we have examined, $[PhBP_3]CoO(2,6\text{-}Me_2\text{-}Ph)$ (**3.4**) and $[PhBP_3]CoOCPh_3$ (**4.11**), both exhibit high spin ground states, and the fact that five-coordinate cobalt(II) systems supported by phosphine ligands invariably populate low spin ground states. The fluorinated aryloxide complex $[PhBP_3]CoO(C_6F_5)$ (**4.3**) is less likely to exhibit π-bonding to the aryl ring due to its electron-withdrawing nature, though interactions with the ortho fluorines of the aryl group cannot be discounted. A similar four-coordinate/five-coordinate equilibrium may explain the change in spin state that is observed in the SQUID data (Figure 4.14).

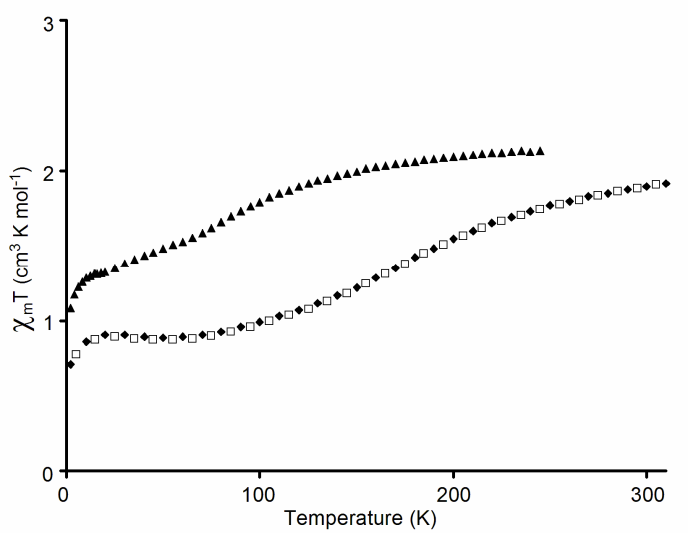

Figure 4.14. SQUID magnetization plot of $\chi_m T$ versus T for [PhBP$_3$]CoO(4-^{t}Bu-Ph) (**4.2**) as the temperature was raised (♦) and then lowered (□), and data for [PhBP$_3$]CoO(C$_6$F$_5$) (**4.3**) (▲) as the temperature was raised.

The complexes supported by the [PhBP$^{i\text{Pr}}_3$] ligand feature two high spin complexes, [PhBP$^{i\text{Pr}}_3$]CoI **(4.12**) and [PhBP$^{i\text{Pr}}_3$]CoOSiPh$_3$ (**4.13**), that exhibit the umbrella distortion, and one thiolate complex, [PhBP$^{i\text{Pr}}_3$]CoSSiPh$_3$ (**4.14**), that exhibits an off-axis distortion and is low spin (vide infra) at low temperature. Structural and magnetic data have been reported previously for [PhBP$^{i\text{Pr}}_3$]CoI (**4.12**). This complex exhibits a high spin ground state configuration and is therefore distinct from its low spin analog [PhBP$_3$]CoI (**3.1**). SQUID data collected on a polycrystalline sample of **4.13** are plotted in Figure 4.15A. The sample is clearly a S = 3/2 system ($\chi_m T_{av}$ (10 K - 300 K) = 2.30 cm^3 K mol^{-1}) and obeys the Curie-Weiss law. Similar magnetic behavior was reported for iodide **4.12**. Magnetization data for the thiolate derivative **4.14** are plotted in Figure 4.15B. The temperature dependence of its magnetic moment is more complex. Below 100 K the sample appears to be low spin ($\chi_m T_{av}$ (10 K - 100 K) = 0.50 cm^3 K

mol^{-1}). A gradual rise in $\chi_m T$ is observed above 100 K and a maximum value of 1.23 cm^3 K mol^{-1} is reached at 300 K, the highest temperature at which the data could be recorded. The magnetic behavior of the sample is fully reversible. The appearance of a gradual spin crossover phenomenon is similar to the rise in magnetic moment that was observed for thiolates **4.4** and **4.6** near room temperature. An interesting observation is that the solution moment of **4.14** at room temperature is 4.0 μ_B, consistent with a fully high spin population. This moment is different from that determined at low temperature by SQUID analysis of the polycrystalline sample, and we therefore elected to further analyze **4.14** by EPR spectroscopy as a powder and as a frozen glass. These data, along with the glassy toluene EPR spectrum of **4.13**, are shown in Figure 4.16. The 20 K glassy toluene spectra of **4.13** and **4.14** (Figure 4.16A and 4.16B) each show spectra characteristic of $S = 3/2$ species. The low field signal present in the glassy spectrum of **4.14** is absent in its powder spectrum at 20 K (Figure 4.16C). There appears therefore to be a stronger preference to populate the high spin configuration in *solution* for this thiolate complex. A different solution conformation of **4.14** may exist than the one that is observed in its solid-state structure at 98 K. Differences in spin behavior between solution and solid samples are not uncommon for spin crossover systems.[48] Even with the stronger donor ligand [$PhBP^{iPr}_3$] these complexes favor the high spin state unless there is a fourth ligand that is an unusually strong donor such as a thiolate ligand. The extreme Co-P axial bond elongation in **4.14** likely reflects a steric compensation that allows the doublet ground state to be populated.

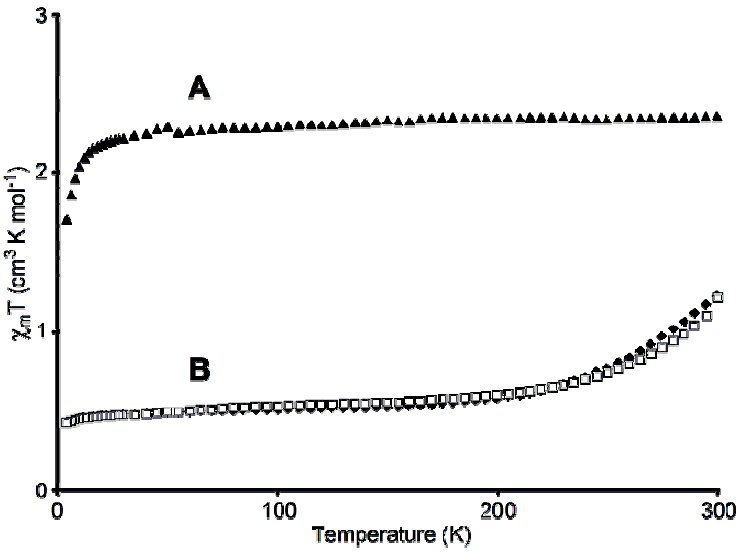

Figure 4.15. SQUID magnetization plot of $\chi_m T$ versus T for (A) [PhBP$^{iPr}_3$]CoOSiPh$_3$ (**4.13**) (▲), and (B) [PhBP$^{iPr}_3$]CoSSiPh$_3$ (**4.14**) as temperature was raised (♦) and then lowered (□).

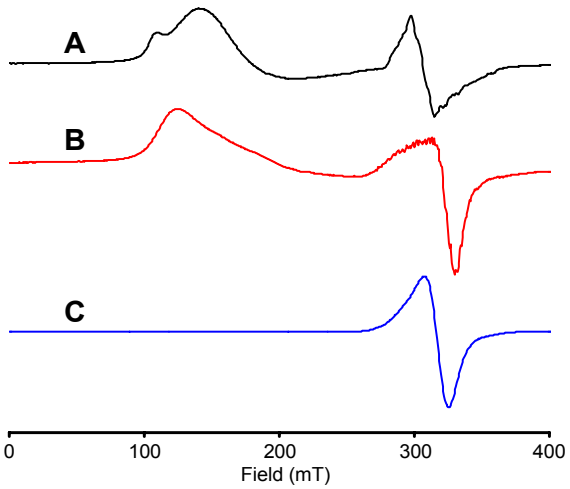

Figure 4.16. Glassy toluene EPR spectra (20 K) of (A) [PhBP$^{iPr}_3$]CoOSiPh$_3$ (**4.13**) (—), and (B) [PhBP$^{iPr}_3$]CoSSiPh$_3$ (**4.14**) (—). Powder sample EPR spectrum (20 K) of (C) [PhBP$^{iPr}_3$]CoSSiPh$_3$ (**4.14**) (—). Instrumental parameters for the spectra can be found in the Experimental Section.

4.2.6 Theoretical analysis of $[BP_3]Co^{II}$-X derivatives

The electronic structure features of umbrella and off-axis geometries share certain similarities, though there are a number of characteristics that distinguish them. To more thoroughly consider the case of their d^7 electronic structures we have undertaken the theoretical DFT examination of one representative complex from each structural subgroup. For this study we chose the siloxide complex $[PhBP_3]CoOSiPh_3$ **4.1** as representative of the umbrella subgroup, and thiolate $[PhBP_3]CoS(2,6\text{-}Me_2\text{-}Ph)$ **4.5** as representative of the off-axis subgroup. Single point electronic structure calculations (DFT) were performed using (i) the experimentally determined X-ray coordinates for each complex as the ground state geometrical structure under (ii) the assumption of a doublet electronic ground state. Each of the structures was subsequently allowed to relax into a theoretically determined global minimum in the absence of geometric constraints, but still under the assumption of a doublet ground state electronic configuration. For each complex, the frontier molecular orbitals obtained by both methods of analysis are qualitatively quite similar. There are, however, noteworthy structural differences between the experimentally and theoretically determined structures.

For pseudotetrahedral **4.1** the predicted frontier molecular orbitals from the geometry-restricted calculation are shown in Figure 4.17. Orbitals calculated for the DFT-optimized structure were calculated and are very similar to those shown here. The singly occupied molecular orbital (SOMO) is energetically well-separated from the lowest unoccupied orbital (LUMO). The lobal representations of the frontier orbitals containing significant d-orbital character map well with those we have sketched qualitatively in Figure 4.2, though the SOMO is predicted by DFT to lie much closer in

energy to the lower set of orbitals than to the LUMO. The SOMO and LUMO orbitals are nearly orthogonal to one another and align reasonably well along the plane containing the Co-O-Si vector. The lowest-lying three orbitals consist of one orbital of dz^2-parentage (HOMO-2) and two orbitals that are canted away from the Co-O-Si vector. While the low symmetry of the structure inevitably gives rise to d-orbital mixing, the lowest-lying pair of orbitals can be very crudely described as *dxy* and dx^2-y^2 type orbitals, where the z-axis is assumed to be coincident with the Co-O-Si vector. Interestingly, there are two high-lying [BP_3]-centered orbitals (HOMO, HOMO-1) comprised within the frontier manifold that would have been difficult to anticipate in the absence of the calculation.

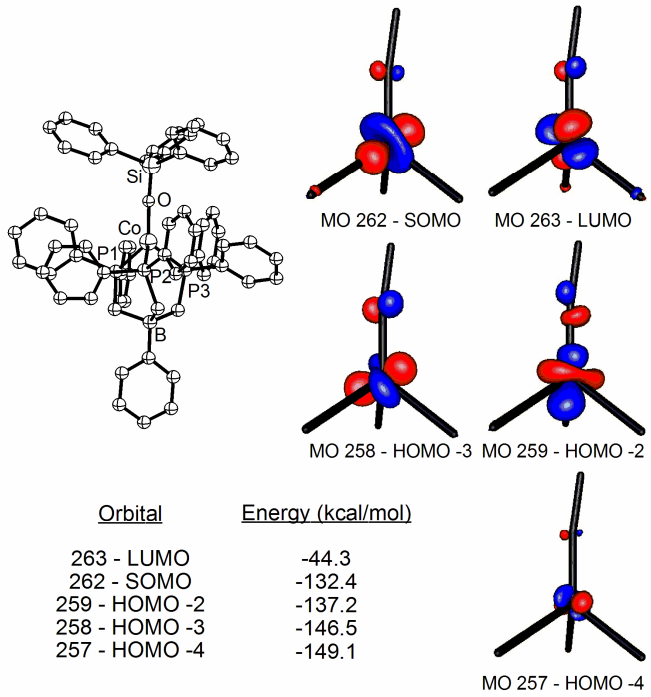

Figure 4.17. Molecular orbitals derived from a single point energy DFT calculation of [$PhBP_3$]$CoOSiPh_3$ (**4.1**) assuming a doublet ground state and the crystallographically determined atomic coordinates.

DFT-minimization of the geometry of **4.1** gives rise to a conformationally similar structure (**4.1**-DFT), with the noteworthy distinction that distortion of one of its Co-P bond distances is grossly exaggerated (2.22 Å, 2.25 Å, 2.43 Å). Despite this structural distinction, the calculation still points to a LUMO that is energetically well-separated from a lower-lying set of d-type orbitals that includes the SOMO. This conclusion is in accord with DFT studies for **4.5**. Table 4.4 compares the core bond lengths and angles of the solid-state structures to the DFT determined structures.

Table 4.4. Experimental and calculated bond lengths and angles for **4.1**, **4.5**, and {**4.15**}.

4.1	Exptl	Calcd	**4.5**	Exptl	Calcd	{**4.15**}	Exptl	Calcd
				Bond Lengths (Å)				
Co-O	1.799	1.849	Co-S	2.167	2.223	Co-O	1.766	1.776
Co-P1	2.156	2.429	Co-P1	2.251	2.418	Co-P1	2.187	2.236
Co-P2	2.284	2.224	Co-P2	2.199	2.271	Co-P2	2.182	2.241
Co-P3	2.169	2.251	Co-P3	2.208	2.286	Co-P3	2.184	2.234
				Bond Angles (deg)				
Co-O-Si	172.5	162.8	Co-S-C46	114.6	119.1	Co-O-Si	178.6	178.7
P1-Co-P2	91.38	88.9	P1-Co-P2	89.44	89.4	P1-Co-P2	90.67	90.8
P1-Co-P3	85.88	94.8	P1-Co-P3	100.23	95.9	P1-Co-P3	90.18	90.8
P2-Co-P3	94.60	88.8	P2-Co-P3	86.73	89.5	P2-Co-P3	90.50	90.5
P1-Co-O	129.45	116.7	P1-Co-S	96.48	99.9	P1-Co-O	125.6	124.4
P2-Co-O	119.42	138.2	P2-Co-S	147.37	145.4	P2-Co-O	124.4	126.4
P3-Co-O	125.82	118.1	P3-Co-S	123.30	122.1	P3-Co-O	124.8	123.5

Lobal representations of the frontier molecular orbitals of the off-axis thiolate complex **4.5** based upon a single-point electronic structure calculation are displayed in Figure 4.18. The LUMO is again energetically well-separated from a set of low-lying d-type orbitals. Certain comparative differences do arise with respect to the MO structure of **4.1**. The LUMO now appears to be coincident with the trigonal plane defined by two Co-P vectors and the Co-S vector, and the SOMO is directed with a lobe that is pointed towards the axial P donor ligand. The shape of the SOMO explains why the axial phosphine ligand is appreciably elongated in the crystal structure of **4.5**. The DFT-minimized structure, **4.5**-DFT, dramatically exaggerates this elongation, as was also observed for the case of **4.1**. The HOMO and HOMO-1 orbitals are no longer ligand centered but now comprise d-type orbitals with additional contributions from the equatorial thiolate ligand. The phasing suggests that the interaction is of Co-S π^* character in each case. The lowest-lying orbital is difficult to distinguish from the HOMO and HOMO-1 orbitals, and the high degree of mixing due to the low symmetry of the system is evident.

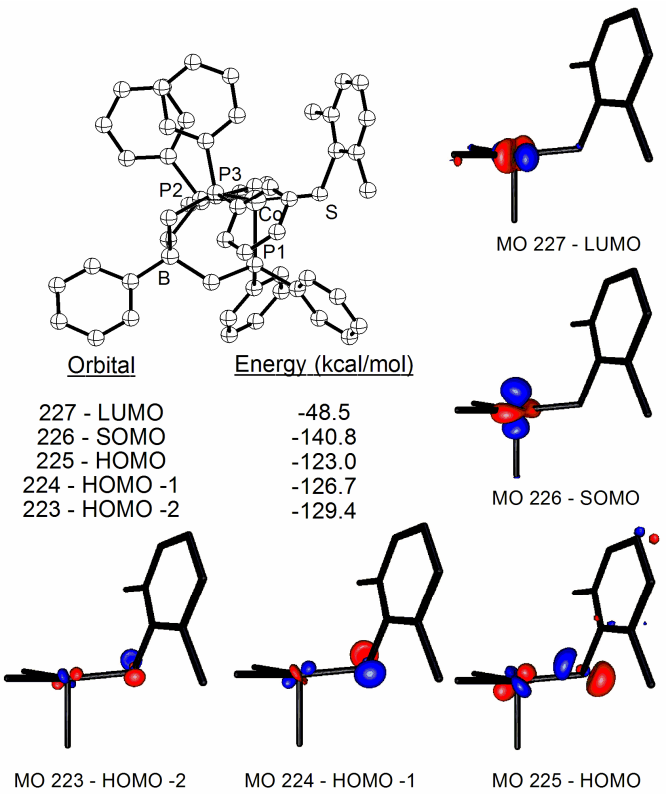

Figure 4.18. Molecular orbitals derived from a single point energy DFT calculation of [PhBP$_3$]CoS(2,6-Me$_2$-Ph) (**4.5**) assuming a doublet ground state and the crystallographically determined atomic coordinates.

The transition state for dissociation of one phosphine ligand should look similar to the highly distorted structures we have calculated for **4.1** and **4.5**. In this context it is interesting to note that the d^7 low spin half-sandwich complex [Tp]Co[Cp*] has been characterized, and dissociation of one of its pyrazolyl donor arms is indeed observed in the solid-state.[9e,f] The authors have suggested that in solution an equilibrium between the κ^2- and κ^3-binding modes is present.[9f] The crystal structure of **4.14** is interesting for comparison in that it provides an experimentally determined ground state structure featuring one Co-P bond that is strikingly elongated by comparison to the other two. In effect, the crystal structure of this complex is a better match for the theoretical structure

obtained for **4.5**, and related d^7 $[BP_3]Ni(NR)$ species, by virtue of the exaggerated distortion.[49] Because the solution magnetic (Evans) and EPR data for **4.15** are indicative of a high spin component, it is reasonable to suggest that an equilibrium mixture between κ^2- and κ^3-binding modes might exist in solution. Nevertheless, it seems more likely to us that the equilibrium is between an umbrella distorted high spin structure, similar to **4.7**, and an off-axis distorted low spin structure in the solid-state.

Our inability to faithfully reproduce the crystallographically determined structures of **4.1** and **4.5** detracts from our confidence to use DFT methods to theoretically predict the ground spin-state of these systems. To illustrate this point, when we calculate the total energy of the DFT-minimized structures of iodide **3.1** assuming a doublet and a quartet state, respectively, the quartet state is energetically favored by 8.8 kcal/mol. This result is in obvious contradiction to the experimentally observed low spin state preference. A general problem associated with open-shell DFT calculations is that there is, as yet, no universally applicable method and basis-set that can be confidently applied to a given system.

The geometries and electronic structures of closed-shell coordination complexes are more reliably predicted by current DFT methods, and we therefore examined diamagnetic $\{\mathbf{4.15}\}^+$. The nature of the SOMO orbital of **4.1** suggests that the removal of one unpaired electron should relieve its distorted structure. This is in fact observed, both crystallographically and theoretically. Recall that XRD analysis of $\{\mathbf{4.15}\}\{BPh_4\}$ revealed an extremely symmetric structure containing a P_3Co subunit defining one half of an octahedron almost perfectly trisected by the Co-O-Si bond vector (Figure 4.5). Complex $\{\mathbf{4.15}\}^+$ can be consequently classified by structure type **E** from Figure 4.2, and

its molecular orbital diagram is therefore anticipated to reflect the two-over-three splitting diagram of an octahedral complex. The presence of degenerate π-binding should give rise to a sizable separation between the upper two and lower three d-orbitals. This picture is evident from the single-point electronic structure calculation performed for {**4.15**}$^{+}$. Lobal representations for the orbitals of dominant d-type contributions are shown in Figure 4.19. As for the MO structure of **4.1**, a number of filled ligand centered orbitals lie at relatively high energy, in this case falling between the lower-lying (a_1 + e) filled d-orbital set comprised of dz^2, *dxy*, and dx^2-y^2 and the upper-lying, empty d-orbital e set comprising *dxz* and *dyz*. These frontier d-orbitals reflect the unmistakable analogy between pseudotetrahedral {**4.15**}$^{+}$ and the electronic structure of sandwich and half-sandwich complexes.[9f,50] The DFT-optimized structure for {**4.15**}$^{+}$ was found to be in good agreement with the crystal structure of {**4.15**}{BPh_4} (Table 4.4).

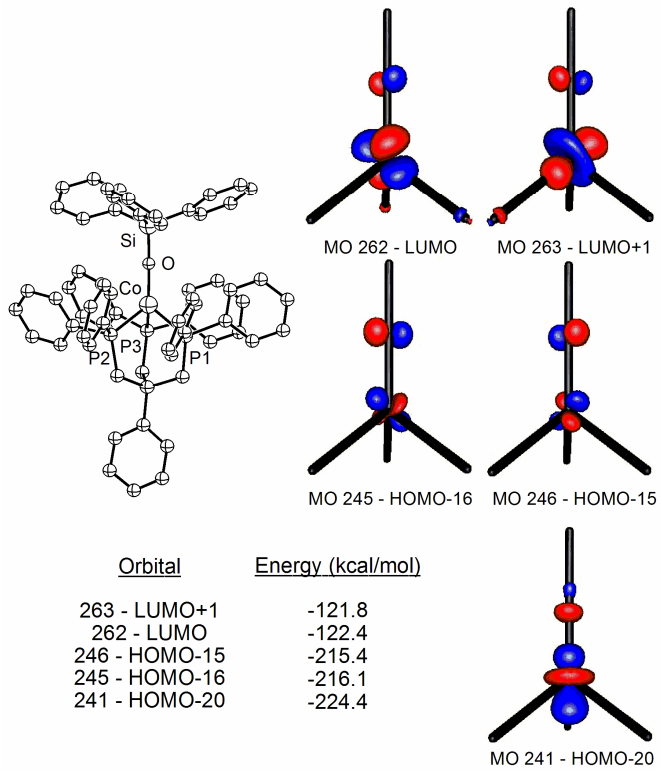

Figure 4.19. Molecular orbitals consisting of significant d-orbital contributions for the frontier region of $\{\mathbf{4.15}\}^{+}$. Orbitals were derived from a single-point electronic structure calculation assuming a singlet ground state and the crystallographically determined atomic coordinates.

4.3 Conclusion

It is evident from the present study that magnetic phenomena for distorted tetrahedral d^7 ions can be much richer then had been appreciated previously. For highly covalent $[BP_3]Co(II)$ complexes, low spin, high spin, and spin crossover complexes are readily accessible for a variety of related geometries best described as pseudotetrahedral with an umbrella or off-axis distortion. The observation of an $S = ½$ ground state for tetracoordinate $[BP_3]Co^{II}X$ complexes appears at this stage to be neither exceptional nor

uncommon–a host of such complexes have now been thoroughly characterized. Given this situation, it is of obvious interest to re-examine other d^7 L_3CoX scaffolds to determine whether access to the $S = ½$ ground state will prove more ubiquitous than was previously thought. Tetracoordinate L_3Co^{II}-SR thiolate complexes should offer a good starting point in this regard, though for the single [Tp]Co(II) thiolate we have examined, the more typical $S = 3/2$ ground state is preferred.

Our data establish that ground spin-state assignments for these types of d^7 ions can be readily made by inspection of their low-temperature solid-state structural, SQUID, and EPR data. The halide structures $[PhBP_3]CoI$ and $[PhBP^{iPr}_3]CoCl$ represent the simplest limiting cases.[15,25] For example, the crystal structure of $[PhBP_3]CoI$ reveals its $S = ½$ ground state by virtue of its three relatively short Co-P distances, with one bond longer than the other two. This contrasts with the structure of $[PhBP^{iPr}_3]CoCl$, in which each Co-P distance is elongated but essentially equidistant, and a threefold axis is more readily discerned. The collection of low temperature data collected for complexes **4.2** and **4.3** serve as a reminder that SQUID or EPR data need to be interpreted cautiously in the absence of structural data. In particular, slippage of a monodentate X-type ligand to a higher coordination mode (e.g., from η^1 to η^3) can confer a spin-state change.

Curious and perhaps still counterintuitive is that the stronger-field donor ligand $[PhBP^{iPr}_3]$ tends to confer the high spin configuration. Such is the case not only for $[PhBP^{iPr}_3]CoCl$, but also for $[PhBP^{iPr}_3]CoI$ (**4.12**) and $[PhBP^{iPr}_3]CoOSiPh_3$ (**4.13**). To account for this, we maintain that conformational constraints imposed by the $[PhBP^{iPr}_3]$ ligand will disfavor short Co-P contacts so as to minimize steric repulsion by the isopropyl groups of this bulky ligand. In the absence of overriding factors, such as strong

π-bonding at the X-linkage, a high spin population is energetically preferred. By choosing a more strongly π-donating X-type linkage, as is the case for the complex [PhBP$^{i\text{Pr}}_3$]CoSSiPh$_3$ (**4.14**), an S = ½ ground state can be realized (at least in the solid-state), but now the requisite distortion that relieves the σ* (and appreciably π*) interaction of the SOMO is far more pronounced than for the case of low spin [PhBP$_3$] systems.

While these examples illustrate the effect that rather dramatic structural and electronic differences can have on the observed ground spin-states of these systems, more subtle differences can have equally striking consequences. For instance, the complex [PhBP$_3$]CoS(2,4,6-^{i}Pr$_3$-Ph) (**4.6**) is an off-axis low spin species, whereas [PhBP$_3$]CoS(2,4,6-^{t}Bu$_3$-Ph) (**4.7**) adopts a distinctly different umbrella distortion and populates a high spin ground state. Even more subtle changes can have profound electronic consequences. Replacement of the trityl C-atom in [PhBP$_3$]CoOCPh$_3$ (**4.11**) by the Si-atom in [PhBP$_3$]CoOSiPh$_3$ (**4.1**) alters the system's ground electronic state from S = 3/2 to S = ½, respectively. This secondary sphere effect is striking and is immediately evident by comparison of the low temperature glassy toluene EPR spectra of the two samples. We have also shown that the spin population of a d^7 L$_3$CoX system can be fine-tuned by adjusting the electron-donor character of the X-type linkage at a site even further removed from the cobalt center. This possibility is evident from the SQUID magnetization and EPR data for [PhBP$_3$]CoOSi(4-NMe$_2$-Ph)$_3$ (**4.9**) and [PhBP$_3$]CoOSi(4-CF$_3$-Ph)$_3$ (**4.10**) and, moreover, suggests that truly cooperative spin crossover d^7 L$_3$CoX platforms might be realized if X-type linkages can be appropriately tailored. This possibility represents an exciting opportunity, as it would enable the

reactivity patterns of structurally related $S = 1/2$ and $S = 3/2$ coordinatively unsaturated d^7 ions to be probed as a function of their spin populations.[32c,51]

4.4 Experimental section

4.4.1 General considerations

General procedures were performed according to Section 2.4.1 and 3.5.1. Magnetic measurements were conducted as described in Section 3.5.2. EPR measurements and simulations were conducted as described in Section 3.5.3.

4.4.2 EPR measurements

Table 4.5. Instrumental parameters for the EPR spectra shown.

Complex Number	**4.1**	**4.2**	**4.3**	**4.4**	**4.5**	**4.6**	**4.7**
Solvent	toluene	toluene	toluene	toluene	toluene	toluene	toluene
Temperature (K)	20	20	20	77	77	10	20
ν (GHz)	9.475	9.474	9.380	9.380	9.379	9.378	9.379
Modulation frequency (kHz)	100	100	100	100	100	100	100
Modulation amplitude (gauss)	4	5	4	4	4	4	4
Microwave power (mW)	0.202	2.02	2.02	0.641	2.02	0.638	2.02
Conversion time (ms)	81.92	81.92	81.92	163.84	81.92	81.92	81.92
Time constant (ms)	20.48	20.48	20.48	40.96	20.48	20.48	20.48
Scans	2	4	3	1	2	1	3

Table 4.5. (cont.)

Complex Number	**4.8**	**4.9**	**4.10**	**4.11**	**4.13**	**4.14**	**4.14**
Solvent	toluene	toluene	toluene	toluene	toluene	toluene	powder
Temperature (K)	20	20	20	20	20	20	20
ν (GHz)	9.380	9.378	9.378	9.379	9.377	9.378	9.382
Modulation frequency (kHz)	100	100	100	100	100	100	100
Modulation amplitude (gauss)	4	4	4	4	4	4	4
Microwave power (mW)	0.638	0.0639	0.00639	0.202	0.639	0.638	0.0638
Conversion time (ms)	81.92	81.92	81.92	81.92	81.92	81.92	81.92
Time constant (ms)	20.48	20.48	20.48	20.48	20.48	20.48	20.48
Scans	1	1	1	1	1	1	3

4.4.3 Computational methods

All calculations were performed using the hybrid DFT functional B3LYP as implemented in the Jaguar 5.0 program package.[52] This DFT functional utilizes the Becke three-parameter functional[53] (B3) combined with the correlation functional of Lee, Yang, and Parr[54] (LYP). LACVP** was used as the basis set. Input coordinates were derived as described in the text from crystallographically determined structures. Spin-states and molecular charges were explicitly stated, and no molecular symmetry was imposed. Default values for geometry and SCF iteration cutoffs were used. All structures

converged under these criteria except for the geometry minimization of **4.1**. In this case, multiple additional cycles showed no more than 1 kcal/mol difference in energy.

The continuous symmetry measurements were determined with the program SHAPE developed at the Universitat de Barcelona, Spain.[55]

4.4.4 Starting materials and reagents

The preparation of [$PhBP_3$]CoI (**3.1**) and ([$PhBP_3$]CoCl) (**3.3**) is described in Chapter 3. [$PhBP^{iPr}_3$]CoI (**4.12**) was prepared according to a literature procedure. The reagents $TlOSiPh_3$,[56] TlO-*p*-^{t}Bu-Ph, TlSPh,[57] HS(2,4,6-^{i}Pr_3-Ph),[58] HS(2,4,6-^{t}Bu_3-Ph),[59] HOSi(*p*-NMe_2-Ph)$_3$,[60] HOSi(*p*-CF_3-Ph)$_3$,[61] {[Cp]$_2$Fe}{BPh_4},[62] and {[Cp]$_2$Fe}{B(3,5-$(CF_3)_2$-Ph)$_4$}[63] were prepared according to literature procedures. TlO(C_6F_5), TlS(2,6-Me_2-Ph), TlS(2,4,6-^{i}Pr_3-Ph), TlS(2,4,6-^{t}Bu_3-Ph), $TlSSiPh_3$, $TlOCPh_3$, TlOSi(*p*-NMe_2-Ph)$_3$, and TlOSi(*p*-CF_3-Ph)$_3$ were prepared via a modification of a general synthetic method reported by Tolman (see below). The reagents HO(*p*-^{t}Bu-Ph), HO(C_6F_5), HSPh, HS(2,6-Me_2-Ph), $HOCPh_3$, $HOSiPh_3$, $HSSiPh_3$, $CoBr_2$, and [K][$Tp^{3,5\text{-}Me2}$] were purchased from commercial vendors and used without further purification. Thallium ethoxide was purchased from Aldrich, filtered through a pad of Celite to remove insoluble black material, and then stored at -35 °C.

General method for the preparation of thallium reagents (modified from Tolman et. al.): The appropriate phenol, thiol, silanol, or silylthiol (about 200 mg) was dissolved in petroleum ether (10 mL) and a minimal amount of THF (if necessary). One equivalent of thallium ethoxide was added as a petroleum ether solution (4 mL), and the reaction mixture was stirred for 30 min. The reaction was preformed in the dark to minimize thallium ethoxide degradation. The precipitates were collected on a medium frit

and washed with petroleum ether (2 x 10 mL) and then dried. The thallium reagents were used without further purification.

4.4.5 Synthesis of compounds

Additional ^{1}H NMR data for [PhBP$_3$]CoI, 3.1. ^{1}H NMR (C_6D_6, 300 MHz): δ 22.3 (6 H, T_1 = 2.4 ms, PhB(C*H*$_2$PPh$_2$)$_3$), 10.8 (12 H, T_1 = 23.6 ms, *meta* P(C$_6$*H*$_5$)$_2$), 7.7 (2 H, T_1 = 40.5 ms, *ortho* B(C$_6$*H*$_5$)), 7.5 (3 H, T_1 = 205 ms, *meta* and *para* B(C$_6$*H*$_5$)), 4.3 (12 H, T_1 = 1.2 ms, *ortho* P(C$_6$*H*$_5$)$_2$), 2.2 (6 H, T_1 = 46.7 ms, *para* P(C$_6$*H*$_5$)$_2$).

Synthesis of [PhBP$_3$]CoOSiPh$_3$, 4.1. A THF (4 mL) solution of TlOSiPh$_3$ (0.173 g, 0.361 mmol) was added dropwise to a stirring solution of [PhBP$_3$]CoI (**3.1**) (0.315 g, 0.361 mmol) in THF (8 mL). The resulting solution was allowed to stir for 10 h. An orange precipitate formed (TlI), which was filtered away over diatomaceous earth. The THF was then removed in vacuo and the resulting solid was dissolved in benzene (4 mL). Crystals were grown via vapor diffusion of petroleum ether into a benzene solution. The purple crystals were dried and weighed (0.300 g, 81% yield). The crystals were recrystallized two additional times (from benzene/petroleum ether) before measurements were taken on the samples (95% yield for each recrystallization). ^{1}H NMR (C_6D_6, 300 MHz): δ 15.6, 10.0, 9.8, 8.6, 8.3, 7.4, 1.1 (br), -2.2. ^{1}H NMR (d$_8$-toluene, 300 MHz): δ 15.4, 9.9, 9.7, 8.6, 8.1, 7.4 (m), 7.1 (m), 1.1 (br), -2.0. UV-vis (C_6H_6) λ_{max}, nm (ε): 557 (700), 763 (310). UV-vis (C_6D_6) λ_{max}, nm (ε): 557 (670), 757 (280), 1136 (320). UV-vis (toluene) λ_{max}, nm (ε): 557 (650), 763 (290). UV-vis (THF) λ_{max}, nm (ε): 557 (670), 761 (300). Evans Method (C_6D_6 – 295 K): 3.42 μ_B; (d$_8$-toluene – 295 K): 3.51 μ_B; (d$_8$-THF – 295 K): 3.54 μ_B. EPR (toluene, 20 K): g_x = 2.03, $a_{x(Co)}$ = 65 gauss, $a_{x(P)}$ = 34 gauss; g_y = 2.05, $a_{y(Co)}$ = 12 gauss, $a_{y(P)}$ = 27 gauss; g_z = 2.21, $a_{z(Co)}$ = 105 gauss, $a_{z(P)}$ = 28 gauss.

Electrochemistry (vs. ferrocene in THF with [TBA][ClO_4] as supporting electrolyte): Co^{II}/Co^{III}, -360 mV; Co^{I}/Co^{II}, -1290 mV. Anal. Calcd for $C_{63}H_{56}BCoOP_3Si$: C, 74.19; H, 5.53. Found: C, 74.27; H, 5.42.

Synthesis of [$PhBP_3$]CoO(4-^{t}Bu-Ph), 4.2. Followed protocol for **4.1**. Used TlO-*p*-^{t}BuPh (85.8 mg, 0.243 mmol) and **3.1** (212 mg, 0.243 mmol). Red-brown crystals of **4.2** were isolated (115 mg, 53% yield). ^{1}H NMR (C_6D_6, 300 MHz): δ 12.3 (br), 9.2, 7.7, 2.1, 1.2, 0.9, 0.5 (br). UV-vis (C_6H_6) λ_{max}, nm (ε): 428 (2300), 567 (1600), 715 (700). Evans Method (C_6D_6): 3.43 μ_B. Electrochemistry (vs. ferrocene in THF with [TBA][PF_6] as supporting electrolyte): Co^{II}/Co^{III}, -390 mV; Co^{I}/Co^{II}, -1330 mV. Anal. Calcd for $C_{55}H_{54}BCoOP_3$: C, 73.92; H, 6.09. Found: C, 73.58; H, 6.01.

Synthesis of [$PhBP_3$]CoO(C_6F_5), 4.3. Followed protocol for **4.1**. Used TlO(C_6F_5) (109 mg, 0.281 mmol) and **3.1**, (245 mg, 0.281 mmol). Olive green crystals of **4.3** were isolated (159 mg, 59% yield). ^{1}H NMR (C_6D_6, 300 MHz): δ 16.9, 10.9, 8.5, 7.5, -1.0, -3.4, -61.8. ^{19}F NMR (C_6D_6, 282 MHz): δ -73.1, -181.0. UV-vis (C_6H_6) λ_{max}, nm (ε): 582 (740), 712 (560). Evans Method (C_6D_6): 3.8 μ_B. Anal. Calcd for $C_{51}H_{41}BCoF_5OP_3$: C, 66.04; H, 4.46. Found: C, 65.19; H, 4.39.

Synthesis of [$PhBP_3$]CoSPh, 4.4. Followed protocol for **4.1**. Used TlSPh (94.0 mg, 0.300 mmol) and **3.1** (261 mg, 0.300 mmol). Red crystals of **4.4** were isolated (193 mg, 75% yield). ^{1}H NMR (C_6D_6, 300 MHz): δ 24.7 (br), 16.7, 10.7, 8.3, 7.7, 7.6, 2.2 (br), 1.4, -3.1 (br), -6.0. UV-vis (C_6D_6) λ_{max}, nm (ε): 460 (3500), 597 (1800), 1204 (270). Evans Method (C_6D_6): 2.43 μ_B. Electrochemistry (vs. ferrocene in THF with [TBA][PF_6] as supporting electrolyte): Co^{II}/Co^{III}, -160 mV; Co^{I}/Co^{II}, -1120 mV. Anal. Calcd for $C_{51}H_{46}BCoP_3S$: C, 71.76; H, 5.43. Found: C, 71.94; H, 5.42.

Synthesis of [PhBP$_3$]CoS(2,6-Me$_2$-Ph), 4.5. Followed protocol for **4.1**. Used TlS(2,6-Me$_2$-Ph) (102 mg, 0.297 mmol) and **3.1** (259 mg, 0.297 mmol). Red crystals of **4.5** were isolated (172 mg, 66% yield). ^{1}H NMR (C_6D_6, 300 MHz): δ 79.8, 26.7, 19.6, 13.1, 9.9, 8.2, 8.0, 0.5 (br), -1.1, -21.1. UV-vis (C_6H_6) λ_{max}, nm (ε): 396 (4600), 486 (3200), 599 (2300), 741 (900). Evans Method (C_6D_6): 2.28 μ_B. Electrochemistry (vs. ferrocene in THF with [TBA][ClO_4] as supporting electrolyte): Co^{II}/Co^{III}, -170 mV; Co^{I}/Co^{II}, -1100 mV. Anal. Calcd for $C_{53}H_{50}BCoP_3S$: C, 72.20; H, 5.72. Found: C, 72.42; H, 5.69.

Synthesis of [PhBP$_3$]CoS(2,4,6-^{i}Pr$_3$-Ph), 4.6. Followed protocol for **4.1**. Used TlS(2,4,6-^{i}Pr$_3$-Ph) (117 mg, 0.265 mmol) and {[PhBP$_3$]CoCl} (**3.3**) (207 mg, 0.265 mmol). Red-brown crystals of **4.6** were isolated (178 mg, 68% yield). ^{1}H NMR (C_6D_6, 300 MHz): δ 46.4 (br), 21.7, 11.6, 9.1, 8.9, 7.8, 7.7, 4.8, 1.3, 0.9. UV-vis (C_6H_6) λ_{max}, nm (ε): 384 (6600), 471 (4200), 609 (3000), 743 (900). Evans Method (C_6D_6): 2.80 μ_B. Electrochemistry (vs. ferrocene in THF with [TBA][PF_6] as supporting electrolyte): Co^{II}/Co^{III}, -80 mV; Co^{I}/Co^{II}, -1190 mV. Anal. Calcd for $C_{60}H_{64}BCoP_3S$: C, 73.54; H, 6.58. Found: C, 73.18; H, 6.57.

Synthesis of [PhBP$_3$]CoS(2,4,6-^{t}Bu$_3$-Ph), 4.7. Followed protocol for **4.1**. Used TlS(2,4,6-^{t}Bu$_3$-Ph) (145 mg, 0.302 mmol) and **3.1** (263 mg, 0.302 mmol). Red crystals of **4.7** were isolated (113 mg, 36% yield). ^{1}H NMR (C_6D_6, 300 MHz): δ 50.8, 16.7, 12.8, 10.6 (br), 9.2, 8.1, 2.3, -3.2 (br), -5.4, -27.0. UV-vis (C_6D_6) λ_{max}, nm (ε): 479 (3600), 640 (1900), 754 (1800), 1190 (430). Evans Method (C_6D_6): 3.90 μ_B. Electrochemistry (vs. ferrocene in THF with [TBA][PF_6] as supporting electrolyte): Co^{II}/Co^{III}, -60 mV;

Co^{I}/Co^{II}, -1080 mV. Anal. Calcd for $C_{63}H_{70}BCoP_3S$: C, 74.04; H, 6.90. Found: C, 73.95; H, 6.98.

Synthesis of [PhBP$_3$]CoSSiPh$_3$, 4.8. Followed protocol for **4.1**. Used $TlSSiPh_3$ (187 mg, 0.376 mmol) and **3.1** (328 mg, 0.376 mmol). Green crystals of **4.8** were isolated (321 mg, 83% yield). ^{1}H NMR (C_6D_6, 300 MHz): δ 46.4, 11.9, 8.7-6.6, 1.3. UV-vis (C_6H_6) λ_{max}, nm (ε): 622 (1300), 747 (670). Evans Method (C_6D_6): 2.53 μ_B. Electrochemistry (vs. ferrocene in THF with [TBA][PF_6] as supporting electrolyte): Co^{II}/Co^{III}, -210 mV (irreversible), Co^{I}/Co^{II}, -1010 mV. Anal. Calcd for $C_{63}H_{56}BCoP_3SSi$: C, 73.04; H, 5.45. Found: C, 73.06; H, 5.49.

Synthesis of [PhBP$_3$]CoOSi(4-NMe$_2$-Ph)$_3$, 4.9. Followed protocol for **4.1**. Used $TlOSi(p\text{-}NMe_2\text{-}Ph)_3$ (228 mg, 0.374 mmol) and ([$PhBP_3$]CoCl) (**3.3**) (292 mg, 0.374 mmol). Layering of petroleum ether (14 mL) onto a toluene solution (4 mL) afforded red crystalline product (173 mg). The recrystallization of the product from the supernatant leads to additional product (115 mg) to give a total yield of 67%. ^{1}H NMR (C_6D_6, 300 MHz): δ 103.7, 14.6, 10.1 (br), 9.5, 8.1, 7.8, 7.4, 2.7, 2.1, -1.0. UV-vis (C_6H_6) λ_{max}, nm (ε): 555 (940), 699 (440), 772 (420). Evans Method (C_6D_6): 3.46 μ_B. Electrochemistry (vs. ferrocene in THF with [TBA][ClO_4] as supporting electrolyte): Co^{II}/Co^{III}, -360 mV; Co^{I}/Co^{II}, -1300 mV. Anal. Calcd for $C_{69}H_{71}BCoN_3OP_3Si$: C, 72.12; H, 6.23; N, 3.66. Found: C, 71.77; H, 6.40; N, 3.52.

Synthesis of [PhBP$_3$]CoOSi(4-CF$_3$-Ph)$_3$, 4.10. Followed protocol for **4.1**. Used $TlOSi(p\text{-}CF_3\text{-}Ph)_3$ (99 mg, 0.145 mmol) and ([$PhBP_3$]CoCl) (**3.3**), (113 mg, 0.145 mmol). The toluene solution (2 mL) was layered with 15 mL of petroleum ether and cooled to -35 ºC until crystals formed. The crystals were then dried in vacuo yielding the pure

compound (117 mg, 66% yield). ^{1}H NMR (C_6D_6, 300 MHz): δ 17.4, 10.7, 9.8 (br), 8.8, 8.5, 7.3, -0.9, -4.2, -81.6 (br). ^{19}F NMR (C_6D_6, 282 MHz): δ -58.1. UV-vis (C_6H_6) λ_{max}, nm (ε): 560 (740), 757 (320). Evans Method (C_6D_6, 298 K): 3.93 μ_B. Electrochemistry (vs. ferrocene in THF with [TBA][ClO_4] as supporting electrolyte): Co^{II}/Co^{III}, -60 mV (irreversible), Co^{I}/Co^{II}, -1080 mV. Anal. Calcd for $C_{66}H_{53}BCoF_9OP_3Si$: C, 64.77; H, 4.36. Found: C, 64.70; H, 4.55.

Synthesis of [PhBP$_3$]CoOCPh$_3$, 4.11. A THF solution (3 mL) of the thallium reagent $TlOCPh_3$ (124 mg, 0.267 mmol) was added to a stirring THF solution (10 mL) of [$PhBP_3$]CoI, **3.1** (233 mg, 0.267 mmol). The solution was stirred for 4 h and a yellow precipitate formed (TlI). The precipitate was removed by filtration over diatomaceous earth. The remaining reaction volatiles were removed in vacuo, and the blue-green powder was then washed with petroleum ether (2 x 10 mL) and dried. The solid was then redissolved in benzene (4 mL) and then triturated with petroleum ether (15 mL). The supernatant was separated from the brown solid via filtration. The blue-green solution was dried in vacuo and then crystallized by vapor diffusion of petroleum ether into a benzene solution (47 mg, 18% yield). ^{1}H NMR (C_6D_6, 300 MHz): δ 20.1, 16.7, 11.3, 9.5, 8.7, 7.9, 7.7, -1.4, -5.0, -83.7. UV-vis (C_6H_6) λ_{max}, nm (ε): 578 (550), 778 (270). Evans Method (C_6D_6, 298 K): 3.75 μ_B. Electrochemistry (vs. ferrocene in THF with [TBA][PF_6] as supporting electrolyte): Co^{II}/Co^{III}, -300 mV; Co^{I}/Co^{II}, -1310 mV. Anal. Calcd for $C_{64}H_{56}BCoOP_3$: C, 76.58; H, 5.62. Found: C, 76.23; H, 5.88.

Additional ^{1}H NMR data for [PhBP$^{i\mathrm{Pr}}_3$]CoI, 4.12. ^{1}H NMR (C_6D_6, 300 MHz): δ 115.6 (6 H, T_1 = 2.6 ms, $PhB(CH_2P^iPr_2)_3$ or $P(CH(CH_3)_2)_2$), 41.6 (6 H, T_1 = 0.9 ms, $PhB(CH_2P^iPr_2)_3$ or $P(CH(CH_3)_2)_2$), 24.1 (18 H, T_1 = 5.6 ms, $P(CH(CH_3)_2)_2$), 12.8 (2 H, T_1

= 17.5 ms, *ortho* B(C_6H_5)), 9.0 (1 H, T_1 = 204 ms, *para* B(C_6H_5)), 7.3 (2 H, T_1 = 244 ms, *meta* B(C_6H_5)), 3.3 (18 H, T_1 = 1.9 ms, P(CH(CH_3)$_2$)$_2$).

Synthesis of [PhBP$^{iPr}_3$]CoOSiPh$_3$, 4.13. A THF solution (2 mL) of the thallium reagent TlOSiPh$_3$ (58 mg, 0.12 mmol) was added to a stirring THF solution (5 mL) of [PhBP$^{iPr}_3$]CoI, **4.12** (81 mg, 0.12 mmol). The solution was stirred for 1 h, and a yellow precipitate formed (TlI). The precipitate was removed by filtration over diatomaceous earth. The remaining reaction volatiles were removed in vacuo, and the purple powder was redisolved in benzene (5 mL). The benzene solution was filtered over diatomaceous earth to remove any residual TlI and then frozen and lyophilized to remove any trace of THF. Vapor diffusion of petroleum ether into a benzene solution (1 mL) afforded purple crystalline product (39 mg, 41% yield). ^{1}H NMR (C_6D_6, 300 MHz): δ 32.8, 21.6, 12.1, 11.0, 9.2, 8.9, 7.5, 7.4, 1.7, -60.3. UV-vis (C_6H_6) λ_{max}, nm (ε): 553 (600), 657 (380), 788 (320). Evans Method (C_6D_6): 4.32 μ_B. Electrochemistry (vs. ferrocene in THF with [TBA][PF_6] as supporting electrolyte): Co^{II}/Co^{III}, 100 mV (irreversible); Co^{I}/Co^{II}, -1690 mV. Anal. Calcd for $C_{45}H_{68}BCoOP_3Si$: C, 66.25; H, 8.40. Found: C, 66.20; H, 8.14.

Synthesis of [PhBP$^{iPr}_3$]CoSSiPh$_3$, 4.14. Followed protocol for **4.13**. Used TlSSiPh$_3$ (161 mg, 0.325 mmol) and **4.12** (216 mg, 0.325 mmol). Green crystals of **4.14** were isolated (167 mg, 62% yield). ^{1}H NMR (C_6D_6, 300 MHz): δ 35.7, 20.7, 11.4, 9.3, 8.7, 7.8, 7.1, 6.2, 5.0, -52.6. UV-vis (C_6H_6) λ_{max}, nm (ε): 604 (420), 664 (520), 747 (1300). Evans Method (C_6D_6): 4.00 μ_B. Electrochemistry (vs. ferrocene in THF with [TBA][PF_6] as supporting electrolyte): Co^{II}/Co^{III}, -140 mV (irreversible), Co^{I}/Co^{II}, -1330 mV. Anal. Calcd for $C_{45}H_{68}BCoP_3SSi$: C, 64.97; H, 8.24. Found: C, 64.77; H, 8.28.

Synthesis of {[PhBP$_3$]CoOSiPh$_3$}{BAr$_4$}, {4.15}{BAr$_4$}. Solid [PhBP$_3$]CoOSiPh$_3$, **4.1**, (98 mg, 0.096 mmol) and {[Cp]$_2$Fe}{B(3,5-(CF$_3$)$_2$-Ph)$_4$} (101 mg, 0.096 mmol) were added to a 20 mL vial and then THF (8 mL) was added. The solution immediately went from purple to green and was stirred for 10 min. The reaction mixture was then dried in vacuo to leave a green powder, which was washed with petroleum ether (3 x 10 mL). The green powder was dried to leave the pure product (140 mg, 77% yield), which was stored at –35 ºC. A similar procedure was used with {[Cp]$_2$Fe}{BPh$_4$} as the oxidant giving the less soluble counteranion (for X-ray crystallography). In this case the dried product was washed with a petroleum ether/benzene mixture (7:3) (3 x 10 mL) to give the final product (51% yield). A single crystal was grown at -35 °C in CH_2Cl_2 using the {BPh$_4$} counteranion. For {**4.15**}{B(3,5-(CF$_3$)$_2$-Ph)$_4$}: ^{1}H NMR (C_6D_6, 300 MHz): δ 8.43 (s, 8 H, *ortho* B(3,5-(CF$_3$)$_2$-C$_6$*H*$_3$)$_4$), 7.81 (d, J = 6.0 Hz, 8 H, *ortho* Si(C$_6$*H*$_5$)$_3$ and *ortho* B(C$_6$*H*$_5$)), 7.67 (t, J = 7.5 Hz, 2 H, *meta* B(C$_6$*H*$_5$)), 7.60 (s, 4 H, *para* B(3,5-(CF$_3$)$_2$-C$_6$*H*$_3$)$_4$), 7.47 (t, J = 7.5 Hz, 1 H, *para* B(C$_6$*H*$_5$)), 7.28 (m, 9 H, *meta* and *para* Si(C$_6$*H*$_5$)$_3$), 7.10 (m, 12 H, *ortho* P(C$_6$*H*$_5$)$_2$), 6.67 (t, J = 7.2 Hz, 6 H, *para* P(C$_6$*H*$_5$)$_2$), 6.40 (t, J = 7.5 Hz, 12 H, *meta* P(C$_6$*H*$_5$)$_2$), 0.98 (br s, 6 H, PhB(C*H*$_2$PPh$_2$)$_3$). ^{31}P{^{1}H} NMR (C_6D_6, 121.4 MHz): δ 64.6. ^{19}F{^{1}H} NMR (C_6D_6, 282 MHz): -58.5. UV-vis (C_6D_6) λ_{max}, nm (ε): 624 (830). Anal. Calcd for $C_{95}H_{68}B_2CoF_{24}OP_3Si$: C, 60.59; H, 3.64. Found: C, 60.59; H, 4.00. For {**4.15**}{BPh$_4$}: Identical UV-vis and ^{31}P NMR were found for the substituted anion.

Synthesis of [Tp$^{3,5\text{-}Me2}$]CoS(2,6-Me$_2$-Ph), 4.16. Anhydrous $CoBr_2$ (61.8 mg, 0.285 mmol) was slurried in THF (13 mL) for 10 min. Solid [K][Tp$^{3,5\text{-}Me2}$] (0.113 g, 0.335 mmol) was added over 30 min. To this solution, TlS(2,6-Me$_2$-Ph) (0.114 g, 0.335 mmol)

was added as a THF (3 mL) slurry and stirred for 30 min. After the addition of the thallium reagent, the solution turned green and white precipitate appeared (TlBr). The solution was filtered over Celite and then dried in vacuo to leave a green powder. The green powder was taken up in toluene (3 mL) and then crystallized by vapor diffusion of petroleum ether giving green crystals (0.043 g, 31% yield). Additional crystallizations can be used to collect additional product giving 69% total yield. ^{1}H NMR (C_6D_6, 300 MHz): δ 68.1, 38.5, 29.4, 16.2, -0.8, -11.4, -38.8. UV-vis (C_6H_6) λ_{max}, nm (ε): 647 (1300). SQUID (10-300 K): χT_{av} = 2.41 cm^3 K mol^{-1}. Anal. Calcd for $C_{23}H_{31}BCoN_6S$: C, 55.99; H, 6.33; N, 17.03. Found: C, 55.72; H, 6.23; N, 17.12.

4.4.6 X-ray experimental information

The general X-ray experimental procedure was performed according to section 2.4.4. Crystallographic information is provided in Table 4.6.

Table 4.6. X-ray diffraction experimental details for $[PhBP_3]CoOSiPh_3$ (**4.1**), $[PhBP_3]CoO(4\text{-}^tBu\text{-}Ph)$ (**4.2**), $[PhBP_3]CoSPh$ (**4.4**), $[PhBP_3]CoS(2,6\text{-}Me_2\text{-}Ph)$ (**4.5**), $[PhBP_3]CoS(2,4,6\text{-}^iPr_3\text{-}Ph)$ (**4.6**), $[PhBP_3]CoS(2,4,6\text{-}^tBu_3\text{-}Ph)$ (**4.7**), $[PhBP_3]CoSSiPh_3$ (**4.8**), $[PhBP_3]CoOSi(4\text{-}NMe_2\text{-}Ph)_3$ (**4.9**), $[PhBP_3]CoOCPh_3$ (**4.11**), $[PhBP^{iPr}_3]CoSSiPh_3$ (**4.14**), $\{[PhBP_3]CoOSiPh_3\}\{BPh_4\}$, $\{$**4.15**$\}\{BPh_4\}$, and $[Tp^{3,5\text{-}Me2}]CoS(2,6\text{-}Me_2\text{-}Ph)$, (**4.16**).

	$[PhBP_3]CoOSiPh_3$, (**4.1**)	$[PhBP_3]CoO(4\text{-}^tBu\text{-}Ph)$, (**4.2**)
Chemical formula	$C_{63}H_{56}BOP_3SiCo \cdot 1½(C_6H_6)$	$C_{55}H_{54}BCoOP_3$
Formula weight	1136.98	893.63
T (K)	98	98
λ (Å)	0.71073	0.71073
a (Å)	13.1013(14)	38.2238(8)
b (Å)	14.4428(16)	38.2238(8)
c (Å)	16.9894(19)	12.4091(5)
α (º)	77.984(2)	90
β (º)	67.962(1)	90
γ (º)	89.536(2)	90
V ($Å^3$)	2905.8(6)	18130.4(9)
Space group	$P\bar{1}$	$I4_1/a$
Z	2	16
Dcalcd (g/cm^3)	1.299	1.310
μ(cm^{-1})	4.44	5.25
R1, wR2 ($I>2\sigma(I)$)[a]	0.0336, 0.0673	0.0560, 0.0808

[a] $R1 = \Sigma \, | \, |F_o| - |F_c| \, | \, / \, \Sigma \, |F_o|$, $wR2 = \{ \, \Sigma \, [\, w(F_o^2 - F_c^2)^2 \,] \, / \, \Sigma \, [\, w(F_o^2)^2 \,] \, \}^{1/2}$

Table 4.6 (cont.)

	$[PhBP_3]CoSPh$, (**4.4**)	$[PhBP_3]CoS(2,6\text{-}Me_2\text{-}Ph)$, (**4.5**)
Chemical formula	$C_{51}H_{41}BCoP_3S$	$C_{53}H_{50}BCoP_3S$
Formula weight	853.59	881.64
T (K)	98	98
λ (Å)	0.71073	0.71073
a (Å)	16.8066(16)	12.0158(9)
b (Å)	14.0767(13)	12.5469(9)
c (Å)	19.2736(18)	15.5078(12)
α (º)	90	77.780(1)
β (º)	113.801(2)	77.546(1)
γ (º)	90	77.919(1)
V ($Å^3$)	4172.0(7)	2198.2(3)
Space group	$P2_1$	$P\bar{1}$
Z	4	2
Dcalcd (g/cm^3)	1.359	1.332
μ(cm^{-1})	6.10	5.80
R1, wR2 ($I>2\sigma(I)$)[a]	0.0463, 0.0661	0.0405, 0.0743

Table 4.6 (cont.)

	[PhBP$_3$]CoS(2,4,6-^{i}Pr$_3$-Ph), (**4.6**)	[PhBP$_3$]CoS(2,4,6-^{t}Bu$_3$-Ph), (**4.7**)
Chemical formula	$C_{60}H_{64}BCoP_3S$	$C_{63}H_{70}BCoP_3S \cdot C_6H_6$
Formula weight	979.82	1100.01
T (K)	98	98
λ (Å)	0.71073	0.71073
a (Å)	15.3738(11)	13.8333(10)
b (Å)	17.3171(13)	13.9539(10)
c (Å)	20.7953(15)	17.5922(13)
α (º)	65.655(1)	99.145(1)
β (º)	87.329(2)	106.587(1)
γ (º)	88.642(2)	107.029(1)
V (Å^3)	5038.5(6)	3000.8(4)
Space group	P$\bar{1}$	P$\bar{1}$
Z	4	2
Dcalcd (g/cm^3)	1.292	1.217
μ(cm^{-1})	5.20	4.40
R1, wR2 (I>2σ(I))[a]	0.0482, 0.0836	0.0663, 0.1133

Table 4.6 (cont.)

	$[PhBP_3]CoSSiPh_3$, (**4.8**)	$[PhBP_3]CoOSi(4\text{-}NMe_2\text{-}Ph)_3$, (**4.9**)
Chemical formula	$C_{63}H_{56}BCoP_3SSi \cdot 2\ C_6H_6$	$C_{69}H_{71}BCoN_3OP_3Si$
Formula weight	1192.09	1149.03
T (K)	98	98
λ (Å)	0.71073	0.71073
a (Å)	11.0416(8)	12.1092(11)
b (Å)	12.8426(9)	12.3919(11)
c (Å)	22.3975(15)	21.3227(19)
α (º)	87.228(1)	80.696(2)
β (º)	81.435(1)	75.993(2)
γ (º)	73.024(1)	72.962(1)
V ($Å^3$)	3003.7(4)	2954.0(5)
Space group	$P\bar{1}$	$P\bar{1}$
Z	2	2
Dcalcd (g/cm^3)	1.318	1.292
μ(cm^{-1})	4.70	4.40
R1, wR2 ($I>2\sigma(I)$)[a]	0.0529, 0.0777	0.0485, 0.0712

Table 4.6 (cont.)

	$[PhBP_3]CoOCPh_3$, (**4.11**)	$[PhBP^{iPr}_3]CoSSiPh_3$, (**4.14**)
Chemical formula	$C_{64}H_{56}BCoOP_3 \cdot C_6H_6$	$C_{45}H_{68}BCoP_3SSi$
Formula weight	1081.85	831.79
T (K)	98	98
λ (Å)	0.71073	0.71073
a (Å)	12.9420(10)	10.3161(4)
b (Å)	20.8485(15)	14.4678(6)
c (Å)	21.5457(16)	29.963(1)
α (º)	77.529(1)	90
β (º)	82.143(1)	90
γ (º)	88.626(1)	90
V ($Å^3$)	5622.9(7)	4472.0(3)
Space group	$P\bar{1}$	$P2_12_12_1$
Z	4	4
Dcalcd (g/cm^3)	1.278	1.235
μ(cm^{-1})	4.40	6.00
R1, wR2 ($I>2\sigma(I)$)[a]	0.0457, 0.0867	0.0431, 0.0606

Table 4.6 (cont.)

	{[PhBP$_3$]CoOSiPh$_3$}{BPh$_4$}, ({**4.15**}{BPh$_4$})	[Tp$^{3,5\text{-}Me2}$]CoS(2,6-Me$_2$-Ph), (**4.16**)
Chemical formula	$C_{87}H_{76}B_2CoOP_3Si \cdot 1½\ CH_2Cl_2$	$C_{23}H_{31}BCoN_6S$
Formula weight	1466.50	493.34
T (K)	98	98
λ (Å)	0.71073	0.71073
a (Å)	13.592(2)	23.0774(18)
b (Å)	14.814(2)	13.6982(10)
c (Å)	19.251(3)	7.9439(6)
α (º)	72.567(3)	90
β (º)	87.945(3)	90
γ (º)	82.565(2)	90
V (Å^3)	3667.0(9)	2511.2(3)
Space group	$P\bar{1}$	P_{nma}
Z	2	4
Dcalcd (g/cm^3)	1.328	1.305
μ(cm^{-1})	4.70	7.90
R1, wR2 (I>2σ(I))[a]	0.0643, 0.1156	0.0468, 0.0722

References cited

1) a) Nishida, Y.; Kida, S. *Bull. Chem. Soc. Jpn.* **1978**, *51*, 143-149. b) Gray, H. B. *Chemical Bonds: An Introduction to Atomic and Molecular Structure*; University Science Books: Mill Valley, CA, 1994.

2) a) Strauss, S. H.; Silver, M. E.; Long, K. M.; Thomson, R. G.; Hudgens, R. A.; Spartalian, K.; Ibers, J. A. *J. Am. Chem. Soc.* **1985**, *107*, 4207-4215. b) Goedken, V. L.; Pluth, J. J.; Peng, S.; Bursten, B. *J. Am. Chem. Soc.* **1976**, *98*, 8014-8021.

3) a) Solomon, E. I.; Rawlings, J.; McMillin, J. R.; Stephens, P. J.; Gray, H. B. *J. Am. Chem. Soc.* **1976**, *98*, 8046-8048. b) Bertini, I.; Luchinat, C. *Acc. Chem. Res.* **1983**, *16*, 272-279. c) Bertini, I.; Lanini, G.; Luchinat, C. *J. Am. Chem. Soc.* **1983**, *105*, 5116-5118. d) Khalifah, R. G.; Rogers, J. I.; Harmon, P. J.; Carroll, S. B. *Biochemistry* **1984**, *23*, 3129-3136. e) Briganti, F.; Pierattelli, R.; Scozzafava, A.; Supuran, C. T. *Eur. J. Med. Chem.* **1996**, *31*, 1001-1010.

4) Maret, W.; Vallee, B. L. "*Cobalt as probe and label of proteins*," *Methods in Enzymology* **1993**, *226*, 52-71.

5) a) Lippard, S. J.; Berg, J. M. *Principles of Bioinorganic Chemistry*; University Science Books: Mill Valley, CA, 1994; Chapter 12. b) Bren, K. L.; Pecoraro, V. L.; Gray, H. B. *Inorg. Chem.* **2004**, *43*, 7894-7896.

6) a) Lever, A. B. P. *Inorganic Electronic Spectroscopy*, 2nd ed.; Elsevier: New York, 1984; pp 480-505. b) Cotton, F. A.; Wilkinson, G. *Advanced Inorganic Chemistry*, 5th ed.; Wiley: New York, 1988; p. 729.

7) For examples of low spin Co(II) octahedral systems see: a) Faus, J.; Julve, M.; Lloret, F.; Muñoz, M. C. *Inorg. Chem.* **1993**, *32*, 2013-2017. b) Santra, B. K.; Lahiri, G. K. *J. Chem. Soc.*, *Dalton Trans.* **1998**, 139-145. c) Iwatsuki, S.; Obeyama, K.; Koshino, N.; Funahashi, S.; Kashiwabara, K.; Suzuki, T.; Takagi, H. D. *Can. J. Chem.* **2001**, *79*, 1344-1351. d) Reinen, D.; Ozarowski, A.; Jakob, B.; Pebler, J.; Stratemeier, H.; Wieghardt, K.; Tolksdorf, I. *Inorg. Chem.* **1987**, *26*, 4010-4017.

8) a) Zarembowitch, J. *New J. Chem.* **1992**, *16*, 255-267. b) Juhász, G.; Hayami, S.; Inoue, K.; Maeda, Y. *Chem. Lett.* **2003**, *32*, 882-883. c) Sieber, R.; Decurtins, S.; Stoeckli-Evans, H.; Wilson, C.; Yufit, D.; Howard, J. A. K.; Capelli, S. C.; Hauser, A. *Chem. Eur. J.* **2000**, *6*, 361-368. d) Gaspar, A. B.; Muñoz, M. C.; Niel, V.; Real, J. A. *Inorg. Chem.* **2001**, *40*, 9-10. e) Faus, J.; Julve, M.; Lloret, F.; Real, J. A.; Sletten, J. *Inorg. Chem.* **1994**, *33*, 5535-5540. f) Kremer, S.; Henke, W.; Reinen, D. *Inorg. Chem.* **1982**, *21*, 3013-3022.

9) For $[Cp]_2Co$ see: a) Gordon, K. R.; Warren, K. D. *Inorg. Chem.* **1978**, *17*, 987-994. b) König, E.; Schnakig, R.; Kremer, S.; Kanellakopulos, B.; Klenze, R. *Chem. Phys.* **1978**, *27*, 331-344. c) Warren, K. D. *Struct. and Bond.* **1976**, *27*, 45-159. For mixed-sandwich complexes see: d) Brunker, T. J.; Barlow, S.; O'Hare, D. *Chem. Commun*. **2001**, 2052-2053. e) Brunker, T. J.; Crowley, A. R.; O'Hare, D. *Organometallics* **2002**, *21*, 3123-3138. f) Brunker, T. J.; Green, J. C.; O'Hare, D. *Inorg. Chem.* **2003**, *42*, 4366-4381.

10) a) Sacconi, L. *Coord. Chem. Rev.* **1972**, *8*, 351-367. b) Morassi, R.; Bertini, I.; Sacconi, L. *Coord. Chem. Rev.* **1973**, *11*, 343-402.

11) a) Kennedy, B. J.; Murray, K. S. *Inorg. Chim. Acta* **1987**, *134*, 249-254. b) Kennedy, B. J.; Fallon, G. D.; Gatehouse, B. M. K. C.; Murray, K. S. *Inorg. Chem.* **1984**, *23*, 580-588.

12) a) Thuéry, P.; Zarembowitch, J. *Inorg. Chem.* **1986**, *25*, 2001-2008. b) Zarembowitch, J.; Kahn, O. *Inorg. Chem.* **1984**, *23*, 589-593.

13) Cirera, J.; Alemany, P.; Alvarez, S. *Chem. Eur. J.* **2004**, *10*, 190-207.

14) See Chapter 2 and Shapiro, I. R.; Jenkins, D. M.; Thomas, J. C.; Day, M. W.; Peters, J. C. *Chem. Commun.* **2001**, 2152-2153.

15) See Chapter 3 and Jenkins, D. M.; Di Bilio, A. J.; Allen, M. J.; Betley, T. A.; Peters, J. C. *J. Am. Chem. Soc.* **2002**, *124*, 15336-15350.

16) Jenkins, D. M.; Peters, J. C. *J. Am. Chem. Soc.* **2003**, *125*, 11162-11163.

17) a) Ray, M.; Hammes, B. S.; Yap, G. P. A.; Rheingold, A. L.; Borovik, A. S. *Inorg. Chem.* **1998**, *37*, 1527-1532. b) Sacconi, L.; Orlandini, A.; Midollini, S. *Inorg. Chem.* **1974**, *13*, 2850-2859. c) Mani, F.; Mealli, C. *Inorg. Chim. Acta* **1981**, *54*, L77-L79.

18) Holm, R. H. *Acc. Chem. Res.* **1969**, *2*, 307-316.

19) Jaynes, B. S.; Doerrer, L. H.; Liu, S.; Lippard, S. J. *Inorg. Chem.* **1995**, *34*, 5735-5744.

20) a) Everett, G. W.; Holm, R. H. *J. Am. Chem. Soc.* **1965**, *87*, 5266-6267. b) Cotton, F. A.; Soderberg, R. H. *J. Am. Chem. Soc.* **1962**, *84*, 872-873.

21) The complex {[$PhBP_3$]Fe≡N(1-Ad)}{NBu_4} has been thoroughly characterized (including by XRD analysis) and features a singlet ground state. Brown, S. D.; Peters, J. C. *J. Am. Chem. Soc.* (*accepted*).

22) Brown, S. D.; Betley, T. A.; Peters, J. C. *J. Am. Chem. Soc.* **2003**, *125*, 322-323.

23) Betley, T. A.; Peters, J. C. *J. Am. Chem. Soc.* **2003**, *125*, 10782-10783.

24) Betley, T. A.; Peters, J. C. *J. Am. Chem. Soc.* **2004**, *126*, 6252-6254.

25) Betley, T. A.; Peters, J. C. *Inorg. Chem.* **2003**, *43*, 5074-5084.

26) Brown, S. D.; Peters, J. C. *J. Am. Chem. Soc.* **2004**, *126*, 4538-4539.

27) Daida, E. J.; Peters, J. C. *Inorg. Chem*. **2004**, *43*, 7474-7485.

28) a) Reinaud, O. M.; Rheingold, A. L.; Theopold, K. H. *Inorg. Chem.* **1994**, *33*, 2306-2308. b) Detrich, J. L.; Konečný, R.; Vetter, W. M.; Doren, D.; Rheingold, A. L.; Theopold, K. H. *J. Am. Chem. Soc.* **1996**, *118*, 1703-1712. c) Jewson, J. D.; Liable-Sands, L. M.; Yap, G. P. A.; Rheingold, A. L.; Theopold, K. H. *Organometallics* **1999**, *18*, 300-305.

29) a) Shirasawa, N.; Akita, M.; Hikichi, S.; Moro-oka, Y. *Chem. Commun.* **1999**, 417-418. b) Shirasawa, N.; Nguyet, T. T.; Hikichi, S.; Moro-oka, Y.; Akita, M. *Organometallics* **2001**, *20*, 3582-3598.

30) a) Schebler, P. J.; Riordan, C. G.; Guzei, I. A.; Rheingold, A. L. *Inorg. Chem.* **1998**, *37*, 4754-4755. b) Schebler, P. J.; Mandimutsira, B. S.; Riordan, C. G.; Laible-Sands, L. M.; Incarvito, C. D.; Rheingold, A. L. *J. Am. Chem. Soc.* **2001**, *123*, 331-332.

31) a) Constable, E. C.; Baum, G.; Bill, E.; Dyson, R.; van Eldik, R.; Fenske, D.; Kaderli, S.; Morris, D.; Neubrand, A.; Neuburger, M.; Smith, D. R.; Wieghardt, K.; Zehnder, M.; Zuberbühler, A. D. *Chem. Eur. J.* **1999**, *5*, 498-508. And references therein. b) Sohrin, Y.; Kokusen, H.; Matsui, M. *Inorg. Chem.* **1995**, *34*, 3928-3934.

32) a) Bally, T.; Borden, W. T. *Rev. Comp. Chem.* **1999**, *13*, 1-97. b) Boone, A. J.; Chang, C. H.; Greene, S. N.; Herz, T.; Richards, N. G. J. *Coord. Chem. Rev.* **2003**, *238-239*, 291-314. c) Carreón-Macedo, J.; Harvey, J. N. *J. Am. Chem. Soc.* **2004**, *126*, 5789-5797.

33) a) Thompson, J. S.; Sorrell, T.; Marks, T. J.; Ibers, J. A. *J. Am. Chem. Soc.* **1979**, *101*, 4193-4201. b) Yoshimitsu, S.; Hikichi, S.; Akita, M. *Organometallics* **2002**, *21*, 3762-3773.

34) a) Jesson, J. P.; Trofimenko, S.; Eaton, D. R. *J. Am. Chem. Soc.* **1967**, *89*, 3148-3158. b) De Alwis, D.; Chanaka, L.; Schultz, F. A. *Inorg. Chem.* **2003**, *42*, 3616-3622.

35) a) Katzin, L. I. *J. Am. Chem. Soc.* **1954**, *76*, 3089-3090. b) Katzin, L. I.; Gebert, E. *J. Am. Chem. Soc.* **1953**, *75*, 2830-3832. c) Schmidtke, H.; Nover, J. *Inorg. Chem. Acta* **1995**, *240*, 231-237.

36) Hayashi, Y.; Yamamoto, T.; Yamamoto, A.; Komiya, S.; Kushi, Y. *J. Am. Chem. Soc.* **1986**, *108*, 385-391.

37) a) Kownacki, I.; Kubicki, M.; Marciniec, B. *Polyhedron* **2001**, *20*, 3015-3018. b) Osakada, K.; Takizawa, T.; Tanaka, M.; Yamamoto, T. *J. Organomet. Chem.* **1994**, *473*, 359-369. c) Tran, D. T. T.; Taylor, N. J.; Corrigan, J. F. *Angew. Chem., Int. Ed. Engl.* **2000**, *39*, 935-937.

38) Archibald, S. J.; Foxon, S. P.; Freeman, J. D.; Hobson, J. E.; Pernutz, R. N.; Walton, P. H. *J. Chem. Soc., Dalton Trans.* **2002**, 2797-2799.

39) The preparation was modified from this reference. See Experimental Section. Jazdzewski, B. A.; Holland, P. L.; Pink, M.; Young Jr., V. G.; Spencer, D. J. E.; Tolman, W. B. *Inorg. Chem.* **2001**, *40*, 6097-6107.

40) Ming, L. *Physical Methods in Bioinorganic Chemistry* (Ed.: L. Que, Jr.); University Science Books: Sausalito, CA, 2000, pp. 375-464.

41) MacBeth, C. E.; Thomas, J. C.; Betley, T. A.; Peters, J. C. *Inorg. Chem.* **2004**, *43*, 4645-4662.

42) Jenkins, D. M.; Betley, T. A.; Peters, J. C. *J. Am. Chem. Soc.*, **2002**, *124*, 11238-11239.

43) a) Avnir, D.; Katzenelson, O.; Keinan, S.; Pinsky, M.; Pinto, Y.; Salomon, Y.; Zabrodsky, H. *Concepts in Chemistry*: *A Contemporary Challenge* (Ed.: D. H. Rouvray); Research Studies Press: Taunton (UK), 1996. b) Alvarez, S.; Avnir, D.; Llunell, M.; Pinsky, M. *New J. Chem*. **2002**, *26*, 996-1009.

44) The atoms in the aryloxide ligand were refined isotropically.

45) For a discussion of EPR of Co(II) see: Banci, L.; Bencini, A.; Benelli, C.; Gatteschi, D.; Zanchini, C. *Struct. Bonding* **1982**, *52*, 37-86.

46) Stelzer, O.; Sheldrick, W. S.; Subramanian, J. *J. Chem. Soc., Dalton Trans.* **1976**, 966-970.

47) Palmer, G. *Physical Methods in Bioinorganic Chemistry* (Ed.: L. Que, Jr.); University Science Books: Sausalito, CA, 2000.

48) Gütlich, P.; Garcia, Y.; Goodwin, H. A. *Chem. Soc. Rev.* **2000**, *29*, 419-427.

49) We very recently obtained the solid-state crystal structure of the low spin half sandwich complex [$PhBP_3$]Co[Cp]. While a thorough discussion of this and related [BP_3]-supported half sandwich complexes is beyond the scope of this discussion, we note that in the crystalline state, [$PhBP_3$]Co[Cp] features a κ^3-bonding mode of the [$PhBP_3$] ligand and features one Co-P bond distance that is extremely distorted (2.479 Å) by comparison to the other two Co-P bond distances (2.242 Å and 2.231 Å). Jacobs, C. S.; Peters, J. C. *unpublished results*.

50) Sohn, Y. S.; Hendrickson, D. N.; Gray, H. B. *J. Am. Chem. Soc*. **1971**, *93*, 3603-3612.

51) Poli, R. *Chem. Rev*. **1996**, *96*, 2135-2204.

52) Jaguar 5.0, Schrodinger, LLC, Portland, Oregon, 2002.

53) Becke, A. D. *J. Chem. Phys.* **1993**, *98*, 5648-5652.

54) Lee, C.; Yang, W.; Parr R. G. *Phys. Rev. B* **1988**, *37*, 785-789.

55) SHAPE. Llunell, M.; Casanova, D.; Cirera, J.; Bofill, J. M.; Alemany, P.; Alvarez, S.; Pinsky, M.; Avnir, D. Version 1.1, Barcelona, 2003.

56) Harvey, S.; Lappert, M. F.; Raston, C. L.; Skelton, B. W.; Srivastava, G.; White, A. H. *J. Chem. Soc., Chem. Commun.* **1988**, *17*, 1216-1217.

57) Detty, M. R.; Wood, G. P. *J. Org. Chem.* **1980**, *45*, 80-89.

58) a) Oae, S.; Togo, H. *Bull. Chem. Soc. Jpn.* **1983**, *56*, 3802-3812. b) Blower, P. J.; Dilworth, J. R.; Hutchinson, J. P.; Zubieta, J. A. *J. Chem. Soc., Dalton Trans.* **1975**, 1533-1541.

59) Bochmann, M.; Webb, K. J. *Inorg. Synth.* **1997**, *31*, 158-162.

60) Gilman, H.; Plunkett, M. A.; Dunn, G. E. *J. Am. Chem. Soc.* **1951**, *73*, 1686-1688. Trichlorosiliane was substituted for tetrachlorosilane.

61) HOSi(*p*-CF_3-Ph) was prepared by the method of: Pauling, H.; Andrews, D. A.; Hindley, N. C. *Helv. Chim. Acta* **1976**, *59*, 1233-1243.

62) a) Connelly, N. G.; Geiger, W. E. *Chem. Rev.* **1996**, *96*, 877-910. b) Jordan, R. F.; LaPointe, R. E.; Bajgur, C. S.; Echols, S. F.; Willett, R. *J. Am. Chem. Soc.* **1987**, *109*, 4111-4113. c) Aggarwal, R. P.; Connelly, N. G.; Crespo, M. C.; Dunne, B. J.; Hopkins, P. M.; Orpen, A. G. *J. Chem. Soc., Dalton Trans.* **1992**, 655-662.

63) Le Bras, J.; Jiao, H.; Meyer, W. E.; Hampel, F.; Gladysz, J. A. *J. Organomet. Chem.* **2000**, *616*, 54-66.

Chapter 5: Synthesis of cobalt imide complexes

The text of this chapter is reproduced in part with permission from:

Jenkins, D. M.; Betley, T. A.; Peters, J. C. *J. Am. Chem. Soc.* **2002**, *124*, 11238-11239.

5.1 Introduction

Atom- and group-transfer reactions mediated by transition metal centers represent a prominent and heavily scrutinized area of research in inorganic chemistry.[1] Not only are such processes finding relevance in the field of catalysis,[2] but they have also been proposed in many processes that occur in metalloprotein active sites. First row transition metals that can accept and/or release oxo and nitrene functionalities are particularly interesting.[3] For the first row metals Fe, Co, Ni, and Cu, isolable complexes with a terminal imido and/or oxo functionality bonded to a single metal center, M=E or M≡E (E = O, NR), are rare.[4] This apparent incompatibility of later metals (groups 9, 10, and 11) with multiply-bonded strong π-donor ligands was overcome in third row transition metal complexes more than 10 years ago (e.g., [Cp*]Ir≡NR and (Mes_3)Ir≡O).[5,6] Recently, the quantity of late-metal (group 8 or later) first row transition metal multiple bonds has enjoyed an upsurge, as a number of these complexes have been synthesized. Terminal oxo and nitride complexes have been prepared for iron,[7] and terminal imido complexes have now been synthesized for iron,[8,9,10] cobalt,[10,11,12,13] and nickel.[14] Many of these imido complexes have been reported to undergo reactions wherein the nitrene functionality is transferred to an organic substrate. Two previously described group transfer reactions, which involve loss of the nitrene functionality, include isocyanate production upon addition of CO[9,11,15] or aziridination upon addition of olefins.[16]

We recently prepared a cobalt(II) complex, $[PhBP_3]$CoI (**3.1**), exhibiting a distorted tetrahedral geometry and an anomalous low spin ground state.[17] The ground-state electronic configuration proposed for **3.1** (Figure 5.1B) arises from a strong axial distortion of the C_{3v} symmetry, enforced by the geometry of the $[PhBP_3]$ ligand and

its strong ligand field donor strength. These factors suggested to us that it should, in principle, be possible to replace the iodide ligand by a divalent, strongly π-donating ligand. This would conceptually afford an 18-electron, closed-shell configuration (Figure 5.1C) similar to that of cobalticinium. We therefore sought to install a terminal imido functionality on the "[$PhBP_3$]Co" unit, which would be the first of its type, and herein report strategies that proved viable.

The primary method of imide synthesis was the oxidative degradation of organic azides added to a Co(I) precursor to give the Co(III) imide. An array of imides, including those containing a variety of alkyl and aryl substituents, can be prepared using this strategy. A secondary approach includes the metathesis of lithium amides with an appropriate Co(III) dihalide precursor. This metathesis methodology was used previously for the preparation of Ir and Ni imido complexes.[5,14]

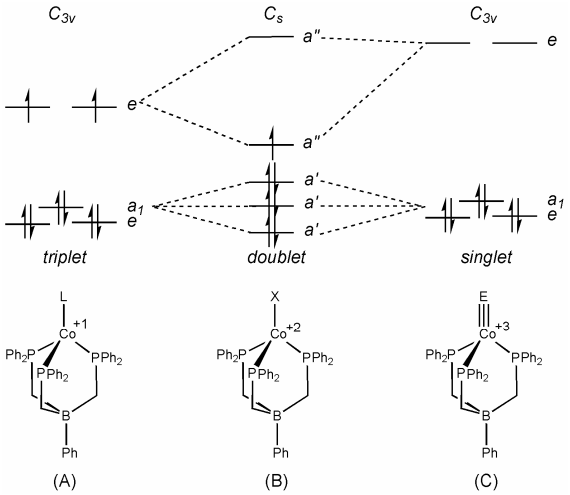

Figure 5.1. Qualitative splitting diagram assuming approximate C_{3v} or C_s symmetry for the frontier orbitals of (A) [$PhBP_3$]Co-L; (B) Jahn-Teller distorted low spin [$PhBP_3$]Co-X; and (C) [$PhBP_3$]Co≡E. The relative orbital energies are represented qualitatively.

In addition to the synthesis and reactivity of these unusual complexes, the electronic structures of these species also are of interest. Theoretical and experimental investigations have been carried out for late-metal third row imides to determine their molecular orbital diagrams, but not for their first row cousins.[5,18] DFT calculations were performed to shed light on the bonding of the cobalt imide complexes presented here. In addition, species such as isolobal $[PhBP_3]CoO$ and $\{[PhBP_3]CoN\}^-$ are addressed.

5.2 Results

5.2.1 Synthesis and characterization of precursors $[PhBP_3]CoI(PMe_3)$ and $[PhBP_3]Co(PMe_3)$

The strategy of preparing Co(III) imides from a two-electron oxidation accompanied by azide degradation required the synthesis of a Co(I) reagent. The synthesis of this key Co(I) precursor begins with the synthesis of the red, five-coordinate Co(II) complex, $[PhBP_3]CoI(PMe_3)$ (**5.1**). The addition of neat PMe_3 to a benzene solution of green $[PhBP_3]CoI$ (**3.1**) gives **5.1** in quantitative yield (Eq. 5.1). The reduction of **5.1** with a sodium/mercury amalgam produces light green $[PhBP_3]Co(PMe_3)$ (**5.2**) in 90% yield with concurrent loss of NaI.

$$\underset{(\mathbf{3.1})}{[PhBP_3]CoI} \xrightarrow{PMe_3} \underset{(\mathbf{5.1})}{[PhBP_3]CoI(PMe_3)} \xrightarrow[-NaI]{Na/Hg} \underset{(\mathbf{5.2})}{[PhBP_3]Co(PMe_3)} \qquad (5.1)$$

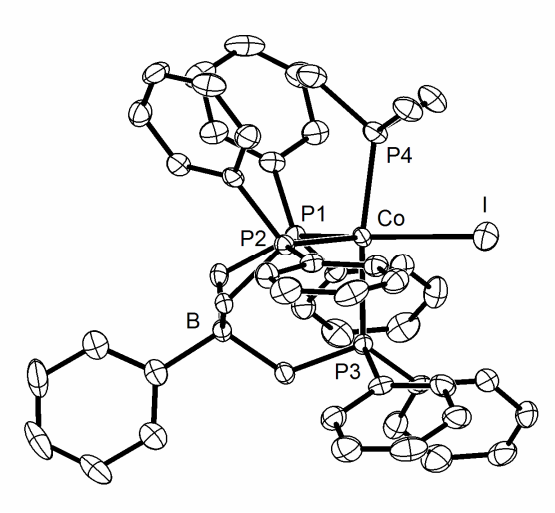

Figure 5.2. Displacement ellipsoids are represented at 50%. Selected interatomic distances (Å) and angles (deg) for $[PhBP_3]CoI(PMe_3)$ (**5.1**): Co-P1, 2.270(1); Co-P2, 2.298(1); Co-P3, 2.353(1); Co-P4, 2.285(1); Co-I, 2.6062(6). P1-Co-P2, 97.72(4); P1-Co-P3, 86.84(4); P2-Co-P3, 89.69(4); P1-Co-P4, 97.42(4); P2-Co-P4, 95.57(4); P3-Co-P4, 172.71(4); P1-Co-I, 137.88(4); P2-Co-I, 124.33(3); P3-Co-I, 90.73(3); P4-Co-I, 82.14(3).

Single crystal X-ray diffraction experiments were undertaken to ascertain the geometry of **5.1** and **5.2**. The distorted trigonal bipyramidal complex $[PhBP_3]CoI(PMe_3)$ has the iodide ligand in the equatorial plane along with two of the three phosphines from the $[PhBP_3]$ ligand (Figure 5.2). Complex **5.1** is structurally very similar to the previously described cationic complex, $[(H_3CC(CH_2PPh_2)_3)CoCl(PMe_3)][BPh_4]$ ($H_3CC(CH_2PPh_2)_3$ = triphos).[19]

Complex **5.2** has nearly C_3 symmetry in the solid state (Figure 5.3). The Co-P bond distances are all near 2.25 Å, while the P-Co-P bond angles are approximately 92°. The PMe_3 ligand sits on an axial site that shows no off-axis distortion (in **5.2**), with each

of the $P_{[PhBP3]}$-Co-P4 angles at approximately 124°. The disordered phenyl ring off the boron was refined isotropically in two orientations with the carbon atoms restrained to ideal geometry using isotropic temperature factors and riding hydrogens. Few Co(I) species similar to **5.2** have been structurally characterized. The homoleptic complex $[Co(PMe_3)_4][BPh_4]$ has been prepared and features some distortion of the P-Co-P angles, which range from 101° to 125°.[20] The only Co(I) complex supported by a tridentate phosphine is $(np_3)CoBr$ (np_3 = tris(2-(diphenylphosphino)ethyl)amine), which is a paramagnetic (S = 1) species that likewise adopts a pseudotetrahedral geometry. The P-Co-P angles in this case are all near 103°, and the P-Co-Br angles are between 113° and 119°.[21] The tighter P-Co-P angles for **5.2** are not surprising, given that the ligand is less flexible than np_3.

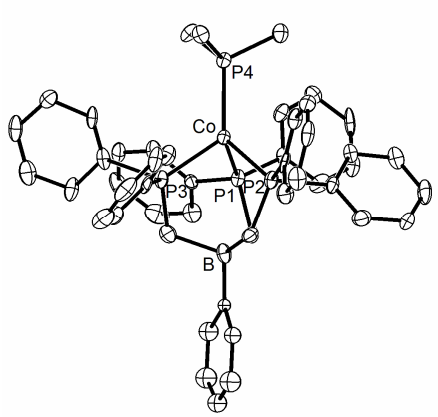

Figure 5.3. Displacement ellipsoids are represented at 50%. The phenyl ring attached to the boron atom in **5.2** is disordered and has been refined isotropically. Selected interatomic distances (Å) and angles (deg) for $[PhBP_3]Co(PMe_3)$ (**5.2**): Co-P1, 2.244(2); Co-P2, 2.250(2); Co-P3, 2.251(2); Co-P4, 2.305(2); P1-Co-P2, 91.82(7); P1-Co-P3, 91.93(8); P2-Co-P3, 92.31(8); P1-Co-P4, 123.39(8); P2-Co-P4, 124.13(8); P3-Co-P4, 123.95(8).

The magnetism of complexes **5.1** and **5.2** was investigated to determine their ground spin states. Both complexes provide paramagnetic ^{1}H NMR spectra in C_6D_6. The solid state magnetization was investigated via SQUID magnetometry; the results are shown in Figure 5.4A. Both complexes obey the Curie-Weiss law, showing spin states of $S = ½$ for **5.1** ($\chi_m T_{av}$ (10-300K) = 0.44 cm^3 K mol^{-1}) and $S = 1$ for **5.2** ($\chi_m T_{av}$ (10-300K) = 1.00 cm^3 K mol^{-1}). It is not surprising that **5.1** is a low spin species, since phosphine ligands often confer low spin configurations for trigonal bipyramidal Co(II) complexes.[22] The Evans's method measurements in C_6D_6 confirm this assignment in solution. The glassy toluene EPR spectra of the complexes are shown in Figure 5.4B. The axial signal ($g_{\|} > g_{\perp}$) for complex **5.1** suggests that the trigonal bipyramidal geometry is present in solution as well as the solid state.[23] The combined data show that [PhBP$_3$]CoI(PMe$_3$) (**5.1**) has a doublet ground state and that [PhBP$_3$]Co(PMe$_3$) (**5.2**) has a triplet ground state. This suggests that the electronic configuration for **5.2** is in accord with the proposed molecular orbital diagram shown in Figure 5.1A.

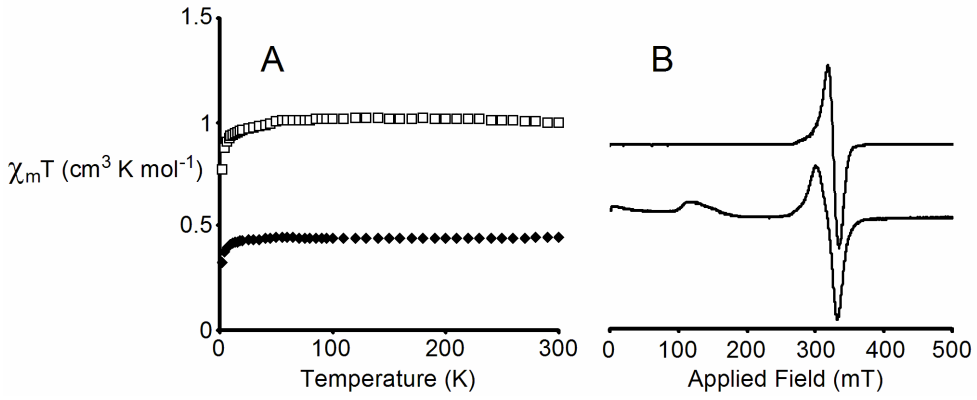

Figure 5.4. (A) SQUID magnetization plot of $\chi_m T$ versus T for [PhBP$_3$]CoI(PMe$_3$) (**5.1**), (♦) and [PhBP$_3$]Co(PMe$_3$) (**5.2**), (□). (B) EPR spectrum of a glassy toluene solution of **5.1** (top) at 50 K and **5.2** (bottom) at 4 K.

5.2.2 Synthesis of imido complexes via azide reduction

A variety of Co(III) imides can be generated from [PhBP$_3$]Co(PMe$_3$), **5.2**. The addition of two equivalents of an arylazide, such as phenylazide, to a benzene solution of **5.2** gives rise to a bright red solution (Eq. 5.2). In addition to the desired imide, [PhBP$_3$]CoNPh (**5.3**), the byproducts Me$_3$P=NPh and N_2 are also formed. The iminophosphorane can be removed by washing the solids with petroleum ether or through crystallization from benzene and petroleum ether. The reaction has proven general for a number of different arylazides with either electron withdrawing and electron donating groups on the aryl ring. Three additional arylimido complexes were synthesized with this methodology, including [PhBP$_3$]CoN-*p*-tolyl (**5.4**), [PhBP$_3$]CoN(4-CF$_3$-Ph) (**5.5**), and [PhBP$_3$]CoN(4-NMe$_2$-Ph) (**5.6**). All four species are diamagnetic and show one broad resonance in the ^{31}P NMR around 68 ppm. The ^{1}H NMR of the species also suggests that they have C_3 symmetry in solution at ambient temperature.

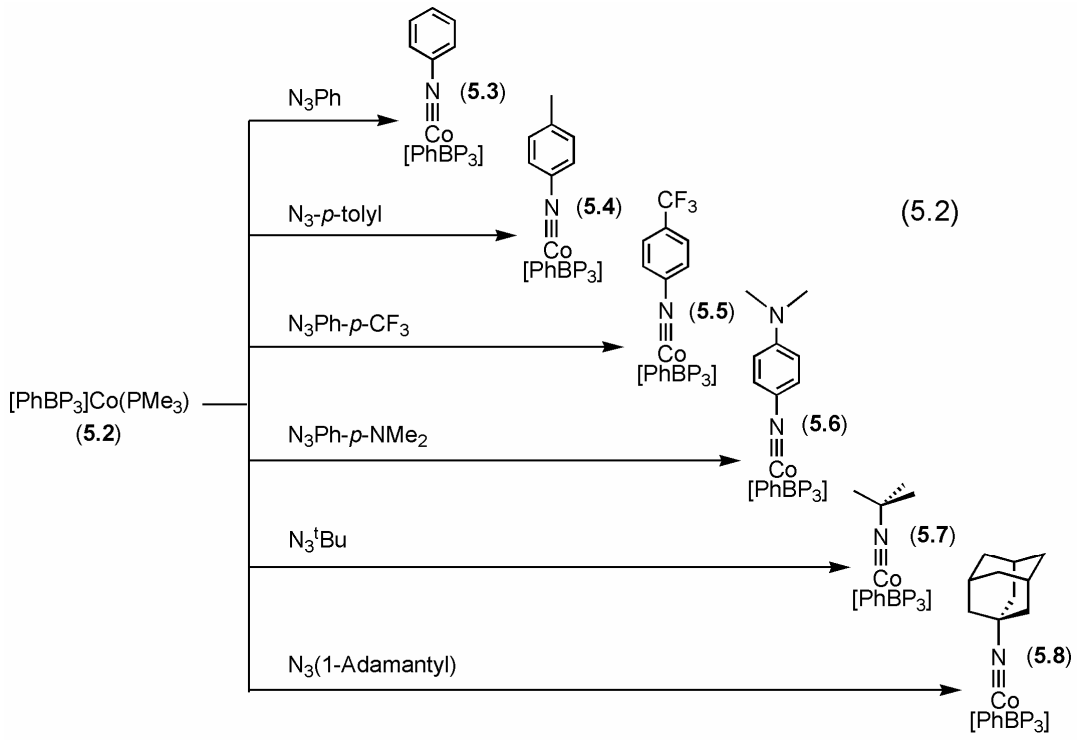

The synthesis of imides from $[PhBP_3]CoPMe_3$ (**5.2**) and alkylazides is also feasible, although the reactions are slower than with the arylazides. For example, the reaction between **5.2** and $N_3{}^tBu$ requires heating at 55 °C for several hours to be driven to completion. Two alkylimide complexes were prepared from **5.2** and their corresponding azides, $[PhBP_3]CoN^tBu$ (**5.7**) and $[PhBP_3]CoNAd$ (**5.8**) (Ad = 1-adamantyl) (Eq. 5.2). These species are diamagnetic and show similar ^1H and ^{31}P NMR spectra to the arylimide complexes. The bright red color of the arylimido complexes, presumably arising from a ligand-to-metal charge transfer band, is not present in the alkylimide complexes. None of the Co(III) imides feature a reversible oxidation or reduction in a cyclic voltamogram between +600 mV to -2000 mV versus ferrocenium. On the other hand, the iron imides prepared in our laboratory, such as $[PhBP_3]FeNAd$, which can be reduced to its Fe(II) anion $\{[PhBP_3]FeNAd\}^-$.[24]

5.2.3 Synthesis of imides via metathesis

Although aryl or alkylazides allow for the synthesis of the Co(III) imide complexes beginning with a Co(I) precursor, we were interested in extending the methodology to more conventional routes. Bergman's iridium imide, $[Cp^*]IrN^tBu$, is synthesized via metathesis using $([Cp^*]IrCl_2)_2$ and four equivalents of $LiNH^tBu$. Likewise, Hillhouse has prepared a three-coordinate nickel(II) imide using amide metathesis followed by oxidation and deprotonation. To evaluate whether a dehydrohalogenation route would work with our system, we needed to synthesize an appropriate Co(III) starting material that would be isoelectronic to $[Cp^*]IrCl_2$. The cyclic voltammogram for **3.1** showed a reversible $Co^{II/III}$ oxidative wave at 10 mV versus ferrocene/ferrocenium, while the chloride derivative $([PhBP_3]Co(\mu\text{-}Cl))_2$ (**3.3**) showed

the same oxidative wave at -80 mV. Since **3.3** is a monomer in solution, this result suggested that **3.3** could be cleanly oxidized using a ferrocenium salt. Addition of excess solid NaCl to a THF solution of **3.3** in the presence of a stoichiometric quantity of $\{[Cp]_2Fe\}\{PF_6\}$ gave the green diamagnetic complex $[PhBP_3]CoCl_2$ (**5.9**) (Eq. 5.3). Complex **5.9** is a five-coordinate complex that has a distorted square pyramidal geometry as can be seen in the solid-state structure in Figure 5.5. The two *trans* angles for P-Co-Cl are both greater than 154°. This complex is structurally analogous to $[(triphos)CoCl_2][BF_4]$ prepared by Huttner and co-workers. Interestingly, this five-coordinate complex **5.9** has only a single ^{31}P NMR resonance at 36 ppm suggesting that the phosphorous atoms exchange positions rapidly on the NMR time scale.

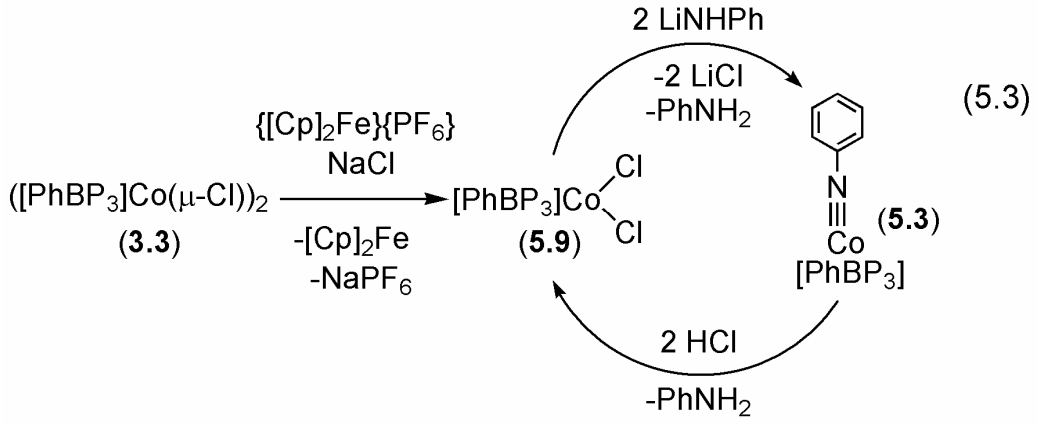

The addition of two equivalents of PhNHLi to a benzene solution of **5.9** immediately causes the reaction mixture to turn red (Eq. 5.3). After purification, the only cobalt product present was identified as $[PhBP_3]CoNPh$ (**5.3**) by comparing its ^1H NMR, ^{31}P NMR, and UV-vis spectra to that of **5.3** prepared by the synthetic route described above. No cobalt amide species is detected, even when a less than one equivalent of PhNHLi is used. ^{31}P NMR shows only the starting material, $[PhBP_3]CoCl_2$ (**5.9**), and the

imide, **5.3**. Conversion of the imide (**5.3**) to the Co(III) dichloride (**5.9**) is also feasible. Addition of two equivalents of HCl in ether to $[PhBP_3]CoNPh$ gives $[PhBP_3]CoCl_2$.

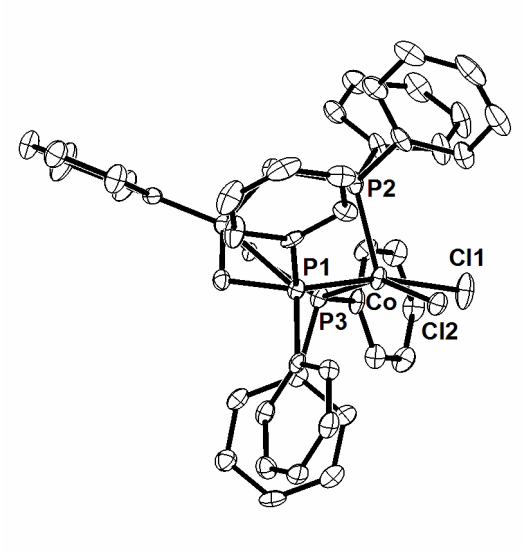

Figure 5.5. Displacement ellipsoids are represented at 50%. Selected interatomic distances (Å) and angles (deg) for $[PhBP_3]CoCl_2$ (**5.9**): Co-P1, 2.268(1); Co-P2, 2.182(1); Co-P3, 2.235(1); Co-Cl1, 2.226(1); Co-Cl2, 2.210(1). P1-Co-P2, 89.77(5); P1-Co-P3, 93.88(4); P2-Co-P3, 88.35(4); Cl1-Co-P1, 165.47(5); Cl1-Co-P2, 104.60(5); Cl1-Co-P3, 88.75(4); Cl2-Co-P1, 84.18(4); Cl2-Co-P2, 117.34(5); Cl2-Co-P3, 154.18(5); Cl1-Co1-Cl2, 87.24(4).

5.2.4 Structural characterization of the Co(III) imides

The structural parameters of two of the cobalt imides were established by single crystal X-ray diffraction. The solid state structures of $[PhBP_3]CoN$-*p*-tolyl (**5.4**) and $[PhBP_3]CoN^tBu$ (**5.7**) are shown in Figure 5.6 and Figure 5.7, respectively. The structure of **5.4** shows a slight distortion from C_3 symmetry; the P-Co-N bond angles vary from 115° to 132°. The short Co-N distance of 1.658(2) Å and the nearly linear Co-N-C(46)

angle of 169.51(2)° suggest a triple bond as shown in Figure 5.1C. Complex **5.7** has even less distortion from C_3 symmetry, since the variance between the P-Co-N angles in this case is less than five degrees, between 122° and 126°. Likewise, the Co-N-C46 angle is more linear at 176.68(13)° and the Co-N bond length is slightly shorter at 1.633(2). These Co-N bond distances are slightly longer than the reported distance of the β-diketiminato supported imide [HC(CMeNC$_6$H$_3$-2,6-Me$_2$)$_2$]CoNAd ([HC(CMeNC$_6$H$_3$-2,6-Me$_2$)$_2$]$^-$ = [Me$_2$NN]), which is 1.624(4) Å. Furthermore, the Co-N-C bond angle for the planar species [Me$_2$NN]CoNAd is slightly more bent at 161.5(3)° than these [PhBP$_3$] supported imides. Another Co(III) imide prepared in our laboratory, [PhBP$^{i\text{Pr}}_3$]CoN-*p*-tolyl ([PhBP$^{i\text{Pr}}_3$] = [PhB(CH$_2$P^{i}Pr$_2$)$_3$]$^-$), features a similar Co-N bond distance (1.667(2) Å) and Co-N-C bond angle (173.2(2)°). More recently, a cationic cobalt(III) imide supported by a neutral tridentate N-heterocyclic carbene ligand has been reported by Meyer and co-workers. The geometry is best described as pseudotetrahedral, and the Co-N bond distance (1.675(2) Å) is only slightly longer than the distances for our cobalt imides. This arylimide complex has Co-N-C bond angle (168.6(2)°) that is very close to the bond angle of **5.4**. Late-metal four-coordinate iron imides feature Fe-N bond lengths and Fe-N-C bond angles that are close to the cobalt imides we have structurally characterized.[8,9]

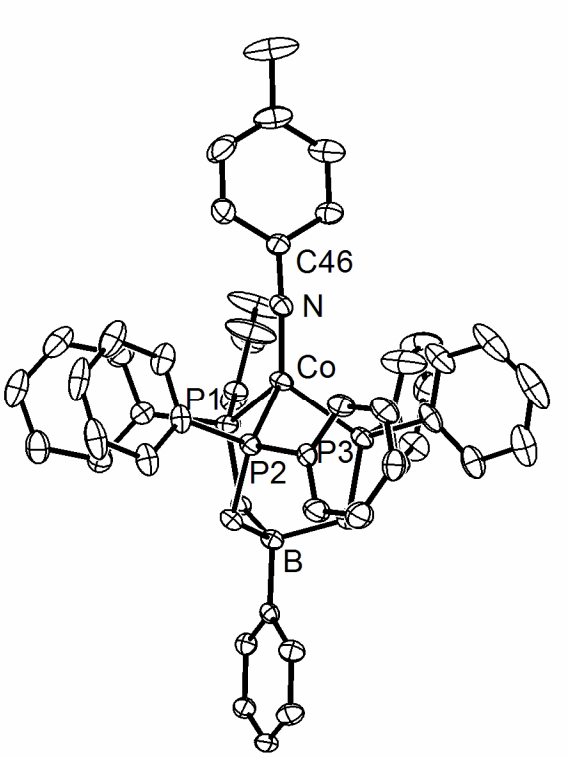

Figure 5.6. Displacement ellipsoids are represented at 50%. Selected interatomic distances (Å) and angles (deg) for [$PhBP_3$]CoN-*p*-tolyl (**5.4**): Co-N, 1.658(2); N-C46, 1.370(2); Co-P1, 2.1719(6); Co-P2, 2.1892(6); Co-P3, 2.1618(6). P1-Co-P2, 93.13(2); P1-Co-P3, 89.07(2); P2-Co-P3, 91.24(2); P1-Co-N, 115.32(6); P2-Co-N, 131.89(6); P3-Co-N, 125.64(6) Co-N-C46, 169.51(2).

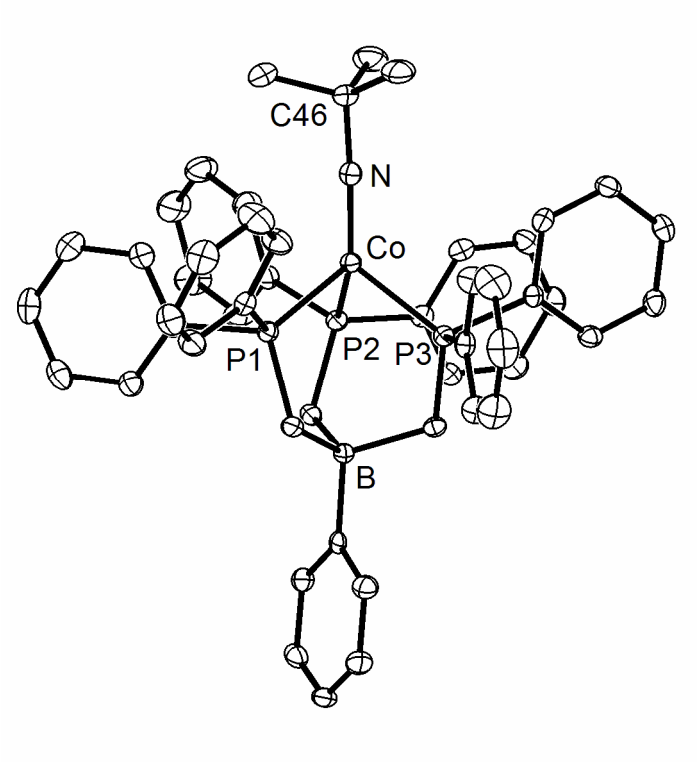

Figure 5.7. Displacement ellipsoids are represented at 50%. Selected interatomic distances (Å) and angles (deg) for $[PhBP_3]CoN^tBu$ (**5.7**): Co-N, 1.633(2); N-C46, 1.441(2); Co-P1, 2.1595(5); Co-P3, 2.1765(5); Co-P2, 2.1823(5). P1-Co-P2, 91.46(2); P1-Co-P3, 92.18(2); P2-Co-P3, 88.95(2); N-Co-P1, 122.24(5); N-Co-P2, 125.24(5); N-Co-P3, 126.49(5).

5.2.5 Reactivity of the Co(III) imide complexes

A catalytic cycle wherein the imide is formed from an organic azide and from which the nitrene functional group could be transferred to an organic compound would be a valuable synthetic tool. Ideally, aziridination could be achieved using these aryl or alkylazides and olefins. Previous examples of aziridination were only successful with tosylazide[25] or, more commonly, the hypervalent iodide reagent PhI=NTs

(Ts = -S(O)$_2$-*p*-tolyl).[26] Notably, Hillhouse and co-workers have been able to perform an aziridination reaction from an isolated Ni imide complex, (dtbpe)NiN(2,6-di-isopropylphenyl) (dtbpe = 1,2-bis(di-tert-butylphosphino)ethane), and ethylene, although they were unable to prepare the imide species from azide degradation. Even with prolonged heating, we have been unable to cause the nitrene functionality from **5.4** to react with an olefin (such as styrene) to give an aziridine (such as 1-*p*-tolyl-2-phenyl-cyclopropane). We have had greater success inducing reactivity between the imide complexes and π-acids. For example, we find that the imido functionality can be transferred slowly from **5.4** to carbon monoxide to produce the isocyanate (O=C=N-*p*-tolyl) (14 equiv of CO, 70 °C, 12 days). The isolated cobalt(I) byproduct (90%) was the diamagnetic dicarbonyl species [PhBP$_3$]Co(CO)$_2$ (**5.10**) (Eq. 5.4). This contrasts to the behavior of Bergman's imide, [Cp*]IrN^{t}Bu, which reacts with CO but does not give the free isocyanate.[5a] Despite attempts to turn over a catalytic cycle, we have been unable to provoke additional azide to react with [PhBP$_3$]Co(CO)$_2$ to form an imide complex and additional isocyanate. This lack of reactivity of the Co(I) dicarbonyl contrasts with a similar species we have prepared in our laboratory, [PhBP$_3$]Fe(CO)$_2$, which reacts with *p*-tolylazide to give the imide complex and *p*-tolyl-isocyanate.

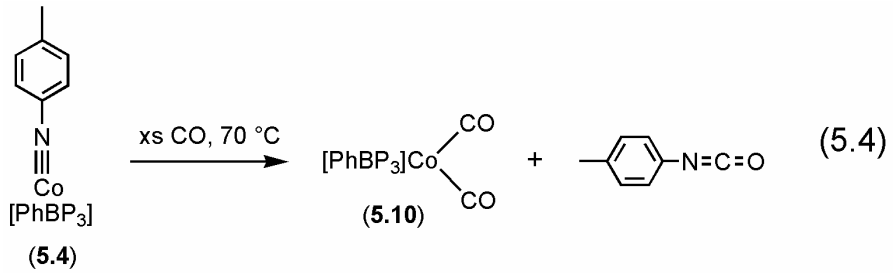

Addition of three equivalents of *tert*-butylisocyanide to **5.4** at ambient temperature gives the mixed carbodiimide *p*-tolyl-N=C=N-^{t}Bu as the organic product

(Eq. 5.5). More than one metal-containing byproduct was detected in this reaction, and an independent synthesis of $[PhBP_3]Co(CN^tBu)_2$ (**5.11**) from $[PhBP_3]CoI(CN^tBu)$ (**5.12**), CN^tBu, and Na/Hg amalgam (see Experimental Section for details) confirmed this species to be one of the two metal-containing products. Two additional peaks in the ^{31}P NMR of the reaction mixture in a ratio of 2:1 suggest that the other metal-containing product is most likely diamagnetic $[\kappa_2\text{-}PhBP_3]Co(CNtBu)_3$, whose synthesis we have yet to independently realize, even by addition of excess CN^tBu to $[PhBP_3]Co(CN^tBu)_2$ (**5.11**). The only reported example of this type of reaction on late metal imides involves an iridium imide complex in which the carbodiimide is not released from the metal center.[5a]

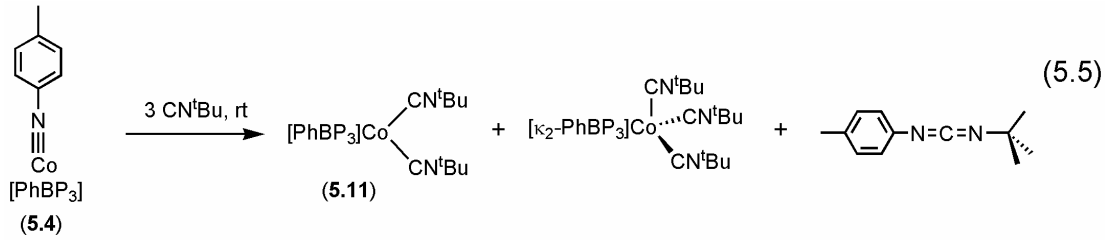

(5.5)

Unlike the related $[PhBP_3]FeN$-*p*-tolyl, which releases aniline as a product when exposed to H_2, none of the cobalt imides we have examined react with H_2.[27] The stability of the complexes is also manifested in their lack of reactivity with oxygen and water; only after prolonged exposure do they degrade. Furthermore, the imides are thermally robust, as **5.4** can be heated for days to 100° in toluene with only modest decomposition.

5.3 Discussion

Due to the unusual nature of this metal-ligand multiple bond, the orbital splitting diagram of these imide species is of interest. The molecular orbital diagrams of late third row transition metal imide bonds have received attention in the past. Bergman suggests that up to d^6 imides would be stable supposing that the d_z^2 orbital does not interact too

strongly with the auxiliary ligand, in his case [Cp*].[5a] Photoelectron spectroscopy studies provided experimental support for this assertion. The suggested d orbital splitting diagram included a low-lying non-bonding *e* set followed by an a_1 orbital and a high-lying π-antibonding *e* set. On the basis of our recent EPR studies of [$PhBP_3$]FeN-*p*-tolyl, it seemed possible that the ground state configuration could best be described as $(d_z^2)^2(d_{x^2-y^2})^2(d_{xy})^1(d_{xz})^0(d_{yz})^0$ for a d^5 imide species. To evaluate whether this was a good model of the cobalt imide complexes, DFT calculations were performed using the X-ray structure of **5.7** as a starting point. In light of the approximate C_{3v} symmetry that this complex adopts, one would expect the *d*-orbitals to transform into two *e* sets (xy, x^2-y^2 and xz, yz) and one a_1 set (d_z^2) as shown in Figure 5.1C. A large HOMO-LUMO is predicted by this model.

The results of the DFT energy minimization and orbital calculation are shown in Figure 5.8. The calculated geometry is in excellent agreement with the experimental geometry, excluding an elongation of each of the Co-P bonds by 0.08 Å. Two ligand-based orbitals (MO 206 and 209) are interspersed near the five d orbitals and involve C-C π-bonds on the phenyl ring attached to the boron. The orbital of a_1 symmetry is the lowest in energy, approximately 6 kcal/mol lower than the non-bonding *e* set (xy, x^2-y^2). The higher lying *e* set (xz, yz) shows strong π-antibonding with the nitrogen, again suggesting a stable triple bond. The large HOMO-LUMO gap, calculated at 91 kcal/mol, is responsible for the stabilization of the metal-ligand multiple bond species, as the π* orbitals are empty. Similar results were obtained from a DFT study of **5.4**. The molecular orbital splitting diagram is reminiscent of the molecular orbital diagram of d^6 sandwich complexes such as $[Cp]_2Fe$ or $\{[Cp]_2Co\}^+$.[28]

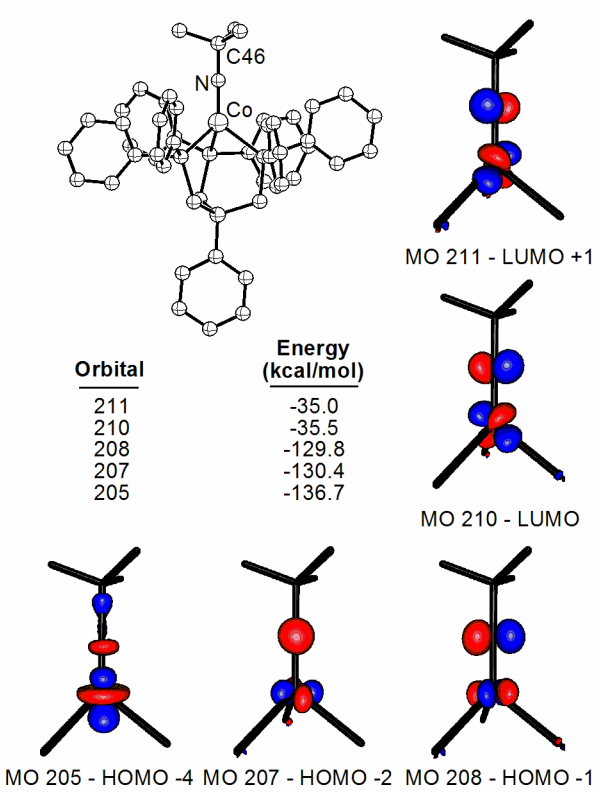

Figure 5.8. Molecular orbitals derived from a DFT energy minimization of $[PhBP_3]CoN^tBu$ (**5.7**) assuming a singlet ground state and the crystallographically determined atomic coordinates as a starting point.

These cobalt(III) imides feature stable cobalt-nitrogen triple bonds in agreement with their symmetry and molecular orbital diagram. The d^6 configuration was shown to be stable for a pseudotetrahedral imide over a decade ago by Bergman. What is perhaps more intriguing is the question of why unsubstituted multiply bonded ligands, such as $[PhBP_3]Co{\equiv}O$, are not stable in this d^6 configuration. The only example of a group 9 or later terminal heteroatom metal-ligand multiple bond remains the d^4 iridium oxo $(Mes)_3Ir{\equiv}O$ (Mes = mesityl) prepared by Wilkinson over a decade ago.[6,29] We propose that the predicted stability of metal-ligand multiple bonds can only be addressed by dividing these species into two classes: terminal, with no additional atoms attached to

multiply bonded ligands (e.g., oxos and nitrides), and non-terminal, with additional atoms attached to multiply bonded ligands (e.g., imidos).

The stability of the two classes is more subtle than can be predicted using a back-of-the-envelope molecular orbital diagram. The nature of the sigma bond between the metal and the ligand must be taken into account. More specifically, the amount of mixing between the p_z and d_z^2 orbitals on the metal and between the p_z and s orbitals on the heteroatom ligand is critical. The d_z^2 orbital is shown in Figure 5.9 for three calculated complexes: $[PhBP_3]CoN^tBu$ (**5.7**) and the hypothetical molecules $[PhBP_3]CoNH$ and $\{[PhBP_3]CoN\}^-$. Owing to its attenuated HOMO-LUMO gap, which arises from the terminally bonded nitride ligand, we anticipate that $\{[PhBP_3]CoN\}^-$ to electronically less stable than $[PhBP_3]CoN^tBu$. The hypothetical cobalt nitride features strong σ-antibonding with the cobalt d_z^2 and the p_z on the nitrogen. This is consistent with a complex synthesized in our laboratory, the d^4 nitride $[PhBP^{iPr}_3]Fe{\equiv}N$,[7a] and suggests that the lone pair on the nitrogen atom has an almost fully *s* orbital character. Oxidizing the species by two electrons would remove electrons from this antibonding orbital.

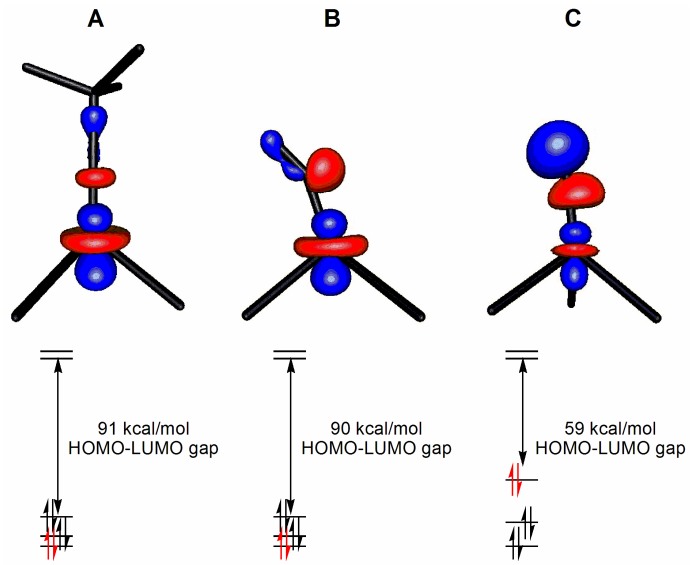

Figure 5.9. Molecular orbital diagrams derived from DFT calculations of $[PhBP_3]CoN^tBu$ (A), $[PhBP_3]CoNH$ (B), and $\{[PhBP_3]CoN\}^-$ (C). Only the central atoms are shown for clarity. The orbital representations show the d_z^2 for each molecule, and its position of the molecular orbital diagram is depicted by the red electrons.

Alternatively, substituted multiply bonded ligand allows the lone pair on the heteroatom to hybridize to an sp configuartion, which lowers the energy of the d_z^2 orbital. Due to the destabilization at the terminal atom, it would seem difficult to stabilize a metal-ligand multiple bond for a terminal atom in a tetrahedral d^6 configuration. More generally, if a late-metal metal-ligand multiple bond for a non-terminal atom is stable for a d^n electron configuration, a terminal atom should only be stable with a d^{n-2} electron configuration. This hypothesis is supported not only by work performed in our laboratory on cobalt and iron, but also by others working in this field. Presently, we have been unable to synthesize a terminal nitride or oxo of Co(III), but the imides are readily accessible. The related $[PhBP_3]Fe$ and $[PhBP^{iPr}_3]Fe$ systems support up to d^6 imides, but

only a d^4 nitride.[7a] Likewise, Hillhouse and co-workers have reported a d^8 imide complex in a trigonal planar geometry, but no corresponding terminal atom metal-ligand multiple bond such as an oxo. This hypothesis does not suggest that the terminal metal-ligand multiple bond is thermodynamically preferred over a bridging species, such as a μ_2-nitride versus a terminal nitride. Warren and co-workers prepared a trigonal planar Co(III) imide featuring an adamantyl group off of the nitrogen, but using smaller substituents such as 3,5-dimethylphenyl formed a bridging bis-μ_2-imide.[12,30] Obviously, this hypothesis only holds if the complexes being compared are of the same geometry.

Our attempts to prepare a $[PhBP_3]Co{\equiv}O$ have failed primarily due to the destabilization of terminal atoms versus non-terminal atoms for a d^6 pseudotetrahedral complex. The Co(III) siloxide $\{[PhBP_3]CoOSiPh_3\}\{BAr_4\}$ ($\{$**4.15**$\}\{BAr_4\}$ (Ar = Ph, or 3,5-$(CF_3)_2$-C_6H_3) is relatively stable, but under no conditions have we been able to remove the silyl group to form $[PhBP_3]Co{\equiv}O$, even though this species is isolobal to the stable imides we have prepared.[31] Likewise, a comparison of the d_z^2 orbitals from $\{$**4.15**$\}$ to the theoretically calculated $[PhBP_3]CoO$ show the same effect as the imide versus nitride (Figure 5.10). In fact, the DFT results for $\{$**4.15**$\}$ suggest that this complex has a molecular orbital diagram similar to the imides but with somewhat weaker π-bonding. In addition to strong σ-antibonding from the d_z^2 orbital, the hypothetical oxo $[PhBP_3]CoO$ is off-axis like the calculated nitride $\{[PhBP_3]CoN\}^-$. This model predicts that in a pseudotetrahedral geometry only a d^4 oxo or nitride such as $\{[PhBP_3]CoN\}^+$ would be stable.

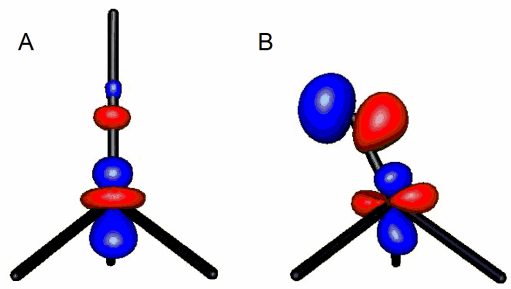

Figure 5.10. Orbital representations showing the d_z^2 orbital: (A) $\{[PhBP_3]CoOSiPh_3\}^+$ ({**4.15**}) and (B) $[PhBP_3]CoO$. Only the central atoms are shown for clarity.

The second fundamental shift in metal-ligand bonds lies in the nature of the R group on the imido nitrogen. More subtly, the parent imide $[PhBP_3]CoNH$ is less stable than $[PhBP_3]CoN^tBu$ (Figure 5.9). While the strong σ-antibonding interaction is not apparent, as in the case of the nitride complex, and the HOMO-LUMO gap is almost as large, the position of the calculated imide does not sit in the axial position, as it has nearly formed an equatorial plane with two of the phosphines. This result suggests that the hybridization on the N-H bond is not as effective as an N-C bond at attenuating the σ-antibonding interaction with the d_z^2 orbital. The NH group is being moved away from the σ-antibonding d_z^2 orbital, suggesting that dimeric NH imides may be electronically favored. To date, efforts to synthesize the parent imide $[PhBP_3]CoNH$ have been unsuccessful. Although bulky substituents on the imide nitrogen, such as a *tert*-butyl group, can favor the formation of terminal imides over other products, particularly bridging imides, it seems likely that the NH fragment is not as favorable electronically as other groups.[32] While it is impossible to separate the steric and electronic issues fully, it

is worth noting that the number of structurally characterized M≡NH imide complexes is far smaller than the number of M≡NR (R = alkyl or aryl) imide species that have been reported.[33] At present, no structurally characterized example of a terminal M≡NH has been reported for an electron count greater than d^3, while M≡NR imides have now been synthesized with electron counts as high as d^8.[34]

The inertness of the Co(III) imides ultimately rests on their electronic stability as closed shell 18 electron species. Saturated imides with a large HOMO-LUMO gap are resistant to giving up the nitrene functionality in group transfer reactions. This explains why this system is so inert, both to air and water, as well as chemical transformations. Comparable imide complexes, such as $[PhBP_3]FeNPh$[9,24,27] and Hillhouse's nickel imide,[14,15,16] are unsaturated species (with 17 and 16 electrons, respectively), which helps explain their greater reactivity. In light of the molecular orbital diagram for the cobalt imide species, it is not surprising that they undergo very few reactions.

5.4 Conclusions

We have synthesized the first imides on cobalt and they are supported by the $[PhBP_3]$ auxiliary ligand. Their synthesis can be adapted either from oxidative degradation of azides with a cobalt(I) precursor or salt metathesis of lithium amides with a Co(III) dihalide complex. The imides only react to give up the nitrene functionality in the case of CO or CN^tBu addition, giving the isocyanate and the carbodiimide as organic by-products respectively. The electronic structure diagram of the imides is similar to the well-known molecular orbital diagram for $\{[Cp]_2Co\}^+$ or $[Cp]_2Fe$ as well as their third row relative, $[Cp^*]IrN^tBu$. These pseudotetrahedral species confirm that the $[PhBP_3]Co{\equiv}ER$ species effectively have an *octahedral* molecular orbital diagram.

5.5 Experimental section

5.5.1 General considerations

General procedures were performed according to Section 2.4.1 and 3.5.1. Magnetic measurements were conducted as described in Section 3.5.2. EPR measurements and simulations were conducted as described in Section 3.5.3.

5.5.2 EPR measurements

Instrumental parameters for the spectra shown:

For $[PhBP_3]CoI(PMe_3)$ (**5.1**) in Figure 5.2: EPR spectrum of a glassy toluene solution of $[PhBP_3]CoI(PMe_3)$ at 50 K. Instrumental parameters: ν = 9.621 GHz, modulation frequency = 100 KHz, modulation amplitude = 2 G, microwave power = 2.017 mW, conversion time = 20.48 ms, time constant = 5.12 ms, 10 scans.

For $[PhBP_3]Co(PMe_3)$ (**5.2**) in Figure 5.2: EPR spectrum of a glassy toluene solution of $[PhBP_3]Co(PMe_3)$ at 4 K. Instrumental parameters: ν = 9.476 GHz, modulation frequency = 100 kHz, modulation amplitude = 15 G, microwave power = 2.01 mW, conversion time = 81.92 ms, time constant = 20.48 ms, 5 scans.

5.5.3 DFT calculations

All calculations were performed using the hybrid DFT functional B3LYP as implemented in the Jaguar 5.0 program package.[35] This DFT functional utilizes the Becke three-parameter functional[36] (B3) combined with the correlation functional of Lee, Yang, and Parr[37] (LYP). LACVP** was used as the basis set. Input coordinates were derived as described in the text from crystallographically determined structures (**5.4**, **5.7**, and {**4.15**}{BPh_4}). The starting structures of $[PhBP_3]CoNH$ and $\{[PhBP_3]CoN\}^-$ used the framework of **5.7** subtracting the *tert*-butyl group off the imide and adding a hydrogen

atom at a reasonable distance in the case of [$PhBP_3$]CoNH. The starting structure of [$PhBP_3$]CoO used the framework of {**4.15**} removing the silyl group. Spin-states and molecular charges were explicitly stated, and no molecular symmetry was imposed. Default values for geometry and SCF iteration cutoffs were used. All structures converged under these criteria.

5.5.4 Starting materials and reagents

The reagents CN^tBu, NaCl, {[Cp]$_2$Fe}{PF_6}, 1-azidoadamantane (1-adamantylazide), PMe_3, CO, 1.0 M HCl in Et_2O, sodium, and mercury metal were purchased from commercial vendors and used without further purification. PhNHLi was freshly prepared by addition of 1 equiv. of 1.6 M BuLi to 1 equiv. of $PhNH_2$ in petroleum ether. The resulting precipitate was collected via vacuum filtration and washed with additional petroleum ether. The reagents N_3Ph,[38] N_3-*p*-tolyl, N_3Ph-*p*-CF_3,[39] N_3Ph-*p*-NMe_2,[40] and $N_3{}^tBu$[41] were prepared according to literature procedures. The preparation of [$PhBP_3$]CoI (**3.1**) and ([$PhBP_3$]Co(μ-Cl))$_2$ (**3.3**) is described in Chapter 3. The preparation of {[$PhBP_3$]CoOSiPh_3}{BAr_4} ({**4.15**}{BAr_4} Ar = Ph or 3,5-$(CF_3)_2$-C_6H_3) is described in Chapter 4.

5.5.5 Synthesis of compounds

Synthesis of [$PhBP_3$]CoI(PMe_3), 5.1. Neat PMe_3 (34 μL, 0.32 mmol) was added via microsyringe to a stirring solution of [$PhBP_3$]CoI (**3.1**) (0.254 g, 0.291 mmol) in benzene (10 mL). The initially green solution turned red instantly. After stirring for 15 min, the solution was frozen, and the benzene was removed by lyophilization to afford a pure red powder (0.272 g, 99 % yield). Crystals were grown via vapor diffusion of petroleum ether into a benzene solution. ^{1}H NMR (C_6D_6, 300 MHz): δ 22.6 (br), 10.8, 9.4 (br), 7.4

(m), 2.2, 1.2 (m). UV-vis (C_6H_6) λ_{max}, nm (ε): 472 (1700). Anal. Calcd for $C_{48}H_{50}BICoP_4$: C, 60.85; H, 5.32. Found: C, 60.88; H, 5.11.

Synthesis of [PhBP$_3$]Co(PMe$_3$), 5.2: A 0.71 % Na/Hg amalgam was prepared by dissolving 7.3 mg (0.32 mmol) of sodium in 1.03 g of mercury. A THF solution (12 mL) of [PhBP$_3$]CoI(PMe$_3$) (**5.1**) (0.272 g, 0.29 mmol) was added to the stirring amalgam suspension in THF (5 mL). The mixture was stirred for 6 h as the color changed from red to brown. The heterogeneous reaction mixture was filtered through Celite to remove the amalgam, and the filtrate was dried in vacuo to a fine brown powder. The brown powder was then dissolved in 15 mL of benzene and stirred vigorously. After 1 h, a white precipitate (NaI) was observed, which was removed by filtration through Celite. The brown filtrate was frozen and dried to a fine brown powder by lyophilization (0.212 g, 90% yield). The product is extremely air sensitive and can be recrystallized via vapor diffusion of petroleum ether into benzene to give light green crystals. ^{1}H NMR (C_6D_6, 300 MHz): δ 42 (br), 15.8, 14.9, 13.2, 8.4, 8.2, 7.4 (m), 1.2 (m), -3.2, -3.6, -7.2 (br). UV-vis (C_6H_6) λ_{max}, nm (ε): 680 (140). Anal. Calcd for $C_{48}H_{50}BCoP_4$: C, 70.26; H, 6.14. Found: C, 70.17; H, 6.11.

Synthesis of [PhBP$_3$]CoNPh, 5.3. A benzene (2 mL) solution of phenylazide (39.2 mg, 0.329 mmol) was added dropwise to a stirring benzene (10 mL) solution of [PhBP$_3$]Co(PMe$_3$) (**5.2**) (135 mg, 0.164 mmol). During the first 15 min, nitrogen evolution was evident, and the brown solution turned deep red. The solution was stirred for an additional 4 h to ensure completion. The solvent was removed by lyophilization. The resulting red powder was washed with petroleum ether (10 mL) to remove the byproduct (Me$_3$P=NPh) and then dried to afford pure product (104 mg, 76%). The product can be recrystallized via vapor diffusion of petroleum ether into benzene. ^{1}H NMR (C_6D_6, 300 MHz): δ 8.191 (d, *J* = 7.8 Hz, 2 H), 8.129 (d, *J* = 7.2 Hz, 2 H), 7.735 (m, 14 H), 7.492 (t, *J* = 7.2 Hz, 1 H), 7.348 (t, *J* = 7.5 Hz, 1 H), 7.059 (t, *J* = 7.5 Hz, 2 H), 6.731 (m, 18 H), 1.481 (br, 6 H). ^{31}P NMR (C_6D_6, 121.4 MHz): δ 69 (br). ESI/MS (m/z): 836 (**5.3** + H^+). UV-vis (C_6H_6) λ_{max}, nm (ε): 418 (7000), 538 (4200). Anal. Calcd for $C_{51}H_{46}BCoNP_3$: C, 73.31; H, 5.55; N, 1.68. Found: C, 72.35; H, 5.43; N, 1.87.

Synthesis of [PhBP$_3$]CoN-*p*-tolyl, 5.4. A benzene (2 mL) solution of *p*-tolylazide (50.6 mg, 0.380 mmol) was added dropwise to a stirring benzene (10 mL) solution of [PhBP$_3$]Co(PMe$_3$) (**5.2**) (156 mg, 0.190 mmol). During the first 15 min, nitrogen evolution was evident, and the brown solution turned deep red. The solution was stirred for an additional 4 h to ensure completion. The solvent was removed by lyophilization. The resulting red powder was washed with petroleum ether (10 mL) to remove the byproduct (Me$_3$P=N-*p*-tolyl) and then dried to afford pure product (157 mg, 97%). The product can be recrystallized via vapor diffusion of petroleum ether into benzene. ^{1}H NMR (C_6D_6, 300 MHz): δ 8.141 (d, *J* = 7.2 Hz, 2 H), 7.764 (m, 14 H), 7.494 (t, *J* = 7.5 Hz, 1 H), 6.857 (d, *J* = 8.1 Hz, 2 H), 6.749 (m, 20 H), 1.769 (3 H), 1.491 (br, 6 H). ^{31}P

NMR (C_6D_6, 121.4 MHz): δ 69 (br). ^{13}C NMR (C_6D_6, 209.5 MHz): δ 138.6, 134.6, 132.6, 131.7, 129.0, 128.9, 128.5, 128.3, 128.2, 125.0, 120.4, 22.7, 12.7 (br). ESI/MS (m/z) : 850 (**5.4** + H^+). UV-vis (C_6H_6) λ_{max}, nm (ε): 420 (5700), 536 (3400). Anal. Calcd for $C_{52}H_{48}BCoNP_3$: C, 73.51; H, 5.69; N, 1.65. Found: C, 73.64; H, 5.61; N, 1.63.

Synthesis of [PhBP$_3$]CoNPh-*p*-CF$_3$, 5.5. A benzene (2 mL) solution of N_3Ph-*p*-CF_3 (95.8 mg, 0.512 mmol) was added to a stirring benzene (10 mL) solution of [PhBP$_3$]Co(PMe$_3$), **5.2**, (210 mg, 0.256 mmol). The reaction mixture was stirred for 5 h at rt and then frozen and dried to a dark red powder by lyophilization. The powder was washed with acetonitrile (2 x 15 mL) and dried affording the product (139 mg, 60% yield). ^{1}H NMR (C_6D_6, 300 MHz): δ 8.11 (d, *J* = 7.2 Hz, 2 H), 7.92 (d, *J* = 7.8 Hz, 2 H), 7.73 (t, *J* = 7.5 Hz, 2 H), 7.66 (m, 12 H), 7.48 (t, *J* = 7.2 Hz, 1 H), 7.23 (d, *J* = 8.1 Hz, 2 H), 6.75 (m, 18 H), 1.46 (br s, 6 H). ^{31}P{^{1}H} NMR (C_6D_6, 121.4 MHz): δ 65 (br). ^{19}F NMR (C_6D_6, 282 MHz): -61.2. UV-vis (C_6H_6) λ_{max}, nm (ε): 422 (6800), 549 (4500). Anal. Calcd for $C_{52}H_{45}BCoF_3NP_3$: C, 69.12; H, 5.02; N, 1.55. Found: C, 68.72; H, 5.41; N, 1.55.

Synthesis of [PhBP$_3$]CoNPh-*p*-NMe$_2$, 5.6. A benzene (2 mL) solution of N_3Ph-*p*-NMe_2 (31.0 mg, 0.191 mmol) was added to a stirring benzene (5 mL) solution of [PhBP$_3$]Co(PMe$_3$), **5.2**, (78.4 mg, 0.096 mmol). The reaction mixture was stirred for 8 h at rt and then frozen and dried to a dark red powder by lyophilization. The powder was washed with petroleum ether (2 x 10 mL), dried, and then dissolved in benzene (2 mL). Crystallization via vapor diffusion of petroleum ether into the benzene solution yielded pure product (52 mg, 62% yield). ^{1}H NMR (C_6D_6, 300 MHz): δ 8.04 (d, J = 8.4 Hz, 2 H), 8.17 (d, *J* = 6.9 Hz, 2 H), 7.84 (m, 12 H), 7.74 (t, *J* = 6.9 Hz, 2 H), 7.49 (t, *J* = 6.6 Hz, 1

H), 6.78 (m, 18 H), 6.34 (d, J = 8.4 Hz, 2 H), 2.33 (s, 6 H), 1.54 (br s, 6 H). $^{31}P\{^{1}H\}$ NMR (C_6D_6, 121.4 MHz): δ 64 (br). UV-vis (C_6H_6) λ_{max}, nm (ε): 454 (10500), 543 (9900). Anal. Calcd for $C_{53}H_{51}BCoN_2P_3$: C, 72.45; H, 5.85; N, 3.19. Found: C, 72.10; H, 5.98; N, 3.07.

Synthesis of [PhBP$_3$]CoN^{t}Bu, 5.7. A benzene (2 mL) solution of $N_3{}^t$Bu (114 mg, 1.16 mmol) was added to a stirring benzene (8mL) solution of [PhBP$_3$]Co(PMe$_3$), **5.2**, (159 mg, 0.194 mmol). The reaction mixture was stirred and heated to 55º C for 6 h. After cooling to rt, the reaction mixture was frozen and dried to a brown powder by lyophilization. This powder was then washed with petroleum ether (2 x 10 mL) and dried to afford the product (41 mg, 26% yield). The product can be crystallized via vapor diffusion of petroleum ether into benzene. ^{1}H NMR (C_6D_6, 300 MHz): δ 8.12 (d, J = 6.9 Hz, 2 H), 7.70 (t, J = 7.8 Hz, 2 H), 7.66 (m, 12 H), 7.46 (t, J = 7.2 Hz, 1 H), 6.78 (m, 18 H), 1.58 (s, 9 H), 1.49 (br s, 6 H). $^{31}P\{^{1}H\}$ NMR (C_6D_6, 121.4 MHz): δ 70 (br). UV-vis (C_6H_6) λ_{max}, nm (ε): 480 (1500).

Synthesis of [PhBP$_3$]CoNAd, 5.8. A benzene (5 mL) solution of 1-azidoadamantane (177 mg, 1.00 mmol) was added to a stirring benzene (7 mL) solution of [PhBP$_3$]Co(PMe$_3$), **5.2**, (205 mg, 0.250 mmol). The reaction mixture was stirred for 2 h at rt and then frozen and dried to a brown powder by lyophilization. The powder was washed with petroleum ether (2 x 10 mL), dried, then washed with acetonitrile (2 x 10 mL), and dried to afford the product (100 mg, 45% yield). ^{1}H NMR (C_6D_6, 300 MHz): δ 8.13 (d, J = 7.2 Hz, 2 H), 7.73 (m, 12 H), 7.71 (t, J = 7.8 Hz, 2 H), 7.47 (t, J = 7.2 Hz, 1 H), 6.80 (m, 18 H), 2.36 (s, 6 H), 1.99 (s, 3 H), 1.71 (s, 6 H), 1.51 (br s, 6 H). $^{31}P\{^{1}H\}$ NMR (C_6D_6, 121.4 MHz): δ 70 (br). UV-vis (C_6H_6) λ_{max}, nm (ε): 479 (1400). Anal.

Calcd for $C_{55}H_{56}BCoNP_3$: C, 73.92; H, 6.32; N, 1.57. Found: C, 73.57; H, 6.46; N, 1.77.

Synthesis of [PhBP$_3$]CoCl$_2$, 5.9. A THF (80 mL) solution of ([PhBP$_3$]Co(μ-Cl))$_2$, **3.3**, (0.936 g, 0.600 mmol) was stirred vigorously prior to addition of solid {[Cp]$_2$Fe}{PF$_6$} (0.437 g, 0.132 mmol). The solution immediately turned bright green. After 5 min, solid NaCl (0.701 g, 1.20 mmol) was added to the solution, which was then stirred for 16 h. The reaction mixture was then filtered through Celite, and the filtrate was dried in vacuo affording a fine green powder. The powder was washed with petroleum ether (3 x 75 mL) to remove [Cp]$_2$Fe. The green powder was dissolved in benzene (150 mL) and was stirred vigorously for 6 h followed by filtration through Celite. The green filtrate was then frozen and dried to an analytically pure powder by lyophilization (0.594 g, 61% yield). The product can be crystallized via vapor diffusion of petroleum ether into benzene. ^{1}H NMR (C_6D_6, 300 MHz): δ 7.91 (d, J = 6.9 Hz, 2 H), 7.73 (m, 12 H), 7.62 (t, J = 6.9 Hz, 2 H), 7.42 (m, 1 H), 6.84 (m, 6 H), 6.68 (m, 12 H), 1.39 (s br, 6 H). ^{31}P{^{1}H} NMR (C_6D_6, 121.4 MHz): δ 36. UV-vis (C_6H_6) λ_{max}, nm (ε): 484 (690), 645 (750). Anal. Calcd for $C_{45}H_{41}BCl_2CoP_3$: C, 66.29; H, 5.07. Found: C, 66.42; H, 4.85.

Alternative synthesis of [PhBP$_3$]CoNPh, 5.3. A benzene (10 mL) solution of [PhBP$_3$]CoCl$_2$, **5.9**, (223 mg, 0.273 mmol) was added to a stirring slurry of PhNHLi (54.2 mg, 0.547 mmol) in benzene (5 mL). The reaction mixture changed from green to red and was stirred for 2 h followed by filtration over Celite. The red filtrate was frozen and dried by lyophilization and then washed with petroleum ether (2 x 10 mL). The red powder was then dried in vacuo (120 mg, 53% yield). Spectroscopic methods indicated that the product was pure **5.3** showing identical UV-vis, ^{31}P NMR, and ^{1}H NMR signals.

Alternative synthesis of [PhBP$_3$]CoCl$_2$, 5.9. A diethyl ether (15 mL) solution of [PhBP$_3$]CoNPh, **5.3**, (82 mg, 0.098 mmol) was stirred vigorously prior to addition of 1.0 M HCl in diethyl ether (196 μL, 0.196 mmol) via micropipette. The reaction mixture immediately changed from red to green and solids precipitated. The reaction mixture was filtered over Celite, and benzene (2 x 10 mL) was used to extract more product from the Celite. The green filtrate was then frozen and dried to a powder by lyophilization and then washed with petroleum ether (2 x 5 mL) and dried in vacuo (32 mg, 40% yield). Spectroscopic methods indicated that the product was pure **5.9** showing identical UV-vis, ^{31}P NMR, and ^{1}H NMR signals.

Synthesis of [PhBP$_3$]Co(CO)$_2$, 5.10. An atmosphere of CO was added to a 200 mL Strauss flask that contained a benzene (8 mL) solution of [PhBP$_3$]CoN-*p*-tolyl (**5.4**) (25.4 mg, 0.030 mmol). The flask was heated to 70 °C in an oil bath for 8 d during which the color changed from deep red to light brown. GC/MS of the reaction mixture showed the formation of phenylisocyanate (m/z = 119). The solution was then frozen, and the solvent was removed by lyophilization. The resulting tan powder was washed with petroleum ether (10 mL) and then dried to afford pure product (22 mg, 90 %). ^{1}H NMR (C_6D_6, 300 MHz): δ 8.084 (d, *J* = 7.2 Hz, 2 H), 7.667 (t, *J* = 7.2 Hz, 2 H), 7.433 (t, *J* = 7.2 Hz, 1 H), 7.377 (m, 12 H), 6.783 (m, 18 H), 1.781 (br s, 6 H). ^{31}P NMR (C_6D_6, 121.4 MHz): δ 35.5. ^{13}C NMR (C_6D_6, 125.7 MHz): δ 211.1, 139.3, 133.3, 131.6, 130.6, 129.9, 129.1, 124.2, 16.7 (br). IR (cm^{-1}, THF): 2008, 1932. UV-vis (C_6H_6) λ_{max}, nm (ε): 440 (880). Anal. Calcd for $C_{47}H_{41}BCoO_2P_3$: C, 70.52; H, 5.16. Found: C, 70.90; H, 5.27.

Synthesis of [PhBP$_3$]Co(CN^{t}Bu)$_2$, 5.11. A 0.61% Na/Hg amalgam was prepared by dissolving 3.3 mg (0.14 mmol) of sodium into 540 mg of mercury. A THF (10 mL)

solution of [PhBP$_3$]CoI(CN^{t}Bu), **5.12** (see below), (136 mg, 0.14 mmol) was added to the stirring amalgam in THF (3 mL). Neat CN^{t}Bu (12 mg, 0.14 mmol, 16 μL) was then added via micropipette. The mixture was stirred for 3 h as the color changed from green to brown. The reaction mixture was then filtered through Celite to remove the amalgam, and the filtrate was dried in vacuo affording a fine brown powder. The brown powder was dissolved in benzene (12 mL) and stirred vigorously. After 1 h, white precipitate (NaI) was observed, which was remove by filtration though Celite. The orange filtrate was frozen and dried to a fine orange powder through lyophilization (129 mg, 100% yield). ^{1}H NMR (C_6D_6, 300 MHz): δ 8.12 (d, J = 6.3 Hz, 2 H), 7.63 (t, J = 7.5 Hz, 2 H), 7.58 (m, 12 H), 7.39 (t, J = 6.3 Hz, 1 H), 6.88 (m, 18 H), 1.75 (s, 6 H), 1.06 (s, 18 H). ^{31}P{^{1}H} NMR (C_6D_6, 121.4 MHz): δ 39. IR (cm^{-1}, THF): 2113, 2040. Anal. Calcd for $C_{55}H_{59}BCoN_2P_3$: C, 72.53; H, 6.53; N, 3.08. Found: C, 72.48; H, 6.92; N, 3.01.

Synthesis of [PhBP$_3$]CoI(CN^{t}Bu), 5.12. A benzene (2 mL) solution of CN^{t}Bu (23.2 mg, 0.279 mmol) was added to a stirring benzene (10 mL) solution of [PhBP$_3$]CoI, **3.1**, (243 mg, 0.279 mmol). The reaction mixture was stirred for 10 h at rt and then frozen and dried to a green powder by lyophilization. The powder was washed with petroleum ether (2 x 15 mL) and dried affording the product (237 mg, 89% yield). ^{1}H NMR (C_6D_6, 300 MHz): δ 10.6 (br), 7.9, 7.7, 7.4, 7.3, 7.0, 2.9 (br). UV-vis (C_6H_6) λ_{max}, nm : 423 (2400), 701 (1100). Anal. Calcd for $C_{50}H_{50}BCoINP_3$: C, 62.92; H, 5.28; N, 1.47. Found: C, 62.76; H, 5.44; N, 1.23.

Addition of CO to [PhBP$_3$]CoN-*p*-tolyl (5.4). To a J. Young tube was added **5.4** (12.7 mg, 0.015 mmol) and ferrocene (2.0 mg) as an internal standard in C_6D_6. The tube was then charged with CO (14 equiv, 0.210 mmol). The J. Young tube was heated for 12 days

at 70 °C in an oil bath. A ^{1}H NMR spectrum of the reaction mixture was compared to a pure sample of *p*-tolylisocyanate, confirming only 30% of the free isocyanate by integration (GC/MS: 133 m/z for *p*-tolylisocyanate). An additional peak in the alkyl region (45% by integration) suggested another product(s), presumably due to isocyanate degradation during the course of the experiment. Only free isocyanate was detected by GC/MS.

Addition of CN^{t}Bu to [PhBP$_3$]CoN-*p*-tolyl (5.4). Neat CN^{t}Bu (27.6 mg, 0.333 mmol, 37.7 μL) was added via micropipette to a stirring solution of [PhBP$_3$]CoN-*p*-tolyl, **5.4**, (94.1 mg, 0.111 mmol) in benzene (8 mL) at ambient temperature. The reaction mixture went from red to brown over 6 h. The solution was frozen and dried to a fine brown powder through lyophilization. The powder was washed with petroleum ether (2 x 10 mL). The petroleum ether fraction was set aside to settle and decanted 30 min later and dried in vacuo. The powder fraction was dried in vacuo. Organic products from the petroleum ether fraction were characterized by GC/MS, which showed ^{t}BuN=C=NPh-*p*-CH$_3$. GC/MS (m/z): 188 (M), 132 (M-^{t}Bu). Inorganic products from the solid showed [PhBP$_3$]Co(CN^{t}Bu)$_2$, **5.11**, (by IR, ^{31}P NMR and ^{1}H NMR) as well as an additional product tentatively assigned as κ$_2$-[PhBP$_3$]Co(CNtBu)$_3$. ^{31}P{^{1}H} NMR (C$_6$D$_6$, 121.4 MHz): δ 45 (2 P), 9 (1 P). IR (cm^{-1}, THF): 2142 (additional peaks may be obscured by overlapping **5.11**).

5.5.6 X-ray experimental information

The general X-ray experimental procedure was performed according to section 2.4.4. Crystallographic information is provided in Table 5.1.

Table 5.1. X-ray diffraction experimental details for [PhBP$_3$]CoI(PMe$_3$) (**5.1**), [PhBP$_3$]Co(PMe$_3$) (**5.2**), [PhBP$_3$]CoN-*p*-tolyl (**5.4**), [PhBP$_3$]CoN^{t}Bu (**5.7**), and [PhBP$_3$]CoCl$_2$ (**5.9**).

	[PhBP$_3$]CoI(PMe$_3$), (**5.1**)	[PhBP$_3$]Co(PMe$_3$), (**5.2**)
Chemical formula	$C_{54}H_{56}BCoIP_4$	$C_{48}H_{50}BP_4Co \cdot C_6H_6$
Formula weight	1025.51	898.61
T (ºC)	-177	-177
λ (Å)	0.71073	0.71073
a (Å)	19.1690(9)	13.204(2)
b (Å)	12.2981(6)	13.313(2)
c (Å)	21.3027(10)	17.112(3)
α (º)	90	72.299(2)
β (º)	105.5100(10)	88.479(2)
γ (º)	90	60.454(2)
V (Å^3)	4839.1(4)	2465.2(7)
Space group	$P2_1/c$	$P\bar{1}$
Z	4	2
Dcalcd (g/cm^3)	1.408	1.211
μ(cm^{-1})	11.61	5.12
R1, wR2 (I>2σ(I))[a]	0.0580, 0.1099	0.1044, 0.1820

[a] $R1 = \Sigma \, | \, |F_o| - |F_c| \, | \, / \, \Sigma \, |F_o|$, $wR2 = \{ \Sigma \, [\, w(F_o^2 - F_c^2)^2 \,] \, / \, \Sigma \, [\, w(F_o^2)^2 \,] \, \}^{1/2}$

Table 5.1. (cont.)

	[PhBP$_3$]CoN-*p*-tolyl (**5.4**)	[PhBP$_3$]CoN^{t}Bu (**5.7**)
Chemical formula	$C_{55}H_{51}BCoNP_3$	$C_{49}H_{50}BNP_3Co \cdot 1½(C_6H_6)$
Formula weight	888.62	932.71
T (ºC)	-177	-177
λ (Å)	0.71073	0.71073
a (Å)	14.1174(11)	11.2939(5)
b (Å)	14.3252(11)	18.4709(8)
c (Å)	22.3306(18)	23.6972(11)
α (º)	90	90
β (º)	96.2060(10)	99.9680(10)
γ (º)	90	90
V (Å^3)	4489.6(6)	4868.8(4)
Space group	$P2_1/c$	$P2_1/n$
Z	4	4
Dcalcd (g/cm^3)	1.315	1.272
μ(cm^{-1})	5.28	4.90
R1, wR2 (I>2σ(I))[a]	0.0439, 0.0648	0.0401, 0.0669

Table 5.1. (cont.)

	$[PhBP_3]CoCl_2$ (**5.9**)
Chemical formula	$C_{45}H_{42}BCl_2P_3Co \cdot 2\ (C_6H_6)$
Formula weight	971.54
T (ºC)	-177
λ (Å)	0.71073
a (Å)	10.8683(12)
b (Å)	13.3303(14)
c (Å)	16.8858(18)
α (º)	93.356(2)
β (º)	96.607(2)
γ (º)	103.506(2)
V ($Å^3$)	2353.7(4)
Space group	$P\bar{1}$
Z	2
Dcalcd (g/cm^3)	1.371
μ(cm^{-1})	6.20
R1, wR2 ($I>2\sigma(I)$)[a]	0.0620, 0.1073

References cited

1) a) Groves, J. T.; Takahashi, T. *J. Am. Chem. Soc.* **1983**, *105*, 2073-2074. b) LaPointe, R. E.; Wolczanski, P. T.; Mitchell, J. F. *J. Am. Chem. Soc.* **1986**, *108*, 6382-6384. c) Cummins, C. C. *Chem. Commun.* **1998**, 1777-1786. d) Donahue, J. P.; Lorber, C.; Nordlander, E.; Holm, R. H. *J. Am. Chem. Soc.* **1998**, *120*, 3259-3260. e) Woo, L. K.

Chem. Rev. **1993**, *93*, 1125-1136. f) Crevier, T. J.; Lovell, S.; Mayer, J. M.; Rheingold, A. L.; Guzei, I. A. *J. Am. Chem. Soc.* **1998**, *120*, 6607-6608.

2) a) Mansuy, D.; Mahy, J.; Dureault, A.; Bedi, G.; Battioni, P. *J. Chem. Soc., Chem. Commun.* **1984**, 1161-1163. b) Li, Z.; Conser, K. R.; Jacobsen, E. N. *J. Am. Chem. Soc.* **1993**, *115*, 5326-5327. c) Evans, D. A.; Faul, M. M.; Bilodeau, M. T. *J. Am. Chem. Soc.* **1994**, *116*, 2742-2743. d) DuBois, J.; Tomooka, C. S.; Hong, J.; Carreira, E. M. *Acc. Chem. Res.* **1997**, *30*, 364-372.

3) a) Tshuva, E. Y.; Lee, D.; Bu, W.; Lippard, S. J. *J. Am. Chem. Soc.* **2002**, *124*, 2416-2417. b) Solomon, E. I.; Brunold, T. C.; Davis, M. I.; Kemsley, J. N.; Lee, S. K.; Lehnert, N.; Neese, F.; Skulan, A. J.; Yang, Y.; Zhou, J. *Chem. Rev.* **2000**, *100*, 235-249. c) Meunier, B. *Biomimetic Oxidations Catalyzed by Transition Metal Complexes*; Imperial College Press: London, 2000. d) Holm, R. H. *Coord. Chem. Rev.* **1990**, *100*, 183-221. e) Matsunaga, P. T.; Hillhouse, G. L.; Rheingold, A. L. *J. Am. Chem. Soc.* **1993**, *115*, 2075-2077. f) Fischer, B.; Enemark, J. H.; Basu, P. J. *Inorg. Biochem.* **1998**, *72*, 13-21. g) Liang, H. C.; Dahan, M.; Karlin, K. D. *Curr. Opin. Chem. Biol*. **1999**, *3*, 168-175.

4) a) Wigley, D. *Prog. Inorg. Chem*. **1994**, *42*, 239-482. b) Nugent, W. A.; Mayer, J. M. *Metal-Ligand Multiple Bonds*; John Wiley and Sons: New York, 1988. c) Thyagarajan, S.; Incarvito, C. D.; Rheingold, A. L.; Theopold, K. H. *Chem. Commun*. **2001**, 2198-2199. d) Lange, S. J.; Miyake, H.; Que, L., Jr. *J. Am. Chem. Soc.* **1999**, *121*, 6330-6331. e) Wang, D.; Squires, R. R. *J. Am. Chem. Soc*. **1987**, *109*, 7557-7558.

5) a) Glueck, D. S.; Wu, J.; Hollander, F. J.; Bergman, R. G. *J. Am. Chem. Soc.* **1991**, *113*, 2041-2054. b) Glueck, D. S.; Hollander, F. J.; Bergman, R. G. *J. Am. Chem. Soc.* **1989**, *111*, 2719-2721.

6) Hay-Motherwell, R. S.; Wilkinson, G.; Hussain-Bates, B.; Hursthouse, M. B. *Polyhedron* **1993**, *12*, 2009-2012.

7) a) Betley, T. A.; Peters, J. C. *J. Am. Chem. Soc.* **2004**, *126*, 6252-6254. b) Ruhde, J. U.; In, J.; Lim, M. H.; Brennessel, W. W.; Bukowski, M. R.; Stubna, A.; Münck, E.; Nam, W.; Que, L., Jr. *Science* **2003**, *299*, 1037-1039 c) MacBeth, C. E.; Golombek, A. P.; Young, V. G., Jr.; Yang, C.; Kuczera, K.; Hendrich, M. P.; Borovik, A. S. *Science* **2000**, *289*, 938-941.

8) Verma, A. K.; Nazif, T. N.; Achim, C.; Lee, S. C. *J. Am. Chem. Soc.* **2000**, *122*, 11013-11014.

9) Brown, S. D.; Betley, T. A.; Peters, J. C. *J. Am. Chem. Soc.* **2003**, *125*, 322-323.

10) Betley, T. A.; Peters, J. C. *J. Am. Chem. Soc.* **2003**, *125*, 10782-10783.

11) Jenkins, D. M.; Betley, T. A.; Peters, J. C. *J. Am. Chem. Soc.* **2002**, *124*, 11238-11239.

12) Dai, X.; Kapoor, P.; Warren, T. H. *J. Am. Chem. Soc.* **2004**, *126*, 4798-4799.

13) Hu, X.; Meyer, K. *J. Am. Chem. Soc.* **2004**, *126*, 16322-16323.

14) Mindiola, D. J.; Hillhouse, G. L. *J. Am. Chem. Soc.* **2001**, *123*, 4623-4624.

15) Mindiola, D. J.; Hillhouse, G. L. *Chem. Commun.* **2002**, 1840-1841.

16) Waterman, R.; Hillhouse, G. L. *J. Am. Chem. Soc.* **2003**, *125*, 13350-13351.

17) See Chapters 2 and 3 as well as: a) Shapiro, I. R.; Jenkins, D. M.; Thomas, J. C.; Day, M. W.; Peters, J. C. *Chem. Commun.* **2001**, 2152-2153. b) Jenkins, D. M.; Di Bilio,

A. J.; Allen, M. J.; Betley, T. A.; Peters, J. C. *J. Am. Chem. Soc.* **2002**, *124*, 15336-15350.

18) Glueck, D. S.; Green, J. C.; Michelman, R. I.; Wright, I. A. *Organometallics* **1992**, *11*, 4221-4225.

19) Heinze, K.; Huttner, G.; Zsolnai, L.; Schober, P. *Inorg. Chem.* **1997**, *36*, 5457-5469.

20) de Carvalho, L. C. A.; Dartiguenave, M.; Dartiguenave, Y.; Beauchamp, A. L. *J. Am. Chem. Soc.* **1984**, *106*, 6848-6849.

21) Ghilardi, C. A.; Mealli, C.; Midollini, S.; Orlandini, A. *Inorg. Chem.* **1985**, *24*, 164-168.

22) a) Sacconi, L. *Coord. Chem. Rev.* **1972**, *8*, 351-367. b) Morassi, R.; Bertini, I.; Sacconi, L. *Coord. Chem. Rev.* **1973**, *11*, 343-402.

23) Bencini, A.; Gatteschi, D. *Trans. Metal Chem.* **1982**, *8*, 97-119.

24) Brown, S. D.; Peters, J. C. *J. Am. Chem. Soc.*, *accepted*.

25) a) Li, Z.; Quan, R. W.; Jacobsen, E. N. *J. Am. Chem. Soc.* **1995**, *117*, 5889-5890. b) Omura, K.; Murakami, M.; Uchida, T.; Irie, R.; Katsuki, T. *Chem. Lett.* **2003**, *32*, 354-355.

26) a) Dauban, P.; Dodd, R. H. *Synlett* **2003**, *105*, 1571-1586. b) O'Conner, K. J.; Wey, S.; Burrows, C. J. *Tetrahedron Lett.* **1992**, *33*, 1001-1004.

27) Brown, S. D.; Peters, J. C. *J. Am. Chem. Soc.* **2004**, *126*, 4538-4539.

28) Warren, K. D. *Struct. and Bond.* **1976**, *27*, 45-159.

29) A platinum terminal oxo complex has recently been reported. See: Anderson, T. M.; Neiwert, W. A.; Kirk, M. L.; Piccoli, P. M. B.; Schultz, A. J.; Koetzle, T. F.; Musaev, D. G.; Morokuma, K.; Cao, R.; Hill, C. L. *Science* **2004**, *306*, 2074-2077. Two points

are worth mentioning about this complex. First, the authors do not characterize it as a metal-ligand multiple bond based on their molecular orbital diagram. They claim it is only a Pt-O single bond. Second, the metal cluster nature of the ligands may stabilize the supposed d^6 configuration by delocalizing electron density away from the Pt center to the ligands.

30) Based on this hypothesis, it should be possible to synthesize a terminal Co(III) d^6 oxo in a trigonal planar geometry given that Hillhouse has prepared a trigonal planar d^8 imide. Warren and co-workers have made the bridged bis-μ_2-oxo instead of a terminal oxo using the same auxiliary ligands that stabilized a terminal imide. This is not surprising given that the bridged oxo may be thermodynamically more stable.

31) See Chapter 4 for synthesis and discussion of $\{[PhBP_3]CoOSiPh_3\}\{BAr_4\}$ (Ar = Ph or 3,5-$(CF_3)_2$-C_6H_3).

32) To try to limit the effects of sterics in protecting the terminal imide, if would be of interest to see if an imido complex with a methyl group off of the nitrogen such as $[PhBP_3]CoNMe$ is stable. The $[PhBP_3]Co$ system so far has not proven to be sterically effected by smaller R groups unlike the Hillhouse, Meyer, Bergman, and Warren systems that either degrade or form bridging imides.

33) Currently only 17 terminal M≡NH species have been reported (CCDC search, 2005). This is two orders of magnitude below the number of M≡NR species reported.

34) For a d^3 M≡NH species see: a) Huynh, M. H.; White, P. S.; John, K. D.; Meyer, T. J. *Angew. Chem., Int. Ed. Engl.* **2001**, *40*, 4049-4051. For d^2 examples see: b) Hagenbach, A.; Strahle, J. *Z. Anorg. Allg. Chem.* **2000**, *626*, 1613-1619. c) Yoshida, T.; Adachi, T.; Yabunouchi, N.; Ueda, T.; Okamoto, S. *Chem. Commun.* **1994**,

151-152. d) Ishino, H.; Tokunaga, S.; Seino, H.; Ishii, Y.; Hidai, M. *Inorg. Chem.* **1999**, *38*, 2489-2496.

35) Jaguar 5.0, Schrodinger, LLC, Portland, Oregon, 2002.

36) Becke, A. D. *J. Chem. Phys.* **1993**, *98*, 5648-5652.

37) Lee, C.; Yang, W.; Parr R. G. *Phys. Rev. B* **1988**, *37*, 785-789.

38) Smith, P. A. S.; Brown, B. B. *J. Am. Chem. Soc.* **1951**, *73*, 2438-2441.

39) Abramovitch, R. A.; Challand, S. R.; Scriven, E. F. V. *J. Org. Chem.* **1972**, *37*, 2705-2710.

40) a) Li, Y.; Kirby, J. P.; George, M. W.; Poliakoff, M.; Schuster, G. B. *J. Am. Chem. Soc.* **1988**, *110*, 8092-8098. b) Smith, P. A. S.; Hall, J. H. *J. Am. Chem. Soc.* **1962**, *84*, 480-485.

41) Bottaro, J. C.; Penwell, P. E.; Schmitt, R. J. *Syn. Comm.* **1997**, *27*, 1465-1467.

Chapter 6: A structurally characterized homobimetallic bridging μ_2-nitride complex of cobalt

6.1 Introduction

Bridging μ_2-nitrides have been shown to be the final product of the chemical splitting of N_2 in molybdenum[1] and niobium[2] systems. Furthermore, the potential for a bridging nitride to be part of the catalytic cycle for biological nitrogen fixation is intriguing in light of the recent X-ray structure of the MoFe-cofactor of nitrogenase, which features an interstitial μ_6-ligand, possibly a nitride.[3] Previously, homobimetallic bridging μ_2-nitrides of many early to mid-transition metals in high oxidation states have been synthesized.[4,5] Examples of this type of complex featuring late metals are limited to examples on Fe,[6,7] Ru,[8] and Os,[9] even though they are monomeric terminal nitride or imido late metal complexes,[10,11] and bridging nitride complexes of higher nuclearity (three or more metal atoms)[12] have been reported. The scarcity of homobimetallic bridging μ_2-nitride complexes for late metals is all the more striking in light of the fact that the related mono-[13] and bis-μ_2-oxo complexes[14] are well-established for groups 9 through 12. Herein we report the first example of a homobimetallic bridging μ_2-nitride complex of cobalt.

6.2 Results and discussion

6.2.1 Synthesis of $([PhBP_3]Co)_2(\mu\text{-}N)$

The synthesis of the bridged nitride can be accomplished by the two routes shown in Eq. 6.1 and Eq. 6.2. The bridged azide complex $([PhBP_3]Co(\mu\text{-}1,3\text{-}N_3))_2$ (**6.1**) ($[PhBP_3]$ = $[PhB(CH_2PPh_2)_3]^-$) is prepared by reacting the previously described $[PhBP_3]CoI$ (**3.1**)[15] with excess TlN_3 in THF (Eq. 6.1). Complex **6.1** is isolated in 66% yield and characterized by IR, UV-vis, and NMR spectroscopy, as well as single crystal X-ray diffraction. The addition of one equivalent of Na/Hg amalgam to **6.1** in THF gives

the desired bridged nitride, $([PhBP_3]Co)_2(\mu\text{-}N)$ (**6.2**), in 90% yield. Complex **6.2** is formally a mixed valent Co^{II}/Co^{III} species. This route to the μ_2-bridging nitride manifold is similar to that employed in our laboratory for the preparation of the low valent Fe^{II}/Fe^{II} μ_2-nitride, $\{([PhBP_3]Fe)_2(\mu\text{-}N)\}\{Na(THF)_5\}$. The bridged nitride complex, **6.2**, is deep red in color and has two charge transfer bands in its UV-vis spectrum at 395 (ε = 21800 M^{-1} cm^{-1}) and 549 (ε = 8800 M^{-1} cm^{-1}) nm; the near-IR region of the spectrum shows no additional bands, in contrast to the NIR bands of related $\{([PhBP_3]Fe)_2(\mu\text{-}N)\}\{Na(THF)_5\}$.

$$[PhBP_3]CoI \;(\mathbf{3.1}) \xrightarrow[-TlI]{TlN_3} ([PhBP_3]Co(\mu\text{-}1,3\text{-}N_3))_2 \;(\mathbf{6.1}) \xrightarrow[-NaN_3\ -N_2]{Na/Hg} ([PhBP_3]Co)_2(\mu\text{-}N) \;(\mathbf{6.2}) \qquad (6.1)$$

An alternate route (Eq. 6.2) proceeds via the addition of $TlPF_6$ and acetonitrile to a THF solution of **3.1** to give the green cationic bis-acetonitrile complex, $\{[PhBP_3]Co(NCCH_3)_2\}\{PF_6\}$, **6.3**, in 95% yield. Complex **6.3** can be reduced with $[Cp]_2Co$ in THF to give the neutral paramagnetic mono-acetonitrile adduct, $[PhBP_3]Co(NCCH_3)$ **6.4** in 78% yield.

$$[PhBP_3]CoI \;(\mathbf{3.1}) \xrightarrow[-TlI]{TlPF_6,\ 2\ NCCH_3} \{[PhBP_3]Co(NCCH_3)_2\}\{PF_6\} \;(\mathbf{6.3}) \xrightarrow[-CH_3CN\ -\{[Cp]_2Co\}\{PF_6\}]{[Cp]_2Co} [PhBP_3]Co(NCCH_3) \;(\mathbf{6.4})$$

$$[PhBP_3]Co(NCCH_3) \;(\mathbf{6.4}) \xrightarrow{N_3(SiMe_3)} ([PhBP_3]Co)_2(\mu\text{-}N) \;(\mathbf{6.2}) \qquad (6.2)$$

Addition of 20 equivalents of $(Me_3Si)N_3$ (Me_3Si = TMS) to a THF solution of **6.4** turns the solution from brown to dark red characteristic of **6.2**. Pure **6.2** was obtained in 17% yield by crystallization of the reaction mixture upon standing for one day.

Trimethylsilylazide has previously been shown to be an effective nitrogen transfer agent to give terminal nitride complexes.[16] Notably, the reactivity of **6.4** with $(Me_3Si)N_3$ is very different from the reactivity of the $[Tp^{R,R}]CoN_2$ ([Tp] = hydro-tris(pyrazolyl)borate, R = ^{i}Pr or ^{t}Bu) complexes reported by Theopold and co-workers, which undergo intramolecular C-H bond activation to form amides.[17]

6.2.2 Structural characterization and magnetic studies of precursors

The solid-state structures of the precursor compounds are of interest. Both **6.1** and **6.3** were studied by X-ray diffraction. The coordination geometry for each metal center within **6.1** is best described as a distorted square pyramidal with a crystallographic inversion center present (Figure 6.1). A small amount (< 3%) of $[PhBP_3]Tl$ co-crystallized in the sample leading to some disorder in the structure. The bond lengths and angles of **6.1** are similar to those of its cationic analogue $[(H_3CC(CH_2PPh_2)_3)Co(\mu_2\text{-}1,3\text{-}N_3)]_2[BPh_4]_2$, ($H_3CC(CH_2PPh_2)_3$ = triphos).[18] Notably, the structure differs somewhat from $([PhBP_3]Co(\mu\text{-}Br))_2$ (**3.2**) and $([PhBP_3]Co(\mu\text{-}Cl))_2$ (**3.3**) as **6.1** has shorter Co-P bonds. In addition, one of the P-Co-N bond angles is nearly linear (N1-Co1-P2, 174.01(10)).

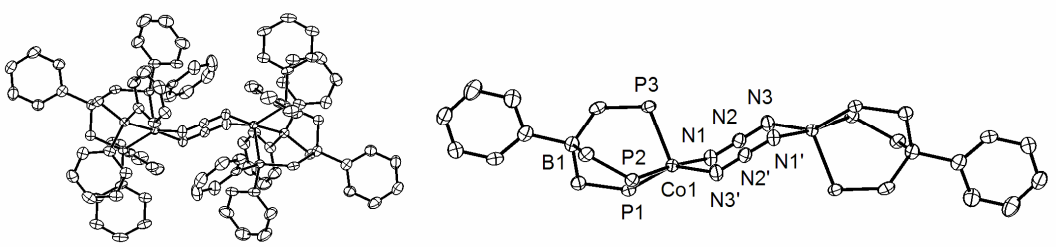

Figure 6.1. Displacement ellipsoids are represented at 50%. The structure on the right is shown without aryl carbon atoms for clarity. Selected interatomic distances (Å) and angles (deg) for $([PhBP_3]Co(\mu\text{-}1,3\text{-}N_3))_2$, (**6.1**): Co1-P1, 2.232(1); Co1-P2, 2.203(1); Co1-P3, 2.255(1); Co1-N1, 1.977(3); Co1-N3', 1.955(3). P1-Co1-P2, 89.32(5); P1-Co1-P3, 95.97(5); P2-Co1-P3, 91.45(5); N1-Co1-P1, 90.85(11); N1-Co1-P2, 174.01(10); N1-Co1-P3, 94.48(10); N3'-Co1-P1, 149.44(11); N3'-Co1-P2, 88.44(10); N3'-Co1-P3, 114.55(11); N3'-Co1-N1, 88.36(14).

The solid-state structure determined for **6.3** reveals a square pyramidal geometry about Co, similar to what is observed for dicationic $[(triphos)Co(NCCH_2CH_3)_2][BF_4]_2$ (Figure 6.2).[19] This contrasts to a similar five-coordinate "$[PhBP_3]Co$" species, namely, $[PhBP_3]CoI(PMe_3)$, which features a trigonal bipyramidal geometry. The geometry difference for these species is also observed in solution by EPR (see below). The axial Co-P bond (Co-P1, 2.331(1)) is elongated compared to the other two equatorial Co-P bonds (2.238(1) and 2.253(1)).

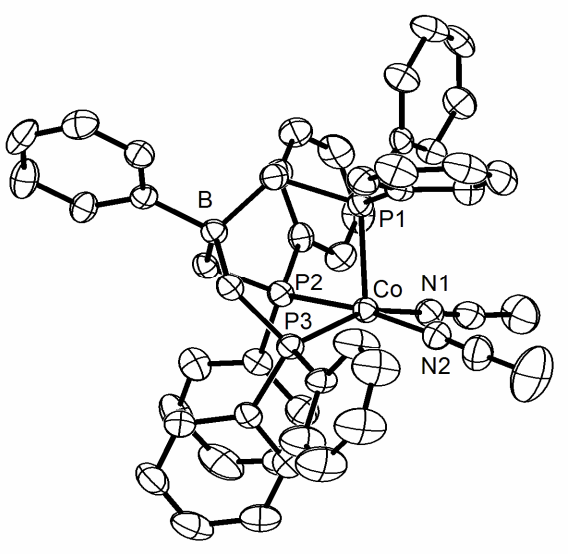

Figure 6.2. Displacement ellipsoid representation (50%) for $\{[PhBP_3]Co(NCCH_3)_2\}^+$ (**6.3**) with the anion omitted for clarity. Selected interatomic distances (Å) and angles (deg): Co-P1, 2.331(1); Co-P2, 2.238(1); Co-P3, 2.253(1); Co-N1, 1.947(3); Co-N2, 1.914(2). P1-Co-P2, 90.01(3); P1-Co-P3, 96.11(3); P2-Co-P3, 87.90(3); N1-Co-P1, 105.92(7); N1-Co-P2, 91.45(7); N1-Co-P3, 157.96(7); N2-Co-P1, 97.34(7); N2-Co-P2, 172.54(7); N2-Co-P3, 90.02(7); N1-Co-N2, 87.79(10).

Complex **6.3** was determined to be low spin by SQUID magnetometry with an average magnetic moment ($\chi_m T_{av}$, 10 to 300 K) of 0.60 cm^3 K mol^{-1}. The complex obeys the Curie-Weiss law. The EPR spectrum of **6.3**, taken in a mixture of benzene and acetonitrile, shows well-defined hyperfine (I_{Co} = 7/2) and superhyperfine (3 x I_P = ½) coupling. The coupling parameters were successfully simulated, and the experimental and simulated spectra are shown in Figure 6.3. The spectrum shows an axial signal ($g_\perp > g_{||}$) typical of low spin Co(II) square pyramidal structures.[20] This confirms that the

species maintains its solid-state geometry in solution and contrasts with $[PhBP_3]CoI(PMe_3)$, which shows an axial EPR spectrum with $g_{\parallel} > g_{\perp}$.

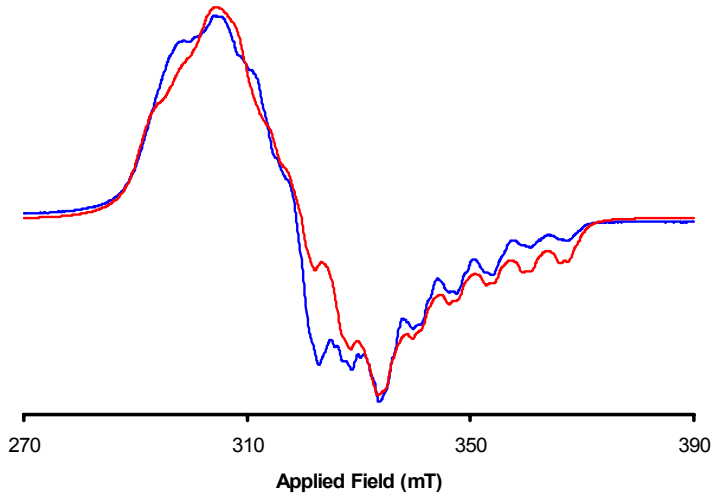

Figure 6.3. EPR spectrum of $\{[PhBP_3]Co(NCCH_3)_2\}\{PF_6\}$ (**6.3**) in a mixture of benzene and acetonitrile at 77 K. The blue line (—) is the experimental spectrum, and the red line (—) is the simulated spectrum. Simulated Parameters: $g_x = 2.150$, $a_{x(Co)} = 22$ gauss, $a_{x(P)} = 26$ gauss; $g_y = 2.176$, $a_{y(Co)} = 54$ gauss, $a_{y(P)} = 15$ gauss; $g_z = 1.974$, $a_{z(Co)} = 65$ gauss, $a_{z(P)} = 17$ gauss. See Experimental Section for instrumental parameters.

6.2.3 Structural characterization of $([PhBP_3]Co)_2(\mu\text{-}N)$

The solid state structure of **6.2** is of significant interest, and suitable crystals for X-ray diffraction were grown from methylene chloride and petroleum ether (Figure 6.4). The solid-state structure obtained includes disorder of the phosphine ligands coordinated to Co2 (approximately 9% of the lattice features molecules with phosphines in the second, chemically equivalent, position). In addition, the crystal suffers from racemic

twinning in the orthorhombic space group $Pna2_1$. The structure of **6.2** presented herein is the best data set obtained from X-ray diffraction studies of a number of different crystalline samples derived from different recrystallization attempts. The molecular structures obtained for the other crystals all indicated similar metrics for the cobalt complex, and therefore the identity of **6.2** is not in question. The Co1-N and Co2-N bonds are quite short, 1.623(8) Å and 1.648(8) Å respectively, suggesting significant metal-ligand multiple bond character. Recently published terminal cobalt imides have Co-N bond distances of 1.658(2) Å for $[PhBP_3]Co{\equiv}N(p\text{-tolyl})$ and 1.624(4) Å for a β-diketiminato supported terminal imide.[21] These short Co-N bonds compare well to bridging μ_2-nitrides of iron, although it should be noted that in the latter cases the iron centers are high valent Fe^{III}/Fe^{IV} or Fe^{IV}/Fe^{IV}.[4,7] These bond distances are also significantly shorter than in the published bridged μ_2-imides of Co (Co-N(R)-Co), which have Co-N bond distances between 1.97 and 2.05 Å.[21,22] The Co-P distances of **6.2** shown are within 0.02 Å of 2.25 Å, which is characteristic of low spin cobalt complexes previously studied, and likewise the P-Co-P angles are barely greater than 90°. Interestingly, the Co1-N-Co2 angle is slightly bent at 155.3(6)°, making this angle more acute than previously examined iron μ_2-nitrides, which typically have Fe-N-Fe bond angles between 170 and 180°.[4,7] The exception to this trend is $\{([PhBP_3]Fe)_2(\mu\text{-}N)\}\{Na(THF)_5\}$, which has an Fe1-N-Fe2 bond angle of 135.9(3).

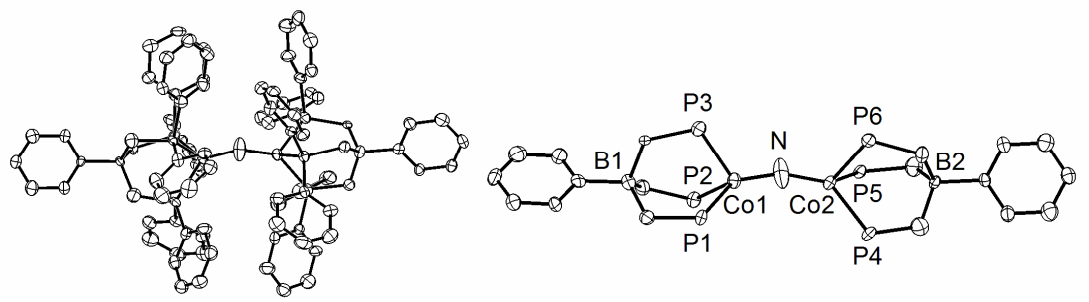

Figure 6.4. Displacement ellipsoids are represented at 50%. The structure on the right is shown without aryl carbon atoms for clarity. Selected interatomic distances (Å) and angles (deg) for ($[PhBP_3]Co)_2(\mu$-N) (**6.2**): Co1-P2, 2.238(2); Co1-P3, 2.258(2); Co1-P1, 2.259(2); Co1-N, 1.623(8); Co2-P6, 2.243(3); Co2-P5, 2.249(2); Co2-P4, 2.254(2); Co2-N, 1.648(8). Co1-N-Co2, 155.3(6).

6.2.4 Magnetic characterization of $([PhBP_3]Co)_2(\mu$-N)

Since **6.2** is a paramagnetic complex, we decided to investigate its magnetic properties using variable temperature SQUID magnetization measurements. The complex was determined to have only one unpaired electron with $\chi_m T_{av}$ (10 K to 300 K) equaling 0.60 cm^3 K mol^{-1}, obeying the Curie-Weiss law (Figure 6.5A). This result rules out the possibility of strong anti-ferromagnetic coupling to give one unpaired electron at low temperature. Variable temperature EPR studies performed in glassy toluene show only one signal in the temperature range of 5 to 60 K. The spectrum shows no well-resolved coupling or anisotropy, and the signal is centered at $g \approx 2.11$ (Figure 6.5B). This result corroborates the SQUID assignment of one unpaired electron for the molecule since no low field signals indicative of high spin cobalt are observed.[23] These combined results

suggest that the species may be a valence localized Co^{II}/Co^{III} species wherein both metal ions are low spin.

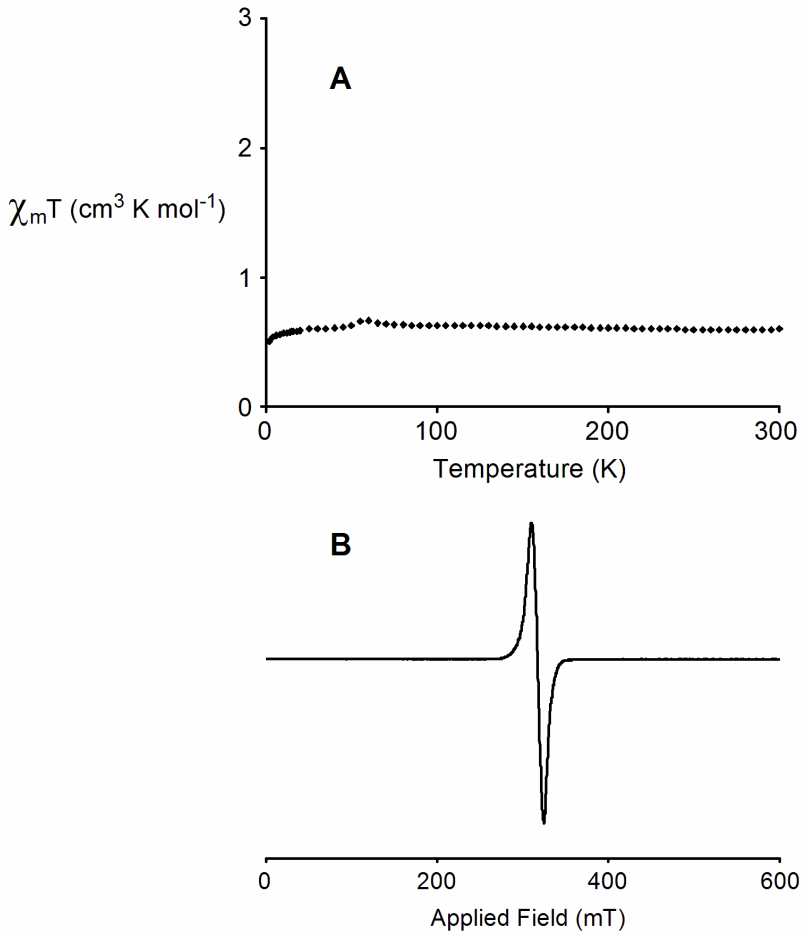

Figure 6.5. (A) SQUID plot of $\chi_m T$ (cm^3 K mol^{-1}) versus T for ([PhBP$_3$]Co)(μ-N), **6.2**, (♦). (B) EPR spectrum of ([PhBP$_3$]Co)$_2$(μ-N), **6.2**, in toluene at 30 K. See Experimental Section for instrumental parameters.

6.3 Conclusion

In summary, we have expanded the family of homobimetallic bridging μ_2-nitride complexes to include a Group 9 metal, cobalt. The bridged nitride exhibits short Co-N bond distances, typical of bridging nitride moieties, although the slightly bent

Co1-N-Co2 angle is unusual compared to most analogous bridging Fe μ_2-nitride complexes. The species is a low spin complex (S = ½) with one unpaired electron.

6.4 Experimental section

6.4.1 General considerations

General procedures were performed according to Section 2.4.1 and 3.5.1. Magnetic measurements were conducted as described in Section 3.5.2. EPR measurements and simulations were conducted as described in Section 3.5.3.

6.4.2 EPR measurements

Instrumental parameters for the spectra shown:

For $\{[PhBP_3]Co(NCCH_3)_2\}\{PF_6\}$ (**6.3**) in Figure 6.3: EPR spectrum of $\{[PhBP_3]Co(NCCH_3)_2\}\{PF_6\}$ in a mixture (1:1) of benzene and acetonitrile at 77 K. Instrumental parameters: ν, 9.509 GHz, Modulation frequency, 100 kHz, Modulation Amplitude, 4 G, Microwave Power, 12.755 mW, Conversion Time, 20.48 ms, Time Constant, 5.12 ms, Scans, 20.

For $([PhBP_3]Co)_2(\mu\text{-}N)$ (**6.2**) in Figure 6.5: EPR spectrum of $([PhBP_3]Co)_2(\mu\text{-}N)$ (**6.2**) in toluene at 30 K. Instrumental parameters: ν, 9.379 GHz; Modulation frequency, 100 kHz; Modulation Amplitude, 2 G; Microwave Power, 0.638 mW; Conversion Time, 81.92 ms; Time Constant, 20.48 ms; Scans, 1.

6.4.3 Starting materials and reagents

The preparation of $[PhBP_3]CoI$ (**3.1**) is described in Chapter 3. The reagent TlN_3 was prepared according to a literature procedure.[24] The reagents $TlPF_6$, $[Cp]_2Co$, $(TMS)N_3$, sodium, and mercury metal were purchased from commercial vendors and used without further purification.

6.4.4 Synthesis of compounds

Synthesis of ([PhBP$_3$]Co(μ_2-1,3-N$_3$))$_2$, 6.1. The reagents TlN_3 (1.73 g, 7.03 mmol) and [PhBP$_3$]CoI, **3.1**, (0.613 g, 0.703 mmol) were mixed together as solids in a 250 mL Erylenmeyer flask, and THF (150 mL) was added. The reaction mixture was stirred for 24 h and then filtered over Celite. The THF was removed under reduced pressure, and the red powder was extracted with 100 mL of CH_2Cl_2. This solution was filtered over Celite and then the solvent was removed in vacuo (0.364 g, 66% yield). The red powder can be crystallized by vapor diffusion of petroleum ether into a CH_2Cl_2 solution. ^{1}H NMR (CD_2Cl_2, 300 MHz): δ 8.06, 7.45 (d, J = 6.9 Hz), 7.26 (t, J = 7.5 Hz), 7.08 (t, J = 7.5 Hz), 5.87, 3.28 (br s). UV-vis (THF) λ_{max}, nm (ε): 375 (8600), 518 (3900). IR (cm^{-1}, THF): 2070. Anal. Calcd for $C_{90}H_{82}B_2Co_2N_6P_6$: C, 68.72; H, 5.25; N, 5.34. Found: C, 68.80; H, 5.52; N, 5.14.

Synthesis of ([PhBP$_3$]Co)$_2$(μ-N), 6.2. Neat N_3(TMS) (0.572 g, 4.96 mmol) was added to a THF solution (2 mL) of [PhBP$_3$]Co(NCCH$_3$), **6.4**, (0.195 g, 0.248 mmol) and mixed for one minute. The solution was allowed to stand for 24 h, and red crystals formed. The red crystals were washed with petroleum ether (3 x 3 mL) then dissolved in benzene (3 mL), which was frozen and lyophilized to remove solvent (0.032 g, 17% yield). ^{1}H NMR (C_6D_6, 300 MHz): δ 9.4, 8.5, 7.9, 7.6, 3.3, 0.5. UV-vis (C_6H_6) λ_{max}, nm (ε): 395 (21800), 549 (8800). SQUID (average from 10 – 310 K): $\chi_m T$ = 0.60 cm^3 K mol^{-1}. Anal. Calcd for $C_{90}H_{82}B_2Co_2NP_6$: C, 71.92; H, 5.50; N, 0.93. Found: C, 70.42; H, 5.30; N, 1.05.

Alternative Synthesis of ([PhBP$_3$]Co)$_2$(μ-N), 6.2. A 0.52 % Na/Hg amalgam was prepared by dissolving 6.2 mg (0.27 mmol) of sodium into 1.2 g of mercury. A THF solution (15 mL) of ([PhBP$_3$]Co(μ_2-1,3-N$_3$))$_2$, **6.1**, (0.212 g, 0.270 mmol) was added to

the amalgam and allowed to stir for 14 h. The reaction mixture was then filtered through Celite to remove the amalgam, and the filtrate was dried in vacuo affording a fine red powder. The powder was dissolved in benzene (12 mL) and stirred vigorously. The solution was then filtered over Celite, and the solvent was removed under reduced pressure (0.183 g, 90% yield). The compound can be crystallized in CH_2Cl_2 at -35 °C. This preparation gave the same spectra as the above method.

Synthesis of {[PhBP$_3$]Co(NCCH$_3$)$_2$}{PF$_6$}, 6.3. A THF (3 mL) solution of $TlPF_6$ (0.042 g, 0.12 mmol) was added to a THF (10 mL) solution of [PhBP$_3$]CoI, **3.1**, (0.101 g, 0.116 mmol) causing the green reaction mixture to become cloudy. An excess of acetonitrile (approximately 5 to 15 equivalents) was added to the mixture causing an instant color change to yellow. An orange solid precipitated after 4 h leaving a green supernatant. The solution was filtered over Celite and then concentrated to dryness under reduced pressure. The resulting powder was dissolved in benzene (8 mL), and vapor diffusion of petroleum ether afforded green crystals (0.107 g, 95.7% yield). Note: the crystals grown for the X-ray diffraction experiment contained the $\{BF_4\}$ counteranion instead of $\{PF_6\}$. ^{1}H NMR (CD_3CN, 300 MHz): δ 10.4 (br), 7.2, 7.0, 3.6, 3.1 (br), 1.7. UV-vis (C_6H_6) λ_{max}, nm (ε): 740 (280). SQUID (average from 10 – 310 K): $\chi_m T$ = 0.60 cm^3 K mol^{-1}. EPR (77 K, benzene/acetonitrile): g_x = 2.150, $a_{x(Co)}$ = 22 gauss, $a_{x(P)}$ = 26 gauss; g_y = 2.176, $a_{y(Co)}$ = 54 gauss, $a_{y(P)}$ = 15 gauss; g_z = 1.974, a_z = 65 gauss, $a_{z(P)}$ = 17 gauss. Anal. Calcd for $C_{49}H_{47}BCoP_4N_2F_6$: C, 60.58; H, 4.87; N, 2.88. Found: C, 60.59; H, 5.39; N, 2.23.

Synthesis of [PhBP$_3$]Co(NCCH$_3$), 6.4: A THF solution (3 mL) of $[Cp]_2Co$ (0.0789 g, 0.417 mmol) was added to a stirring THF solution (15 mL) of

{[$PhBP_3$]Co($NCCH_3$)$_2$}{PF_6}, **6.3**, (0.413 g, 0.426 mmol). The solution was stirred for 16 h and then filtered over Celite followed by removal of the solvent under reduced pressure. The powder was reconstituted in 12 mL of benzene and stirred followed by filtration over Celite. The solution was then frozen and lyophilized (0.255 g, 78% yield). ^{1}H NMR (C_6D_6, 300 MHz): δ 16.0, 15.0, 13.7, 12.2, 10.4, 8.1, 7.2, 5.5. IR (cm^{-1}, THF): 2045. Anal. Calcd for $C_{47}H_{44}BCoNP_3$: C, 71.80; H, 5.65; N, 1.78. Found: C, 71.44; H, 5.82; N, 1.20.

6.4.5 X-ray experimental information

The general X-ray experimental procedure was performed according to section 2.4.4. Crystallographic information is provided in Table 6.1.

Table 6.1. X-ray diffraction experimental details for $([PhBP_3]Co(\mu_2\text{-}1,3\text{-}N_3))_2$ (**6.1**), $([PhBP_3]Co)_2(\mu\text{-}N)$, (**6.2**), and $\{[PhBP_3]Co(NCCH_3)_2\}\{BF_4\}$ (**6.3**).

	$([PhBP_3]Co(\mu_2\text{-}1,3\text{-}N_3))_2$ (**6.1**)	$([PhBP_3]Co)_2(\mu\text{-}N)$, (**6.2**)
Chemical formula	$C_{90}H_{84}B_2Cl_{0.76}Co_{1.95}N_6P_6Tl_{0.05}$	$C_{90}H_{82}B_2NP_6Co_2$
Formula weight	1587.53	1502.87
T (ºC)	-177	-177
λ (Å)	0.71073	0.71073
a (Å)	13.0507(12)	40.978(4)
b (Å)	14.4544(13)	13.3841(13)
c (Å)	14.6285(13)	13.7861(14)
α (º)	100.286(2)	90
β (º)	111.438(1)	90
γ (º)	114.974(1)	90
V ($Å^3$)	2139.6(3)	7560.9(13)
Space group	$P\bar{1}$	$Pna2_1$
Z	1	4
Dcalcd (g/cm^3)	1.551	1.320
μ(cm^{-1})	43.6	6.14
R1, wR2 ($I>2\sigma(I)$)[a]	0.0704, 0.1306	0.0814, 0.1070

[a] $R1 = \Sigma \, | \, |F_o| - |F_c| \, | \, / \, \Sigma \, |F_o|$, $wR2 = \{ \Sigma \, [\, w(F_o^2 - F_c^2)^2 \,] \, / \, \Sigma \, [\, w(F_o^2)^2 \,] \, \}^{1/2}$

Table 6.1. (cont.)

	$\{[PhBP_3]Co(NCCH_3)_2\}\{BF_4\}$ (**6.3**)
Chemical formula	$C_{49}H_{47}BN_2P_3Co \cdot BF_4$
Formula weight	913.35
T (ºC)	-177
λ (Å)	0.71073
a (Å)	19.2341(13)
b (Å)	13.1806(9)
c (Å)	19.6043(13)
α (º)	90
β (º)	115.234(1)
γ (º)	90
V ($Å^3$)	4495.8(5)
Space group	$P2_1/c$
Z	4
Dcalcd (g/cm^3)	1.349
μ(cm^{-1})	5.42
R1, wR2 ($I>2\sigma(I)$)[a]	0.0531, 0.0819

References cited

1) a) Cherry, J. F.; Stephens, F. H.; Johnson, M. J. A.; Diaconescu, P. L.; Cummins, C. C. *Inorg. Chem.* **2001**, *40*, 6860-6862. b) Solari, E.; Da Silva, C.; Iacono, B.; Hesschenbrouck, J.; Rizzoli, C.; Scopelliti, R.; Floriani, C. *Angew. Chem. Int. Ed.* **2001**, *40*, 3907-3909.

2) a) Mindiola, D. J.; Meyer, K.; Cherry, J. F.; Baker, T. A.; Cummins, C. C. *Organometallics* **2000**, *19*, 1622-1624. b) Caselli, A.; Solari, E.; Scopelliti, R.; Floriani, C.; Re, N.; Rizzoli, C.; Chiesi-Villa, A. *J. Am. Chem. Soc.* **2000**, *122*, 3652-3670.

3) Einsle, O.; Tezcan, F. A.; Andrade, S. L. A.; Schmid, B.; Yochida, M.; Howard, J. B.; Rees, D. C. *Science* **2002**, *297*, 1696-1700.

4) Floris, B.; Donzello, M. P.; Ercolani, C. *The Porphyrin Handbook* **2003**, *18*, 1-62.

5) Holl, M. M. B.; Kersting, M.; Pendley, B. D.; Wolczanski, P. T. *Inorg. Chem.* **1990**, *29*, 1518-1526.

6) A Fe^{II}/Fe^{II} bridged nitride has been recently prepared in our laboratory. Brown, S. D.; Peters, J. C. *J. Am. Chem. Soc., accepted*.

7) a) Dutta, S. K.; Beckmann, U.; Bill, E.; Weyhermüller, T.; Weighardt, K. *Inorg. Chem.* **2000**, *39*, 3355-3364. b) Li, M.; Shang, M.; Ehlinger, N.; Schulz, C. E.; Scheidt, W. R. *Inorg. Chem.* **2000**, *39*, 580-583. c) Jüstel, T.; Müller, M.; Weyhermüller, T.; Kressl, C.; Bill, E.; Hildebrandt, P.; Lengen, M.; Grodzicki, M.; Trautwein, A. X.; Nuber, B.; Wieghardt, K. *Chem. Eur. J.* **1999**, *5*, 793-810. d) Scheidt, W. R.; Summerville, D. A.; Cohen, I. A. *J. Am. Chem. Soc.* **1976**, *98*, 6623-6628.

8) a) Bonomo, L.; Solari, E.; Scopelliti, R.; Floriani, C. *Angew. Chem. Int. Ed.* **2001**, *40*, 2529-2531. b) Sun, X.; Liang, J.; Che, C.; Zhu, N.; Zhang, X. X.; Gao, S. *Chem. Commun.* **2002**, 2090-2091. c) Jüstel, T.; Bendix, J.; Metzler-Nolte, N.; Weyhermüller, T.; Nuber, B.; Weighardt, K. *Inorg. Chem.* **1998**, *37*, 35-43.

9) Newton, C.; Edwards, K. D.; Ziller, J. W.; Doherty, N. M. *Inorg. Chem.* **1999**, *38*, 4032-4037.

10) a) Brown, S. D.; Peters, J. C. *J. Am. Chem. Soc.* **2004**, *126*, 4538-4539. b) Brown, S. D.; Betley, T. A.; Peters, J. C. *J. Am. Chem. Soc.* **2003**, *125*, 322-323. c) Betley, T. A.; Peters, J. C. *J. Am. Chem. Soc.* **2003**, *125*, 10782-10783. d) Betley, T. A.; Peters, J. C. *J. Am. Chem. Soc.* **2004**, *126*, 6252-6254. e) Glueck, D. S.; Wu, J.; Hollander, F. J.; Bergman, R. G. *J. Am. Chem. Soc.* **1991**, *113*, 2041-2054. f) Mindiola, D. J.; Hillhouse, G. L. *J. Am. Chem. Soc.* **2001**, *123*, 4623-4624.

11) See Chapter 5 and: Jenkins, D. M.; Betley, T. A.; Peters, J. C. *J. Am. Chem. Soc.* **2002**, *124*, 11238-11239.

12) a) Martinengo, S.; Ciani, G.; Sironi, A.; Heaton, B. T.; Mason, J. J. *J. Am. Chem. Soc.* **1979**, *101*, 7095-7097. b) Martinengo, S.; Ciani, G.; Sironi, A. *J. Chem. Soc., Chem. Commun.* **1984**, 1577-1578. c) Skapski, A. C.; Ciechanowicz, M.; Griffith, W. P.; Pawson, D. *J. Chem. Soc. D., Chem. Commun.* **1971**, 876.

13) a) Ge, Y.; Peng, F.; Sharp, P. R. *J. Am. Chem. Soc.* **1990**, *112*, 2623-2640. b) Bag, B.; Mondal, N.; Mitra, S; Rosair, G. *Chem. Commun.* **2000**, 1729-1730.

14) a) Hikichi, S.; Yoshizawa, M.; Sasakura, Y.; Akita, M.; Moro-oka, Y. *J. Am. Chem. Soc.* **1998**, *120*, 10567-10568. b) Mahadevan, V.; Hou, Z.; Cole, A. P.; Root, D. E.; Lal, T. K.; Solomon, E. I.; Stack, T. D. P. *J. Am. Chem. Soc.* **1997**, *119*, 11996-11997.

15) See Chapter 2, Chapter 3, and: a) Shapiro, I. R.; Jenkins, D. M.; Thomas, J. C.; Day, M. W.; Peters, J. C. *Chem. Commun.* **2001**, 2152-2153. b) Jenkins, D. M.; Di Bilio, A. J.; Allen, M. J.; Betley, T. A.; Peters, J. C. *J. Am. Chem. Soc.* **2002**, *124*, 15336-15350.

16) a) Eikey, R. A.; Khan, S. I.; Abu-Omar, M. M. *Angew. Chem. Int. Ed.* **2002**, *41*, 3592-3595. b) Montilla, F.; Galindo, A.; Monge, Á; Gutiérrez-Puebla, E. *J. Organomet. Chem.* **2002**, *662*, 59-62.

17) Thyagarajan, S.; Shay, D. T.; Incarvito, C. D.; Rheingold, A. L.; Theopold, K. H. *J. Am. Chem. Soc.* **2003**, *125*, 4440-4441.

18) Bencini, A.; Ghilardi, C. A.; Midollini, S.; Orlandini, A. *Inorg. Chem.* **1989**, *28*, 1958-1962.

19) Mann, S.; Huttner, G.; Zsolnai, L.; Heinze, K.; Jacob, V.; Antelmann, B.; Driess, A.; Schiemenz, B. *Z. Naturforsch., B. Chem. Sci.* **2000**, *55*, 638-650.

20) Bencini, A.; Gatteschi, D. *Trans. Metal Chem.* **1982**, *8*, 97-119.

21) Dai, X.; Kapoor, P.; Warren, T. H. *J. Am. Chem. Soc.* **2004**, *126*, 4798-4799.

22) Link, H.; Fenske, D. *Z. Anorg. Allg. Chem.* **1999**, *625*, 1878-1884.

23) Pilbrow, J. R. *Transition Ion Electron Paramagnetic Resonance*; Clarendon Press: Oxford, 1990.

24) McEwan, W. S.; Williams, M. M. *J. Am. Chem. Soc.* **1954**, *76*, 2182.

Chapter 7: Diazoalkane complexes of cobalt

The text of this chapter is reproduced in part with permission from:

Jenkins, D. M.; Betley, T. A.; Peters, J. C. *J. Am. Chem. Soc.* **2002**, *124*, 11238-11239.

7.1 Introduction

Diazoalkanes have been used as reagents for a wide range of metal-catalyzed transformations[1,2] including the cyclopropanation of olefins.[3] In addition, diazoalkanes can act as versatile ligands in transition metal complexes, as these ligands can adopt a plethora of monomeric bonding modes when bound to a metal center.[4] While all of the bonding modes shown in Figure 7.1 have been structurally characterized, type **B** is the most common.[5] The electronic nature of the ligand is highly dependent on the substituents on the carbon atom. For example, resonance stabilization from aryl substituents often provides more stable diazoalkane complexes.

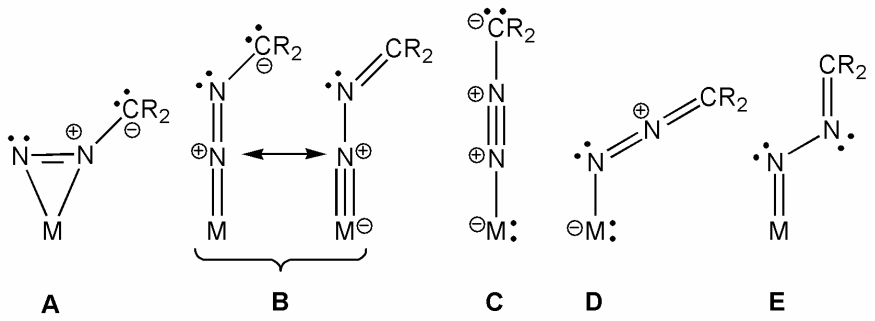

Figure 7.1. Structurally characterized examples have been prepared for each of these monomeric bonding modes of diazoalkanes (A-E). See reference 4.

The degradation of metal-bound diazoalkanes is a common method for preparing transition metal carbenes.[6] A common application of carbene complexes is olefin metathesis.[7] For example, one of the most active olefin metathesis catalysts, Grubbs's catalyst ($RuCl_2(=CHPh)(PPh_3)_2$), is prepared by diazoalkane addition to the precursor ($RuCl_2(PPh_3)_3$) resulting in the carbene complex.[8] We chose to investigate the properties of cobalt diazoalkane complexes with the aspiration of synthesizing a related cobalt

alkylidene complex. To date, there are no examples of structurally characterized Schrock-type cobalt carbenes; however, complexes with this ligand motif have been prepared for other first-row metals such as iron,[9] nickel,[10] and, more recently, copper.[11] Furthermore, Schrock-type carbenes have been prepared using the second- and third-row group 9 metals rhodium[12] and iridium.[13,14] This chapter discusses the synthesis of a number of cobalt diazoalkane complexes, including examples that adopt binding modes **A** and **B** and attempts to generate a cobalt alkylidene.

7.2 Results

7.2.1 Synthesis of diazoalkane complexes

Based on our success in synthesizing imide species such as $[PhBP_3]CoN^tBu$ (**5.7**) through two electron oxidative degradation of organic azides, we were interested in generating a carbene from a free diazoalkane using a similar oxidative group transfer strategy.[15] A five coordinate cobalt(III) carbene complex such as $[PhBP_3]Co(=CR_2)(PR_3)$ (R = aryl or alkyl; $[PhBP_3] = [PhB(CH_2PPh_2)_3]^-$) would be isoelectronic to Bergman's carbene, $[Cp^*]Ir(=CH_2)(PMe_3)$, suggesting that the target cobalt carbene complex would be a reasonable synthetic goal.

Ideally, synthesis of a Co(III) carbene could begin with the same type of Co(I) precursor as used for the imide synthesis. It was necessary to prepare an additional Co(I) starting material, in addition to the previously described $[PhBP_3]CoPMe_3$ (**5.2**), since a more sterically bulky apical phosphine ligand such as PPh_3 may be required to stabilize the proposed five-coordinate carbene. Addition of free PPh_3 to a solution of $[PhBP_3]CoI$ (**3.1**) in the presence of sodium/mercury amalgam gives $[PhBP_3]Co(PPh_3)$, **7.1** (Eq. 7.1). This species is paramagnetic ($S = 1$) and has a similar pale green color to **5.2**.

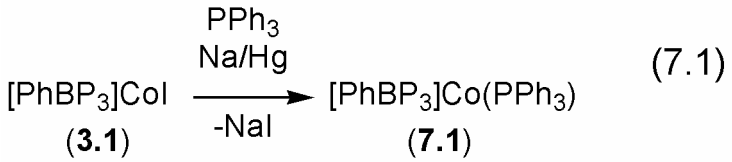

(7.1)

It was found that two equivalents of N_2CPh_2 react with $[PhBP_3]CoPMe_3$ (**5.2**) to generate the diazophosphazene $Me_3P{=}N_2CPh_2$ and the thermally stable diazoalkane adduct, $[PhBP_3]CoN_2CPh_2$, **7.2** (Eq. 7.2), rather than undergo carbene transfer and concomitant expulsion of N_2. Complex **7.2** is a red diamagnetic solid with a single ^{31}P NMR peak at 60 ppm, indicative of local C_3 symmetry about the cobalt center. Evidence for a diazoalkane adduct included a positive test for nitrogen upon combustion analysis and the lack of the signature $^{13}C\{^1H\}$ NMR peak (> 200 ppm) expected for a carbene moiety. Neither heating the complex nor adding Lewis acids such as $Sm(OTf)_3$ (OTf = $-OSO_2CF_3$) triggered the loss of N_2 to yield a carbene complex. Furthermore, addition of an alkene, such as styrene, to the diazoalkane complex does not lead to cyclopropanation, even with elevated temperature (100 °C).

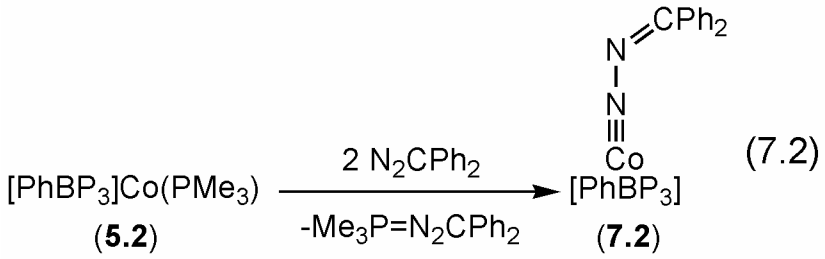

(7.2)

Interestingly, the addition of less sterically hindered diazoalkanes, such as N_2CHPh to $[PhBP_3]CoPMe_3$ (**5.2**), does not result in the formation of a clean diazoalkane complex. In an attempt to trap the potential carbene, a more sterically encumbered Co(I) precursor, $[PhBP_3]Co(PPh_3)$ (**7.1**), was used. Addition of excess N_2CHPh to **7.1** at -30 °C yielded a blue product that had a single new peak in the ^{31}P NMR spectrum at 42 ppm. The observation of PPh_3 at -6 ppm in the ^{31}P NMR spectrum suggests that the product

formed was not a species like $[PhBP_3]Co(=CHPh)(PPh_3)$, but either the diazoalkane adduct $[PhBP_3]CoN_2CHPh$ or possibly the carbene $[PhBP_3]Co{=}CHPh$ (Eq. 7.3). Upon warming to room temperature, the reaction mixture returned to a pale green color, and **7.1** was evident as the only metal containing species detected by ^1H NMR and UV-vis spectroscopy. The organic byproduct was determined by GC/MS to be *trans*-stilbene (by fragmentation). Although we have been unable to isolate the product, spectroscopic differences (^{31}P NMR, UV-vis) suggest that the reaction with N_2CHPh did not result in the same type of diazoalkane adduct as $[PhBP_3]CoN_2CPh_2$, **7.2**.

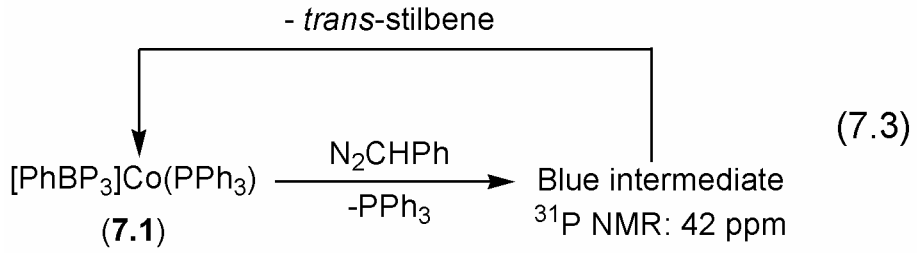

(7.3)

With this in mind, we set out to synthesize a *stable* diazoalkane adduct with a different bonding mode from **7.2** (vide infra) or perhaps with a carbene complex. Addition of $N_2CH(TMS)$ (TMS = $SiMe_3$) as a 2.0 M hexanes solution to a THF solution of **7.1** yields a stable blue product, $[PhBP_3]CoN_2CH(TMS)$ (**7.3**), based on structural characterization (vide infra) (Eq. 7.4). Complex **7.3** can be purified by crystallization from THF and petroleum ether at -30 °C. This species gives a nearly identical ^{31}P NMR resonance (42 ppm) and UV-vis absorption spectra (λ_{max} = 583 nm) as the blue intermediate of the reaction between **7.1** and N_2CHPh, indicating that the blue product is most likely $[PhBP_3]CoN_2CHPh$. Complex **7.3** is stable in the solid state at -30 °C for days although it decomposes at ambient temperature.

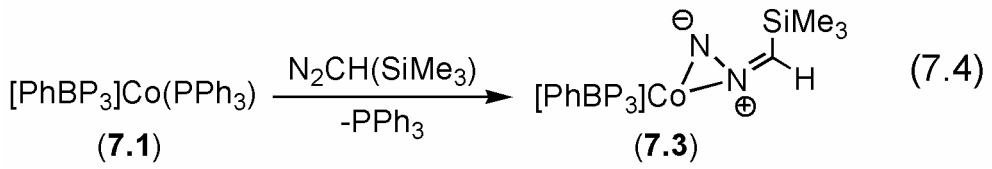

(7.4)

7.2.2 Solid-state structures of the diazoalkane complexes

The collection of single crystal X-ray diffraction data was necessary to unambiguously assign the bonding mode of the different diazoalkane complexes $[PhBP_3]CoN_2CPh_2$ (**7.2**) and $[PhBP_3]CoN_2CH(TMS)$ (**7.3**). The solid-state structures of **7.2** and **7.3** show very different bonding modes and are consistent with their different colors and ^{31}P NMR spectra. Complex **7.2** has a similar Co-N1 distance (1.667(2) Å) as the imido complexes $[PhBP_3]CoN$-*p*-tolyl, **5.4**, and $[PhBP_3]CoN^tBu$, **5.7** (1.658(2) and 1.633(2) Å, respectively) and exhibits a similar slightly bent Co-N1-N2 angle of 163.1(2)° (Figure 7.2). The very short Co-N bond in **7.2** is the second shortest metal-nitrogen bond structurally characterized for an end-on bound diazoalkane.[16] Furthermore, the N1-N2 bond (1.280(2) Å) is elongated in comparison to other group 9 terminally bound diazoalkane adducts (~ 1.16 Å)[14c,17] and significantly shorter than a true N-N single bond (~ 1.45 Å).[18] This suggests that the terminal nitrogen of the diazoalkane possesses significant metal-ligand multiple bond character, with the $-NCPh_2$ moiety effectively acting as the terminal functional group of an imide (i.e., $Co{\equiv}N\text{-}N{=}CPh_2$). This bonding mode has been well described before by Haymore and is common for Group 6 transition metals. Notably, this complex is the first example that displays end-on bonding of a diazoalkane ligand to cobalt.

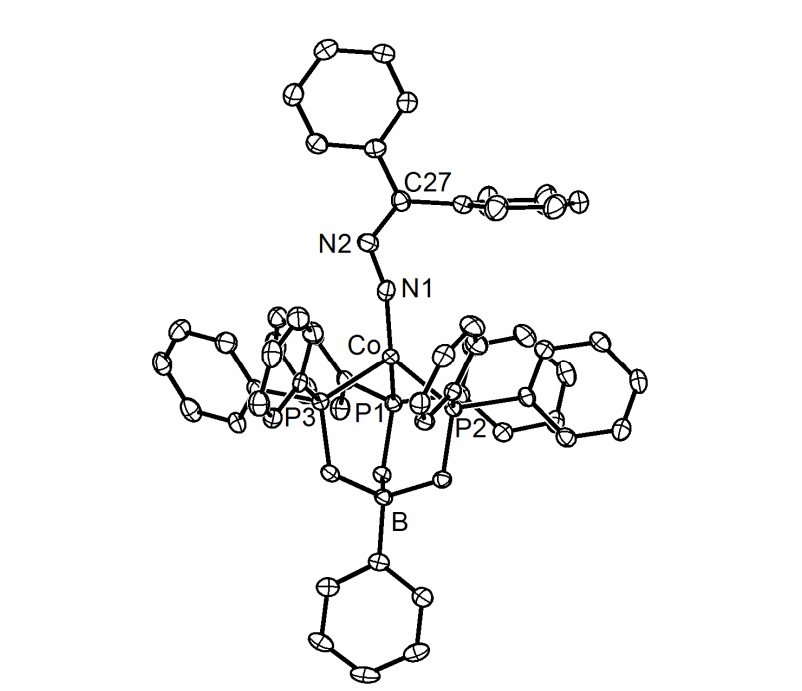

Figure 7.2. Displacement ellipsoid representation (50%) for $[PhBP_3]CoN_2CPh_2$ (**7.2**). Selected interatomic distances (Å) and angles (deg): Co-N1, 1.667(2); N1-N2 1.280(2); N2-C27, 1.311(2); Co-P1, 2.157(1); Co-P2, 2.184(1); Co-P3, 2.181(1). P1-Co-P2, 90.09(2); P1-Co-P3, 92.31(2); P2-Co-P3, 94.07(2); N1-Co-P1, 125.00(6); N1-Co-P2, 128.86(6); N1-Co-P3, 117.13(6); Co-N1-N2, 163.1(2); N1-N2-C27, 123.1(2).

In contrast, $[PhBP_3]CoN_2CH(TMS)$ (**7.3**) is a side-bound diazoalkane adduct, with a Co-N1 bond distance of 1.788(3) Å and a Co-N2 bond distance of 1.857(4) Å (Figure 7.3). These distances are significantly shorter than the only other reported side-bound diazoalkane of cobalt, $(PMe_3)_3Co(CH_3)(N_2C_5H_4)$, which had bond lengths of 1.994 and 1.914 Å for Co-N1 and Co-N2, respectively.[19] Moreover, these Co-N distances are the shortest nitrogen-metal linkages reported for any side-bound

diazoalkane complex found in the literature. The shortest M-N1 and M-N2 distances reported previously are 1.874(3) Å and 1.834(3) Å, for (^{t}BuNC)$_2$Ni(diazofluorene) (diazofluorene = $N_2C_{13}H_8$).[20] Furthermore, the N1-N2 bond distance in **7.3** of 1.289(4) Å is slightly elongated when compared to the N-N bond distances within similar side-bound diazoalkanes, which typically fall between 1.21 and 1.27 Å.[21] These bond distances suggest that the π-bond is quite strong and that the π* orbital is also quite substantial, weakening the N1-N2 bond.

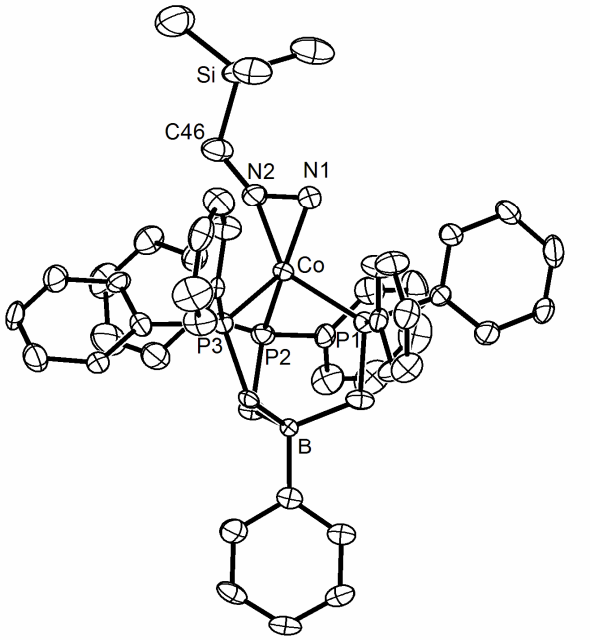

Figure 7.3. Displacement ellipsoid representation (50%) for [PhBP$_3$]CoN$_2$CH(TMS) (**7.3**). Selected interatomic distances (Å) and angles (deg): Co-N1, 1.788(3); Co-N2, 1.857(4); N1-N2, 1.289(4); N2-C46, 1.324(5); Co-P1, 2.214(1); Co-P2, 2.212(1); Co-P3, 2.182(1). Co-N1-N2, 72.2(2); Co-N2-C46, 161.6(3); N1-N2-C46, 131.4(4); N2-C46-Si, 121.3(4); P1-Co-P2, 92.97(5); P1-Co-P3, 91.20(5); P2-Co-P3, 88.34(5).

7.3 Discussion

The end-on diazoalkane [$PhBP_3$]CoN_2CPh_2 (**7.2**), which is best represented by the type **B** bonding mode in Figure 7.1, is remarkably stable, and we have been unable to induce the loss of N_2 under any condition. Given the stability and lack of reactivity of the isolobal imide complexes we have prepared such as [$PhBP_3$]CoN-*p*-tolyl, **5.4**, it is not surprising that **7.2** is so stable. Furthermore, it is noteworthy that this complex is the first example of a type **B** bonding mode involving a group 9 metal. This lack of type **B** diazoalkanes complexes of group 9 metals is not unexpected since type **B** complexes are electronically similar to imides, and few group 9 imides have been prepared until very recently.[22] What is particularly significant in assigning **7.2** as a type **B** complex is the expanded N1-N2 bond distance of 1.280(2) Å. Other group 9 end-on diazoalkanes feature N-N bond distances that are much closer to 1.15 Å, suggesting more N-N multiple bond character as seen in the type **C** bonding mode.[5d,23]

The reaction between N_2CHPh and [$PhBP_3$]$Co(PPh_3)$ (**7.1**) suggests that sterics and electronics play some role in determining the bonding mode of the diazoalkane ligand. The less sterically encumbered N_2CHPh diazoalkane appears to be going through a side-bound intermediate similar to **7.3** prior to loss of N_2 and formation of stilbene. It is perhaps surprising that we have been unable to trap a carbene in this case. A Co(I) species such as [$PhBP_3$]$Co(PMe_3)$ should be poised to make [$PhBP_3$]$Co(=CHPh)(PMe_3)$, which is isoelectronic to Bergman's carbene [Cp*]$Ir(=CH_2)(PMe_3)$. It is intriguing that a side-bound diazoalkane is formed given the inherent stability of the previously reported imides and the ability of a similar diazoalkane **7.2** to form an imide-like structure similar to [$PhBP_3$]CoN-*p*-tolyl, **5.4**. The lack of a second phenyl ring on the diazoalkane may

destabilize the anionic resonance form of type **B** (Figure 7.1B, left), allowing other bonding modes to be electronically favored.

While $[PhBP_3]CoN_2CH(TMS)$ (**7.3**) is more stable than the product of **7.1** and N_2CHPh, it also degrades at ambient temperature over a period of hours. This species is best described as a type **A** diazoalkane. The bonding mode of the species makes the assignment of the cobalt oxidation state ambiguous. Since it is diamagnetic, the bonding scheme in this compound can be compared to related complexes, such as $[PhBP_3]Co^{I}(CO)_2$ (**5.10**) or $[PhBP_3]Co^{III}Cl_2$ (**5.9**). The bonding mode can either be described as one of two limiting cases: type **A** in Figure 7.1, suggesting Co(I), or as the resonance structure shown in Eq. 7.4, suggesting Co(III). The very short Co-N bonds do not necessarily favor one limiting resonance structure type over another.

The energy difference between the two structure types is noticeable upon the addition of $N_2CH(Mes)$ (Mes = mesityl) to $[PhBP_3]Co(PMe_3)$ (**5.2**) in benzene. The solution turns red immediately, but the ^{31}P NMR spectrum suggests that the reaction is quite complicated, as peaks at 59 (br), 40.5, 23.5, and 16.2 are observed. A control reaction between free PMe_3 and $N_2CH(Mes)$ confirmed that the peak at 23.5 ppm is due to $Me_3P{=}N_2CH(Mes)$. $N_2CH(Mes)$ was added to $[PhBP_3]Co(NCCH_3)$ (**6.4**), to simplify the reaction and to suppress the formation of the byproduct, which resulted in two peaks in the ^{31}P NMR at 59 (br) and 40.5 in a ratio of 3:2. This suggests that both the end-on (59 ppm) and side-on (40 ppm) diazoalkane species were formed by the addition of $N_2CH(Mes)$ to a Co(I) precursor. The implication is that the two species are close in energy if both bonding modes can be formed with a single diazoalkne. The ability to observe both the side-bound and end-on conformational isomers of a diazoalkane is

notable since only one other transition metal system, $[Cp^*]_2Ti$, can accommodate both end-on[24] and side-on[21a,25] bonding modes without significant ligand modifications.

7.4 Conclusions

Cobalt diazoalkanes complexes that exhibit two different bonding modes, side-on and end-on, have been prepared with the same auxiliary ligand, [$PhBP_3$]. The end-on diazoalkane complex is the first of this type involving cobalt and shows one of the shortest metal-nitrogen bonds for this ligand class. The side-bound diazoalkane is stable at low temperature and features the shortest metal-nitrogen bonds for a structurally characterized side-bound diazoalkane. Although it is rare to stabilize more than one bonding mode on a single transition metal system, it appears that the energy difference between the end-on and side-on bonding modes is small enough that the nature of the specific diazoalkane ligand dictates the bonding mode.

7.5 Experimental section

7.5.1 General considerations

General procedures were performed according to Sections 2.4.1 and 3.5.1.

7.5.2 Starting materials and reagents

The preparation of [$PhBP_3$]CoI (**3.1**), [$PhBP_3$]Co(PMe_3) (**5.2**), and [$PhBP_3$]Co($NCCH_3$) (**6.4**) are described in Chapters 3, 5, and 6, respectively. The reagents PPh_3, 2.0 M $N_2CH(TMS)$ in hexanes, sodium, and mercury metal were purchased from commercial vendors and used without further purification. The reagents N_2CPh_2,[26] N_2CHPh,[27] and $N_2CH(Mes)$[28] were prepared according to literature procedures.

7.5.3 Synthesis of compounds

Synthesis of [$PhBP_3$]Co(PPh_3), 7.1. A 0.60% Na/Hg amalgam was prepared by dissolving 6.0 mg (0.26 mmol) of sodium into 1.0 g of mercury. A THF (3 mL) solution of PPh_3 (67.9 mg, 0.259 mmol) was then added to the stirring amalgam followed by the addition of a THF (15 mL) solution of [$PhBP_3$]CoI, **3.1**, (215 mg, 0.247 mmol). The mixture was stirred for 12 h as the color changed from green to brown. The reaction mixture was then filtered through Celite to remove the amalgam, and the filtrate was dried in vacuo, affording a fine brown powder. This brown powder was dissolved in benzene (15 mL) and stirred vigorously. After 1 h, white precipitate (NaI) was observed, which was removed by filtration though Celite. The brown filtrate was frozen and dried to a fine brown powder through lyophilization and was washed with petroleum ether (2 x 10 mL) and dried. The powder was then dissolved in benzene (2 mL) and triturated with petroleum ether (15 mL), which caused a green powder to crash out of solution. The supernatant was decanted, and the green powder was washed with petroleum ether (2 x 10 mL) and then dried in vacuo leaving the pure green product (118 mg, 48% yield). ^{1}H NMR (C_6D_6, 300 MHz): δ 18.5 (br), 14.7, 11.7, 8.5, 8.1, 7.6, 4.3, 3.6, -4.0, -5.7 (br). UV-vis (C_6H_6) λ_{max}, nm (ε): 694 (220). Anal. Calcd for $C_{63}H_{56}BCoP_4$: C, 75.16; H, 5.61. Found: C, 75.17; H, 5.30.

Synthesis of [$PhBP_3$]CoN_2CPh_2, 7.2. A benzene (2 mL) solution of diazodiphenylmethane (N_2CPh_2) (55.4 mg, 0.285 mmol) was added dropwise to a stirring benzene (4 mL) solution of [$PhBP_3$]Co(PMe_3), **5.2**, (117 mg, 0.143 mmol). During the first 10 min the brown solution turned deep red. The solution was stirred for an additional 4 h to ensure completion, and the solvent was then removed via lyophilization. The

resulting red powder was washed with petroleum ether (2 x 10 mL) to remove the byproduct, $Me_3P(N_2CPh_2)$. The red powder was taken up in benzene and crystallized by vapor diffusion of petroleum ether to afford analytically pure crystals (67 mg, 50 %). ^{1}H NMR (C_6D_6, 500 MHz): δ 8.14 (d, *J* = 7.0 Hz, 2 H), 7.89 (br, 4 H), 7.72 (t, *J* = 7.0 Hz, 2 H), 7.57 (m, 12 H), 7.48 (t, *J* = 7.0 Hz, 1 H), 7.18 (m, 6 H), 6.76 (m, 18 H), 1.48 (br, 6 H). ^{31}P{H} NMR (C_6D_6, 121.4 MHz): δ 60.1 (br). ^{13}C{H} NMR (C_6D_6, 209.5 MHz): δ 163.5, 139.5, 139.2, 138.2, 132.7, 132.6, 129.6, 129.2, 128.9, 128.8, 128.3, 124.9, 13.4 (br). UV-vis (C_6H_6) λ_{max}, nm (ε): 454 (6400), 520 (5400), 712 (4300). Anal. Calcd for $C_{58}H_{51}BCoN_2P_3$: C, 74.21; H, 5.48; N, 2.98. Found: C, 74.56; H, 5.47; N, 3.05.

Synthesis of [PhBP$_3$]CoN$_2$CH(TMS), 7.3. A 2.0 M solution of $N_2CH(TMS)$ (0.50 mL, 1.0 mmol) in hexanes was added to a stirring THF solution (3 mL) of $[PhBP_3]Co(PPh_3)$, **7.1**, (0.217 g, 0.216 mmol). The solution was stirred for 15 min and then petroleum ether (12 mL) was added. The solution was then cooled to -35 °C for 48 h until blue crystals formed (0.180 g, 97% yield). Elemental analysis failed due to decomposition. ^{1}H NMR (d_8-toluene, 300 MHz): δ 8.09 (d, *J* = 7.2 Hz, 2 H), 7.65 (t, *J* = 7.5 Hz, 2 H), 7.46 (m, 13 H), 6.74 (m, 18 H,), 6.66 (s, 1 H), 1.52 (br s, 6 H), 0.52 (s, 9 H). ^{31}P{^{1}H} NMR (d_8-toluene, 121.4 MHz): δ 42.5. UV-vis (C_6H_6) λ_{max}, nm (ε): 583 (2000).

Addition of N$_2$CHPh to [PhBP$_3$]Co(PPh$_3$), 7.1. Addition of excess (approximately 20 equiv.) N_2CHPh as a d_8-toluene solution to a d_8-toluene solution of $[PhBP_3]Co(PPh_3)$, **7.1**, at -30 °C gave a blue product that had ^{31}P NMR peaks at 42.1 and -6.8 (free PPh_3). The absorption spectrum of the reaction mixture showed a peak at 655 nm. After two hours at ambient temperature, ^{1}H NMR confirmed the return of **7.1**. A GC/MS trace of the reaction mixture confirmed the presence of *trans*-stilbene (m/z = 180).

Addition of $N_2CH(Mes)$ to $[PhBP_3]Co(PMe_3)$, 5.2. Addition of excess (approximately 10 equiv.) $N_2CH(Mes)$ as a C_6D_6 solution to a C_6D_6 solution of $[PhBP_3]Co(PMe_3)$, **5.2**, at ambient temperature gave a red mixture that had ^{31}P NMR peaks at 59 (br), 40.5, 23.5 and 16.2 ppm. The peak at 23.5 ppm was confirmed to be $Me_3P{=}N_2CH(Mes)$ by an independent synthesis.

Addition of $N_2CH(Mes)$ to $[PhBP_3]Co(NCCH_3)$, 6.4. Addition of excess (approximately 10 equiv.) $N_2CH(Mes)$ as a C_6D_6 solution to a C_6D_6 solution of $[PhBP_3]Co(NCCH_3)$, **6.4**, at ambient temperature gave a red mixture that had peaks at 59 (br) and 40.5 ppm in the ^{31}P NMR spectrum.

7.5.4 X-ray experimental information

The general X-ray experimental procedure was performed according to section 2.4.4. Crystallographic information is provided in Table 7.1.

Table 7.1. X-ray diffraction experimental details for $[PhBP_3]CoN_2CPh_2$ (**7.2**) and $[PhBP_3]CoN_2CH(SiMe_3)$ (**7.3**).

	$[PhBP_3]CoN_2CPh_2$ (**7.2**)	$[PhBP_3]CoN_2CH(SiMe_3)$ (**7.3**)
Chemical formula	$C_{58}H_{51}BCoN_2P_3$	$C_{57.5}H_{63}BCoN_2P_3Si$
Formula weight	938.66	778.27
T (ºC)	-177	-177
λ (Å)	0.71073	0.71073
a (Å)	13.1284(8)	16.5731(15)
b (Å)	16.5975(11)	13.2889(12)
c (Å)	21.8205(14)	23.277(2)
α (º)	90	90
β (º)	97.168(1)	97.231(2)
γ (º)	90	90
V (Å^3)	4717.5(5)	5085.7(8)
Space group	$P2_1/n$	$P2_1/n$
Z	4	4
Dcalcd (g/cm^3)	1.322	1.271
μ(cm^{-1})	5.07	5.00
R1, wR2 (I>2σ(I))[a]	0.0466, 0.0693	0.0582, 0.0830

[a] $R1 = \Sigma \, | \, |F_o| - |F_c| \, | \, / \, \Sigma \, |F_o|$, $wR2 = \{ \, \Sigma \, [\, w(F_o^2 - F_c^2)^2 \,] \, / \, \Sigma \, [\, w(F_o^2)^2 \,] \, \}^{1/2}$

References cited

1) a) Kanemasa, S.; Kanai, T. *J. Am. Chem. Soc.* **2000**, *122*, 10710-10711. b) Gothelf, K. V. *Cycloadd. React. Org. Synth.* **2002**, 211-247.

2) a) Maruoka, K.; Concepcion, A. B.; Yamamoto, H. *Synthesis* **1994**, 1283-1290. b) Maruoka, K.; Concepcion, A. B.; Yamamoto, H. *Synlett* **1994**, 521-523.

3) a) Penoni, A.; Wanke, R.; Tollari, S.; Gallo, E.; Musella, D.; Ragaini, F.; Demartin, F.; Cenini, S. *Eur. J. Inorg. Chem.* **2003**, 1452-1460. b) Li, Y.; Huang, J.; Zhou, Z.; Che, C. *J. Am. Chem. Soc.* **2001**, *123*, 4843-4844. c) Davies, H. M. L.; Bruzinski, P. R.; Fall, M. J. *Tet. Lett.* **1996**, *37*, 4133-4136.

4) Hillhouse, G. L.; Haymore, B. L. *J. Am. Chem. Soc.* **1982**, *104*, 1537-1548.

5) For an example of type **A** see: a) Nakamura, A.; Yoshida, T.; Cowie, M.; Otsuka, S.; Ibers, J. A. *J. Am. Chem. Soc.* **1977**, *99*, 2108-2117. For examples of type **B** see: b) Curtis, M. D.; Messerle, L. *Organometallics* **1987**, *6*, 1713-1717. c) Harada, Y.; Mizobe, Y.; Aoshima, T.; Oshita, H.; Hidai, M. *Bull. Chem. Soc. Jpn.* **1998**, *71*, 183-190. For examples of type **C** see: d) Werner, H.; Mahr, N.; Wolf, J.; Fries, A.; Laubender, M.; Bleuel, E.; Garde, R.; Lahuerta, P. *Organometallics* **2003**, *22*, 3566-3576. e) Nikonov, G. I.; Putala, M.; Zinin, A. I.; Kazennova, N. B.; Lemenovskii, D. A.; Batsanov, A. S.; Struchkov, Y. T. *J. Organomet. Chem.* **1993**, *452*, 87-90. For an example of type **D** see: f) Kromm, K.; Hampel, F.; Gladysz, J. A. *Organometallics* **2002**, *21*, 4264-4274. For examples of type **E** see: g) Gerlach, C. P.; Arnold, J. *Organometallics* **1997**, *16*, 5148-5157. h) Lemenovski, D. A.; Nikonov, G. I.; Brusova, G. P.; Kuzmina, L. G.; Stankovie, E.; Putala, M. *J. Organomet. Chem.* **1995**, *496*, 227-232.

6) a) Werner, H. *J. Organomet. Chem.* **1995**, *500*, 331-336. b) Cohen, R.; Rybtchinski, B.; Gandelman, M.; Rozenberg, H.; Martin, J. M. L.; Milstein, D. *J. Am. Chem. Soc.* **2003**, *125*, 6532-6546.

7) a) Chatterjee, A. K.; Choi, T.; Sanders, D. P.; Grubbs, R. H. *J. Am. Chem. Soc.* **2003**, *125*, 11360-11370. b) Trnka, T. M.; Morgan, J. P; Sanford, M. S.; Wilhelm, T. E.; Scholl, M.; Choi, T.; Ding, S.; Day, M. W.; Grubbs, R. H. *J. Am. Chem. Soc.* **2003**, *125*, 2546-2558.

8) Schwab, P.; Grubbs, R. H.; Ziller, J. W. *J. Am. Chem. Soc.* **1996**, *118*, 100-110.

9) a) Mahias, V.; Cron, S.; Toupet, L.; Lapinte, C. *Organometallics* **1996**, *15*, 5399-5408. b) Klose, A.; Solari, E.; Floriani, C.; Re, N.; Chiesi-Villa, A.; Rizzoli, C. *Chem. Commun.* **1997**, 2297-2298. c) Esposito, V.; Solari, E.; Floriani, C.; Re, N.; Rizzoli, C.; Chiesi-Villa, A. *Inorg. Chem.* **2000**, *39*, 2604-2613. d) Li, Y.; Huang, J.; Zhou, Z.; Che, C.; You, X. *J. Am. Chem. Soc.* **2002**, *124*, 13185-13193.

10) Mindiola, D. J.; Hillhouse, G. L. *J. Am. Chem. Soc.* **2002**, *124*, 9976-9977.

11) Dai, X.; Warren, T. H. *J. Am. Chem. Soc.* **2004**, *126*, 10085-10094.

12) a) Schwab, P.; Mahr, N.; Wolf, J.; Werner, H. *Angew. Chem., Int. Ed. Engl.* **1993**, *32*, 1480-1482. b) Werner, H.; Schwab, P.; Bleuel, E.; Mahr, N.; Steinert, P.; Wolf, J. *Chem. Eur. J.* **1997**, *3*, 1375-1384. c) Pechmann, T.; Brandt, C. D.; Werner, H. *Organometallics* **2003**, *22*, 3004-3006.

13) Klein, D. P.; Bergman, R. G. *J. Am. Chem. Soc.* **1989**, *111*, 3079-3080.

14) a) Fryzuk, M. D.; MacNeil, P. A.; Rettig, S. J. *J. Am. Chem. Soc.* **1985**, *107*, 6708-6710. b) Gritjahn, D. B.; Bikzhanova, G. A.; Collins, L. S. B.; Concolino, T.; Lam, K.; Rheingold, A. L. *J. Am. Chem. Soc.* **2000**, *122*, 5222-5223. c) Ortmann, D.

A.; Weberndörfer, B.; Ilg, K.; Laubender, M.; Werner, H. *Organometallics* **2002**, *21*, 2369-2381.

15) See Chapter 5 for a discussion of the synthesis of cobalt imide complexes.

16) The only shorter M-N bond for a diazoalkane is found on $(Ph_2N)_3VN_2CH(TMS)$ (V-N, 1.665(4) Å). See: Song, J.; Gambarotta, S. *Chem. Eur. J.* **1996**, *2*, 1258-1263.

17) Werner, H.; Mahr, N.; Wolf, J.; Fries, A.; Laubender, M.; Bleuel, E.; Garde, R.; Lahuerta, P. *Organometallics* **2003**, *22*, 3566-3576.

18) Greenwood, N. N.; Earnshaw, A. *Chemistry of the Elements*; Reed Elsevier: Oxford, UK, 1997.

19) Errors are not given for the bond lengths. Klein, H.; Ellrich, K.; Hammerschmitt, B.; Koch, U.; Cordier, G. *Z. Naturforsch., B* **1990**, *45*, 1291-1303.

20) Nakamura, A.; Yoshida, T.; Cowie, M.; Otsuka, S.; Ibers, J. A. *J. Am. Chem. Soc.* **1977**, *99*, 2108-2117.

21) a) Polse, J. L.; Andersen, R. A; Bergman, R. G. *J. Am. Chem. Soc.* **1996**, *118*, 8737-8738. b) Latham, I. A.; Leigh, G. J.; Huttner, G.; Jibrill, I. *J. Chem. Soc., Dalton Trans.* **1986**, 377-383.

22) a) Glueck, D. S.; Wu, J.; Hollander, F. J.; Bergman, R. G. *J. Am. Chem. Soc.* **1991**, *113*, 2041-2054. b) Glueck, D. S.; Hollander, F. J.; Bergman, R. G. *J. Am. Chem. Soc.* **1989**, *111*, 2719-2721. c) Betley, T. A.; Peters, J. C. *J. Am. Chem. Soc.* **2003**, *125*, 10782-10783. d) Jenkins, D. M.; Betley, T. A.; Peters, J. C. *J. Am. Chem. Soc.* **2002**, *124*, 11238-11239. e) Dai, X.; Kapoor, P.; Warren, T. H. *J. Am. Chem. Soc.* **2004**, *126*, 4798-4799. f) Hu, X.; Meyer, K. *J. Am. Chem. Soc.* **2004**, *126*, 16322-16323.

23) Werner, H.; Schneider, M. E.; Bosch, M.; Wolf, J.; Teuben, J. H.; Meetsma, A.; Troyanov, S. I. *Chem. Eur. J.* **2000**, *6*, 3052-3059.

24) Kool, L. B.; Rausch, M. D.; Alt, H. G.; Herberhold, M.; Hill, A. F.; Thewalt, U.; Wolf, B. *J. Chem. Soc., Chem. Commun.* **1986**, 408-409.

25) a) Polse, J. L.; Kaplan, A. W.; Andersen, R. A.; Bergman, R. G. *J. Am. Chem. Soc.* **1998**, *120*, 6316-6328. b) Kaplan, A. W.; Polse, J. L.; Ball, G. E.; Andersen, R. A.; Bergman, R. G. *J. Am. Chem. Soc.* **1998**, *120*, 11649-11662.

26) a) Regitz, M.; Maas, G. *Diazo Compounds: Properties and Synthesis*; Academic Press: New York, 1986, p. 326. b) Fischer, W.; Anselme, J. *J. Am. Chem. Soc.* **1967**, *89*, 5312-5313.

27) Creary, X. *J. Am. Chem. Soc.* **1980**, *102*, 1611-1618.

28) Wulfman, D. S.; Yousefian, S.; White, J. M. *Synth. Commun.* **1988**, *18*, 2349-2352.